

LASER SURFACE CLADDING OF STEEL

by LUCINO TAPIA-VILLANUEVA

A Thesis presented for the degree
of master of Philosophy of the
University of London

October 1980

John Percy Research Group
in Process Metallurgy
Department of Metallurgy & Material
Science
Imperial College of Science & Technology
London SW7 2BP

ABSTRACT

A novel method of cladding with stainless steel, a nickel base alloy (monel), and a copper base alloy (tin-bronze) has been developed; the technique is to use a laser beam to melt the alloy in powder form onto the surface of a base metal to give it the improved properties of the cladding alloy. Applications of this work are in the area of protection against corrosion and others.

The present work was done using powdered 316 stainless steel 300 mesh, monel and copper-tin (tin-bronze) (also as fine powders) as the surfacing material and mild steel (En 3) as the base plate. Both surfacing materials and baseplate were supplied by British Steel Corporation (Scottish Laboratories), and the experiments were carried out at Imperial College with a CO₂ continuous wave laser of 2 kilowatts.

The independent variables which defined the process for a single run were:

- a) total incident beam power P (W)
- b) incident beam diameter D (mm)
- c) traverse speed of incident beam V (mm/s)
- d) powder bed thickness d (mm)

On the other hand the dependent variables were found to be:

- a) continuity of bead
- b) width of the bead, w (mm)
- c) height of the bead, h (mm)
- d) spreading
- e) solidified contact angle, θ (degrees)
- f) depth of the heat-affected zone (HAZ), Z (mm)
- g) dilution (%)
- h) deposition rate, (Kg/Hr)
- i) microstructure in both surface cladding and baseplate (HAZ)

A study was made of the effect of the process parameters on the quality of deposit and metallurgical bond formed for single runs. This was then extended to multiple track runs in which the additional parameters of track overlap and degree of preheat of the substrate were also studied.

Some parameter correlations were established between deposit quality width, height, solidified contact angle, depth of the heat-affected zone, rate of deposition and degree of dilution with (P/DV) and (P/V) .

The previously noted advantages of using a laser for cladding have been justified in this work. Those advantages were:

- a) precise control of energy input
- b) localisation of heat
- c) minimal heat-affected zone and therefore thermal distortion and interface embrittlement
- d) a relatively tranquil process suffering from low dilution compared to other surfacing processes
- e) a rapid process, resulting in high quench rates and therefore homogeneous deposits

The quality of the deposits made here has shown that smooth surface deposits of controlled depth are possible, this could be useful in reducing finishing costs in an industrial process.

	TITLE	i
	ABSTRACT	ii
	CONTENTS	iv
CHAPTER 1		1
1.	INTRODUCTION	2
1.1	LASER MACHINES	3
1.2	CLASSES OF CO ₂ LASER	5
1.2.1	SLOW-AXIAL-FLOW CO ₂ LASER	5
1.2.2	FAST-AXIAL-FLOW CO ₂ LASER	6
1.2.3	TRANSVERSE-FLOW CO ₂ LASER	7
1.3	GAS LASER	7
1.4	GAS CONTAMINATION	15
CHAPTER 2		18
2.	SURFACE HEAT TREATING WITH A LASER BEAM	19
2.1	CLASSIFICATION OF METAL SURFACE CLADDING	20
2.1.1	PLASMA ARC-POWDER SURFACE CLADDING	20
2.1.2	PLASMA-ARC-ROD CAST SURFACE CLADDING	21
2.1.3	PLASMA-ARC-ROD CAST-POWDER SURFACE CLADDING	21

2.2.	LASER CLADDING	22
2.2.1	LASER BEAM DIAMETER	23
2.2.2	DILUTION IN SURFACE CLADDING	26
2.2.3	MATERIALS	29
2.2.3.1	BASE METAL	29
2.2.3.2	METAL CLADDING	29
2.2.3.2.1	316 STAINLESS STEEL	29
2.2.3.2.1.1	INFLUENCE OF PRINCIPAL CONSTITUENTS	30
2.2.3.2.1.1.1	ADDITION OF CHROMIUM	30
2.2.3.2.1.1.2	ADDITION OF NICKEL	31
2.2.3.2.1.1.3	ADDITION OF MOLYBDENUM	31
2.2.3.2.1.2	PHYSICAL METALLURGY OF AUSTENITIC STAINLESS STEEL	32
CHAPTER 3		34
3.	EXPERIMENTAL PROCEDURE	35
3.1	STAINLESS STEEL SURFACE CLADDING	35
3.2	MONEL SURFACE CLADDING	36
3.3	TIN-BRONZE SURFACE CLADDING	36
3.4	SINGLE TRACK DEPOSIT	37
3.4.1	SPECIMEN PREPARATION BEFORE CLADDING	37
3.4.2	SPECIMEN PREPARATION AFTER CLADDING	38

3.5	MULTIPLE TRACK DEPOSITS	41
3.5.1	SPECIMEN PREPARATION BEFORE CLADDING	41
3.5.2	SPECIMEN PREPARATION AFTER CLADDING	42
3.6	MICROHARDNESS MEASUREMENT	46
3.7	CALCULATING DILUTION	46
3.8	EQUIPMENT	47
3.8.1	CO ₂ GAS LASER OF 2,000 WATTS	47
3.8.1.1	OPTICAL AND SUPPORT STRUCTURE SYSTEM	48
3.8.1.2	POWER SUPPLIES AND CONTROLS	48
3.8.1.3	WATER FLOW SYSTEM	49
3.8.1.4	GAS FLOW SYSTEM	50
3.8.1.5	MOVEMENT OF WORKPIECE	50
CHAPTER 4		55
4.	DESCRIPTION OF THE RESULT TRACK DEPOSITS	57
4.1	316 STAINLESS STEEL SURFACE CLADDING	57
4.1.1	HEIGHT & WIDTH - 316 STAINLESS STEEL	61
4.2	TIN-BRONZE SURFACE CLADDING	82
4.2.1	HEIGHT & WIDTH - TIN - BRONZE	82
4.3	MONEL SURFACE CLADDING	92
4.3.1	HEIGHT & WIDTH - MONEL	92
4.4	DEVELOPING SECTION SURFACE CLADDING	109

4.5	QUANTITATIVE DILUTION	118
4.5.1	316 STAINLESS STEEL-DILUTION IN SURFACE CLADDING	118
4.5.2	TIN-BRONZE-DILUTION IN SURFACE CLADDING	119
4.6	DEPOSITION RATE IN SURFACE CLADDING	127
4.6.1	DEPOSITION RATE FOR 316 STAINLESS STEEL	127
4.6.2	DEPOSITION RATE FOR TIN-BRONZE	134
4.7	SOLIDIFICATION IN TYPE 316 STAINLESS STEEL	
	SURFACE CLADDING	136
4.8	METALLOGRAPHIC OBSERVATIONS	143
4.8.1	316 STAINLESS STEEL SURFACE CLADDING	143
4.8.2	MICROSTRUCTURES IN THE HEAT-AFFECTED ZONE	
	SUBSTRATE	147
4.9	SURFACE CLADDING COMPOSITION	154
4.10	RESULTANT HARDNESS IN THE CLAD LAYER	162
4.10.1	RESULTANT HARDNESS IN 316 STAINLESS STEEL	
	CLADDING	162
4.10.2	RESULTANT HARDNESS IN THE HEAT-AFFECTED ZONE SUBSTRATE	162-a
4.10.3	RESULTANT HARDNESS ON SELECTED SPECIMENS	
	316 STAINLESS STEEL SURFACE CLADDING	176
4.11	RESULTANT SURFACE CLADDING ON MULTIPLE RUN DEPOSITS	176
4.12	METALLOGRAPHIC OBSERVATION ON MULTIPLE RUNS	182
4.12.1	316 STAINLESS STEEL SURFACE CLADDING	182
4.12.2	HEAT-AFFECTED ZONE SUBSTRATE	182
4.13	WETTING AND SPREADING OF MOLTEN	

	CLADDING ALLOY ON A BASE METAL	183
4.14	VISCOSITY IN SURFACE CLADDING	194
4.15	MECHANICAL PROPERTIES IN SURFACE CLADDING	194
4.15.1	BEND TEST	194
4.15.2	SHEAR TEST	195
CHAPTER 5		197
	CONCLUSIONS	197

APPENDICES		202
I.1	OPERATING CONDITIONS AND RESULTS SINGLE TRACK DEPOSITS, 316 STAINLESS STEEL SURFACE CLADDING	203
I.2	OPERATING CONDITIONS AND RESULTS SINGLE TRACK DEPOSITS, TIN-BRONZE SURFACE CLADDING	228
I.3	OPERATING CONDITIONS AND RESULTS SINGLE TRACK DEPOSITS, MONEL SURFACE CLADDING	230
I.4	OPERATING CONDITIONS AND RESULTS MULTIPLE TRACK DEPOSITS, 316 STAINLESS STEEL SURFACE CLADDING	237
II.1	SECTIONAL AREA, PERCENTAGE DILUTION, DEPOSITION RATE AND SOLIDIFIED CONTACT ANGLE AS A FUNCTION OF THE APPLIED SPECIFIC ENERGY AND POWDER THICKNESS	241
II.2	SECTIONAL AREAS, PERCENTAGE DILUTION, DEPOSITION RATE AND SOLIDIFIED CONTACT ANGLE AS A FUNCTION OF THE APPLIED SPECIFIC ENERGY FOR A 1.00mm POWDER THICKNESS OF TIN-BRONZE	244
II.3	DEPOSIT TOUGHNESS AND ADHERENCE AS MEASURED BY BEND AND SHEAR TESTS	245
	NOMENCLATURE	246
	TABLES	249
	REFERENCES	250
	LIST OF FIGURES	253
	ACKNOWLEDGMENTS	263

CHAPTER 1

1 INTRODUCTION

1.1 LASER MACHINES

1.2 CLASSES OF CO₂ LASERS1.2.1 SLOW-AXIAL-FLOW CO₂ LASER1.2.2 FAST-AXIAL-FLOW CO₂ LASER1.2.3 TRANSVERSE-FLOW CO₂ LASER

1.3 GAS LASER

1.4 GAS CONTAMINATION

1. INTRODUCTION

Laser cladding is one of the new applications for a high power continuous wave CO₂ laser in material processing. There are as yet very few published references to it. It has recently become a method of production, but only in a few factories (e.g. Rolls Royce). However, the process can be considered an excellent technique for improving the resistance of metals against corrosion and high temperature environments.

The technique consists of placing a cladding alloy face to face with a base plate to be clad and using a continuous wave output laser beam to melt the alloy onto the surface.

The aim in the present research is to make use of powdered 316 stainless steel, monel and tin-bronze as cladding alloys, mild steel (En 3) as base plate, and a continuous wave CO₂ laser beam of 2 kilowatts as a heat source to produce an adherent surface cladding, with the minimum possible of dilution, to provide smooth surface cladding with homogeneous microstructure and hardness across it; to provide high density-low porosity as well as to minimize interdiffusion between the cladding alloy and the base plate; to avoid effects on the base plate (big heat-affected zone) and finally, to make the process as flexible as possible.

1.1 LASER MACHINES

The laser has been widely and successfully used in the fields of welding, cutting and surface treatment of materials due to its ability to place rapidly and precisely high intensity energy which is chemically clean (1, 2, 3, 4).

In the last decade different types of lasers have been developed for these industrial applications. The types of laser used are CO₂ gas lasers, He-Ne gas, argon ion, Nd:YAG solid state lasers, ruby and Nd:Glass solid state laser. For more details of these commercial lasers used in material processing see Table 1. However, only the CO₂ gas laser will be described here because this is the kind of laser used in these experiments.

TABLE 1:

COMMERCIAL LASER USED IN MATERIAL PROCESSING (21)

LASER	TYPE OF MATERIAL	TYPE OF OPERATION	WAVELENGTH (μm)	POWER (w)	PULSE REP. RATE (pps)	PULSE LENGTH	TYPICAL USE
CO ₂	MOLECULAR GAS	CONTINUOUS	10.6	100-SEVERAL THOUSAND	-	-	SEAM WELDS
CO ₂	MOLECULAR GAS	REPETITIVELY PULSED	10.6	100 (AVERAGE)	100	100 μs	SEAM WELDS HOLE DRILLING
CO ₂	MOLECULAR GAS	TEA	10.6	10 ⁷	UP TO 100	10 μs	HOLE DRILLING MARKING
Nd:YAG	SOLID STATE	CONTINUOUS	1.06	UP TO 1000	-	-	SEAM WELDS
Nd:YAG	SOLID STATE	REPETITIVELY Q-SWITCHED CONTINUOUSLY PUMPED	1.06	10 ⁴ (PEAK) 10 (AVERAGE)	$\geq 25,000$	200 nsec	COMPONENT FABRICATION AND TRIMMING
Nd:YAG	SOLID STATE	PULSED PUMPED	1.06	10 ⁴ (PEAK)	100	1-10 msec	SPOT AND SEAM WELDS, MARKING
RUBY	SOLID STATE	NORMAL PULSE	0.6943	10 ⁵ (PEAK)	SINGLE PULSE	0.25-5msec	SPOT WELDS AND SINGLE HOLES
Nd:GLASS	SOLID STATE	NORMAL PULSE	1.06	10 ⁶ (PEAK)	SINGLE PULSE	0.5-10msec	SPOT WELDS AND SINGLE HOLES

1.2 Classes of CO₂ Lasers

CO₂ lasers are used in material processing which have beam powers from 100 w to 100kw. They produce a 10.6 μ m infra red radiation with an efficiency of conversion of electrical excitation to optical beam power of between 10-20%. They may be classified according to the gas flow or the method of excitation e.g. slow axial flow, fast axial flow, transverse flow, TEA (Transversely Excited Atmospheric).

1.2.1 Slow-Axial Flow CO₂ laser

Slow axial flow CO₂ lasers were the first CO₂ lasers.

They consisted of a water-cooled tube with mirrors on both ends through which the laser gas mixture (CO₂, N₂ & He) flowed, the low pressure gas was excited by an electric plasma discharge. The gas mixture was cooled by heat conduction to the cool side walls of the discharge tube.

Continuous wave CO₂ lasers cannot operate efficiently at temperatures much above 300°C. The maximum electrical power, which can be delivered to the glass tube must be less than about 500 W/m of discharge tube, at the conversion efficiency of 10%, which corresponds to an output power of 50 W/m.

If the input power were increased then the gas would overheat and so the laser optical power would not increase, neither could the input power be increased if the tube diameter were increased, because then

the gas in the centre of the tube would overheat due to the longer conduction path to the cooled wall. If the gas pressure were increased then the uniform electrical glow discharge between the electrodes would become filamentary in nature and consequently the output power would be reduced. Thus, the only way to increase the output power is to increase the length of the glass tube. The output power in this type of laser could be 10 kilowatts but the length of such a device would be of the order of 100 meters.

1.2.2 Fast Axial-Flow CO₂ Laser.

The discharge in this category of high power, continuous wave CO₂ laser takes place in a series of long glass tubes. The discharge is usually parallel to the flow direction. The loss of heat from the discharge tube is by convection rather than by conduction, because of the high flow rates involved (the control laser 2KW CW CO₂ laser has velocities up to 500 m/s). These machines work on a closed cycle gas flow with a small purge. Commercial machines using this principal are available from 500W to 6000W. The specific output power is approximately 500 W/m with a uniform electric discharge. The 2 kilowatts CO₂ laser used in this work is of this type. It will be described in section 3.8.

1.2.3 Transverse-Flow- CO₂ Laser

In this class of laser, the gas flow is perpendicular to both the electric discharge and the optic axis, giving rise to a cross flow configuration. This has the advantage that the time of residence of the lasing gas in the optical cavity is much shorter than in the axial flow devices, resulting in the possibility of much higher power density and consequently much more power per unit length of optical cavity.

In this system a uniform electric discharge is required over a much larger area than in the axial-flow system.

This is achieved by having specially shaped electrodes (Rogowski electrodes) (e.g. Culham CL5 5kW CW CO₂ laser) or by ionising the lasing gas by firing an electron beam through it (e.g. Avco Everett 15 kW CW CO₂ laser).

1.3 GAS LASER

The lasing action is usually obtained in a gas laser by subjecting it to an electric discharge (the alternative being chemical or gas dynamic excitation). The energetic electrons provided by the discharge collide with the active gas particles (atoms or molecules) which are excited to their higher energy levels from which they will spontaneously descend to lower energy levels. The excess of energy

is emitted in the form of photons or light quanta.

If an excited atom or molecule is struck by one of these photons it will be stimulated to change to a lower energy state thus producing another photon. This amplification is the basic laser mechanism. (The word LASER standing for LIGHT AMPLIFICATION BY THE STIMULATED EMISSION OF RADIATION).

To achieve this optical gain it is necessary that the population density of particles in the upper energy level exceed that in the lower energy level (known as a "population inversion"). It is also necessary that the absolute number of atoms or molecules excited to the upper level be large and that the gas particles leave the lower laser level just as fast as they arrived from the upper level. So the depopulation or de-excitation of the particles in the lower laser level is just as important as the ground state to the upper laser level, since a particle that has already contributed to the laser output must return to the ground state so it is available again for excitation to the upper level in order to produce additional laser power.

The quantity of energy wasted by the particle in returning from the lower laser level to the ground state is equal to the difference

between the energy needed to excite the particle to the upper laser level and the energy of the photon of light which is emitted when the particle makes the transition from the upper laser level to the lower laser level; so the absolute maximum efficiency of the laser system is given by the emitted energy divided by the excitation energy. For a carbon dioxide laser the maximum theoretical, or quantum, efficiency is approximately 45%.

In practice the efficiency of the gas laser is lower than its quantum efficiency, which implies that there is not a perfect state of collision between an atom and an energetic electron in the gas discharge.

Some techniques have been developed for the excitation of the gas laser in the discharge, such as electron-beam-sustained, ultraviolet radiation, radiofrequency-stabilized, etc. The ideal selection of these excitation mechanisms, combined with a high quantum efficiency could be the prescription for obtaining a high working efficiency in gas lasers.

The electron energy level spectra of molecular gases is extremely complicated. However, a molecule can also have energy levels

arising from vibrational and rotational motion. Thus for a given electron configuration of a gas molecule, there are several almost equally spaced vibrational levels, and for each vibrational level there are a number of rotational levels. Such excited states are of low energy and hence usually emit photons in the infra red end of the spectrum.

The use of molecular gases has been found useful for continuous-wave laser oscillation; the vibrational-rotational levels belonging to the electron ground state of the molecule are ideal for efficient and powerful laser systems in the infrared region. The vibrational levels of the electron ground state are very close to the ground level of the molecule, and thus the laser photon energy is a sizable fraction of the total energy needed to excite the molecule from the ground state to the upper laser level. The result is a very high quantum efficiency compared with that of an atomic-gas infrared laser. In addition, since the vibrational levels are close to the ground state of the molecule, almost all the electrons present in the discharge will be effective in the required excitation process. This fact ensures a

high working efficiency as well as high power output, because at these conditions a large population density of molecules in the upper laser can be obtained.

Carbon dioxide has been found suitable for continuous-wave laser oscillation because it is one of the simplest of the triatomic molecules. Moreover, a large amount of spectroscopic information exists about its vibrational-rotational transitions. The carbon dioxide molecule, as is well known, is linear and symmetric in configuration and has three degrees of vibrational freedom as it can be seen on right top fig. 1-1. In the first degree, atoms of the molecule vibrate along the internuclear axis in a symmetric manner; the mode of vibration is called the symmetric stretch mode and is denoted, ν_1 . In the second symmetric mode of vibration, the oscillation of the atoms is perpendicular to the internuclear axis; this mode is called the bending mode and is denoted ν_2 . The third is an asymmetric stretch mode of vibration along the internuclear axis and is denoted ν_3 . The energies of the vibrations are quantized by the rules of quantum mechanics and as they are all different, the carbon

dioxide molecule can be excited to have any linear combination of the three individual modes of vibration. For this reason the vibrational state of the molecule must be described by the three quantum numbers, μ_1 , μ_2 , and μ_3 , which represent the quantum of the μ_1 , μ_2 , and μ_3 modes of vibration to which the molecule is excited and then a description of a given vibrational level would accordingly take the form $(\mu_1 \mu_2 \mu_3)$.

The energy-level diagram of some of the low-lying vibrational states of carbon dioxide is shown in fig 1.1, where the various vibrational levels with different quanta in modes μ_1 , μ_2 and μ_3 form equally spaced ladders. The lifetime of carbon dioxide molecules in the various states is shown together with the probability of excitation by electron impact from the ground state. The level designated 001 is suitable for the upper laser level and the 100 and 020 levels form the respective lower laser levels. The $001 \rightarrow 100$ vibrational-rotational transitions produce infrared radiation near 10.6 microns wavelength and from this lower level decays to the ground state through radiative and collision-induced transitions to the lower 010 level, which in turn decays to the ground state.

A similar mechanism can be taken by $001 \rightarrow 020$ vibrational-rotational transitions to produce infrared radiation near 9.6 microns wavelength and from this lower level decays to the ground state as in the above case.

Particularly important in raising the working efficiency of carbon dioxide lasers is the fact that nitrogen has only one vibrational state and the energy level of this state is almost identical to the (001) vibrational state of carbon dioxide. This means that by adding nitrogen to the carbon dioxide more of the energy in the electric discharge is converted to a level similar to that of (001) CO_2 . The nitrogen can only lose its excitation energy by collision with a CO_2 molecule or the container walls.

Helium is also added to the lasing gas mixture to increase its thermal conductivity and to stabilise the electric discharge.

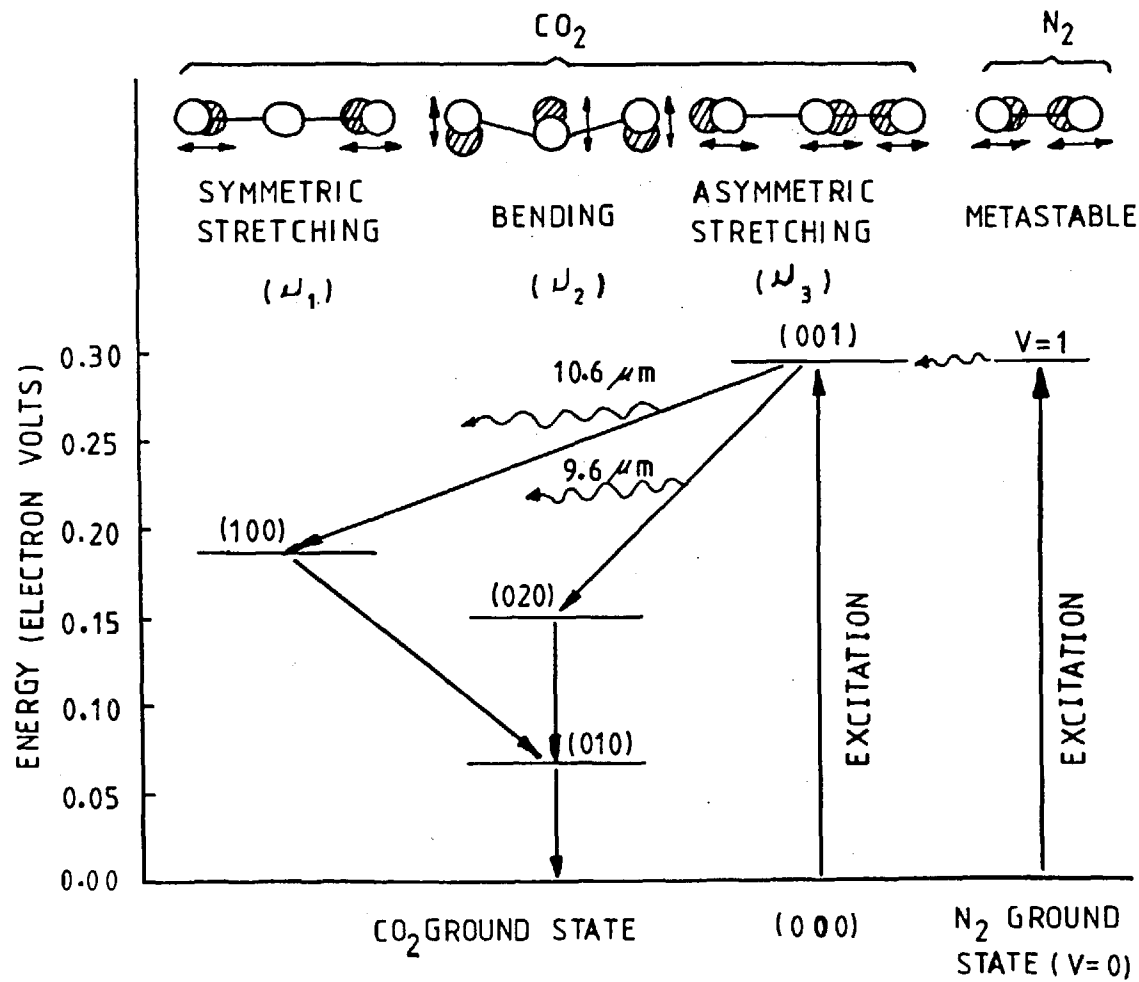


FIG 1.1 OSCILLATION MODES AND VIBRATIONAL ENERGY LEVELS OF CARBON DIOXIDE AND NITROGEN MOLECULE.

1.4 Gas Contamination

One of the limitations in operating high power continuous wave CO_2 lasers has been the effects of small concentrations of impurities which may be present in the fresh CO_2 - N_2 -He lasing gas mixture or generated in the chemical reaction during the discharge (5).

In fig 1.2 are shown some of the various reaction products that can occur in the electric excitation of the mixture CO_2 - N_2 -He, where oxygen-nitrogen reactions are the worst contaminants and NO_2 is the most adverse to laser efficiency.

The presence of contaminants in the carbon dioxide electric-discharge laser alters the discharge impedance which is determined by the balance achieved between the production and loss of charged particles. The neutral gas temperature is determined by the power input to the discharge and is therefore a function of the discharge impedance; moreover, small-signal gain is degraded by its extreme sensibility to changes in the gas temperature. Thus the impurities either upset the plasmas stability, lead to overheating of the gas, or to absorption of the radiation in the cavity.

Variations in impedance and small-signal gain may also be produced by plasma instabilities, which manifest themselves in two

different forms: in the first there are moving striations in the positive column, which do not alter the glow character of the discharge, but cause fluctuations in the sidelight emission. These striations may have the effect of allowing the discharge to operate at a lower average electric field than in their absence; the second form of instability is the sudden constriction of the glow into a bright filament, which may be accompanied by a drop in impedance and degradation of the small-signal gain.

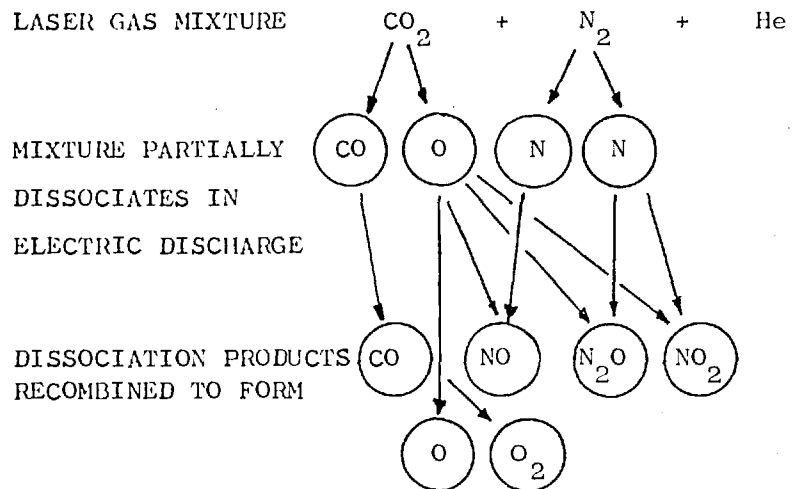


FIG. 1.2 CHEMICAL REACTIONS IN GAS LASER.

NITROGEN-OXYGEN
CONTAMINATION EFFECTS

CONTAMINANT	EFFECTS
NO	GAIN AND PLASMA IMPEDANCE BEGAN TO DECREASE AT 0.1% (*), COMPLETE LOSS OF GAIN 1.5%.
NO ₂	0.04% CAUSE PLASMA INSTABILITIES; COMPLETE LOSS OF GAIN AT 0.1%.
N ₂ O	0.08% CAUSED PLASMA INSTABILITIES; COMPLETE LOSS OF GAIN AT 0.2%.

* RELATIVE TO THE TOTAL FLOW RATE.
REFERENCE 5.

- 2 SURFACE HEAT TREATING WITH LASER BEAM
- 2.1 CLASSIFICATION OF METAL SURFACE CLADDING
 - 2.1.1 PLASMA ARC-POWDER SURFACE CLADDING
 - 2.1.2 PLASMA ARC-ROD CAST SURFACE CLADDING
 - 2.1.3 PLASMA ARC-ROD CAST-POWDER SURFACE CLADDING
- 2.2 LASER CLADDING
 - 2.2.1 LASER BEAM DIAMETER
 - 2.2.2 DILUTION IN SURFACE CLADDING
 - 2.2.3 MATERIALS
 - 2.2.3.1 BASE METAL
 - 2.2.3.2 METAL CLADDING
 - 2.2.3.2.1 316 STAINLESS STEEL
 - 2.2.3.2.1.1 INFLUENCE OF PRINCIPAL CONSTITUENTS
 - 2.2.3.2.1.1.1 ADDITION OF CHROMIUM
 - 2.2.3.2.1.1.2 ADDITION OF NICKEL
 - 2.2.3.2.1.1.3 ADDITION OF MOLYBDENUM
 - 2.2.3.2.1.2 PHYSICAL METALLURGY OF AUSTENITIC STAINLESS STEEL

2. Surface Heat Treating with a Laser Beam

In the field of heat treatment of the surface of materials, various techniques have been developed making use of a laser beam, such as surface hardening (3,6), glazing (7), alloying (6), and cladding (8). The aim of the processes is to improve the surface properties of metals.

Surface cladding, in which we are interested at present, is a technique similar to conventional hardfacing. The process is effected by using a controlled heat source, with the aim of melting cast rod, powder alloys or both cast rod-powder alloy and causing the cladding to flow onto the surface of a base metal.

The heat source could be oxygen-acetylene, flames, arc-plasmas, electron beam, laser beam, etc. The one selected is made according to many factors, such as economic rate of production, quality, equipment versatility, etc.

In this choice the laser is the latest and least understood process.

It has advantages, though, which are already apparent. It only heats a small area, it is a chemically clean heat source, it is easily automated, it can be operated in the air at atmospheric pressure and it does not generate x-radiation. These advantages

distinguish it from all other heat sources.

2.1 Classification of Metal Surface Cladding

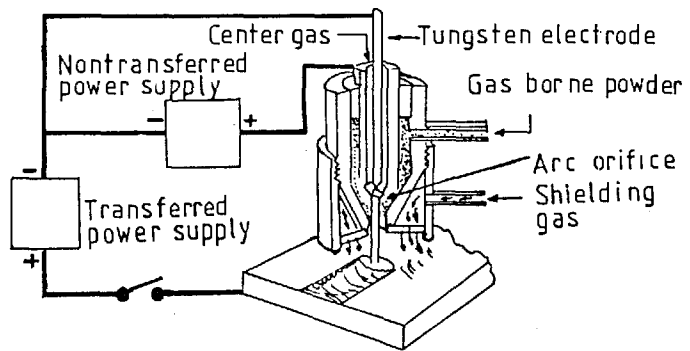
The ordinary industrial method for surface cladding metals is to use an arc as a heat source with the cladding in the form of a powder, wire or both. This being the principal process with which laser cladding must compete. It is now described briefly. (Electroplating and cementation are not cladding processes in the same sense, differing profoundly in the quality, structure and thickness of deposit).

2.1.1 Plasma Arc-Powder Surface Cladding

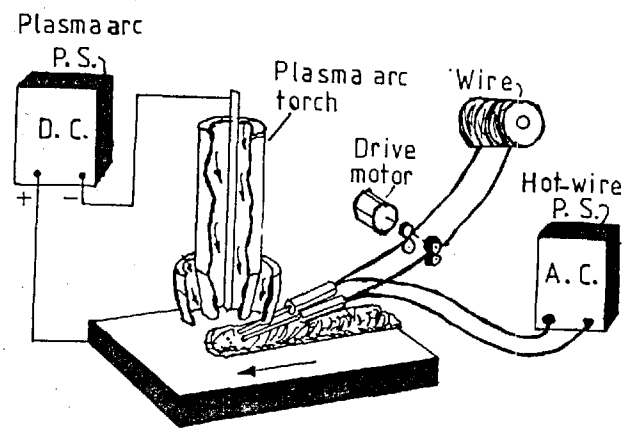
The adherence of the cladding using this technique is described by R.S. Suchowski and E Garrabrant (9). The technique is similar to the gas tungsten-arc process, except that it makes use of a constricted arc and employs filler metal in powder form which is directed through the arc in an argon atmosphere.

The powder is melted and the molten droplets^{are} joined to the base metal under a shielding gas. A sketch is shown in opposite of the next page.

The results obtained using this technique have been found acceptable industrially, as it gives low dilution, a high deposition rate



Schematic view of plasma arc weld surfacing electrode holder (9).



Schematic representative of the plasma arc hot-wire surfacing process (10).

and good deposition thickness.

2.1.2 Plasma Arc-Rod Cast Surface Cladding

Another process has been developed for metal surface cladding in which plasma arc and hot wire are used; Garrabrant E.C. and R.S. Zuchnowsky (10) describe the process. Basically the technique employs two sources of heat, one of them for the desired fusion on the base metal, by a transferred plasma arc with its direct current power supply; and the second one for the filler metal: this source of heat comes from the resistance heating of the two filler metal wires, and this is done with an alternating current power supply, the filler wires being continuously fed to the molten area where the electric circuit is completed. In conclusion, the function of the plasma arc is to melt only the top of the substrate and completely melt the filler metal which was heated previously, the system being shielded through the plasma arc torch. The results have been successful and are finding industrial application. A sketch is shown in opposite.

2.1.3 Plasma Arc-Rod Cast-Powder Surface Cladding

The third method for surface cladding metals to be described in

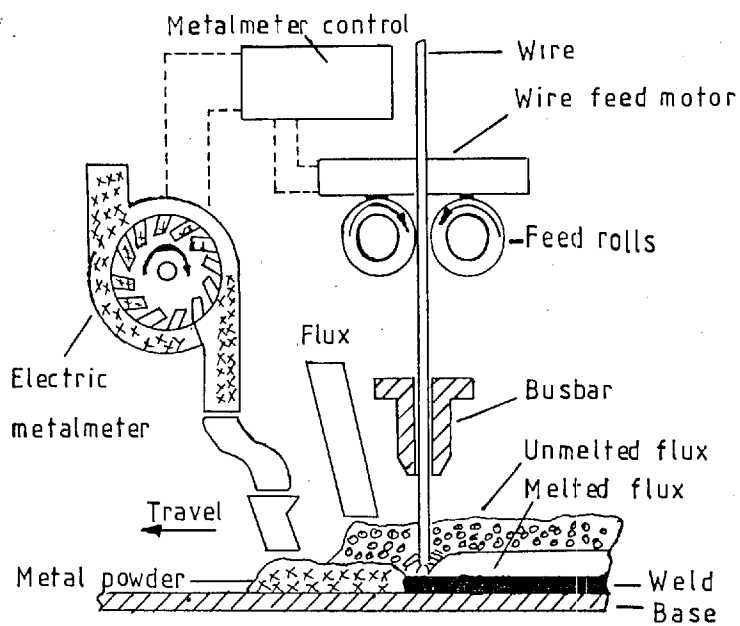


Diagrama of Bulkweld process for powdered filler additions to submerged arc welding, (11).

The present report is to make use of a plasma arc, cast rod, and filler powder metal. This process is called bulk process weld using flux (11). Basically the technique consists in feeding metal powder from an electric metalmeter to the workpiece just ahead of the consumable electrode wire, which at the same time controls the flow rate of the powder and keeps the ratio powder/wire constant. The powder is melted and mixed with the electrode when an arc is passed between the electrode and the base metal as well as the granular metal. A sketch is shown in opposite.

The "bulk" process has advantages (11) over other surfacing processes (Hot Rolled Annealed Bar Mill Clad, Manual Surface Deposit, Gas Metal Arc Surface Cladding) for its low dilution, high deposition rate, corrosion resistance, and low cost.

2.2 Laser Cladding

Laser cladding is the technique of passing a defocused laser beam over the powder alloys to be melted and causing the cladding alloy to flow onto the surface of a base metal to provide improved properties, such as corrosion or wear resistance.

Laser beams offer potential capability for precise control of

energy to melt a powder alloy both in power and spatial distribution. The metallurgical bond is excellent with a very low dilution and high deposition rate.

Dilution can be defined as the degree of admixture between the cladding alloy and base metal. Basically low dilutions in surface cladding are obtained by the control of heat input and power density with elimination of local melting of the base metal which would cause excess dilution of the clad surface. Dilution is undesirable because there is usually a substantial loss of properties as dilution of the cladding metal increases. However at the interface some dilution is required for a good metallurgical bond. Though the thinner this interface can be the ^{the amount of the} less expensive cladding _^ material will be required.

2.2.1 Laser Beam Diameter

It is essential to know the diameter of the laser beam on the work piece; in fact it can be argued that a knowledge of this independent variable is more important than a knowledge of the total laser power (12). Consequently a good optical beam is

desired. In order to achieve this, it is essential that the gas laser medium exhibit either no significant refractive distortions, or small fixed optical distortions which can be compensated by corrective optics techniques.

There are many difficulties in measuring the beam diameter.

Single isotherm measuring techniques are simple and quick to use, e.g. burn marks in acrylic, asbestos board, or paper, as used in this work. But they are not accurate since the measured diameter is a function of the exposure time of the beam power. Methods of measuring multiple isotherms are very much more complicated to use, but are more accurate if they can be evaluated. e.g. photon drag detector, linear response photographic paper. The problem of evaluation lies in the fact that the power distribution often has multiple peaks in it, so what is the definition of the diameter then?

Normally the beam diameter is defined as that radial location on a GAUSSIAN beam profile where the power intensity W/mm^2 has fallen to $1/e^2$ of the central value.

With irregular beams this value can be found by passing the beam

through variable apertures to find which size produces $(1-1/e^2)$ of the total power or the beam can be used to heat the surface of a block, the temperature rise measured and the rate compared to the heating rate from a Gaussian beam via a **mathematical model** :

the thermal rise time method (12). This gives the gaussian beam diameter equivalent to the heating effect of the incident beam.

The laser used here, a fast axial flow 2kW CW CO₂ laser

manufactured by Control Laser Ltd., produced a near Gaussian beam of 22mm exit diameter from the cavity.

The process of cladding requires this power to be accurately and uniformly spread over a certain area (\sim 1-2mm diameter). This careful control of power means a control of the amount of base metal and hence dilution.

In these experiments the beam was simply defocused, thus any irregularity in the beam profile or mode structure would be reflected in the process. To avoid this the beam can be spread by restoring from oscillating mirrors, or reformed by reflecting off faceted mirrors as practised at Culham Laboratories and Avco Ltd. Both these processes allow the greater freedom of using

a square or rectangle of heat in place of a circle.

Recently Ream S.L (13) has recommended using a convex beam integrator in laser heat treatment. This technique consists in dividing the output beam into small parts and applying each one to the same localization of the work surface making use of a mirror with convex shape and covered with irregular facets. Problems were encountered due to diffraction and interference effects but these could possibly be eliminated by use of other optical techniques.

2.2.2

Dilution in Surface Cladding

Dilution is the degree of admixture between the deposited metal and the base metal, or, quantitatively, fig 2.1 defines dilution and illustrates that the percentage of dilution equals the amount of base metal melted (area B), divided by the sum of the clad metal deposited and base metal melted (area A + area B), the quotient of which is multiplied by 100.

$$\% \text{ dilution} = \frac{B}{A+B} \times 100$$

where:

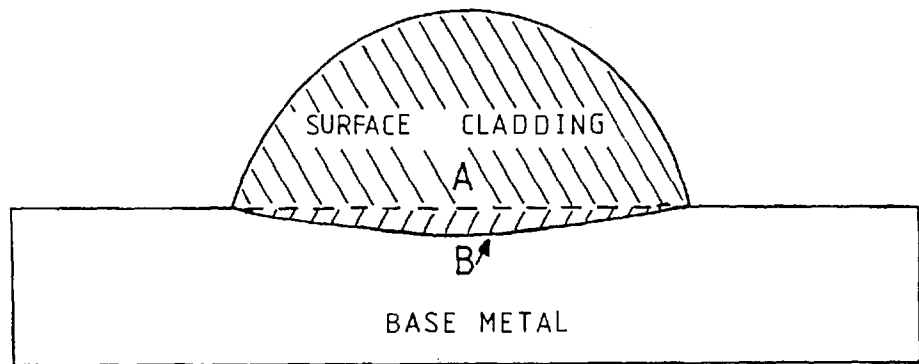
A = partial area of deposit on the base metal (mm^2)

B = Partial area of deposit penetrated on the base metal (mm^2)

$A + B =$ total area of deposit on the base metal (mm^2)

The level of dilution, which affects the composition and properties of the clad layer, is dependent on the quantity of base metal melted (control of the heat input) and the level of turbulence in the melt pool. The laser generated melt pool has only convection and surface tension forces causing turbulence; which compares favourably with arc processes and flame processes where there are also electromagnetic and aerodynamic forces stirring the melt.

Some intermixing at the interface is required in order to get a good metallurgical bond and avoid having an abrupt change in the coefficient of expansion. However this can be very small ($10\mu\text{m}$). The smaller it is the less will be the quantity of cladding material needed.



$$\% \text{ DILUTION} = \frac{B}{A+B} \times 100$$

FIG 2.1 DILUTION OF SURFACE CLADDING. THE BEAD, A, AND PENETRATION, B, BOTH AREAS A AND B ARE THE SAME CLADDING ALLOY, BUT ARE SHADED DIFFERENTLY TO ILLUSTRATE THE CALCULATION OF DILUTION.

2.2.3. Materials

2.2.3.1 Base Metal

The material used in this research as base metal was mild steel (En 3) with chemical composition.

%C	%Mn	%P	%S
0.16/0.24	0.50/0.90	0.05 MAX	0.05 MAX

This type of steel is one of the most widely employed and generally used of all engineering materials.

En 3 steel is readily weldable by ordinary fusion methods and that must be taken into account in making surface cladding on it.

The specimens used were in the form of rolled plate of 12mm thickness, 75mm width and 300mm length respectively, and were cleaned to remove impurities from the surface by surface grinding and degreasing.

2.2.3.2 Metal Cladding

2.2.3.2.1 Stainless Steel

Austenitic stainless steel was used in powder form type 316

of - 300 and 300 mesh and chemical composition.

%C	%Cr	%Ni	%Si	%Mn	%P	%S	%Mo
0.08	16.5/18.5	10.0/13.0	0.20/1.00	0.5//2.0	0.04	0.03	2.0/3.0

First of all stainless steels are a group of ferrous alloys that have at least 12% chromium necessary to produce passivity which is the principal characteristic producing extremely high levels of corrosion resistance.

Type 316 stainless steel is a typical austenitic stainless steel with additions of molybdenum (2.0/3.0%) for the stabilization of the carbides present in it; This material is used for its excellent corrosion resistance in chemical equipment and process plant industries, as well as where a clean surface and hygienic conditions are essential.

2.2.3.2.1.1 Influence of Principal Constituents

2.2.3.2.1.1.1 Addition of Chromium

Chromium, according to classical theories, acts by forming a surface film on the metal, comprising oxides impermeable to and insoluble in corrosive media.

2.2.3.2.1.1.2 Addition of Nickel

The addition of nickel to the steel is made with the aim of stabilizing austenite and modifies the structure of the steel, and gives rise to an alloy with improved ductility, high temperature mechanical strength and weldability. The addition of sufficient nickel to the steel results in a fully austenitic structure at room temperature.

2.2.3.2.1.1.3 Addition of Molybdenum

The passivity and chemical resistance of stainless steel are influenced by addition of molybdenum to reduce acids and chloride solutions where the passivity of chromium itself is less stable. Molybdenum, ^{like} chromium and silicon, is a ferrite former and stabilizer.

In addition to the effects of various elements on corrosion resistance and mechanical properties, a wide range of grade steels can be obtained according to various services requirements.

316 austenitic stainless steel offers a wide range of mechanical properties, such as good ductility and modest strength,

so for its high toughness is suitable for low temperatures as well as offering high strength at elevated temperatures (good creep).

Austenitic stainless steels with a high percentage of nickel cannot be hardened by heat treatment, but with a low percentage of nickel some are age-hardenable as well as all being readily strainhardened by cold forming.

Austenitic stainless steels are readily welded by all common fusion processes as well as easily cut, but because of their high ductility and rapid workhardening some precautions should be taken in machining.

2.2.3.2.1.2 Physical Metallurgy of Austenitic Stainless Steels

The chemical composition of type 316 stainless steel, as well as some grade austenitic, was so designed that when these alloys are solidified from the melt the resultant austenitic structure has a percentage of delta-ferrite, which is useful for avoiding hot cracking during solidification.

The volume fraction of the delta-ferrite in the resultant structure thus depends principally on the chemical composition of the alloy, but also obviously on the heat input condition used in the process which influences the solidification rate.

The ranges of delta-ferrite pre-and postwelded in austenitic stainless steels is quite important, firstly, as mentioned above for preventing hot tearing, and secondly for achieving various types of corrosion resistance.

At high temperatures the reaction in 316 austenitic stainless steel are quite complicated and interesting principally because of the instability of the delta ferrite that may transform to austenite as well as precipitating carbides and intermetallics. The carbides in the austenitic matrix can be $M_{23}C_6$, M_6C and intermetallics such as sigma phase (σ), CHI phase (χ) and laves phase (η).

CHAPTER 3

- 3 EXPERIMENTAL PROCEDURE
- 3.1 STAINLESS STEEL SURFACE CLADDING
- 3.2 MONEL SURFACE CLADDING
- 3.3 TIN-BRONZE SURFACE CLADDING
- 3.4 SINGLE TRACK DEPOSIT
 - 3.4.1 SPECIMEN PREPARATION BEFORE CLADDING
 - 3.4.2 SPECIMEN PREPARATION AFTER CLADDING
- 3.5 MULTIPLE TRACK DEPOSITS
 - 3.5.1 SPECIMEN PREPARATION BEFORE CLADDING
 - 3.5.2 SPECIMEN PREPARATION AFTER CLADDING
- 3.6 MICROHARDNESS MEASUREMENT
- 3.7 CALCULATING DILUTION
- 3.8 EQUIPMENT
 - 3.8.1 CO₂ GAS LASER OF 2,000 WATTS
 - 3.8.1.1 OPTICAL AND SUPPORT STRUCTURE SYSTEM
 - 3.8.1.2 POWER SUPPLIES AND CONTROLS
 - 3.8.1.3 WATER FLOW SYSTEM
 - 3.8.1.4 GAS FLOW SYSTEM
 - 3.8.1.5 MOVEMENT OF WORKPIECE

Experimental Procedure

A Control Laser continuous wave CO₂ laser of 2 kilowatts at Imperial College was used as the heat source for cladding powder type 316 stainless steel, monel and tin-bronze onto a substrate of mild steel.

3.1 Stainless Steel Surface Cladding

Surface cladding with 316 stainless steel was done under different operating conditions; of the following independent variables:

- (a) Laser beam power, (W)
- (b) Laser beam diameter, (mm)
- (c) Transverse speed, (mm/s)
- (d) Powder bed thickness, (mm)

The operating conditions are shown in Appendix 1.1

For multiple runs two more variables were included:

- (e) overlap, (mm)
- (f) Preheat, (°C)

The powder was replaced on the substrate and the laser beam transversed through the powder.

3.2 Monel Surface Cladding

Surface cladding with monel powder was done in two different ways. The first used a procedure similar to 316 stainless steel surface cladding, the effect of the same variables being studied.

In the second method the powder was blown into the laser interaction zone making use of a deloro-stellite flame spray gun which introduced another variable:

(e) Mass flow rate of powder, (Kg/Hr)

The different operating conditions are shown in Appendix 1.3, applying the same technique of blowing the powder. Multiple runs were done with two additional variables:

(g) Overlap, (mm)

(h) Preheat, ($^{\circ}$ C)

3.3 Tin-bronze Surface Cladding

15 single runs and 4 multiple runs of surface cladding with bronze powder were done. The variables explored on a single run were:

(a) Incident laser beam power, (W)

- (b) Laser beam diameter, (mm)
- (c) Traverse speed, (mm/s)
- (d) Powder bed thickness, (mm)

On the other hand for a multiple run only one additional variable was included:

- (e) Overlap, (mm)

The operating conditions are shown in Appendix 1.2

3.4 Single Track Deposits

The objective in making these layers was to find the behaviour of the laser beam under different operating conditions and to find the optimum operating region defined from: continuous track, good adherence, high deposition rate, low dilution and the minimum possible heat affected zone.

3.4.1 Specimen Preparation Before Cladding

The base metal of mild steel to be clad was cleaned with alcohol to take off impurities and mounted on a movable x-y table beneath the laser nozzle. This table was hydraulically actuated to give controlled and steady speeds to over a distance of 18 inches.

The baseplate was positioned perpendicular to the laser nozzle at a carefully measured working distance from the nozzle. A bed of powder of known thickness was laid on it. The laser beam diameter on the base plate surface was calculated from a knowledge of the focal position and nozzle plate working distance. The specimen was moved away from the laser nozzle, a speed selected and the specimen was passed under the laser nozzle. When the specimen was under it, the beam was switched on and the powder was melted by the laser beam, solidifying as a single track behind the path of the beam. The arrangement for making single-runs is shown in Fig 3.1.

For each run a record was made of the run number, total power, working distance, traverse speed and powder thickness. For the next run the unmelted powder was removed and reformed for the next traverse with different operating conditions, and so on.

3.4.2 Specimen Preparation after Cladding

All the resulting beads were photographed and cut sectionally as well as mounted in resin, polished and etched in a 2% nital

solution that developed only the base metal structure which was observed by light microscopy to analyse the interface between surface cladding and base metal, resulting structures, and underbead cracks. All the sectional views of the beads were photographed, from which measurements were made of the resulting bead dimensions. Their respective sectional areas were calculated, after which the percentage dilution and the deposition rates as well as the depth of the heat affected zone were determined. Contact angles were also measured. All working conditions and results are shown in Appendix 1 and II.

Selected specimens were polished and etched in different solutions with the aim of developing the cladding alloy structure. It was found that the Kalling's reagent (2g of Cu Cl_2 , 40 ml of HCl , 60 ml ETHANOL (95%) and 20 ml of WATER - developing time was around 15 minutes) and a mixture of acid solutions (10 ml of HNO_3 , 20 ml of HCl and 30 ml of H_2O - developing time was around 5 minutes) were the most appropriate developer of the stainless steel structure. The solution of acids seem to give the best results. On selected specimens microhardness measurements across the surface cladding were taken.

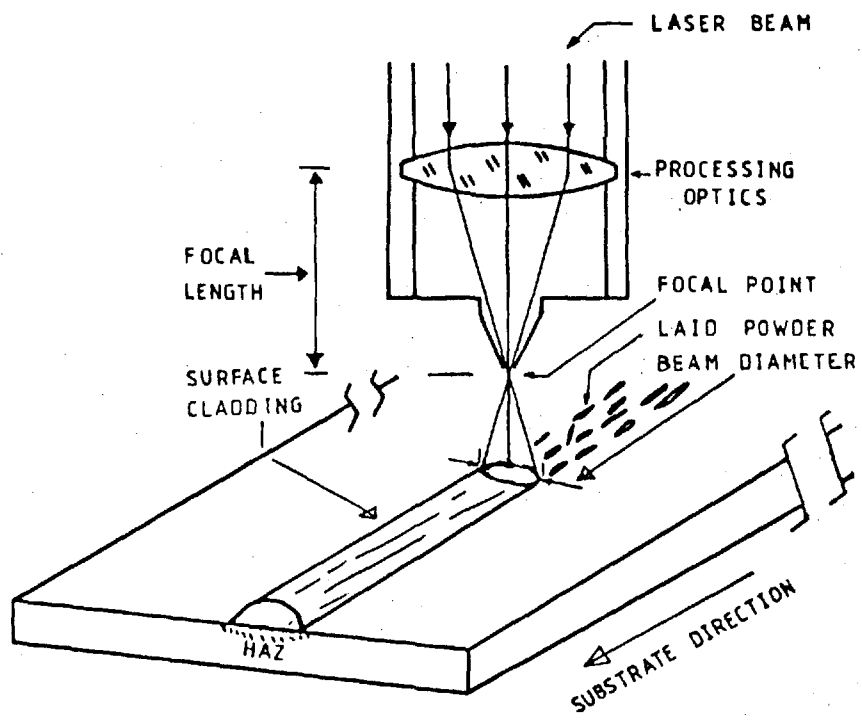


FIG 3.1 ARRANGEMENT OF THE APPARATUS FOR MAKING A SINGLE BEAD SURFACE CLADDING.

3.5 Multiple Track Deposits

The aim of these operations was to produce overlapped tracks which could be considered as single large area surfaces. The conditions for making multiple-runs were the same as the optimum operating conditions for the deposition of a single track-run.

3.5.1 Speciment Preparation before Cladding

The operations were based on mounting the steel slab between two shims and connecting it to a movable x-y table located beneath the stationary laser nozzle. A drawing representation is shown in Fig 3.2 for stainless steel and tin-bronze surface cladding and in Fig 3.3 that used for monel surface cladding. When the metal base was mounted on the movable x-y table, the base metal was preheated by a gas burner underneath the slab to different temperatures which were measured by a thermocouple set up in the metal base and shielding the surface substrate with argon on top while the preheating was done. When the temperature was + 50 °C of the required value, the preheat was stopped and the top surface substrate was covered with a bed of powder, previously measured and then the laser beam was passed

repeatedly forwards and backwards through the powder bed in the x-direction with a set movement in the Y-direction between passes. The Y-direction increments for each specimen were varied to allow the effect of overlap to be studied.

3.5.2 Specimen Preparation after Cladding

The top view of the runs MI to M20 of stainless steel, BM14 to BM19 of tin-bronze, and M45 to M49, M110 to M112 of monel was photographed, and each one was sectioned, polished, and etched in a 2% nital solution, as for the single tracks to study the different morphology presented in the interface between the surface cladding alloy and the base metal. The sectioned surface cladding was photographed with the aim of showing the effects of the degree of preheat and overlap.

All specimens were polished and etched in Kalling's reagent, and the resulting structures were analysed at high magnification and selected samples were photographed. Again all specimens were polished and etched in a mixture of acid solutions and the resulting structures were analysed and photographed. Both etching in Kalling's reagent and mixture of acids were found to be best for developing stainless steel structures.

For the determination of some mechanical properties of the surface cladding, all multiple-run samples were sent to British Steel Corporation (Scottish Laboratories) who performed bend and shear tests according to ASTM A264 for evaluation of the ductility and adherence of the surface cladding onto the base plate. The results are shown in table A3 and Appendix II.3.

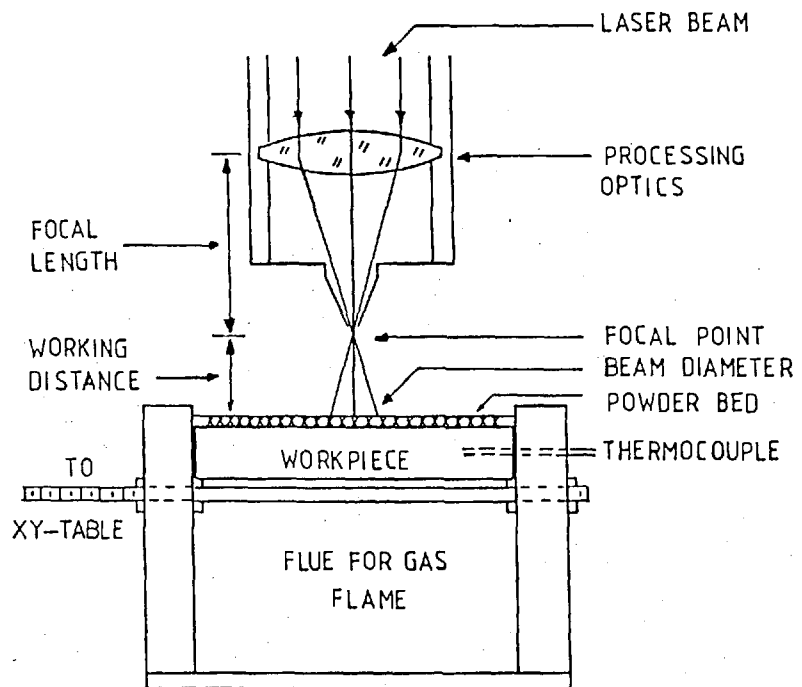


FIG 3.2 ARRANGEMENT OF THE APPARATUS



FIG 3.3 PHOTOGRAPH OF THE ARRANGEMENT OF APPARATUS FOR MONEL SURFACE CLADDING.

3.6 Microhardness Measurements

The microhardness measurements were done on akashi microhardness tester which had been fitted with a load of 200 g. The measurements were taken on a transverse section from the top of the surface cladding through the interface and into the substrate. The selected specimens were polished and etched in 2% nital solution followed by the microhardness measurement.

The vickers hardness number can be estimated from the indentation by a conversion equation, or by standard tables.

The operation of the machine is to indent the specimen structure with the previously set load (200 g) and then take an ocular measurement of the resulting indent (μ).

The size of the indent is converted as the hardness value.

3.7 Calculating Dilution

All specimens were cut sectionally and polished as well as etched in a 2% nital solution, the aim being to distinguish

the interface between surface cladding and base metal. The section view of each specimen was projected on a projector; a picture was drawn of each one; and from that, and taking the surface of the substrate as reference, the bead and penetrating areas of the surface cladding were calculated. By applying the equation described in section 2.2, the percentage of dilution was calculated. The resulting dilutions are shown in Appendix II.

3.8 Equipment

3.8.1 CO₂ Gas Laser of 2 Kilowatts

The Control Laser 2 kilowatts continuous wave laser at Imperial College has been developed by Control Laser Ltd (previously British Oxygen Co., Industrial Power Beams Division) and the British Welding Institute.

The system is operated semi automatically with safety interlocks.

Basically the system consists of five subsystems: optical and support structure system, power supplies and control gas flow system, water flow system and beam manipulator.

3.8.1.1 Optical and Support Structure System

The optical system consists of four pairs of discharge tubes which are supported on a rigid structure, four meters long. These form the laser cavity.

The total optical cavity is 8 meters long folded in the middle. The output beam is passed through a gallium arsenide window which isolates the cavity vacuum from the atmosphere. A pneumatically operated shutter is provided after the output window for beam on-off operation, when the beam is "off" the shutter mirror reflects the output beam into a water calorimeter to monitor the power. There is a fifth mirror which is used for directing the output beam through a lens (KCl) to the workpiece.

3.8.1.2 Power Supplies and Controls

The overall efficiency of the laser in converting electricity into optical power is around 10-20%. Thus at 2kw optical power 10-20 kw of electrical power has to be discharged into the tubes.

Thus the laser power supply is up to 100 amps at 450 volts.

This three phase system passes through a transformer after which it is rectified into four ballasted supplies of up to 30,000 volts at 200 mA. This is sufficient to make the tubes self starting.

The remaining power is required to drive the gas blower.

If any of the essential services fail then the laser is automatically shut down. The essential services are cooling water supplies, gas supplies, or inspection covers opened.

3:8.1.3

Water Flow System

Three water flows are provided for cooling system components.

The primary water circuit is used for cooling of the inlet block to the ovens, the gas heat exchangers, the rootes blower and the cathode box. The secondary water circuit is used for cooling all mirrors and the output window.

A tertiary deionised water circuit is used in the calorimeter.

If any of these circuits fails the laser is switched off.

3.8.1.4 Gas Flow System

A roots blower is provided for circulating the lasing gas mixture-carbon dioxide, nitrogen and helium-through the laser cavity at the rate of 2,500 cubic feet per minute. Three heat exchangers are provided, one of them situated at a point before the gas mixture passes through the blower and the other two after the gases have been passed through the blower. Their purpose is to cool the gas to bring the carbon dioxide back to its ground state (see section 1.3) A small gas purge reduces the build up of contaminants. This purged gas can be passed through a catalyst in the ovens and so recycled. This reduces the gas consumption by around a factor of 5.

An illustration of the control laser 2 kw fast axial flow CO₂ laser, which was used for these experiments, is shown in Fig 3.4.

3.8.1.5 Movement of Workpiece

The workpiece was mounted on an x - y table which was situated below the stationery laser nozzle. This table was moved in

x - y direction at a continuous speed by a hydraulic piston controlled with a setting on a needle valve. The hydraulics were manufactured by "Double A Hydraulics". A photograph of the equipment is shown in Fig 3.5.

PLAN VIEW OF LASER PATH

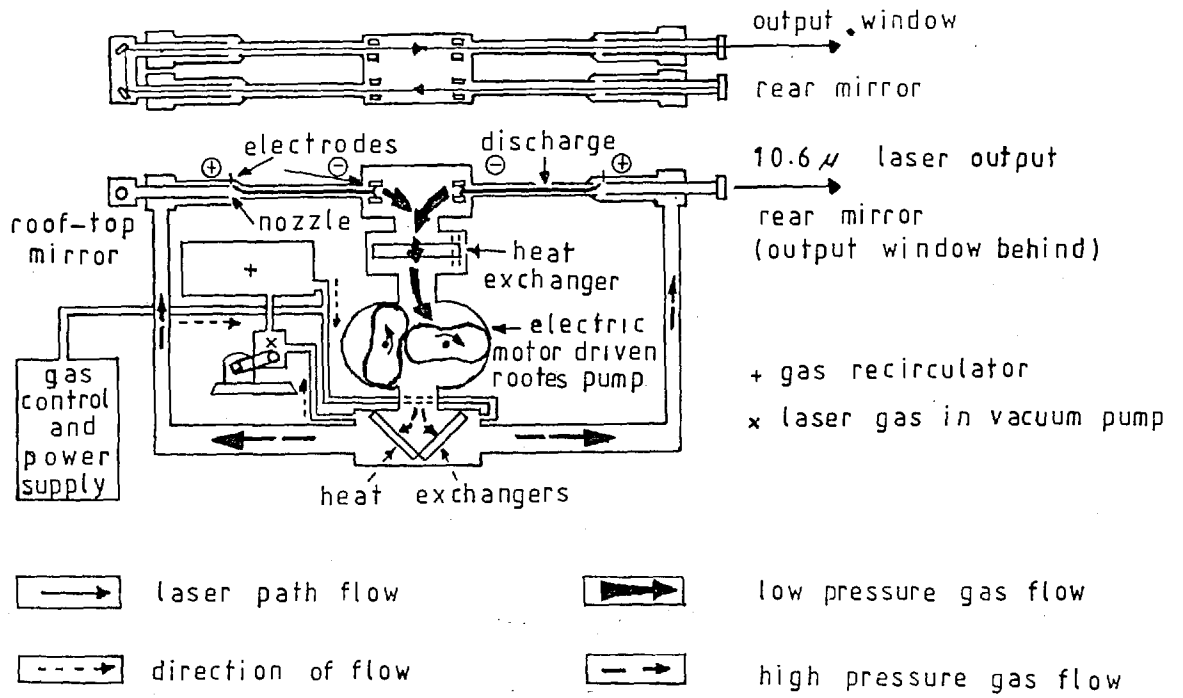


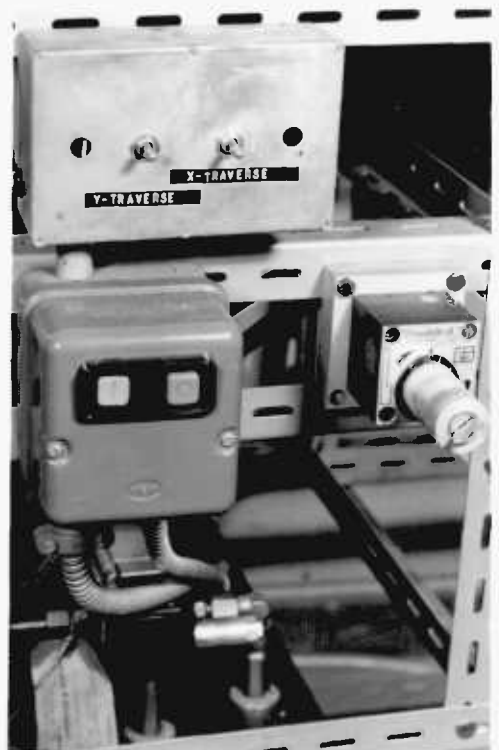
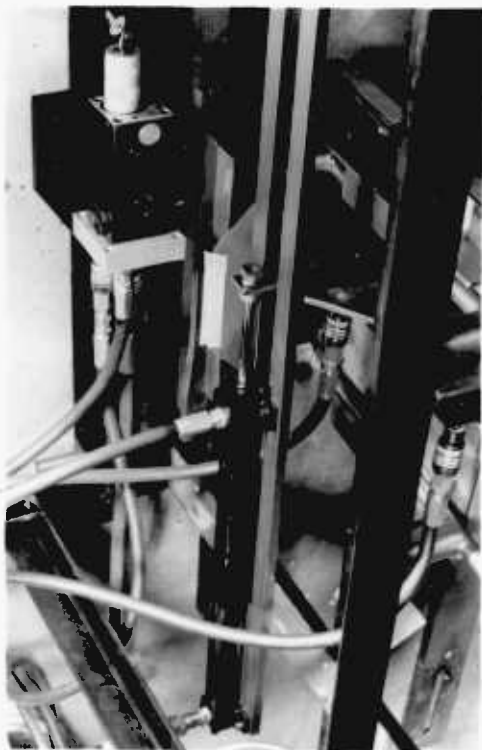
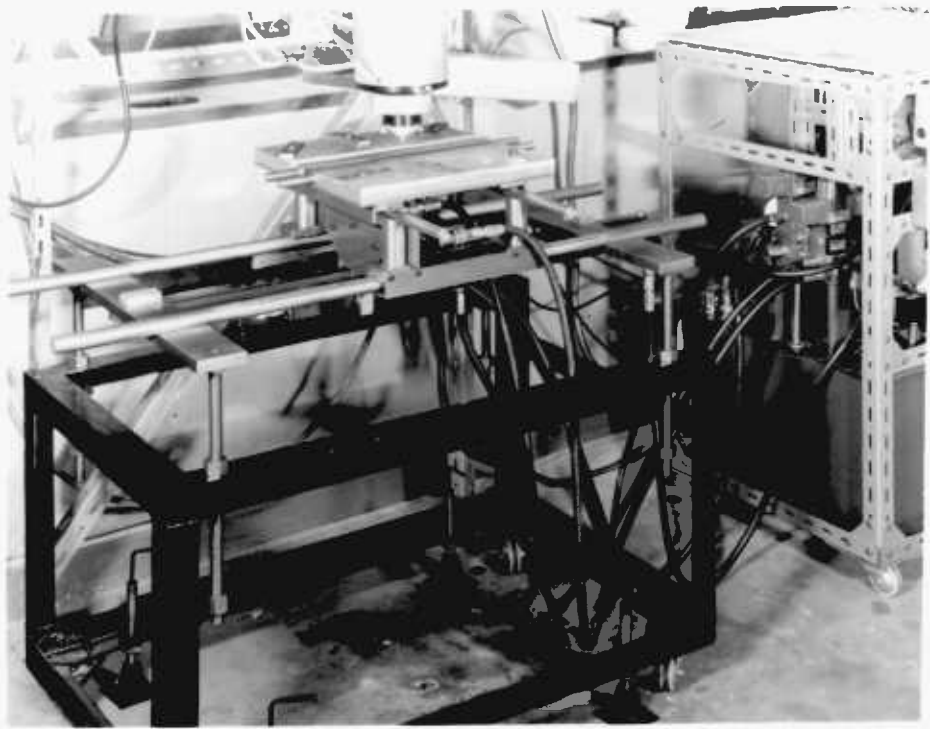
FIG 3.4 BOC 2Kw CO₂ LASER-GAS AND DISCHARGE PATHS.
(REF. 14)

MOVABLE X-Y TABLE

CYLINDER FOR ARRIVE IN X-DIRECTION (left)

SPEED CONTROLLER (right)

FIG 3.5 PHOTOGRAPH OF THE EQUIPMENT (HYDRAULIC X-Y TABLE)



CHAPTER 4

RESULTS

- 4 DESCRIPTION OF THE RESULT TRACK DEPOSITS
- 4.1 316 STAINLESS STEEL SURFACE CLADDING
 - 4.1.1 HEIGHT AND WIDTH - 316 STAINLESS STEEL
- 4.2 TIN-BRONZE SURFACE CLADDING
 - 4.2.1 HEIGHT AND WIDTH-TIN-BRONZE
- 4.3 MONEL SURFACE CLADDING
 - 4.3.1 HEIGHT AND WIDTH-MONEL
- 4.4 DEVELOPED SURFACE CLADDING
- 4.5 QUANTITATIVE DILUTION
 - 4.5.1 316 STAINLESS STEEL-DILUTION IN SURFACE CLADDING
 - 4.5.2 TIN-BRONZE-DILUTION IN SURFACE CLADDING
- 4.6.1 DEPOSITION RATE FOR 316 STAINLESS STEEL
- 4.6.2 DEPOSITION RATE FOR TIN-BRONZE
- 4.7 SOLIDIFICATION IN TYPE 316 STAINLESS STEEL
SURFACE CLADDING
- 4.8 METALLOGRAPHIC OBSERVATIONS
 - 4.8.1 316 STAINLESS STEEL SURFACE CLADDING
 - 4.8.2 MICROSTRUCTURES IN THE HEAT-AFFECTED ZONE
SUBSTRATE
- 4.9 SURFACE CLADDING COMPOSITION
- 4.10 RESULTANT HARDNESS IN THE CLAD LAYER
 - 4.10.1 RESULTANT HARDNESS IN 316 STAINLESS STEEL
CLADDING
 - 4.10.2 RESULTANT HARDNESS IN THE HEAT-AFFECTED ZONE SUBSTRATE

- 4.10.3 RESULTANT HARDNESS ON SELECTED SPECIMENS
 - 316 STAINLESS STEEL SURFACE CLADDING
- 4.11 RESULTANT SURFACE CLADDING ON MULTIPLE RUN DEPOSITS
- 4.12 METALLOGRAPHIC OBSERVATION ON MULTIPLE RUNS
 - 4.11.1 316 STAINLESS STEEL SURFACE CLADDING
 - 4.12.2 HEAT-AFFECTED ZONE SUBSTRATE
- 4.13 WETTING AND SPREADING OF MOLTEN CLADDING ALLOY ON A BASE METAL
- 4.14 VISCOSITY IN SURFACE CLADDING
- 4.15 MECHANICAL PROPERTIES IN SURFACE CLADDING
 - 4.15.1 BEND TEST
 - 4.15.2 SHEAR TEST

4. Description of the Resultant Track Deposits

To produce continuous single tracks some melting of the base metal must take place in order to aid wetting of the substrate by the cladding alloy.

The less melting that occurs the less will be the resultant dilution.

It was found that the continuity and overall structure of the deposit was dependent on the specific energy applied (P/DV , J/mm^2). At high values of the Specific Energy considerable penetration of the base metal occurred giving high levels of dilution, flat or semi-flat bead profile (akin to a bead on plate weld). The whole event being relatively wide with a large heat affected-zone (HAZ) in the substrate.

At intermediate values of the specific energy a semi-circular trace having good adhesion and low dilution was created. The contact angle between the base plate and the cladding increased with decrease in specific energy.

At low values of the specific energy a discontinuous trace was produced with a minimal heat affected zone.

4.1 316 Stainless Steel Surface Cladding

The range of values of the specific energy for the three types of track just described were a function of the powder bed thickness as described in the table 4.1. The operating conditions for all specimens are described in Appendix 1.1

TABLE 4.1 QUALITY OF TRACKS FORM 316 STAINLESS STEEL

RESULTANT TRACKS	BED DEPTH (mm)	SPECIFIC ENERGY RANGE, $S \text{ J/mm}^2$	SPECIMEN NUMBERS (see Appendix 1.1)
DEEP PENETRATION TRACKS	1.00	$P/DV > 44.0 \pm 8.0$	S1, S4, S8, S62, S113 S114, S122, S126
	0.50	$P/DV > 35.0 \pm 8.0$	S36, S41, S45, S85, S88, S97, S131, S133 & Fig 4.1
	0.25	$P/DV > 20.0 \pm 8.0$	S14, S48-S50, S53 S54, S57, S98, S113 S106, S142, S146
GOOD TRACKS	1.00	$44.0 \pm 8.0 > P/DV > 14.0 \pm 5.0$	S5, S6, S9, S10-S13, S20 S59, S60, S63, S65, S66, S67-S72, S116 - S124 & Fig 4.2
	0.50	$35.0 \pm 8.0 > P/DV > 11.0 \pm 5.0$	S26-S34, S37, S38, S42, S75-S78, S80-S83, S134- S139
	0.25	$20.0 \pm 8.0 > P/DV > 10.0 \pm 5.0$	S15-S19
DISCONTINUOUS TRACKS	1.00	$P/DV < 14.0 \pm 5.0$	S2, S3, S7, S21, S61 S64, S66, S67, S111, S112 S115, S121, S127, S128, S129
	0.50	$P/DV < 11.0 \pm 5.0$	S35, S39, S40, S43, S44 S46, S47, S73, S74, S84, S86, S87, S89, S90-S96, S108, S109, S110, S130, S132, S140, S141 & Fig 4.1
	0.25	$P/DV < 10.0 \pm 5.0$	S22-S25, S51, S52, S55, S56 S58, S99, S100, S101, S102, S104, S105, S107, S108, S143, S144, S146, S147, S148



FIG 4.1 HIGH PENETRATION AND DISHOMOGENEOUS —
DEPOSITS; POWER=1 800 W; BEAM DIAMETER=
=7.2, 7.2 AND 5.8 MM; SPEED=5, 15 AND 5
MM/S; POWDER THICKNESS = 0.50 MM.

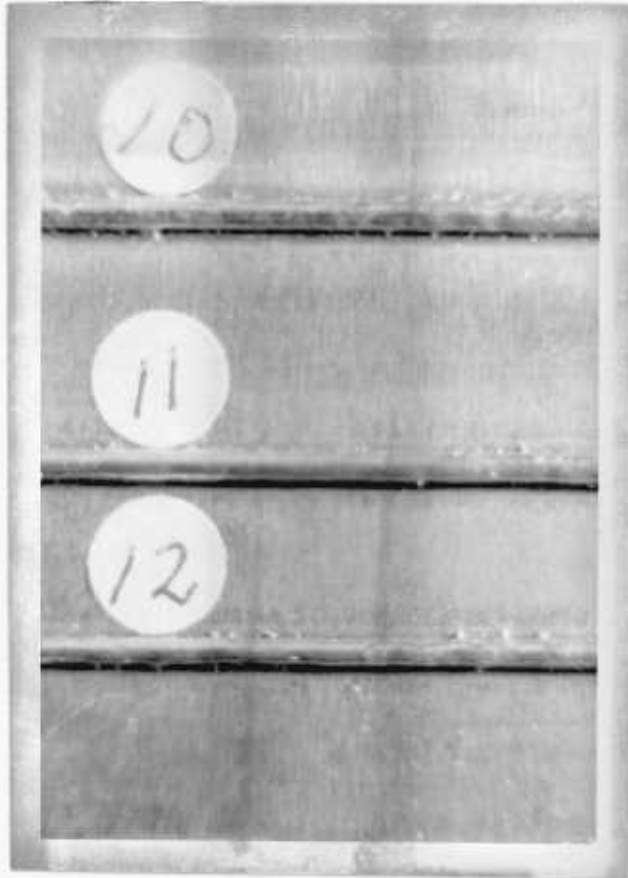


FIG 4.2 HOMOGENEOUS DEPOSITS, POWER=1 600 W;
BEAM DIAMETER=4.3 MM; SPEED =15, 20, —
AND 25 MM/S; POWDER THICKNESS=1.00 MM.

4.1.1 Height and Width of Tracks - 316 Stainless Steel

The resultant height and width of a track were found to be dependent on both specific energy and initial bed depth as shown in graph 4.3 - 4.8, and a plot of deposit ratio vs specific energy is shown in graphs 4.9 - 4.11. Likewise the heat affected zone depended on both specific energy and bed depth. Graphs 4.12 - 4.14

By selecting samples of equal laser power and beam diameter (e.g S4 - S7, S8 - S13 etc) it is possible to see a trend in bead height and width with traverse speed in figs 4.15 - 4.20. It should be noticed that the permissible operating range of specific energy varies to bed depth as illustrated in fig 4.21.

It should be noted that the operating region for producing good tracks (as represented by the range in Specific Energy) is smaller with shallow beds, and very thick beds.

This introduces the idea of their being an optimum bed depth for laser cladding.

No porosity in the stainless steel track was noticed at the interface of tracks. The principal runs recorded in Appendix 1.1 were all pore free.

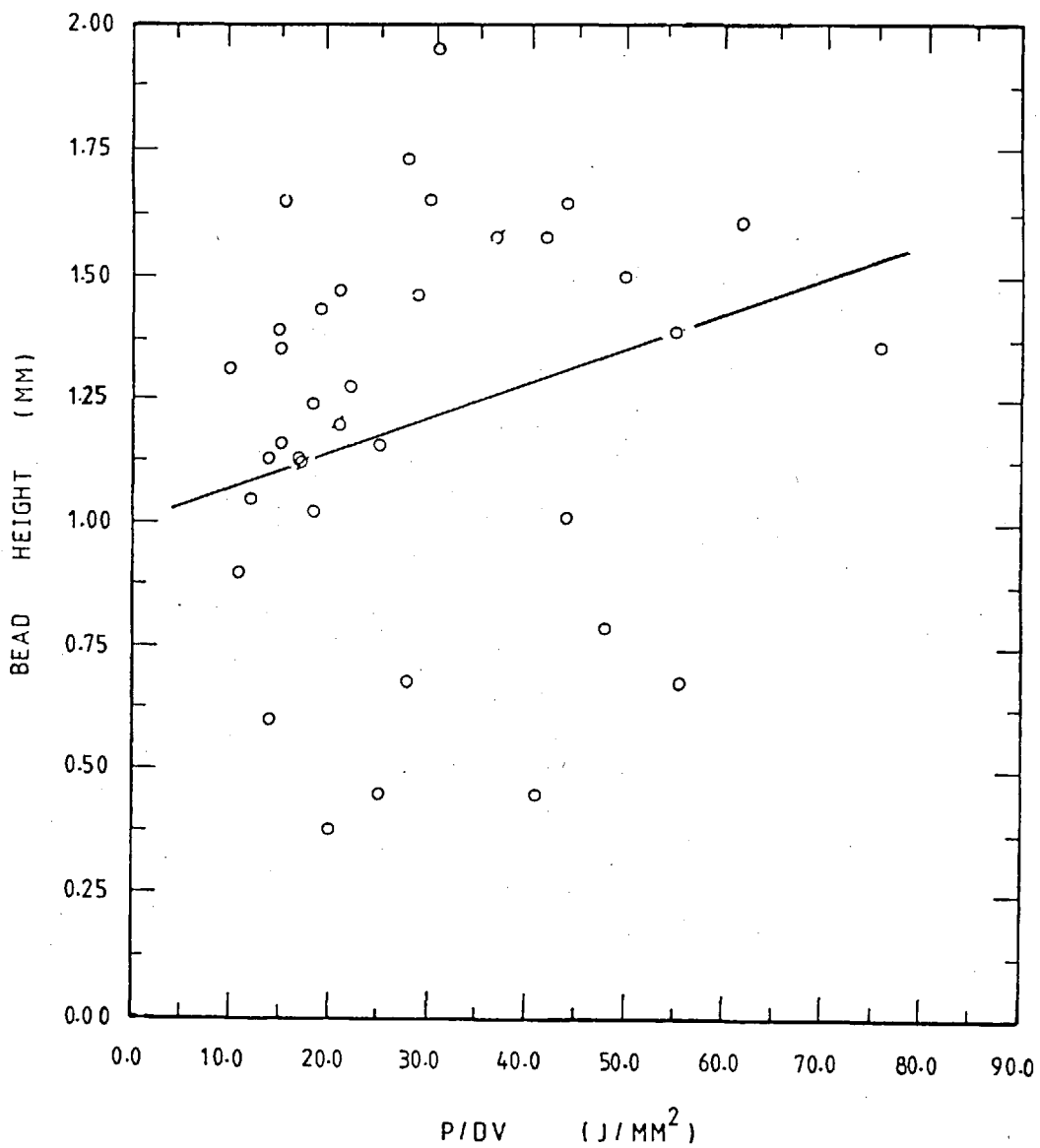


FIG 4.3 BEAD HEIGHT (MM) vs ENERGY/UNIT AREA, P/DV (J/MM²) FOR A 1.00 MM POWDER THICKNESS.

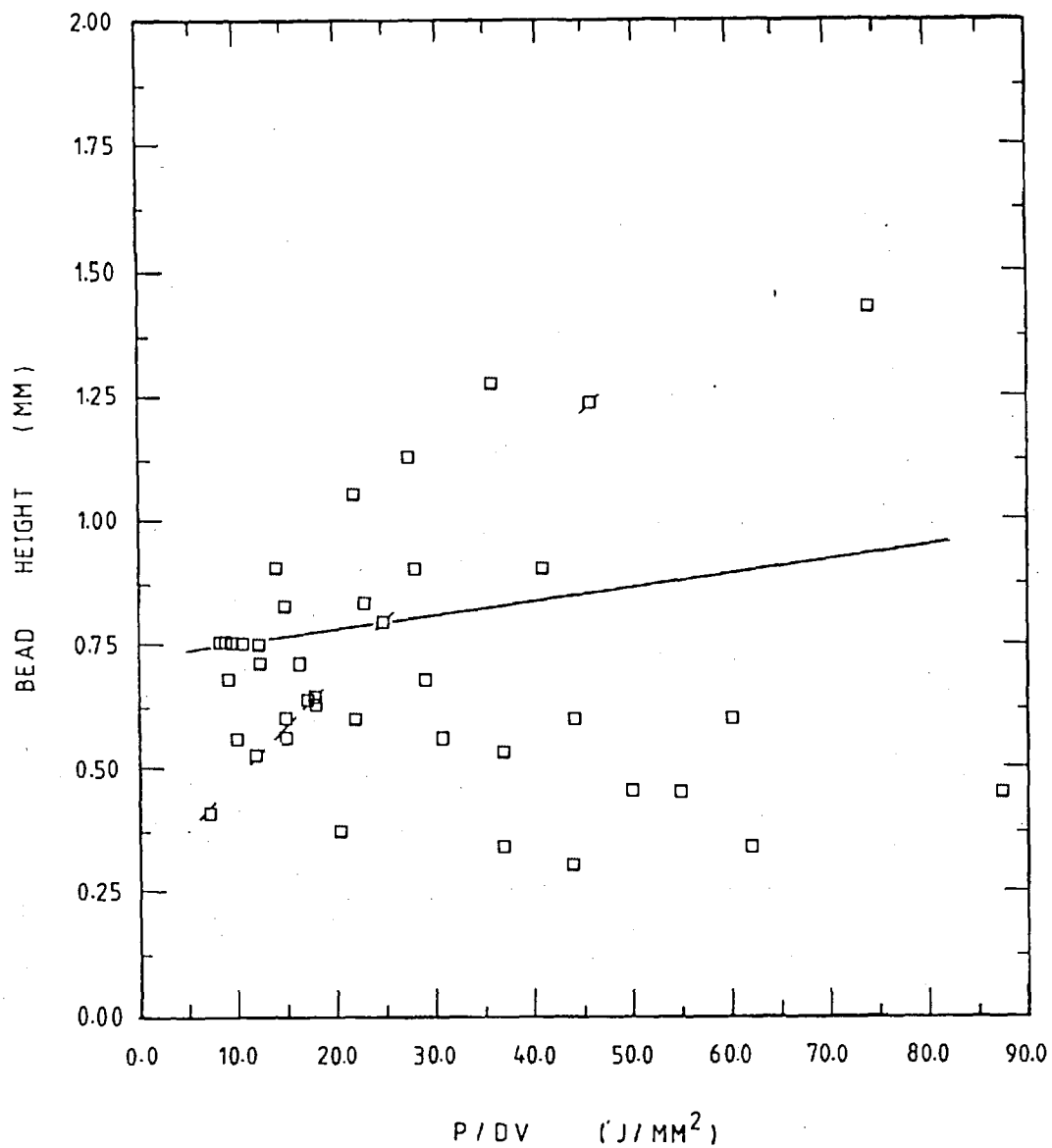


FIG 4.4 BEAD HEIGHT (MM) vs ENERGY/UNIT AREA, P/DV (J/MM²) FOR A 0.50 MM POWDER THICKNESS.

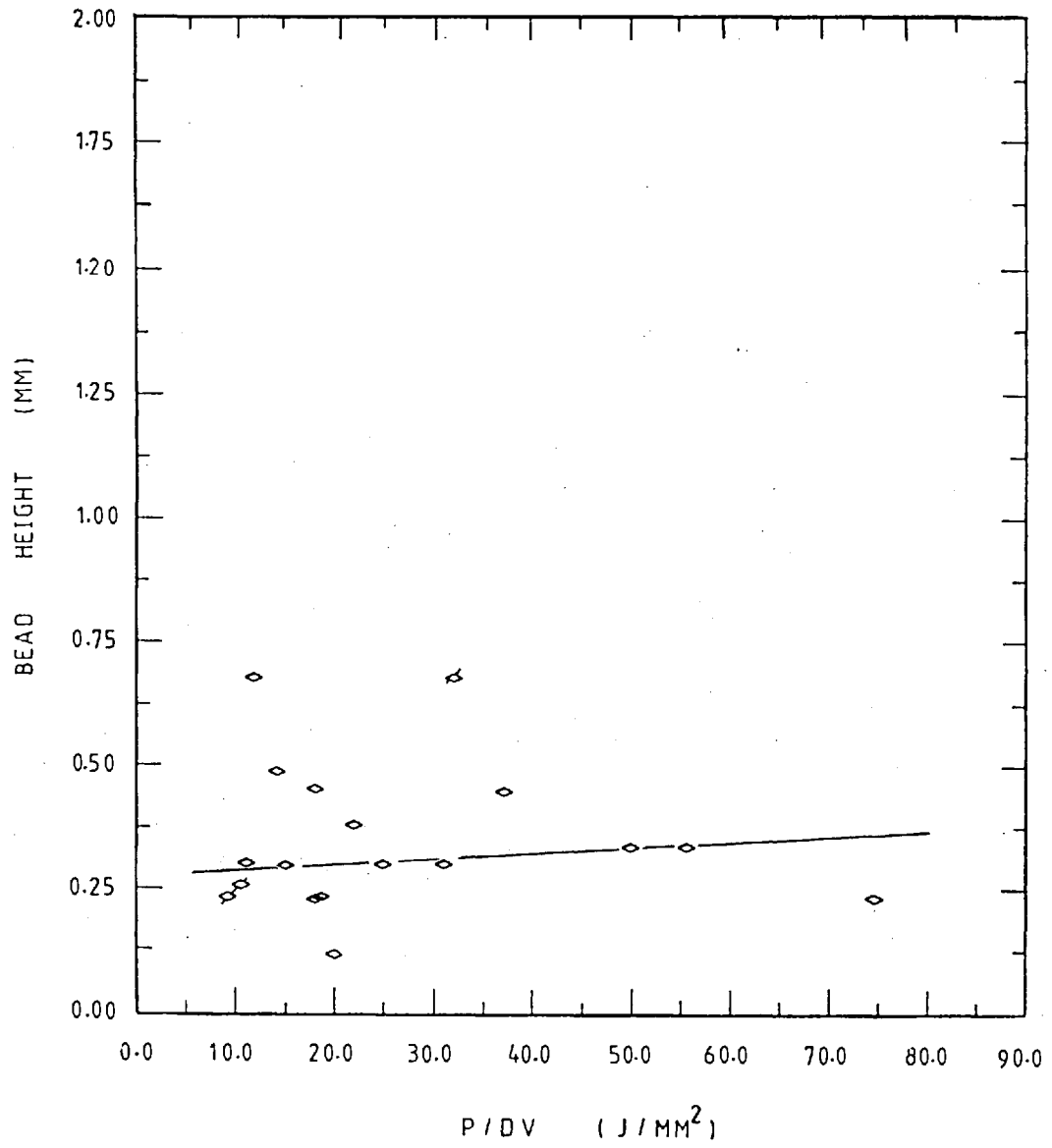


FIG 4.5 BEAD HEIGHT (MM) vs ENERGY/UNIT AREA, P/DV (J/MM²) FOR A 0.25 MM POWDER THICKNESS.

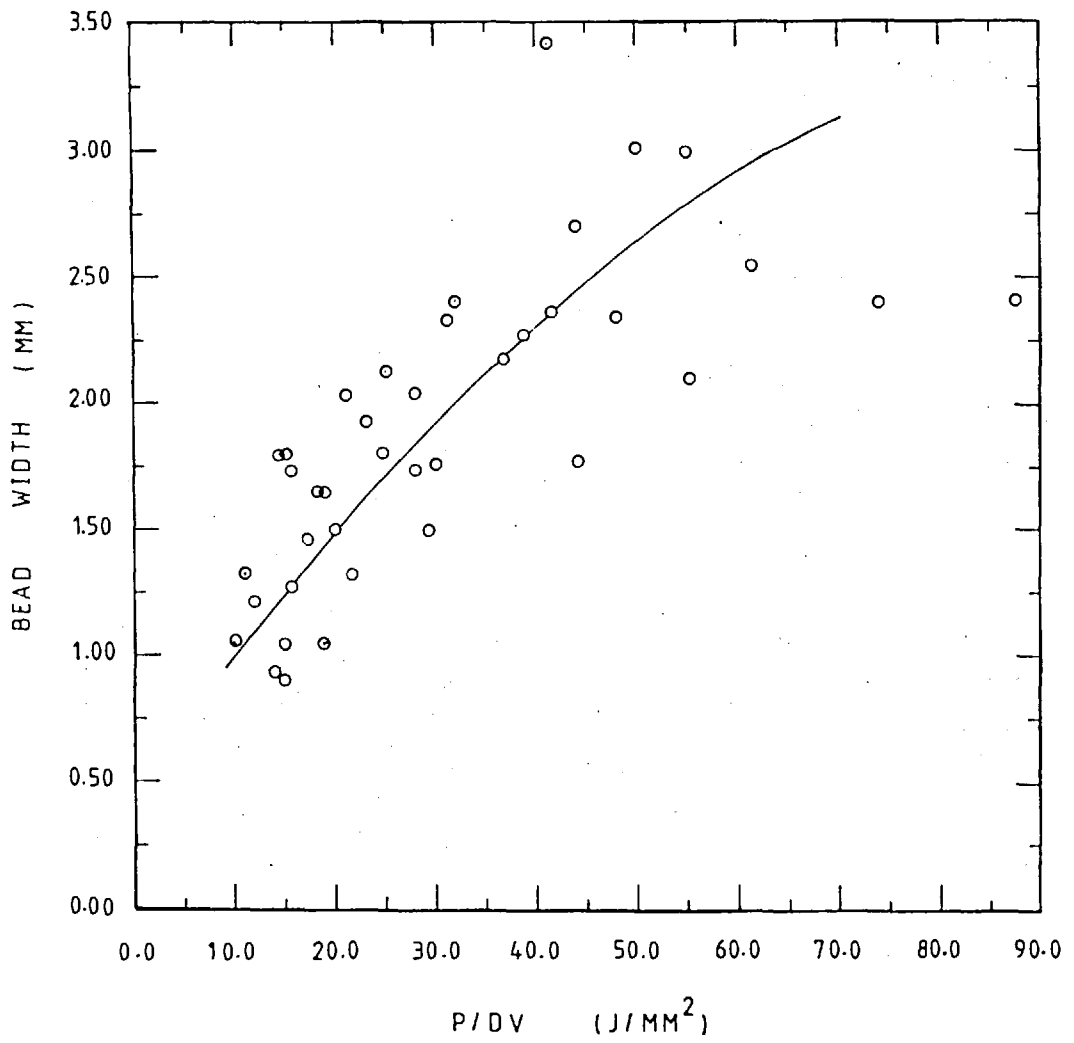


FIG 4.6 BEAD WIDTH (MM) vs ENERGY/UNIT AREA, P/DV (J/MM²) FOR A 1.00 MM POWDER THICKNESS.

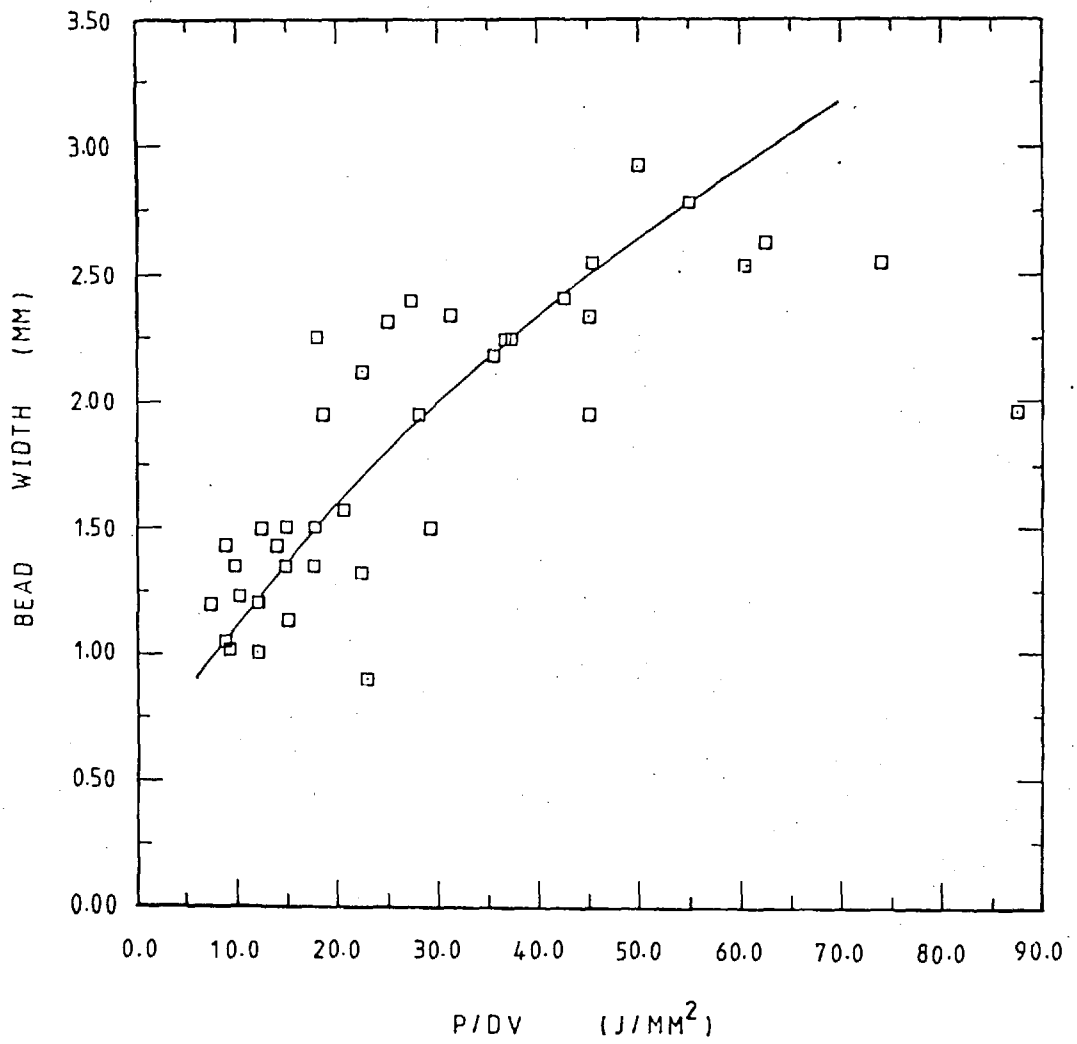


FIG 4.7 BEAD WIDTH (MM) vs ENERGY/UNIT AREA, P/DV (J/MM²) FOR A 0.50 MM POWDER THICKNESS.

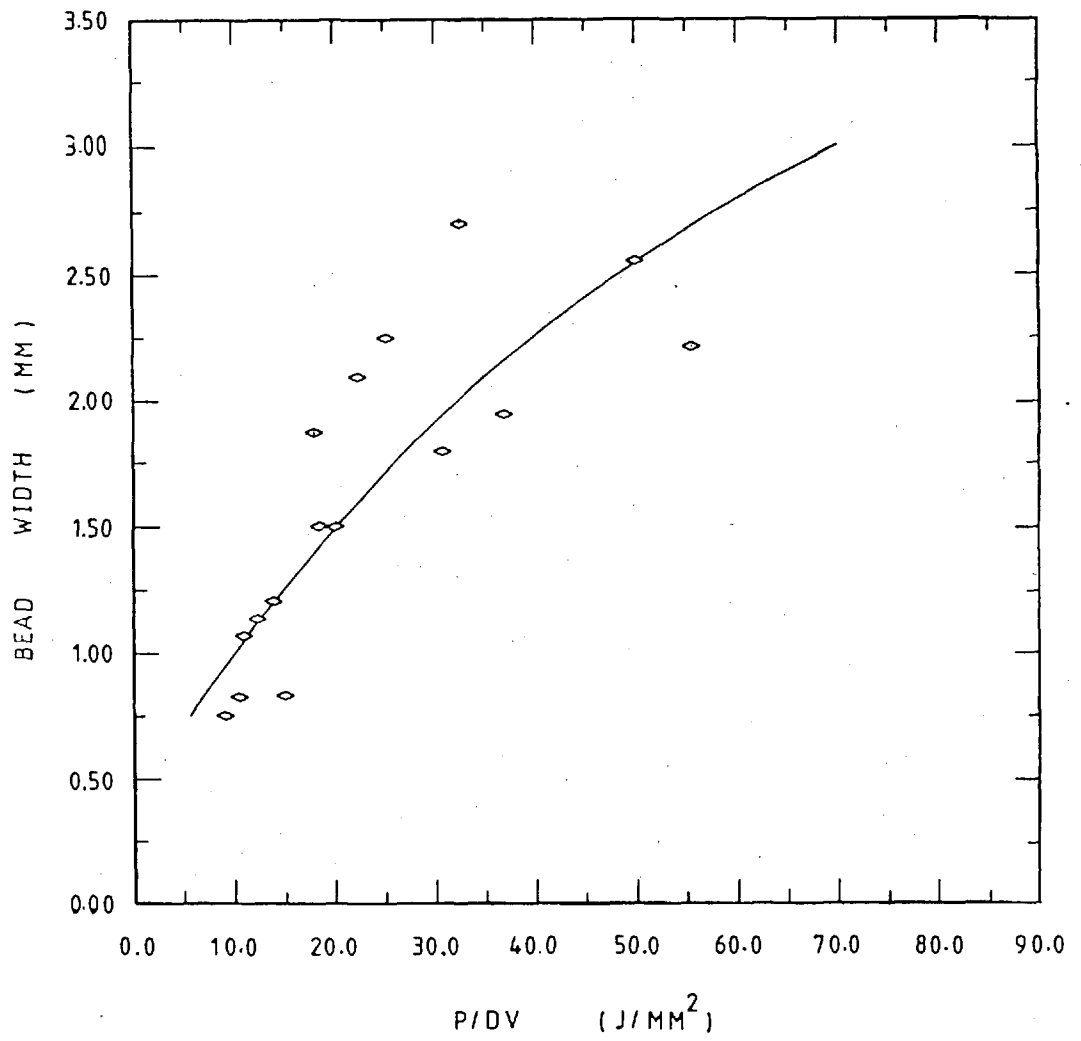


FIG 4.8 BEAD WIDTH (MM) vs ENERGY/UNIT AREA, P/DV (J/MM²) FOR A 0.25 MM POWDER THICKNESS.

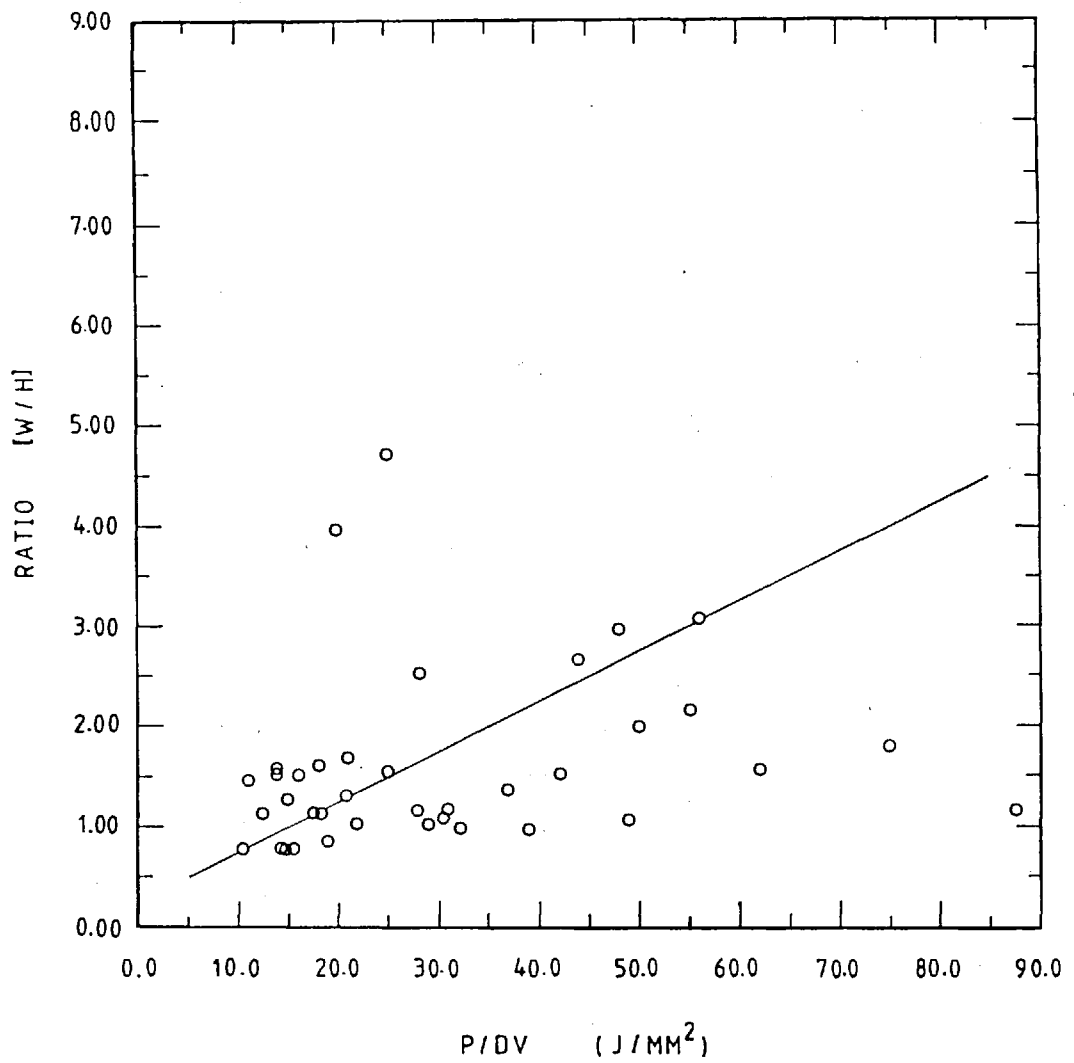


FIG 4.9 RATIO [W/H] vs ENERGY/UNIT AREA, P/DV (J/mm^2) FOR A 1.00 MM POWDER THICKNESS.

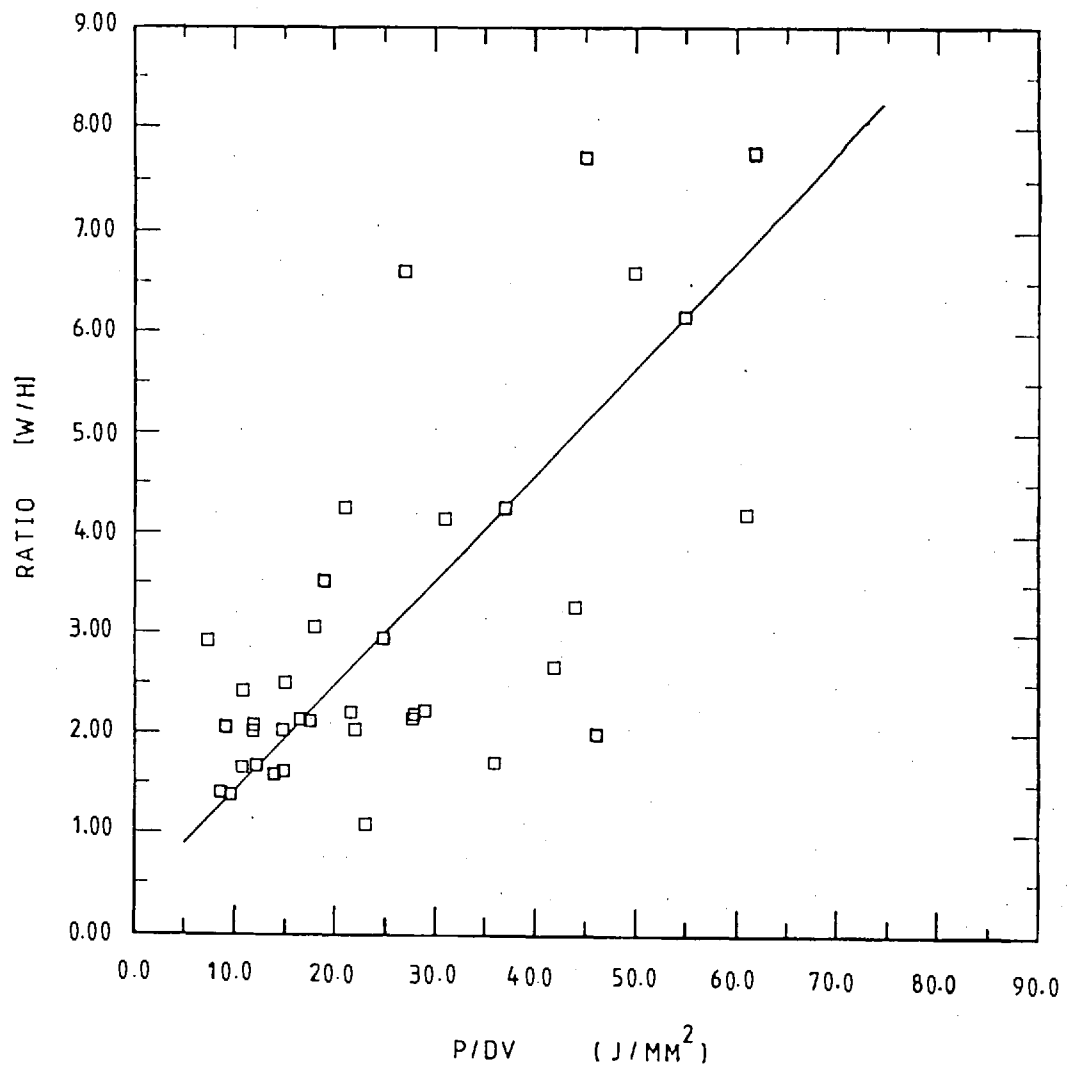


FIG 4.10 RATIO [W/H] vs ENERGY/UNIT AREA, P/DV (J/mm^2) FOR A 0.50 MM POWDER THICKNESS.

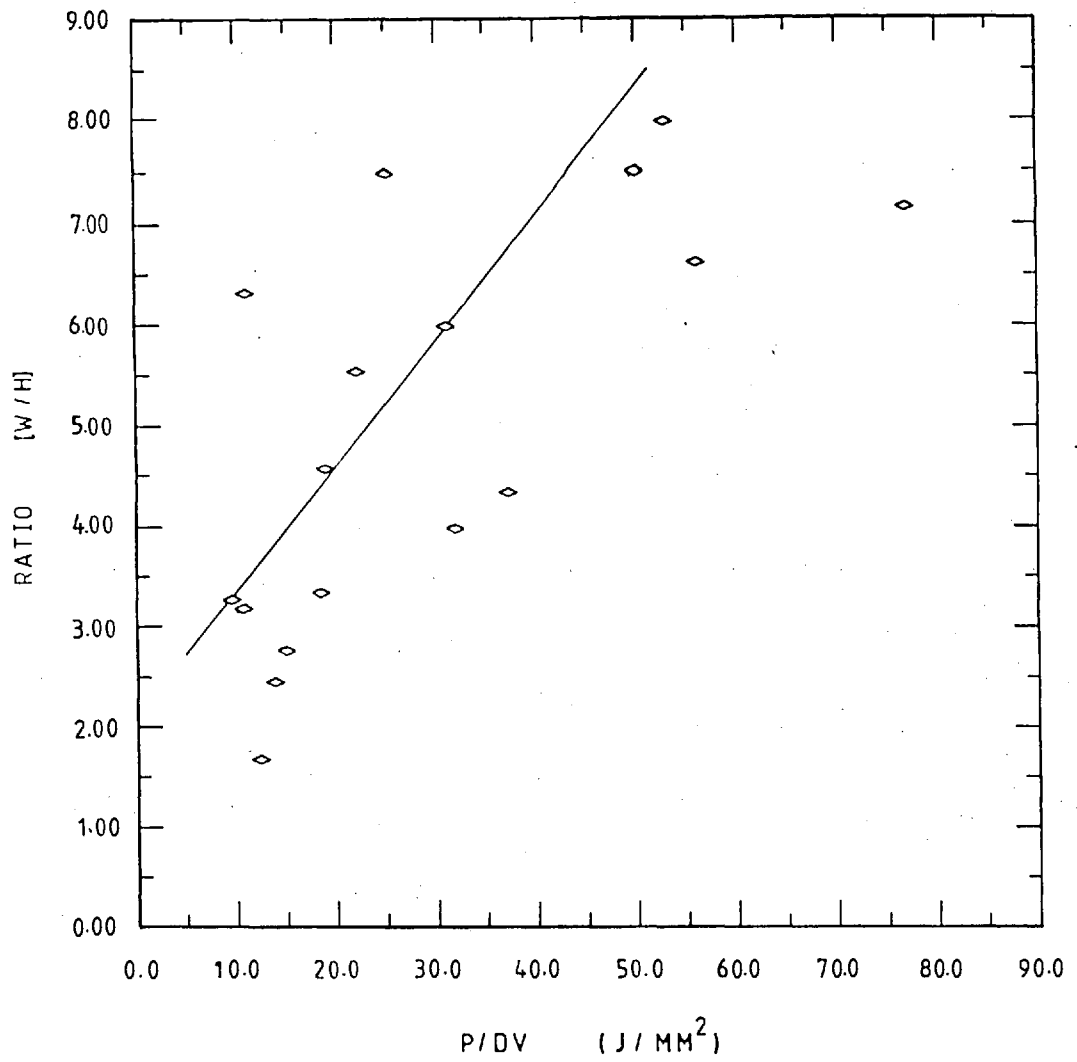


FIG 4.11 RATIO [W/H] vs ENERGY/UNIT AREA, P/DV (J/MM²) FOR A 0.25 MM POWDER THICKNESS.

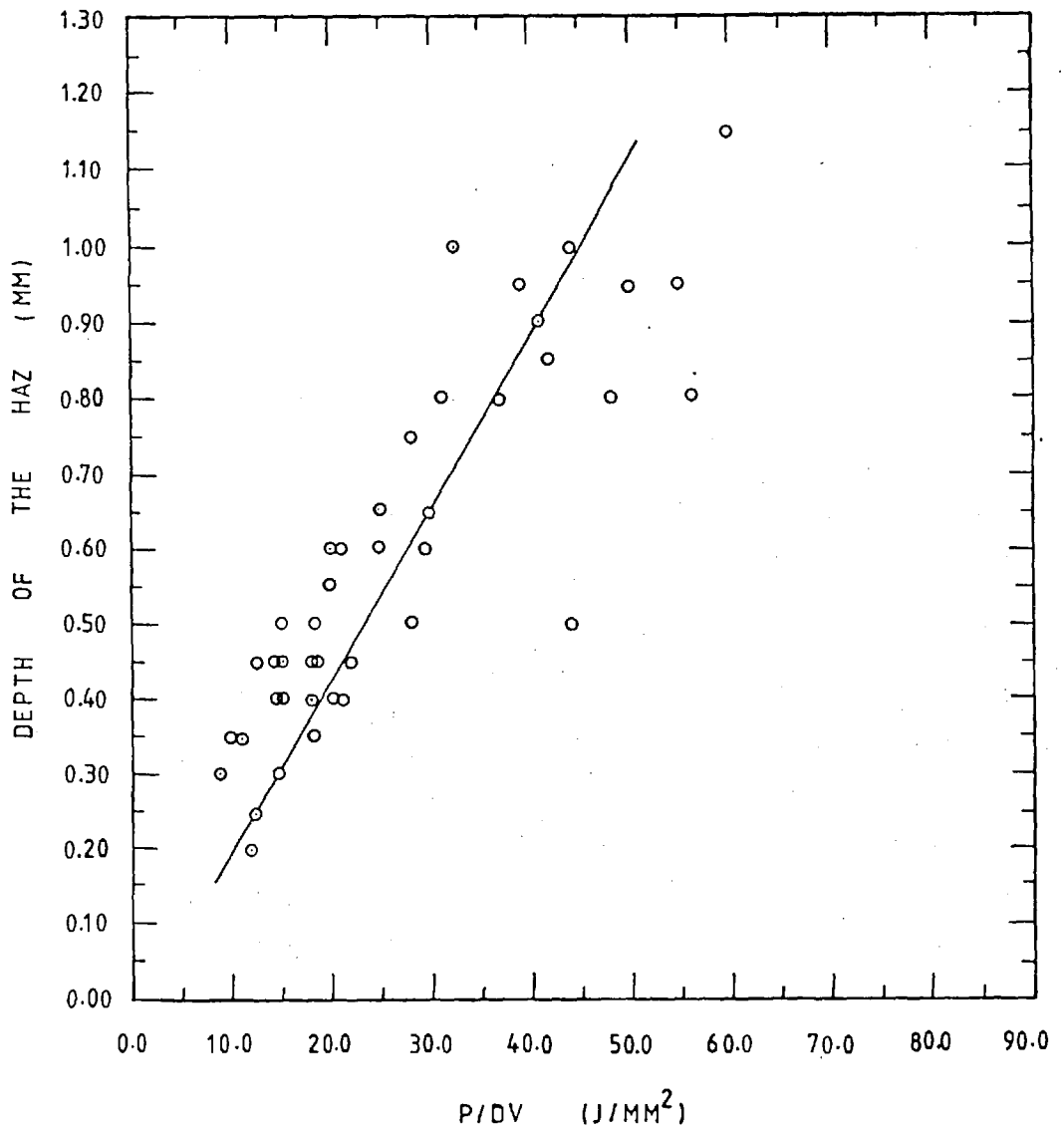


FIG 4.12 DEPTH OF THE HAZ (HEAT-AFFECTED ZONE), (MM) vs ENERGY/ UNIT AREA, P/DV (J/MM²) FOR A 1.00 MM POWDER THICKNESS.

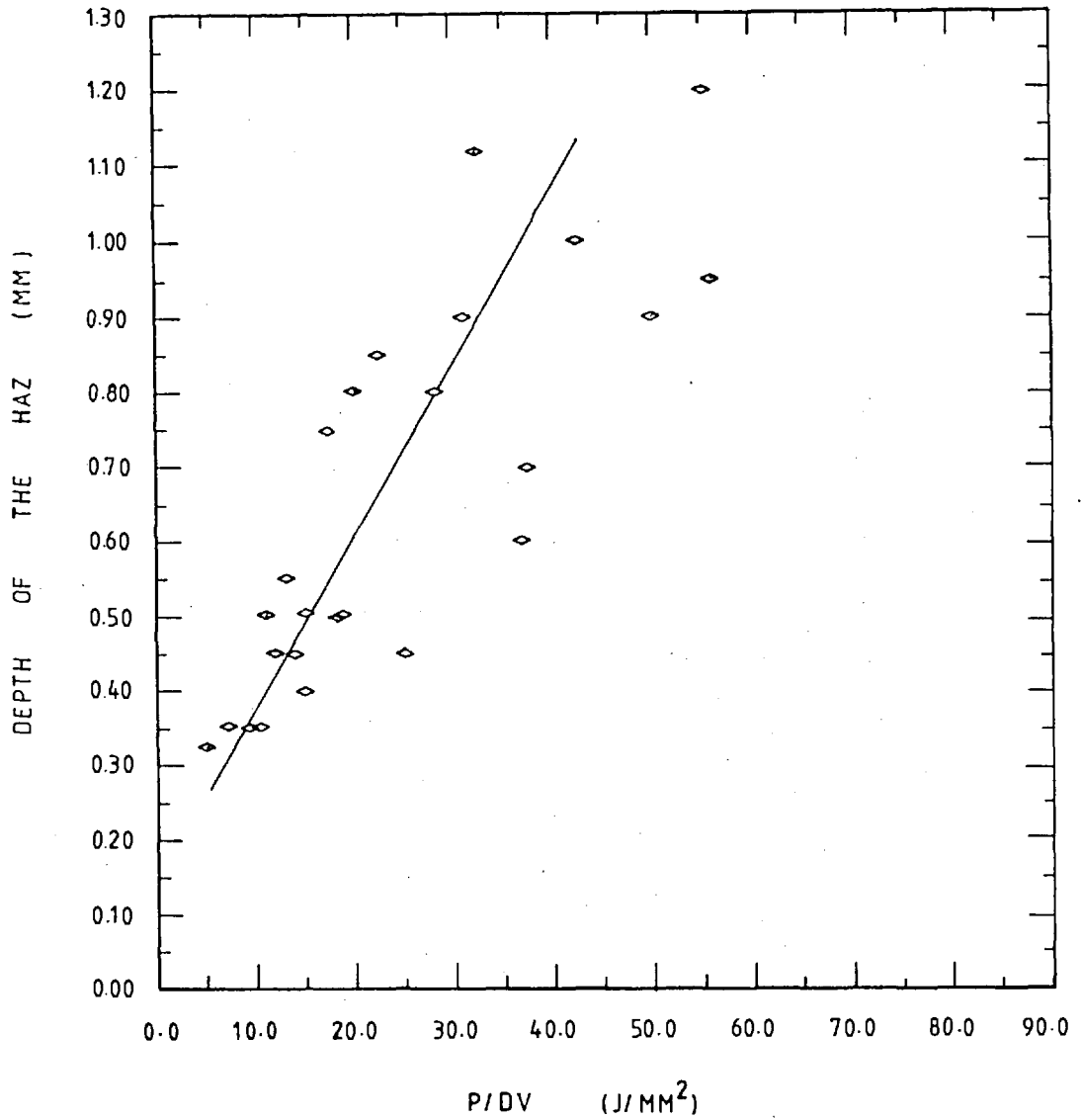


FIG 4.14 DEPTH OF THE HAZ (HEAT-AFFECTED ZONE), (MM) vs ENERGY/ UNIT AREA, P/DV (J/MM²) FOR A 0.25 MM POWDER THICKNESS.

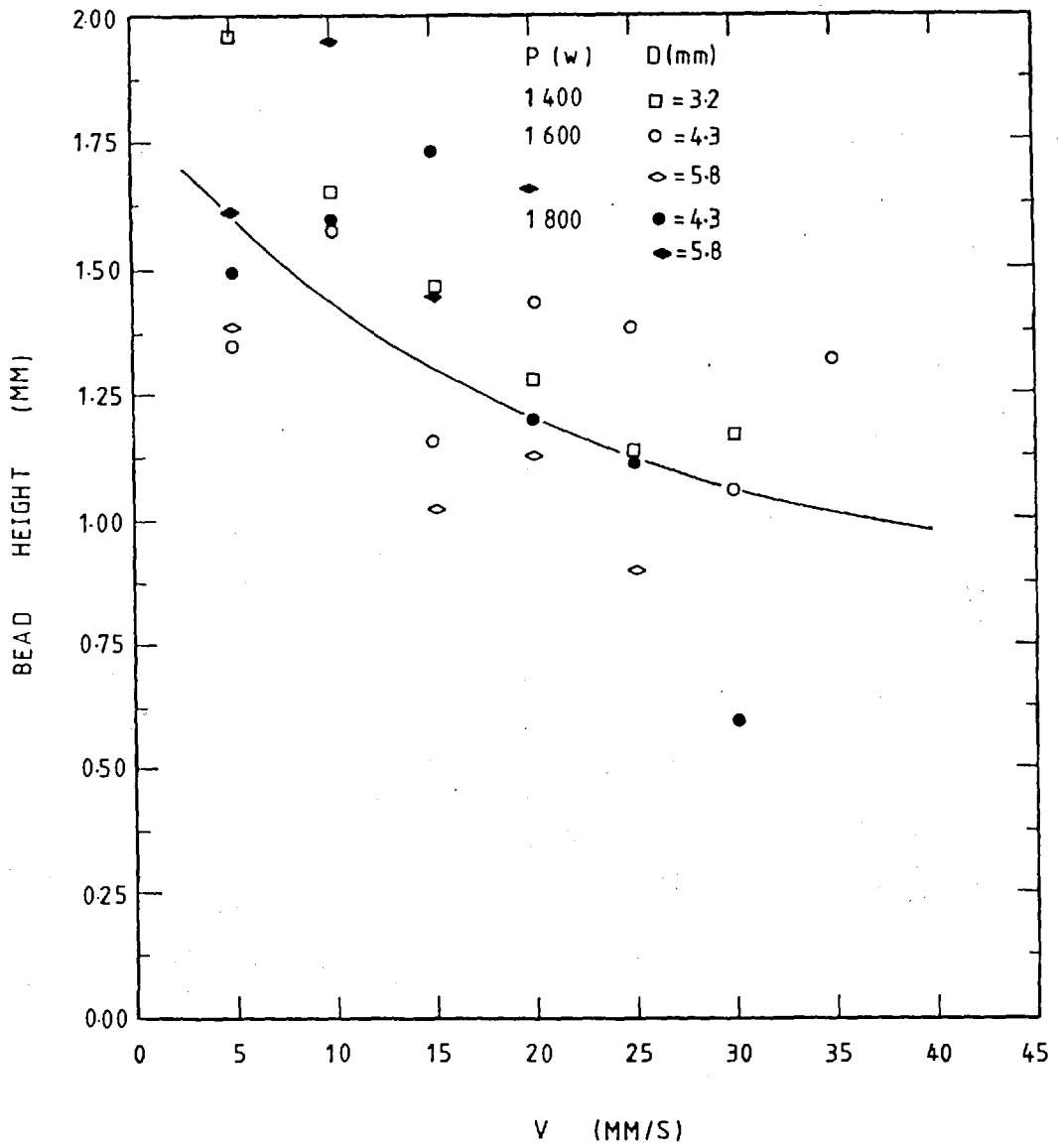


FIG 4.15 BEAD HEIGHT (MM) vs TRAVERSE SPEED (MM/S) FOR A 1.00 MM POWDER THICKNESS.

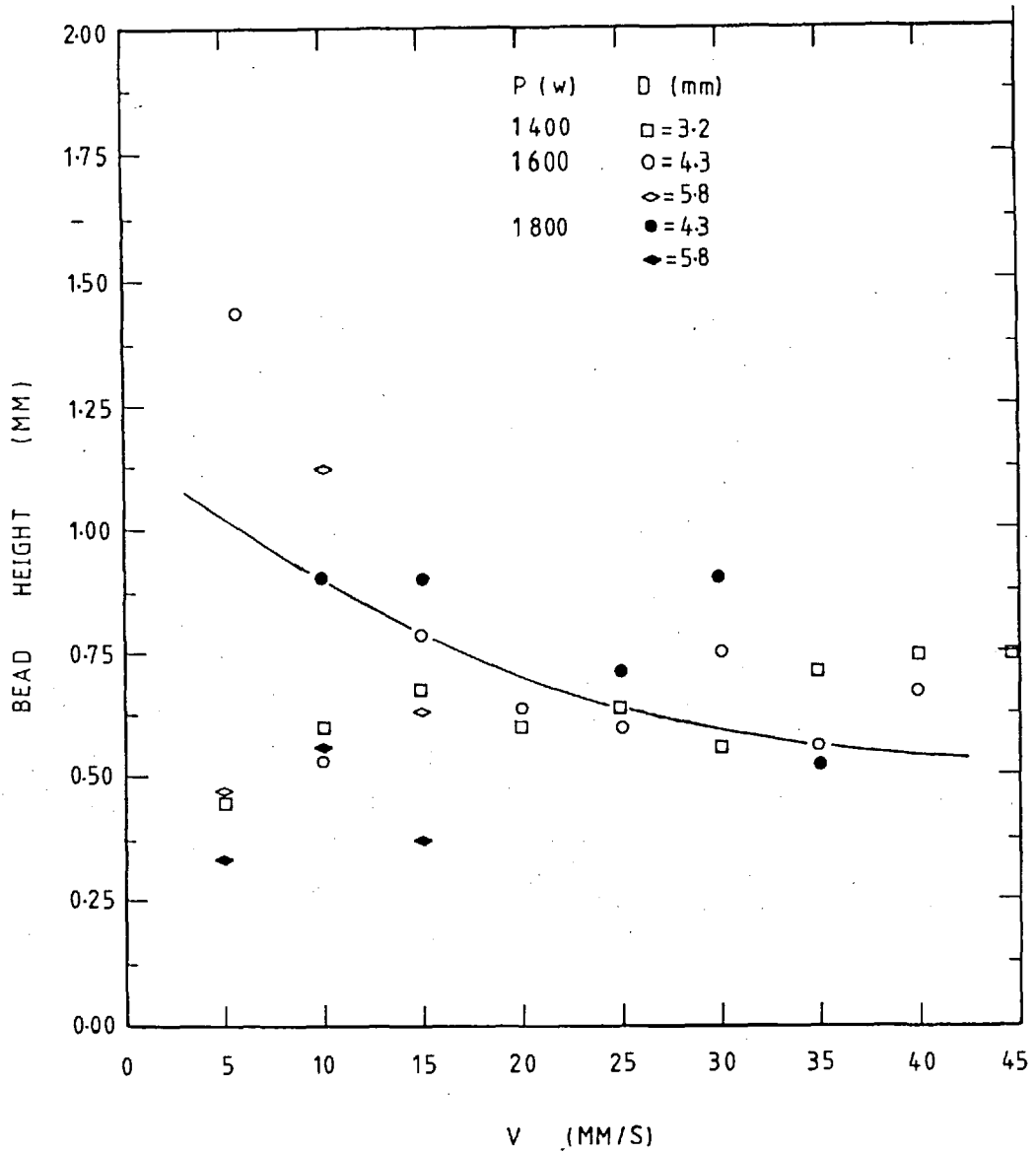


FIG 4.16 BEAD HEIGHT (MM) vs TRAVERSE SPEED (MM/S) FOR A 0.50 MM POWDER THICKNESS.

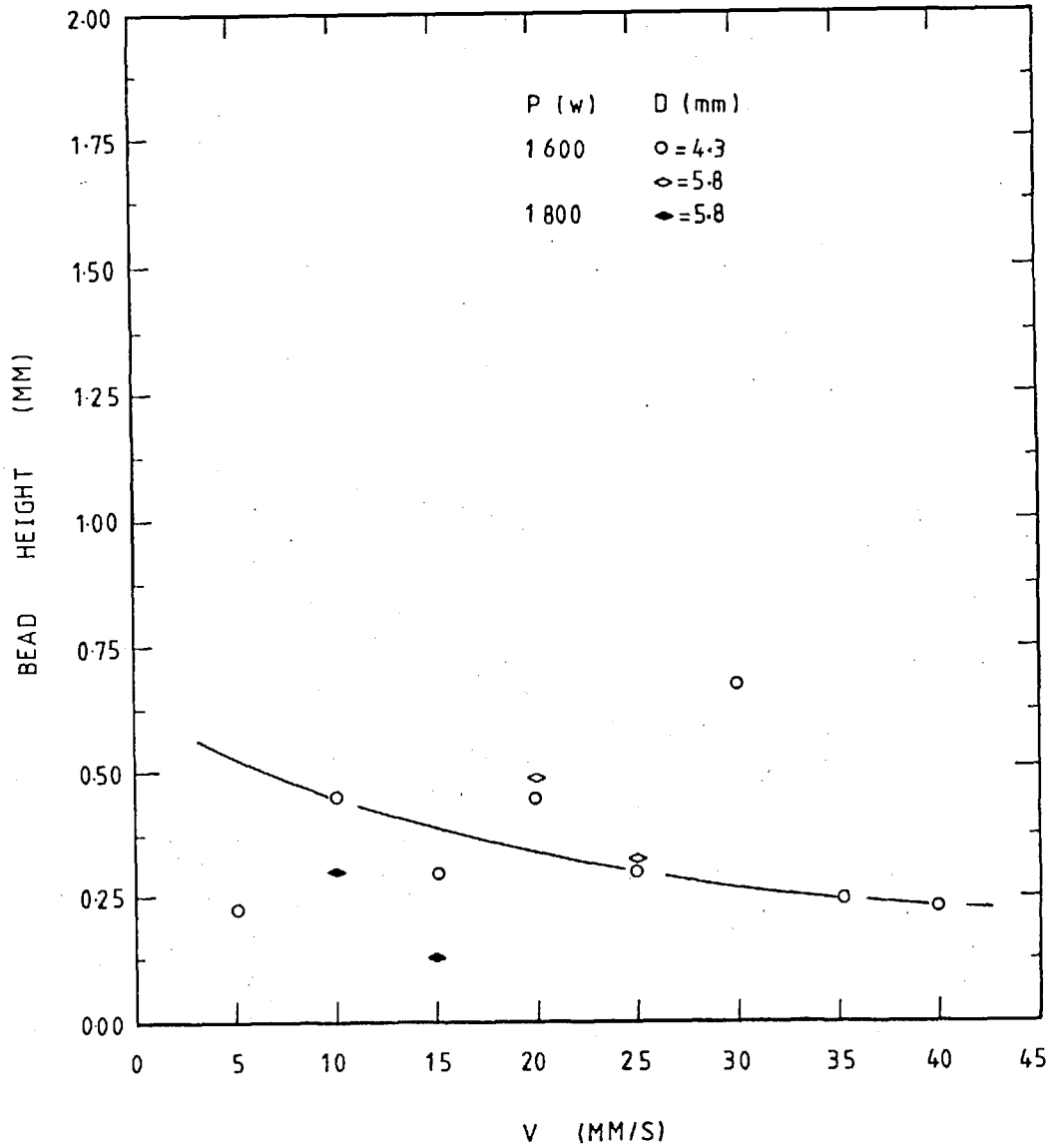


FIG 4.17 BEAD HEIGHT (MM) vs TRAVERSE SPEED (MM/S) FOR A 0.25 MM POWDER THICKNESS.

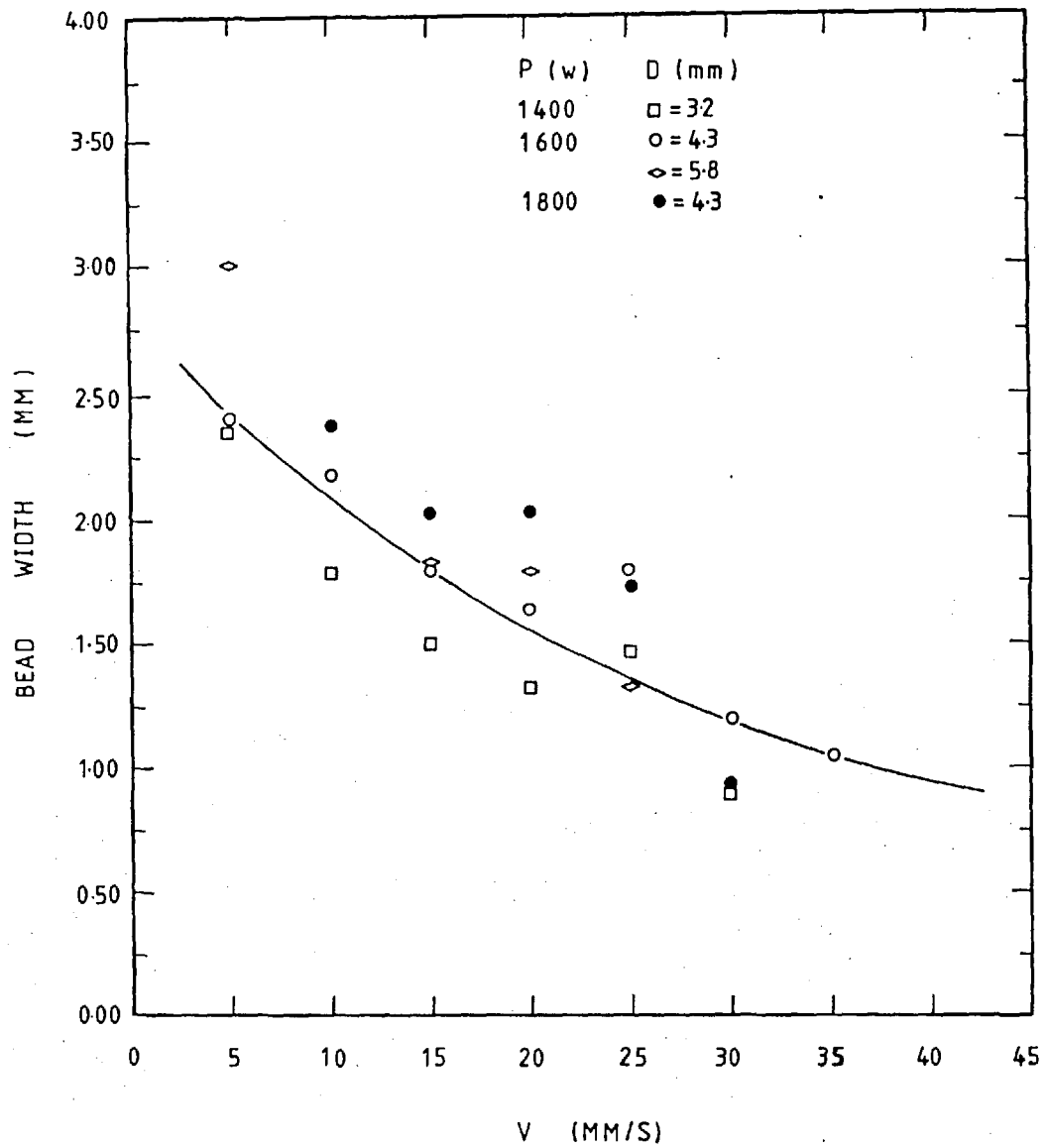


FIG 4.18 BEAD WIDTH (MM) vs TRAVERSE SPEED (MM/S) FOR A 1.00 MM POWDER THICKNESS.

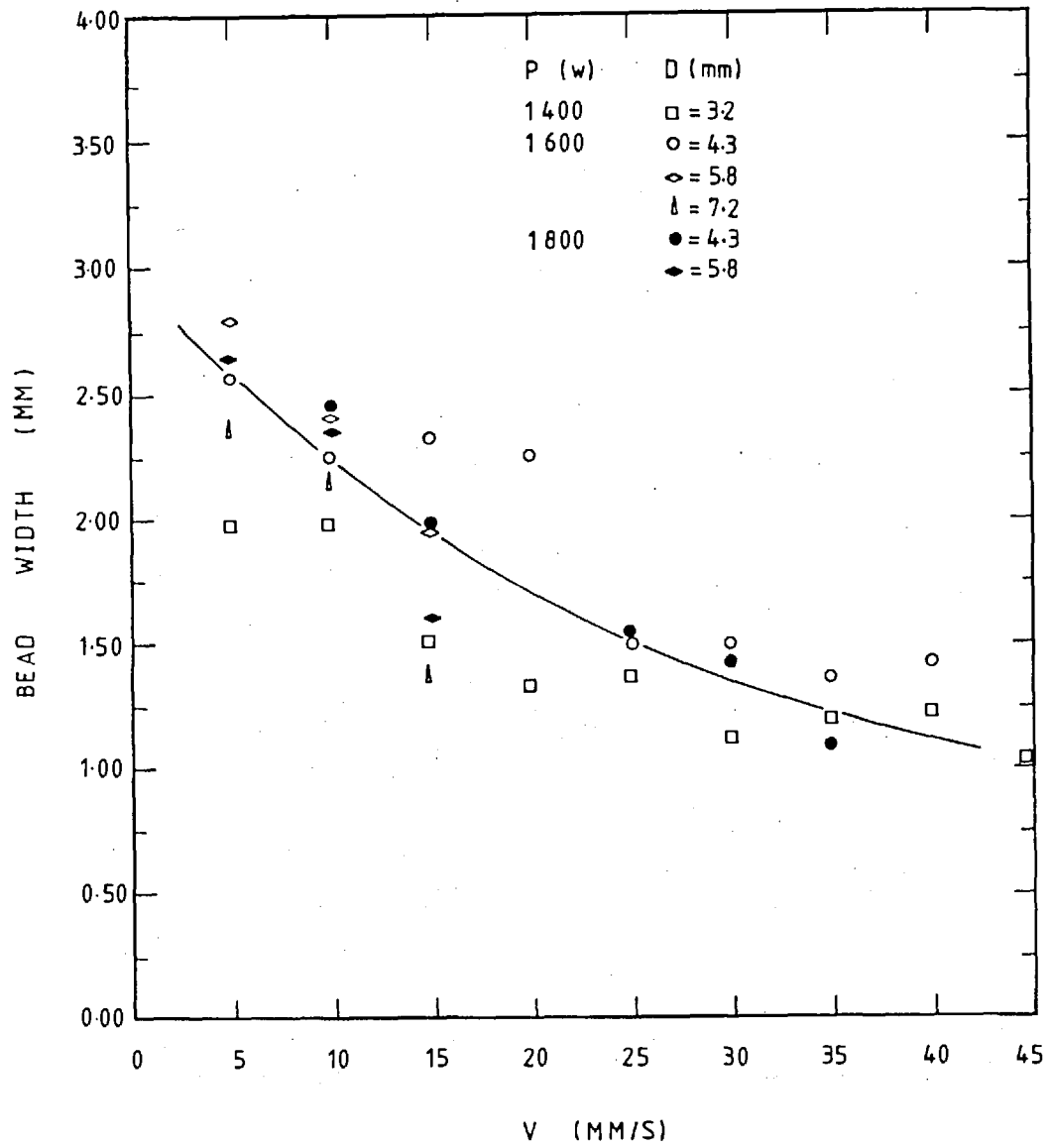


FIG 4.19 BEAD WIDTH (MM) vs TRAVERSE SPEED (MM/S) FOR A 0.50 MM POWDER THICKNESS.

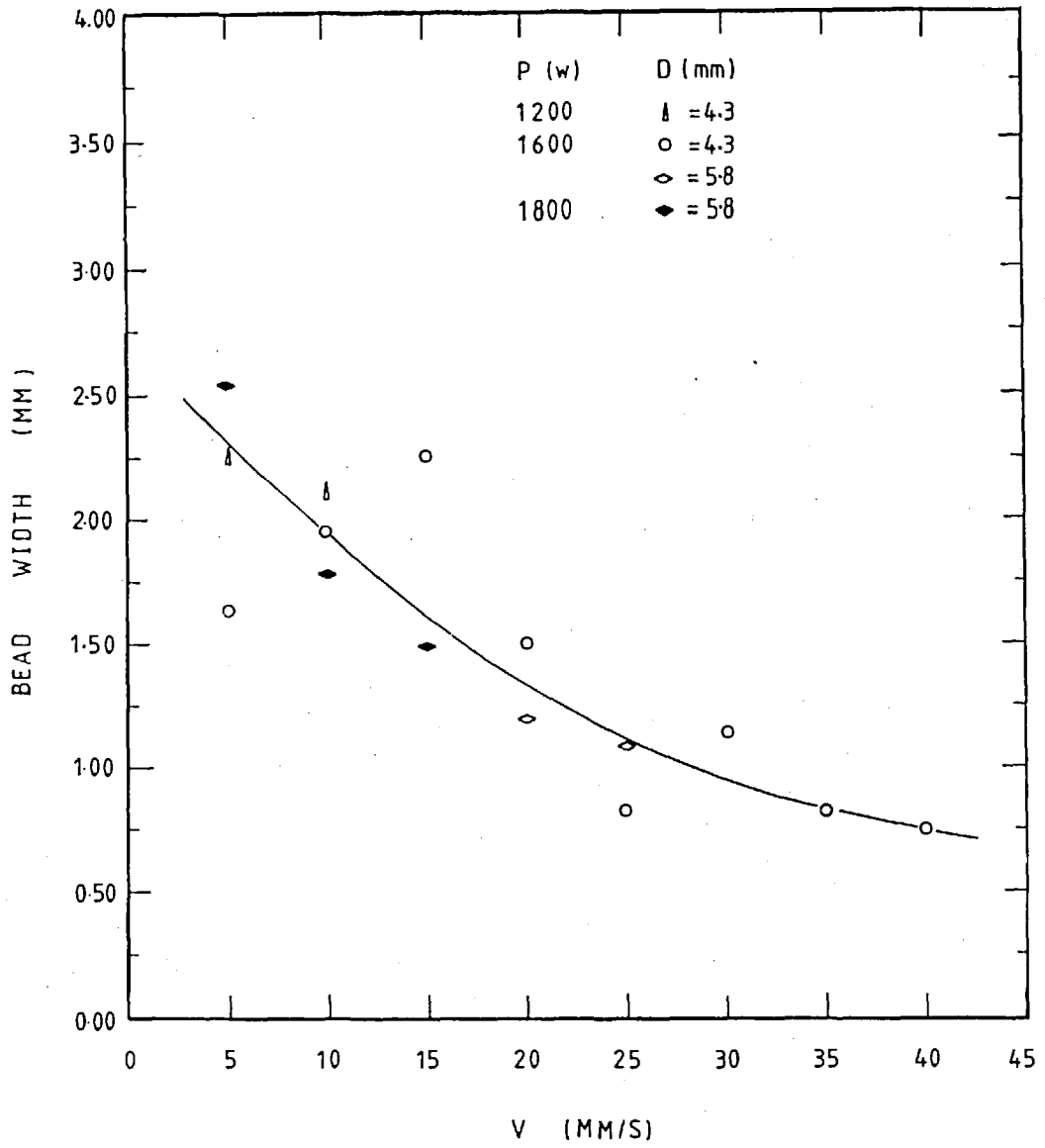


FIG 4.20 BEAD WIDTH (MM) vs TRAVERSE SPEED (MM/S) FOR A 0.25 MM POWDER THICKNESS.

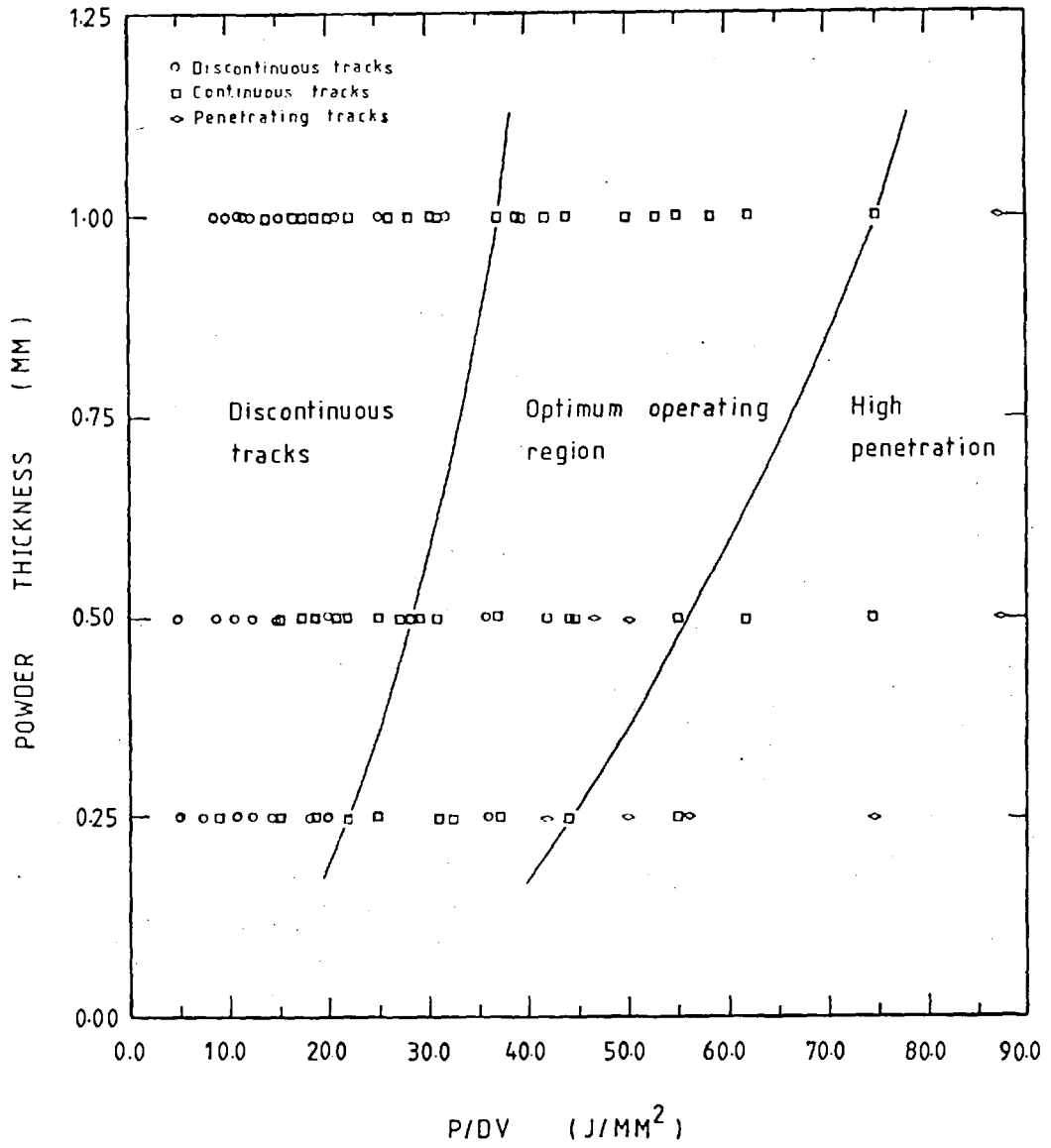


FIG 4.21 POWDER THICKNESS (MM) vs ENERGY/UNIT AREA, P/DV (J/MM²) FOR 316 STAINLESS STEEL.

4.2 Tin Bronze Surface Cladding

Tin bronze has a lower melting point than stainless steel and a different affinity for the base plate mild steel.

The runs were made with only a 1.00mm powder bed depth and these showed the same trends in overall structure observed with the stainless steel. In an attempt to vary the surface wettability runs were made with a bed of only tin bronze powder, a bed where the tin bronze was covered by a layer of boric acid (which is used as a flux in bronzing) and a bed where the boric acid is mixed with the powder. The results are summarized in table 4.2.

High values of specific energy were associated with some porosity in the clad trace.

"Good" traces had no noticeable porosity and ^{only a small} heat affected zone in the base metal, probably due to lower melting point.

4.2.1 Height and Width of Tracks - Tin Bronze

The effect of the boric acid was brighter and smoother tracks with slower traverse and similar with high traverses. The resultant tracks were smaller and wider as can be seen in graphs 4.24 and 4.25, where the track height and width are plotted v.s specific energy and a plot of deposit ratio vs specific energy is shown in graph 4.26.

Likewise the heat affected zone was affected by the boric acid as shown in graph 4.27 and bead height and width vs traverse is plotted in fig 4.28 and 4.29.

TABLE 4.2 QUALITY OF TRACKS MADE WITH TIN-BRONZE

TYPE OF BED (all beds 1.00mm) Deep	QUALITY OF TRACK	SPECIFIC ENERGY Range J/mm ²	SAMPLE No. (operating conditions are given in Appendix I.2)
Neat Powder	Good	150.0 ± 25.0 > P/DV > 10.0 ± 5.0	B1 - B5
	Discontinuous	P/DV < 10.0 ± 5.0	B6
Tin-bronze covered with α0.2 mm boric acid	Good	150.0 ± > P/DV > 10.0 ± 5.0	B07 - B010, B015 & Fig 4.22
	Discontinuous	P/DV < 10.0 ± 5.0	B011 & Fig 4.22
Tin-bronze mixed with 10 vol % boric acid	Good	196.0 > P/DV > 18.25	B112
	Discontinuous	P/DV < 18.25	B113

The cross section of the tracks usually consisted of a central mound as for stainless steel together with extra powder melted into the root as shown in the diagram Fig 4.23.

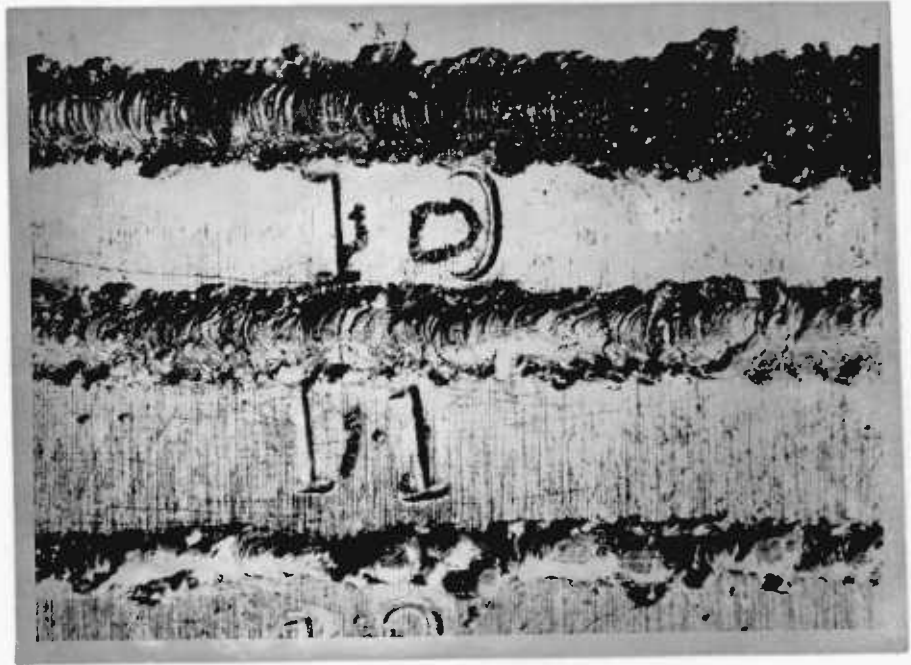


FIG 4.22 GOOD AND DISCONTINUOUS TRACKS, POWER = 1500 W, BEAM DIAMETER = 2.00 MM TRAVERSE SPEED = 20, 40, AND 80 MM/S, POWDER THICKNESS = 1.00 MM, X3.

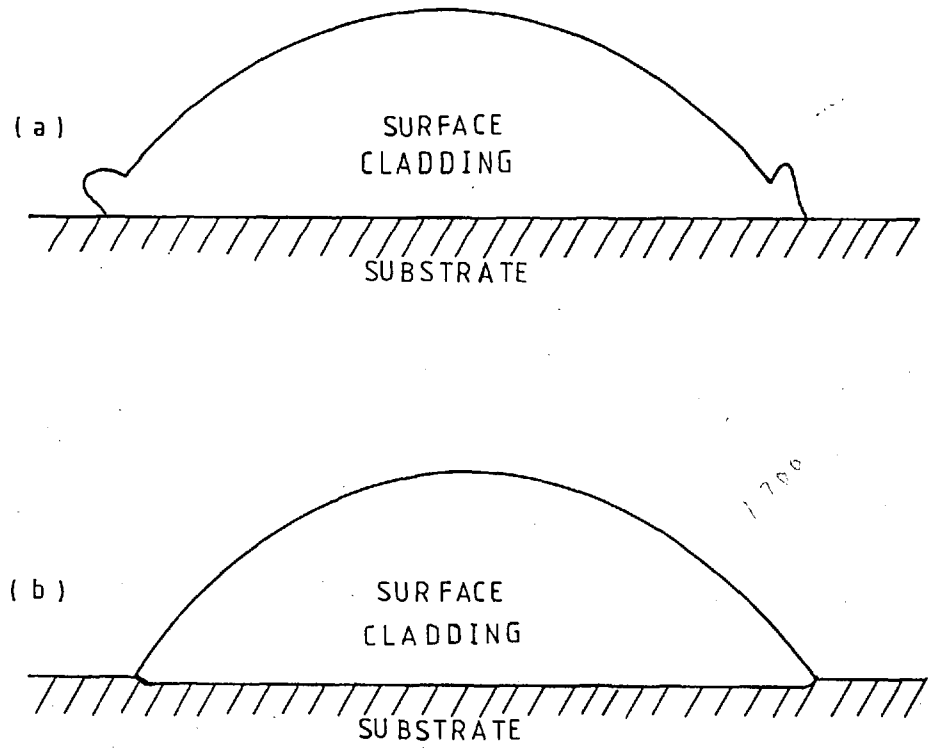


FIG 4.23 DIFFERENT CROSS SECTION PRODUCED BETWEEN
(a) TIN-BRONZE SURFACE CLADDING
(b) 316 STAINLESS STEEL SURFACE CLADDING

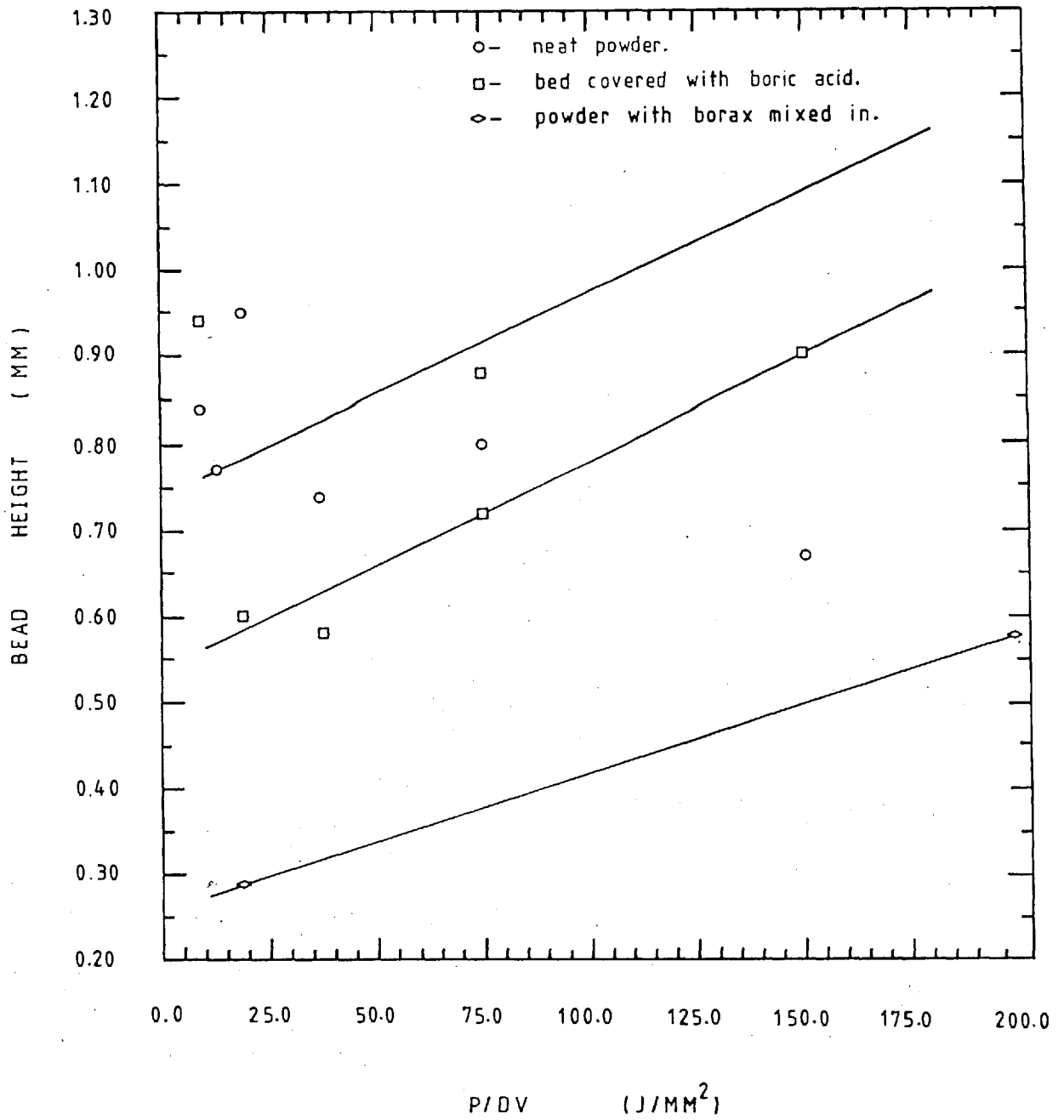


FIG 4.24 BEAD HEIGHT (MM) vs ENERGY/UNIT AREA, P/DV (J/MM²) FOR A 1.00 MM POWDER THICKNESS AND 200 MM BEAM DIAMETER.

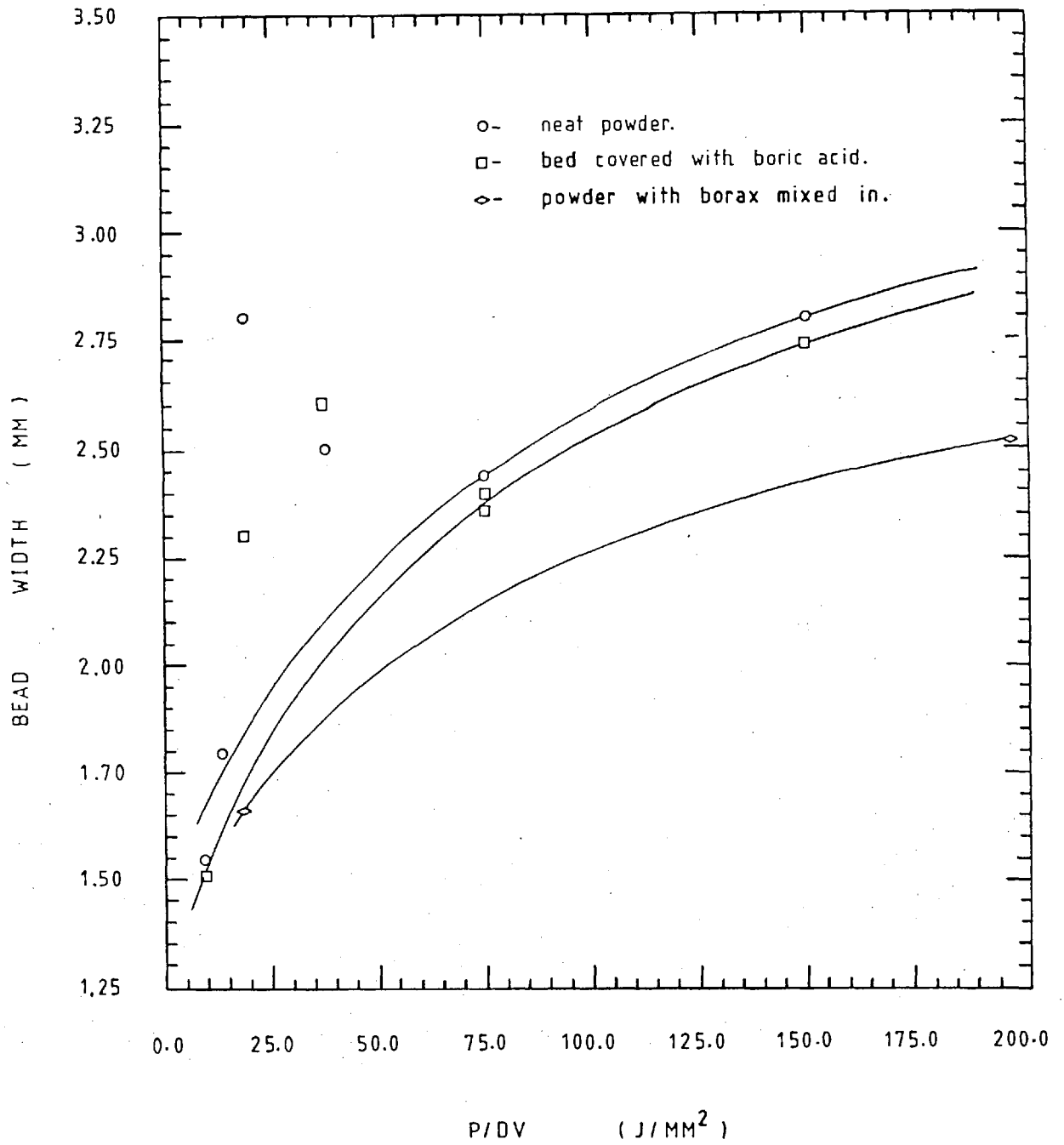


FIG 4.25 BEAD WIDTH (MM) vs ENERGY/UNIT AREA, P/DV (J/MM²) FOR A 1.00 MM POWDER THICKNESS AND 2.00 MM BEAM DIAMETER.

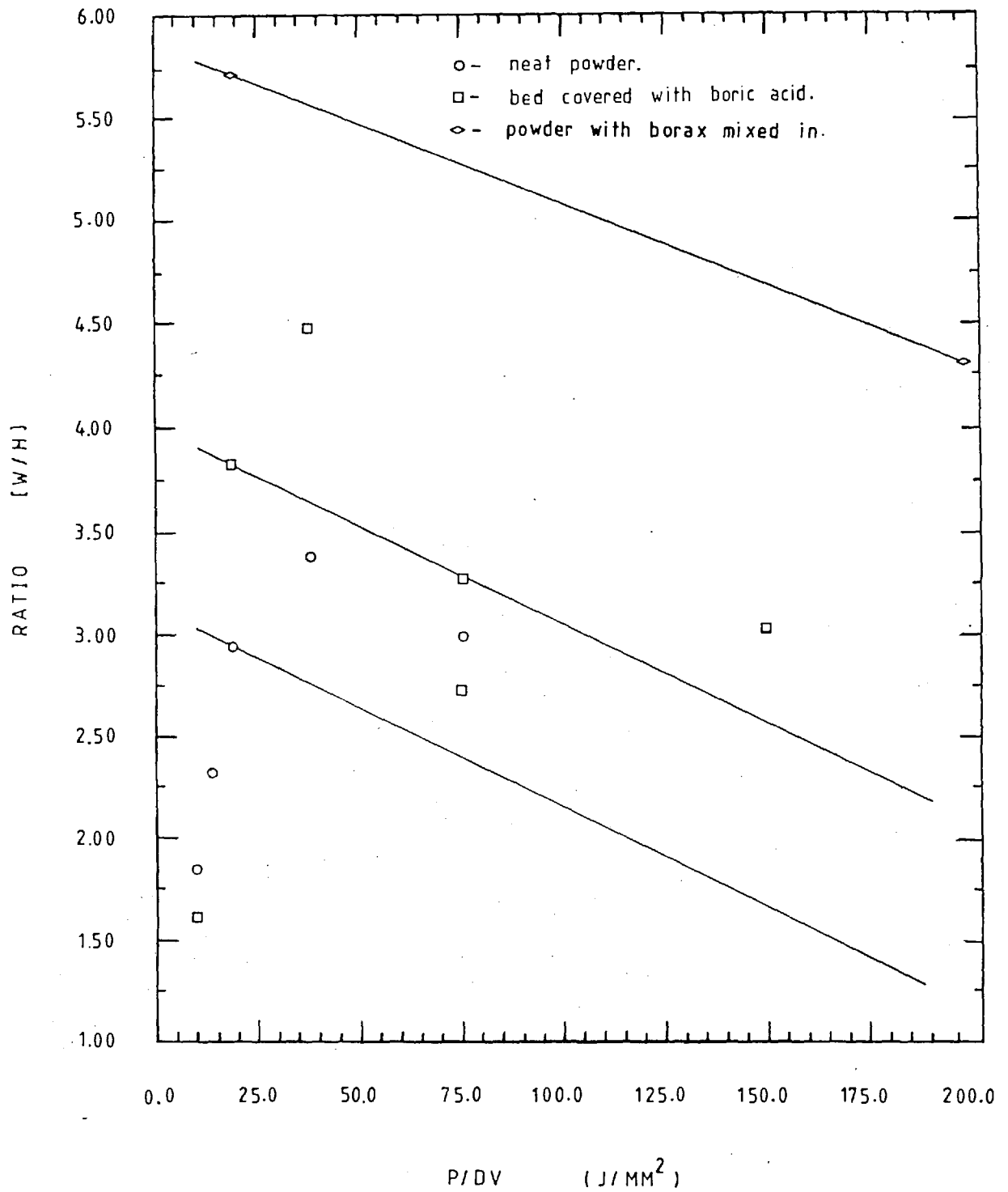


FIG 4.26 RATIO [W/H] (BEAD WIDTH/BEAD HEIGHT) vs ENERGY/UNIT AREA, - P/DV (J/MM²) FOR A 1.00 MM POWDER THICKNESS AND 2.00 MM — BEAM DIAMETER.

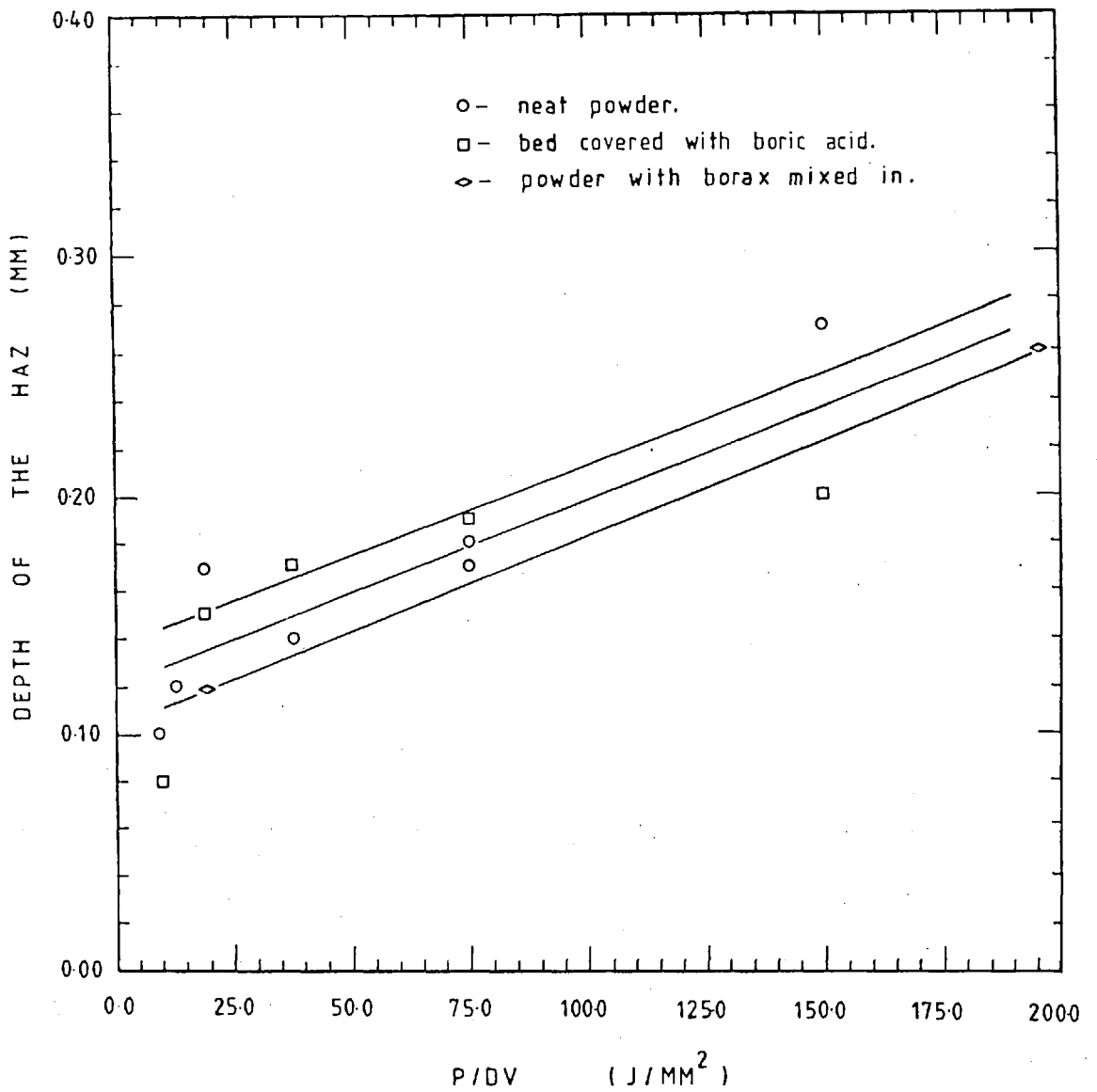


FIG 4.27 DEPTH OF THE HAZ (MM) vs ENERGY/UNIT AREA, P/DV (J/MM²)
FOR A 1.00 MM POWDER THICKNESS AND 2.00 MM BEAM DIAMETER.

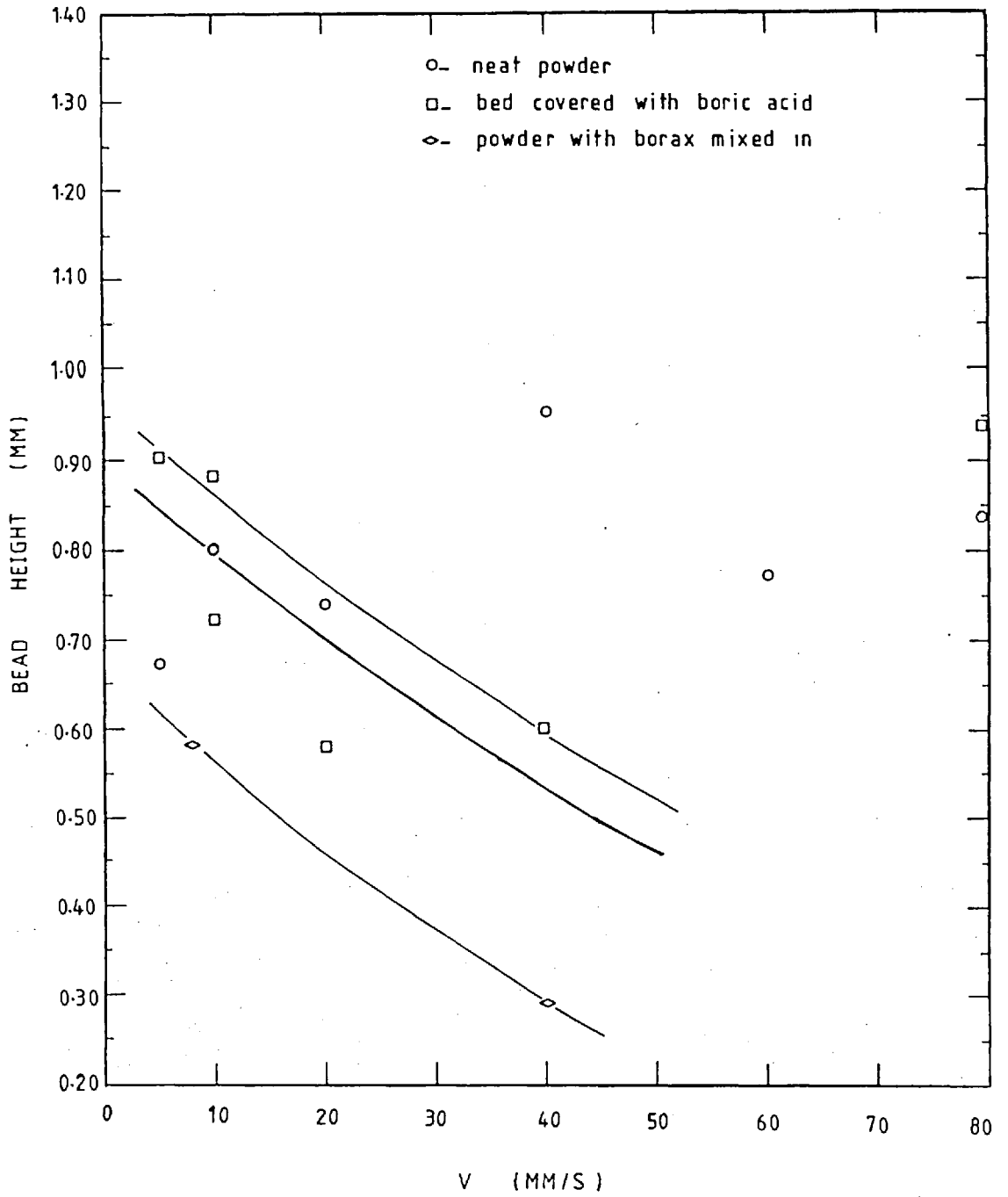


FIG 4.28 BEAD HEIGHT (MM) vs TRAVERSE SPEED (MM/S) FOR A 1.00 MM POWDER THICKNESS AND 200 MM BEAM DIAMETER.

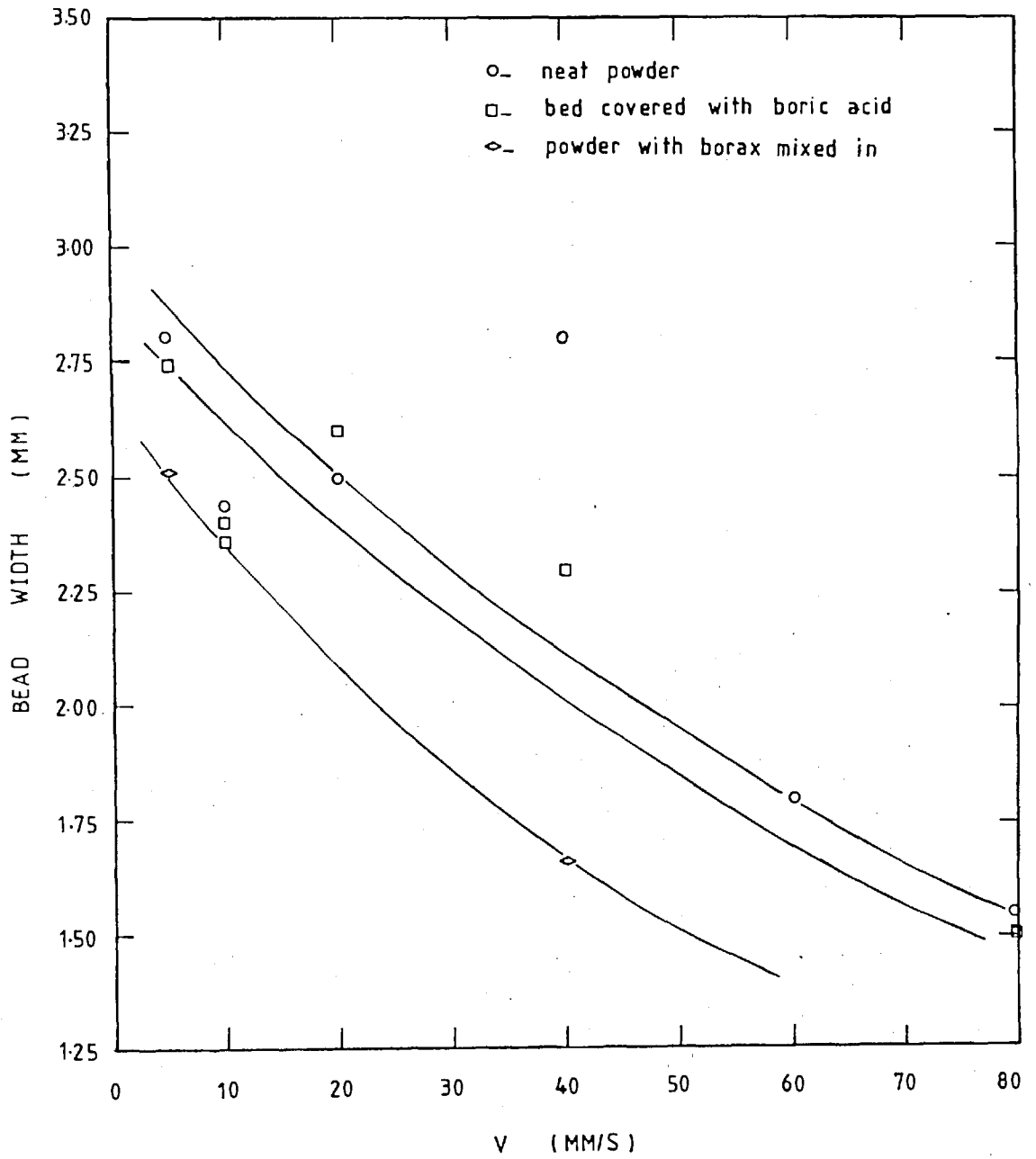


FIG 4.29 BEAD WIDTH (MM) vs TRAVERSE SPEED (MM/S) FOR A 1.00 MM POWDER THICKNESS AND 2.00 MM BEAM DIAMETER.

4.3 Monel Surface Cladding

Monel is one of the most difficult alloys to join onto a base metal, due perhaps to its high melting point.

The runs were made with three different mass flow rates using a stellite gun as described in table 4.3. The operating conditions for all specimens are shown in appendix 1.3.

4.3.1 Height and width of Tracks-Monel

The resultant height and width of the tracks were found to depend on both specific energy and mass flow rate as shown in graphs 4.32 - 4.37, a plot of deposit ratio vs specific energy is shown in graphs 4.38 - 4.40, and plots of bead width vs energy per unit length is shown in figs 4.41 and 4.42.

Likewise, a plot of height and width of the bead vs traverse speed is shown in graphs 4.43 and 4.44.

TABLE 4.3 QUALITY OF TRACKS MADE WITH MONEL

MASS FLOW RATE (Kg/Hr)	QUALITY OF TRACK	SPECIFIC ENERGY J/mm^2	SAMPLE NO (H) (SEE APPENDIX I.3)
2.05	GOOD TRACKS	$80.0 \pm 20.0 J/mm^2$ $> P/DV >$ $30.0 \pm 12.0 J/mm^2$	7,8,9,10,11,36,37,46,47,48, 49,51,52,58,61,68,72,84,92 96,98,99,104
	DISCONTINUOUS TRACKS	$P/DV < 30.0 \pm 12.0 J/mm^2$	12,13,14,15,16,38,39,40,64, 76,80,88,102 & Fig 4.30
	LASER ONLY		5,6
1.37	GOOD TRACKS	$80.0 \pm 20.0 J/mm^2$ $> P/DV >$ $2.50 \pm 10.0 J/mm^2$	17,18,19,20,30,31,32,33,50, 53,54,55,57,60,71,91 & Fig 4.31
	DISCONTINUOUS TRACKS	$P/DV < 25.0 \pm 10.0 J/mm^2$	21,22,29,34,35,67,75,79,87, 101
	LASER ONLY		63,83,95
0.83	GOOD TRACKS	$80 \pm 20.0 J/mm^2$ $> P/DV >$ $25.0 \pm 10.0 J/mm^2$	23,24,41,56,70,90
	DISCONTINUOUS TRACKS	$P/DV < 25.0 \pm 10.0 J/mm^2$	25,26,27,28,42,43,45,59,86,94, 100,3,4.
	LASER ONLY		1,2,62,66,74,78,82

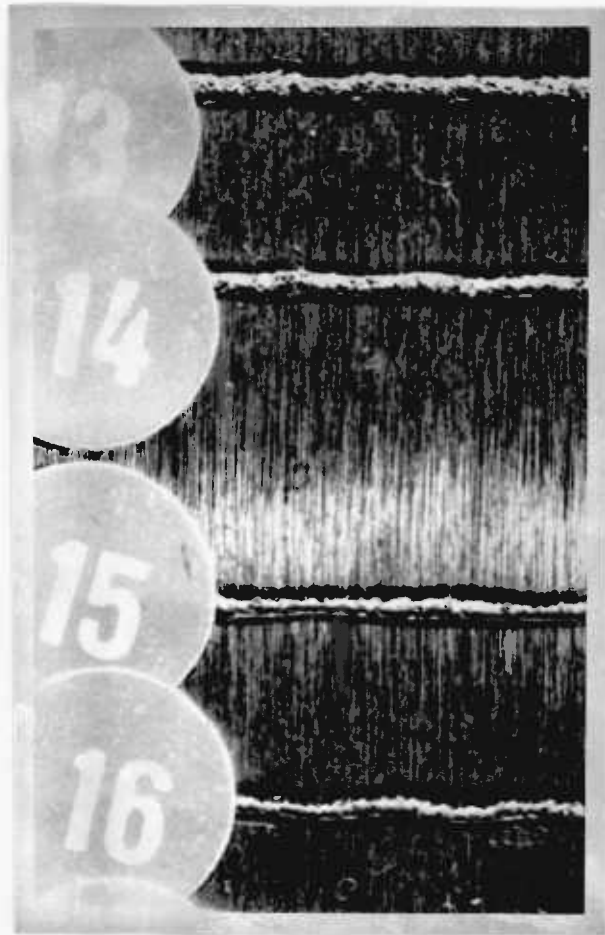


FIG 430 DISCONTINUOUS TRACKS, POWER = 1 600 W, BEAM
DIAMETER = 2.00 MM TRAVERSE SPEED = 35, 40,
45, 50 MM/S, MASS FLOW RATE = 2.05 Kg/Hr, X3.

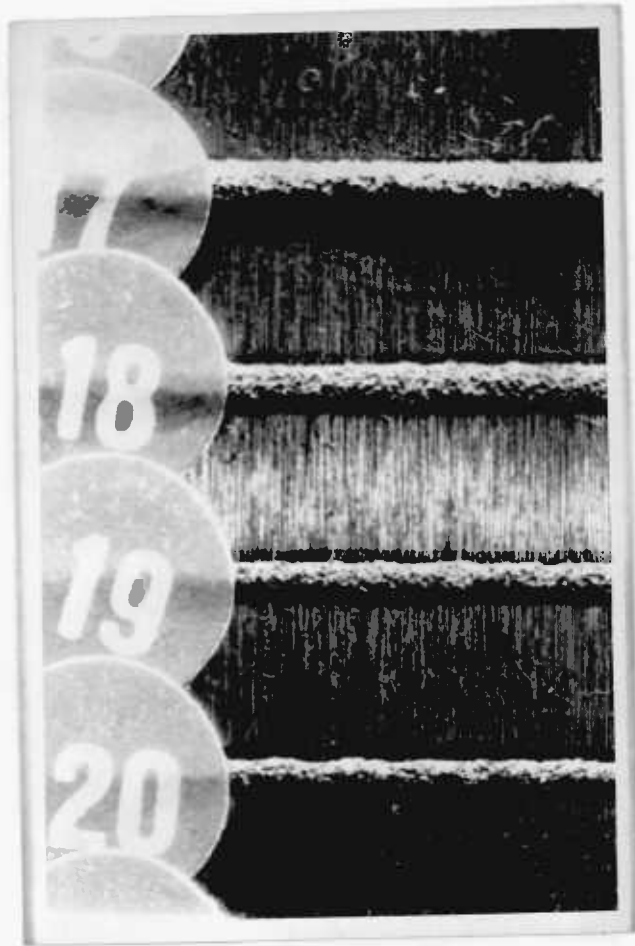


FIG 4.31 CONTINUOUS TRACKS, POWER =1560 W, BEAM DIAMETER =
= 2.00 MM, TRAVERSE SPEED =10, 15, 20, AND 25 MM/S
MASS FLOW RATE =1.37 Kg/Hr, X3.

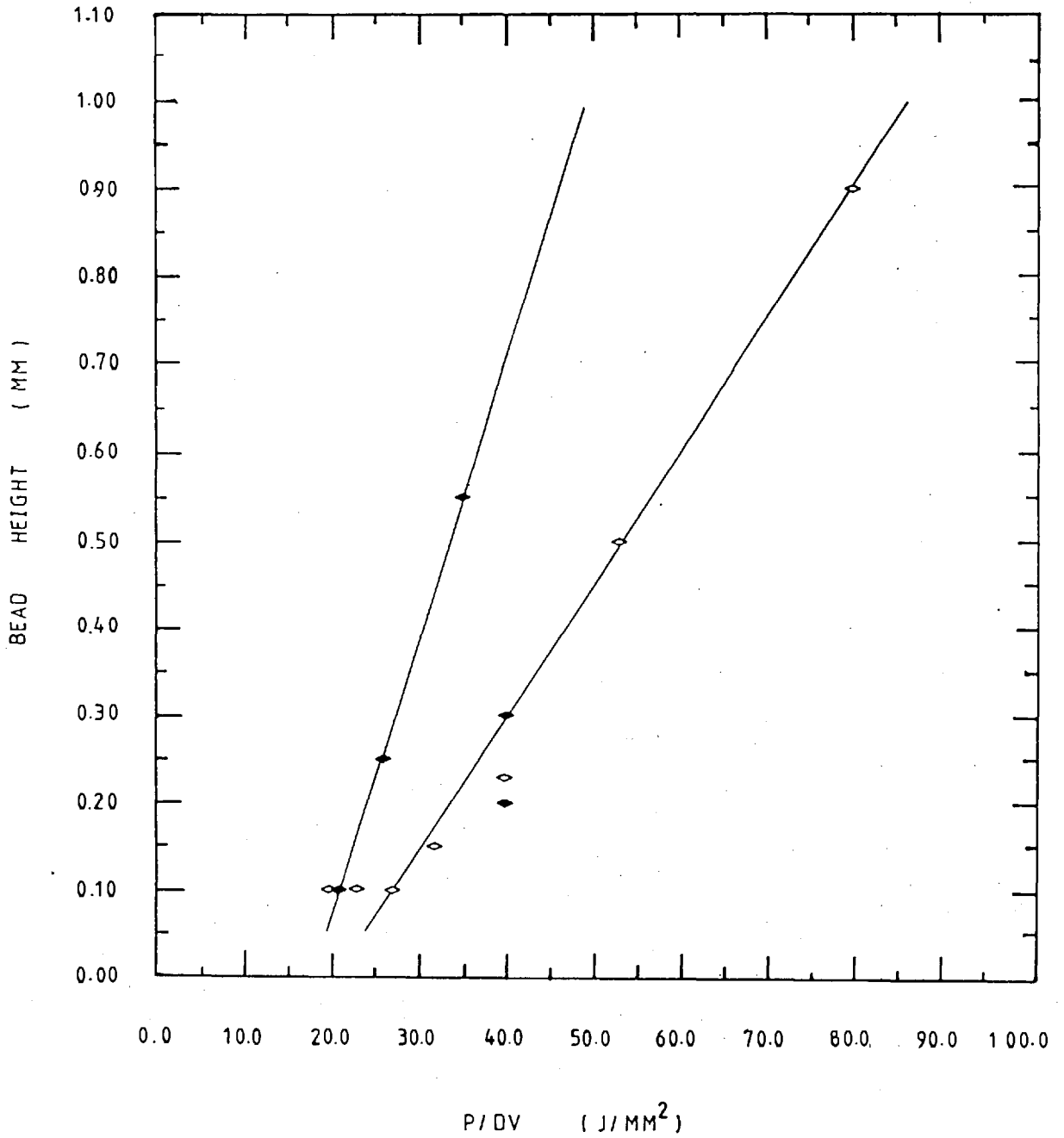


FIG 4.32 BEAD HEIGHT (MM) vs ENERGY/UNIT AREA, P/DV (J/MM²) FOR A MASS FLOW RATE OF 2.05 Kg/Hr, \diamond =2.00 AND \blacklozenge =3.00 MM BEAM - DIAMETER.

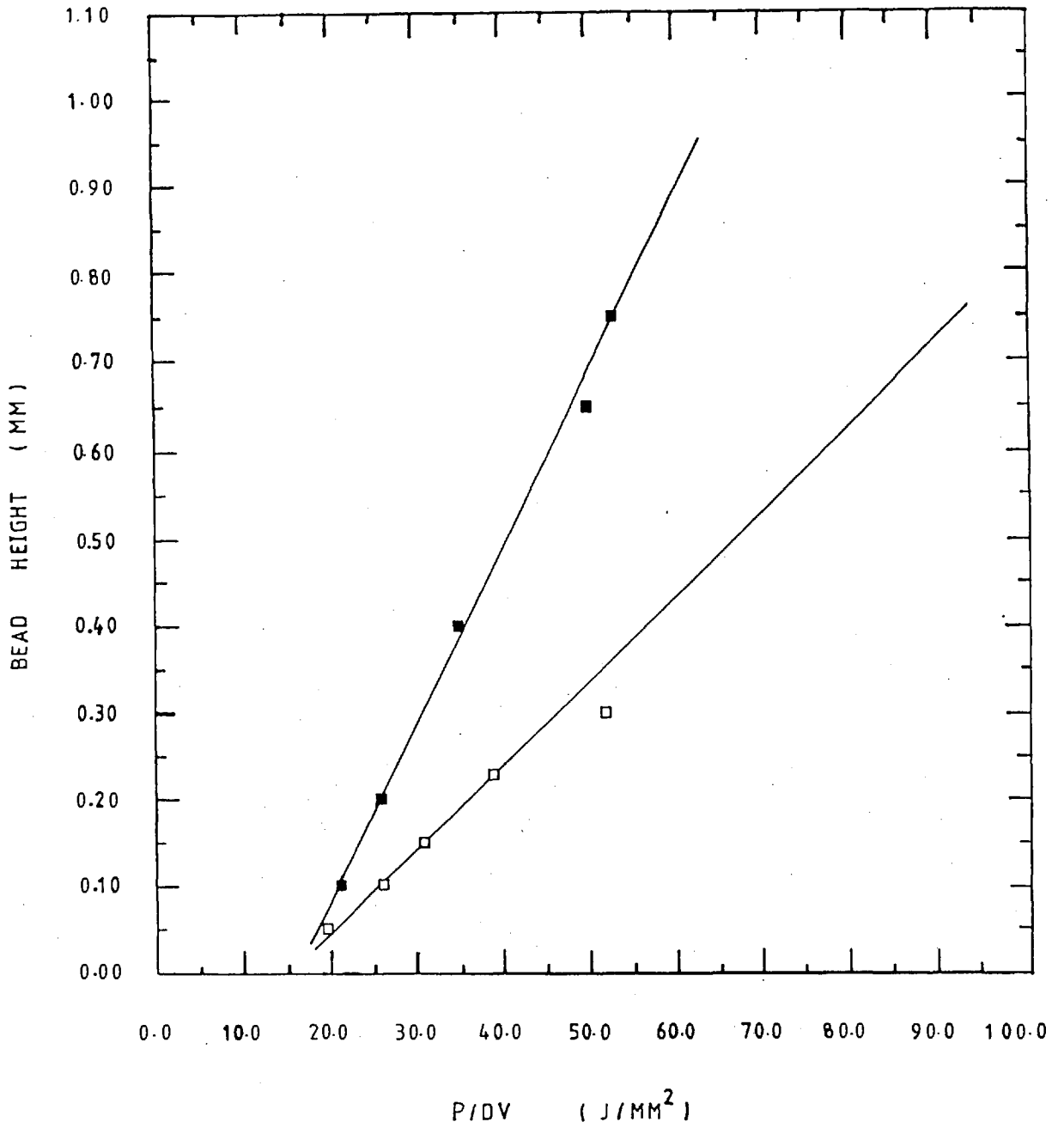


FIG 4.33 BEAD HEIGHT (MM) vs ENERGY/UNIT AREA, P/DV (J/MM^2) FOR A MASS FLOW RATE OF 1.37 Kg/Hr, $\square=2.00$ AND $\blacksquare=3.00$ MM BEAM - DIAMETER.

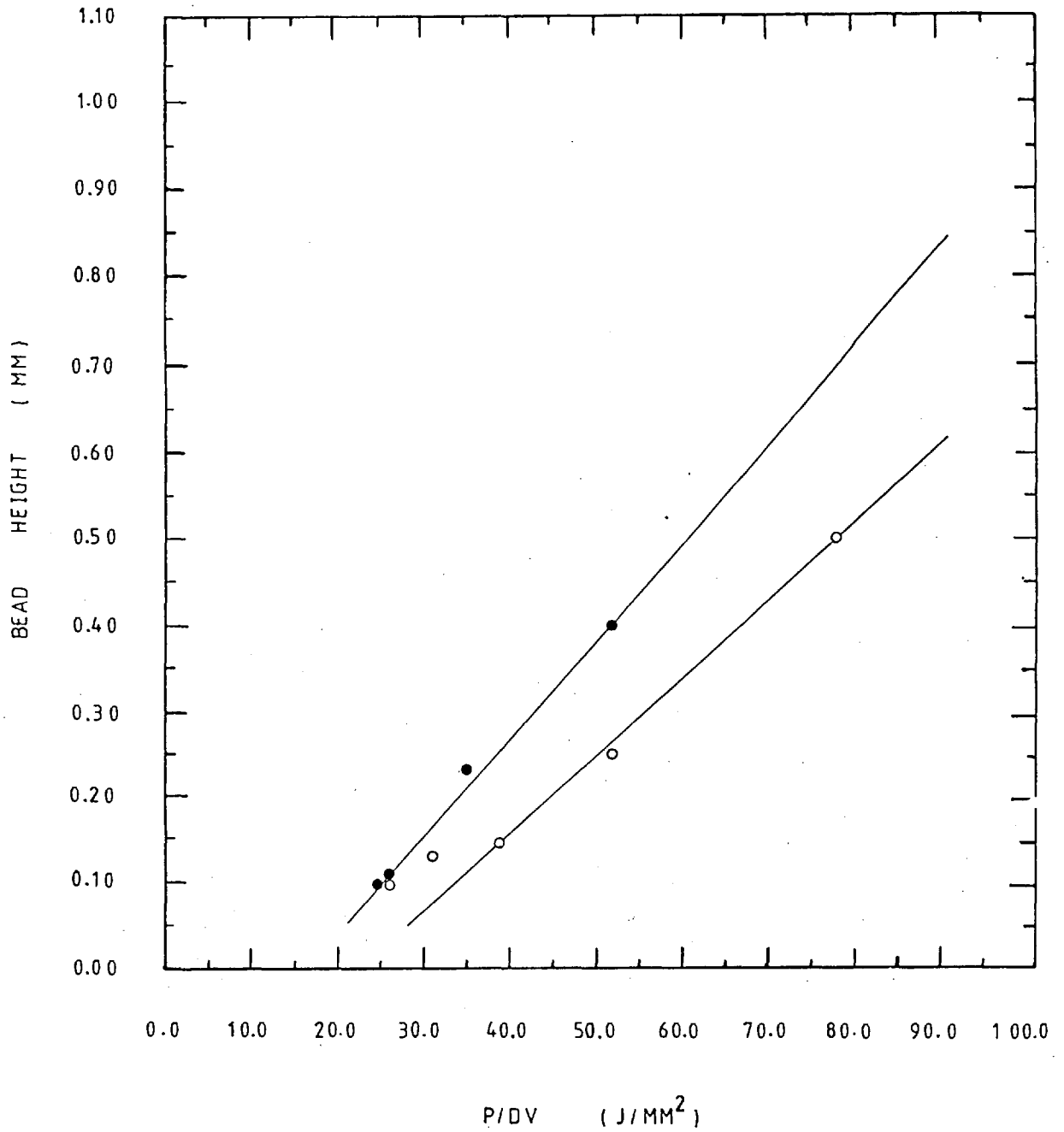


FIG 4.34 BEAD HEIGHT (MM) vs ENERGY/UNIT AREA, P/DV (J/MM²) FOR A MASS FLOW RATE OF 0.83 Kg/Hr, ○ = 2.00 AND ● = 3.00 MM BEAM — DIAMETER.

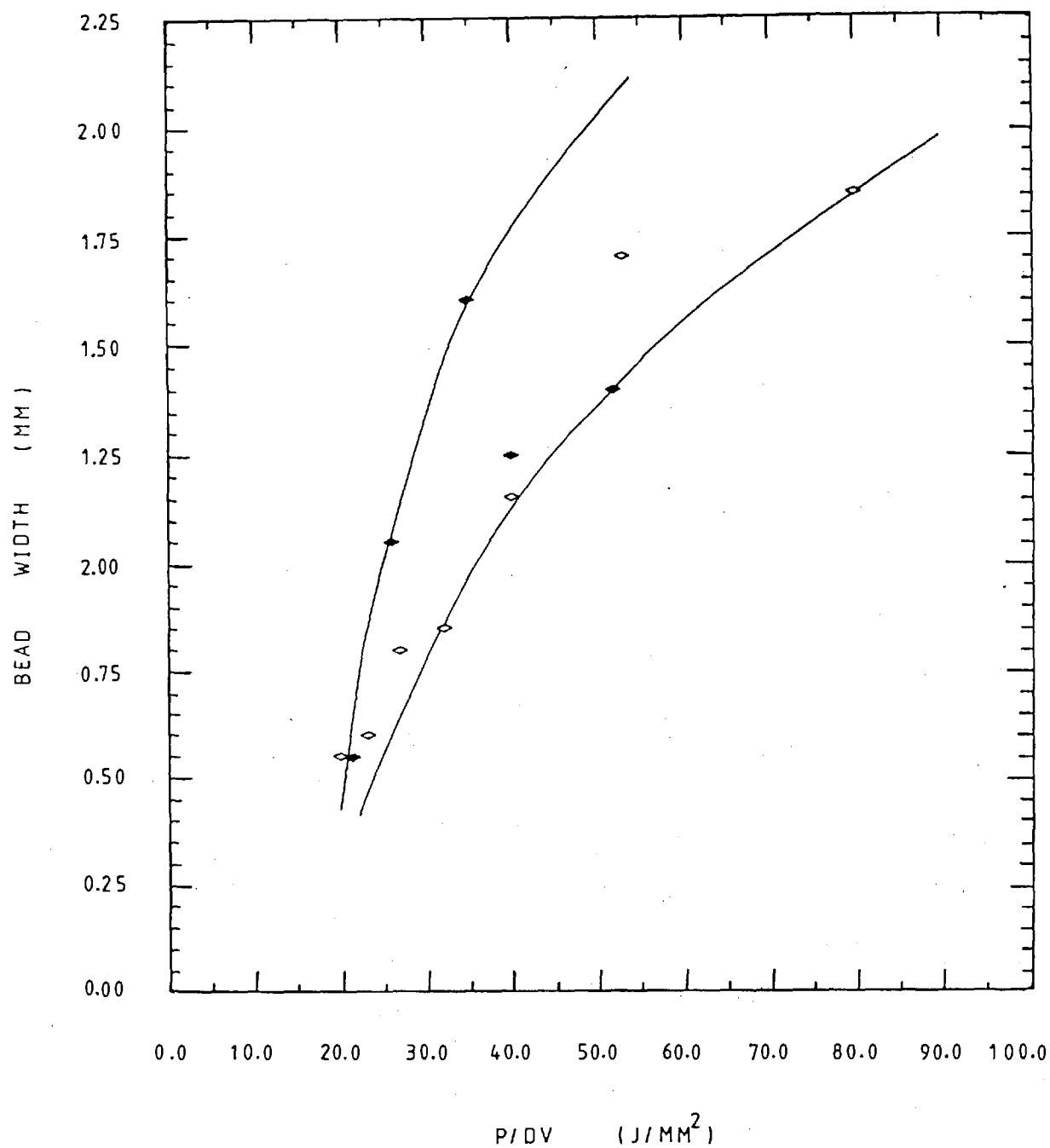


FIG 4.35 BEAD WIDTH (MM) vs ENERGY/UNIT AREA, P/DV (J/MM²) FOR A MASS FLOW RATE OF 2.05 Kg/Hr, ◇ = 2.00 AND ◆ = 3.00 MM BEAM DIAMETER.

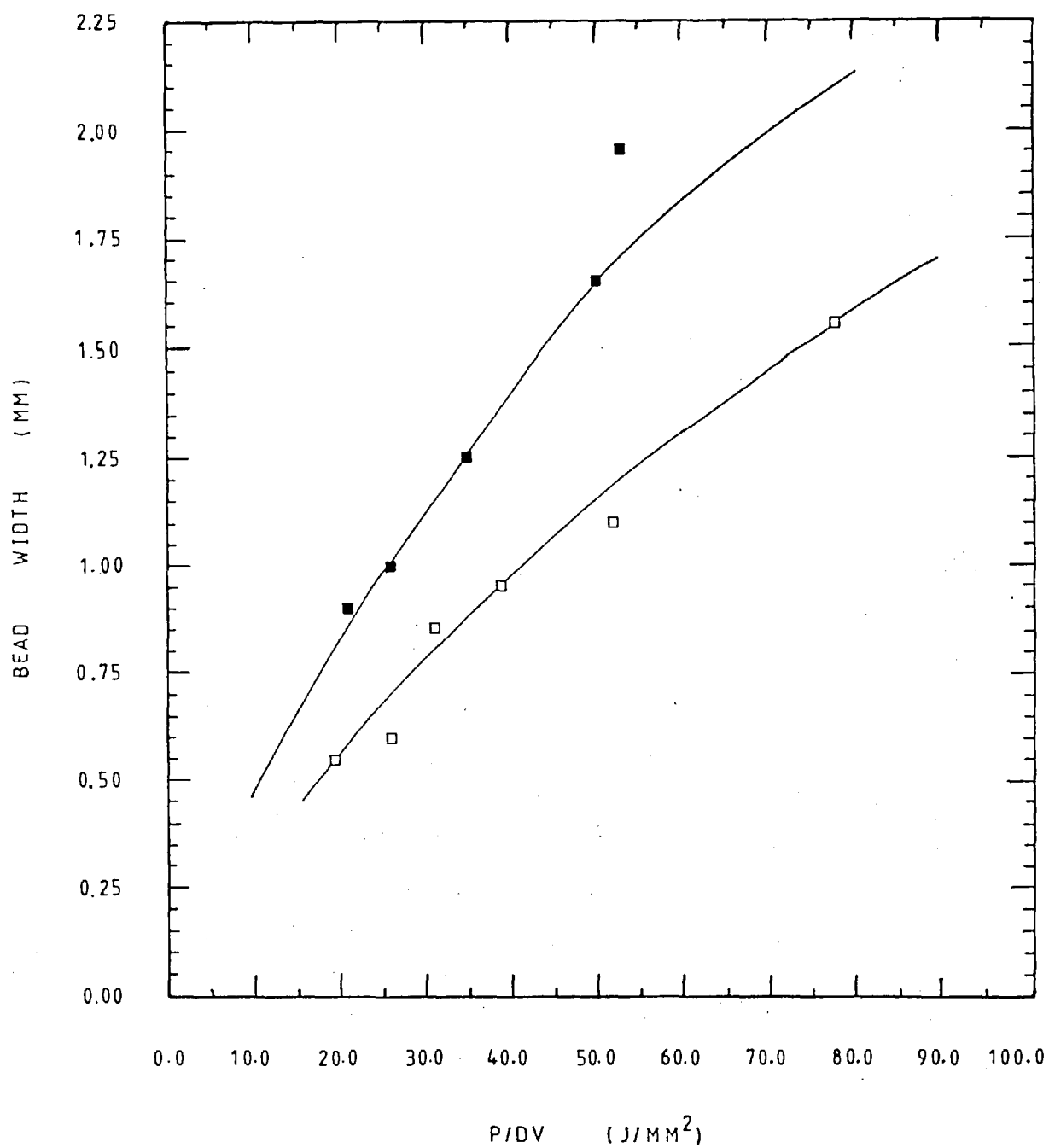


FIG 4.36 BEAD WIDTH (MM) vs ENERGY/UNIT AREA, P/DV (J/MM²) FOR A MASS FLOW RATE OF 1.37 Kg/Hr, \square = 2.00 AND \blacksquare = 3.00 MM BEAM-DIAMETER.

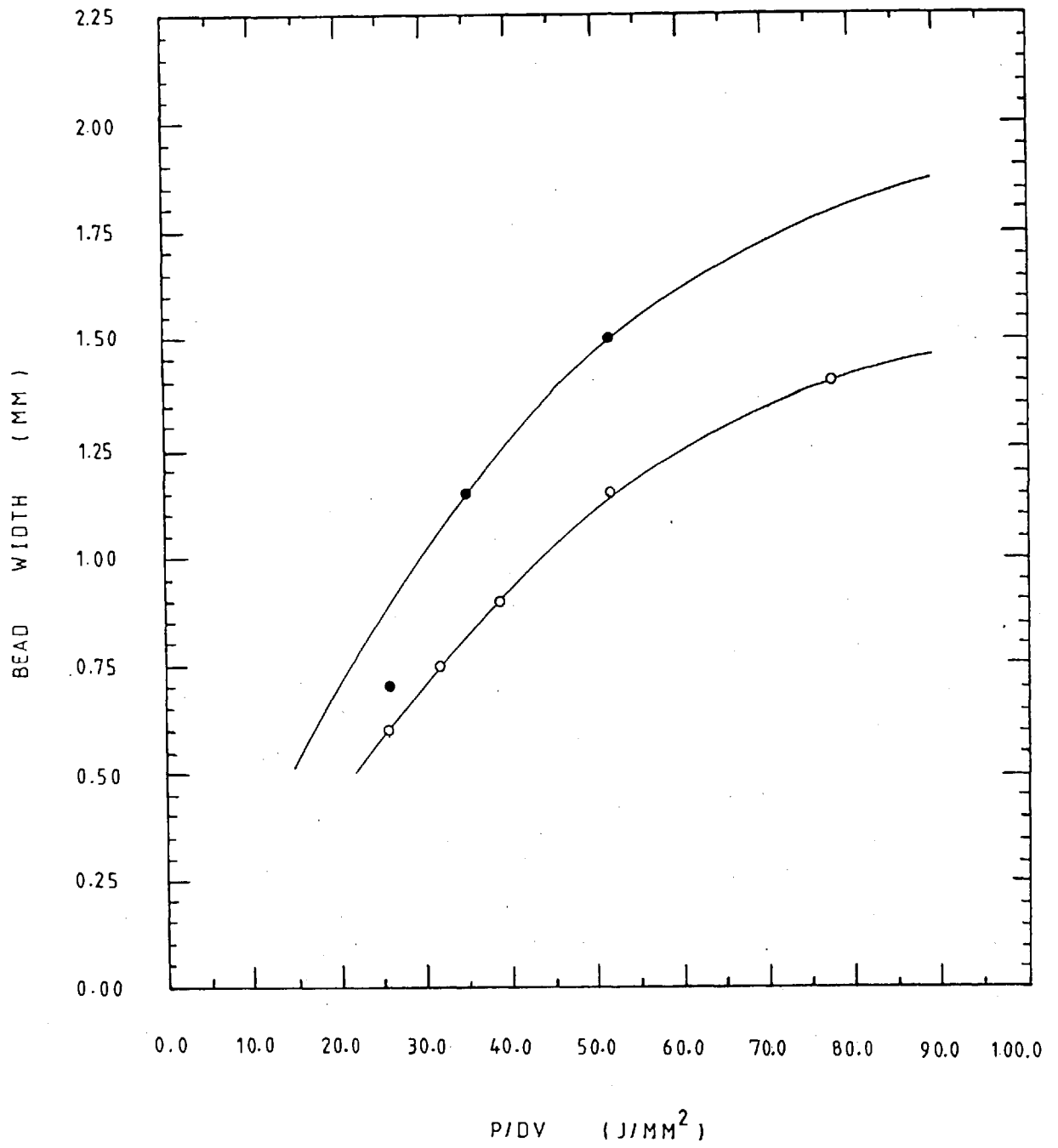


FIG 4.37 BEAD WIDTH (MM) vs ENERGY/UNIT AREA, P/DV (J/MM^2) FOR A MASS FLOW RATE OF 0.83 Kg/Hr, $\circ = 2.00$ AND $\bullet = 3.00$ MM BEAM DIAMETER.

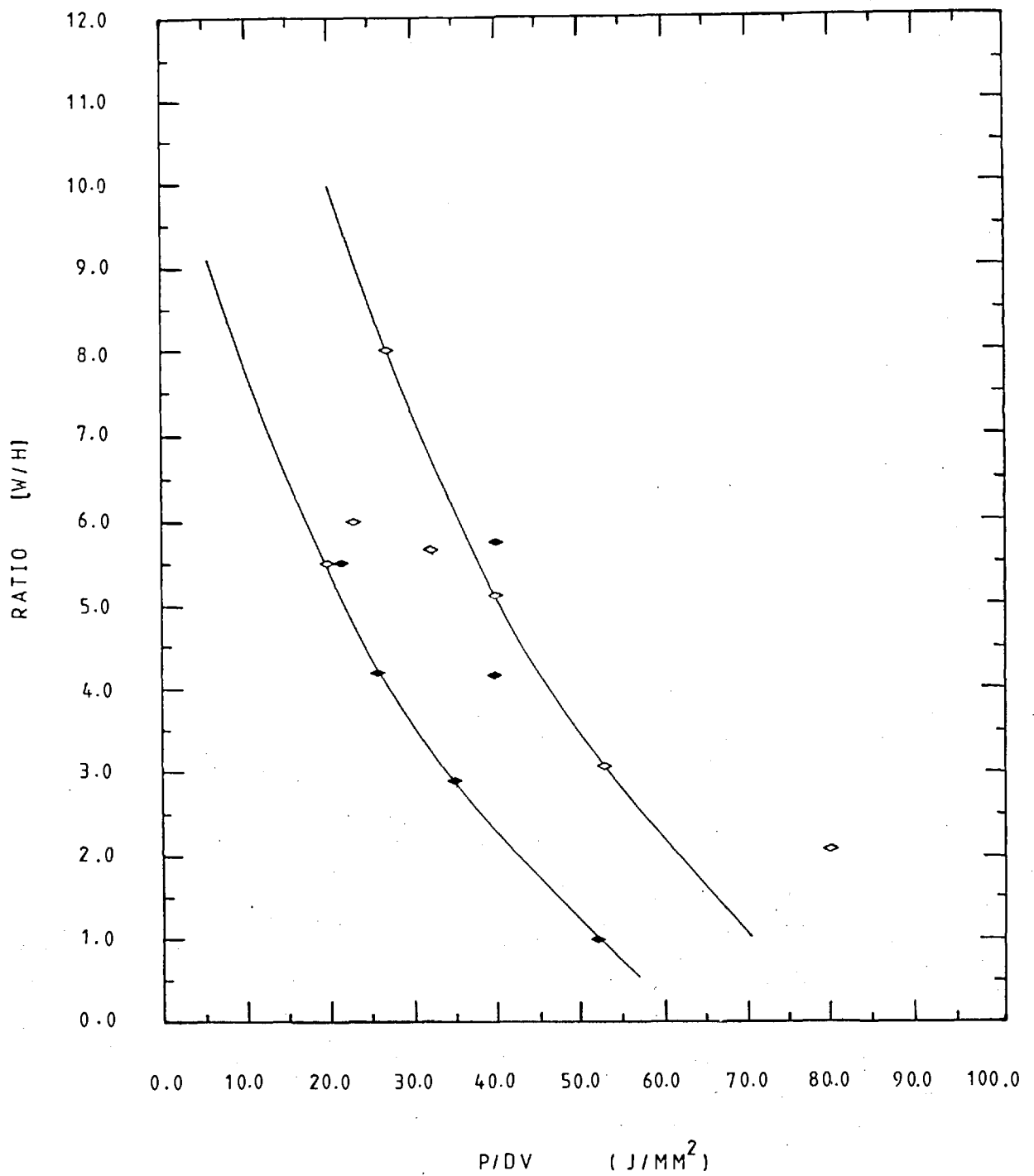


FIG 4.38 RATIO [W/H] (BEAD WIDTH/BEAD HEIGHT) vs ENERGY/UNIT AREA, P/DV (J/MM²) FOR A MASS FLOW RATE OF 2.05 Kg/Hr, \diamond = 2.00 AND \blacklozenge = 3.00 MM BEAM DIAMETER.

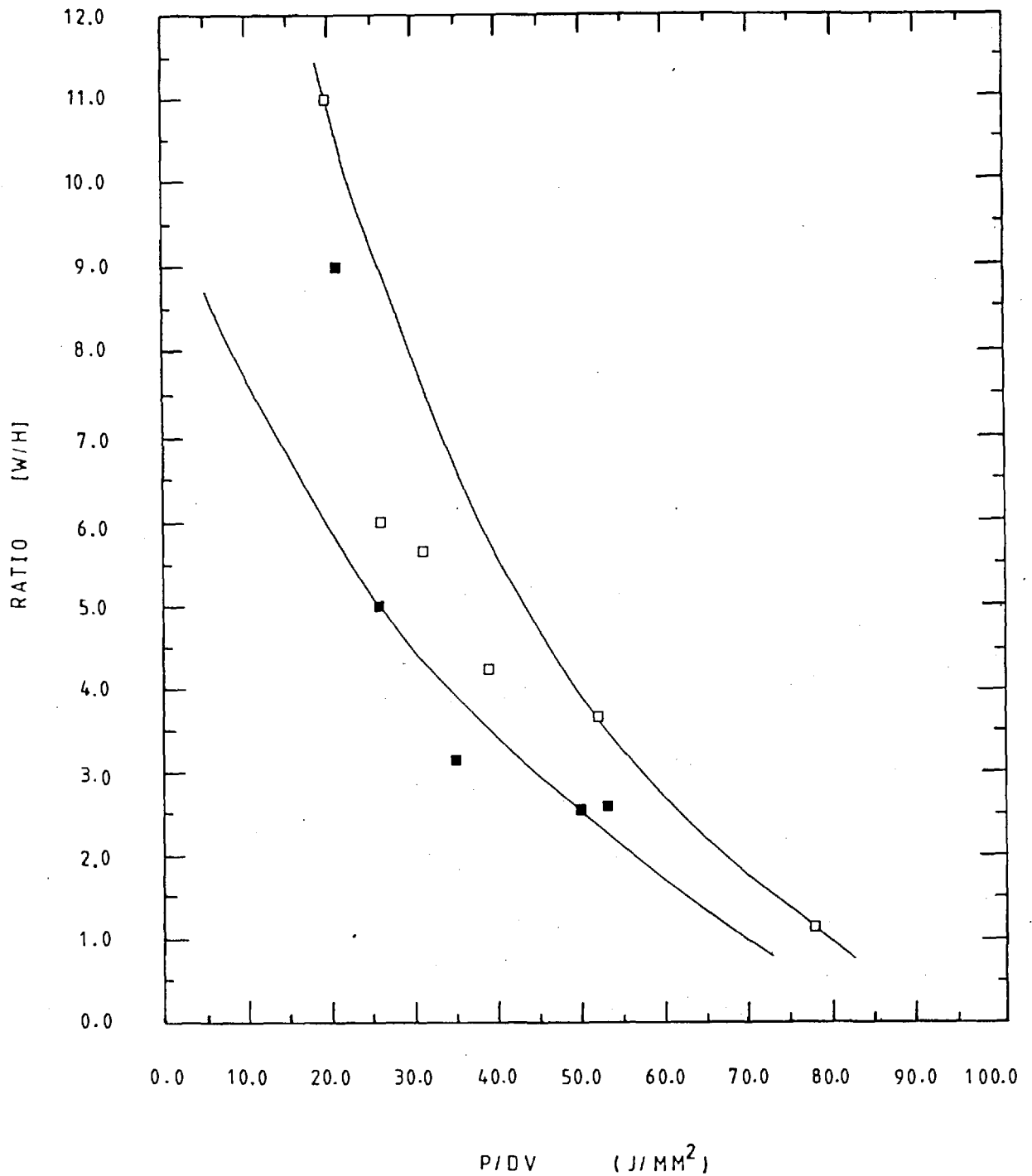


FIG 4.39 RATIO [W/H] (BEAD WIDTH/BEAD HEIGHT) vs ENERGY/UNIT AREA, P/DV (J/MM²) FOR A MASS FLOW RATE OF 1.37 Kg/Hr, □ = 2.00 AND ■ = 3.00 MM BEAM DIAMETER.

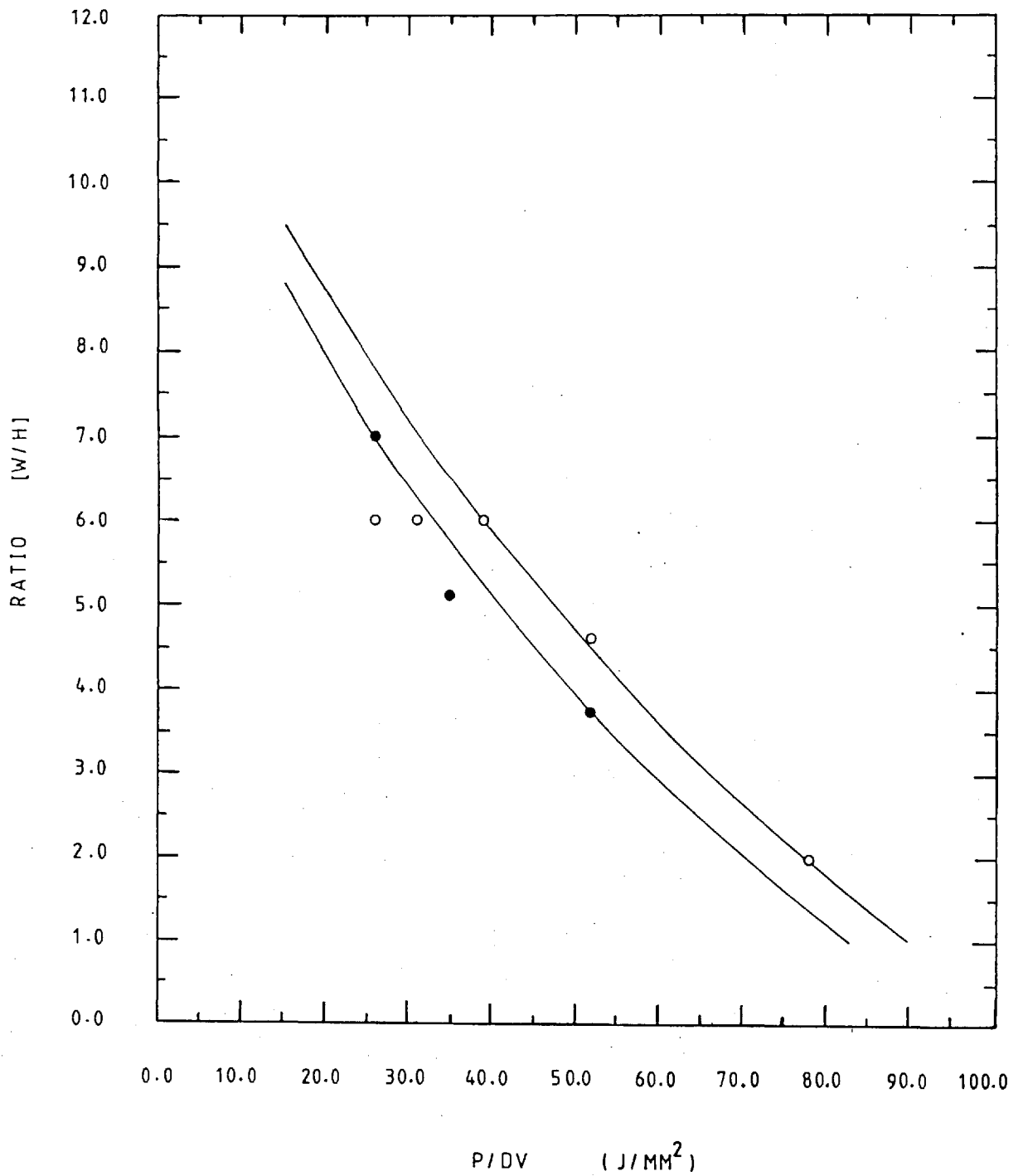


FIG 4.40 RATIO $[W/H]$ (BEAD WIDTH/BEAD HEIGHT) vs ENERGY/UNIT AREA, P/DV (J/MM^2) FOR A MASS FLOW RATE OF 0.83 Kg/Hr, $\phi=2.00$ AND $\bullet=3.00$ MM BEAM DIAMETER.

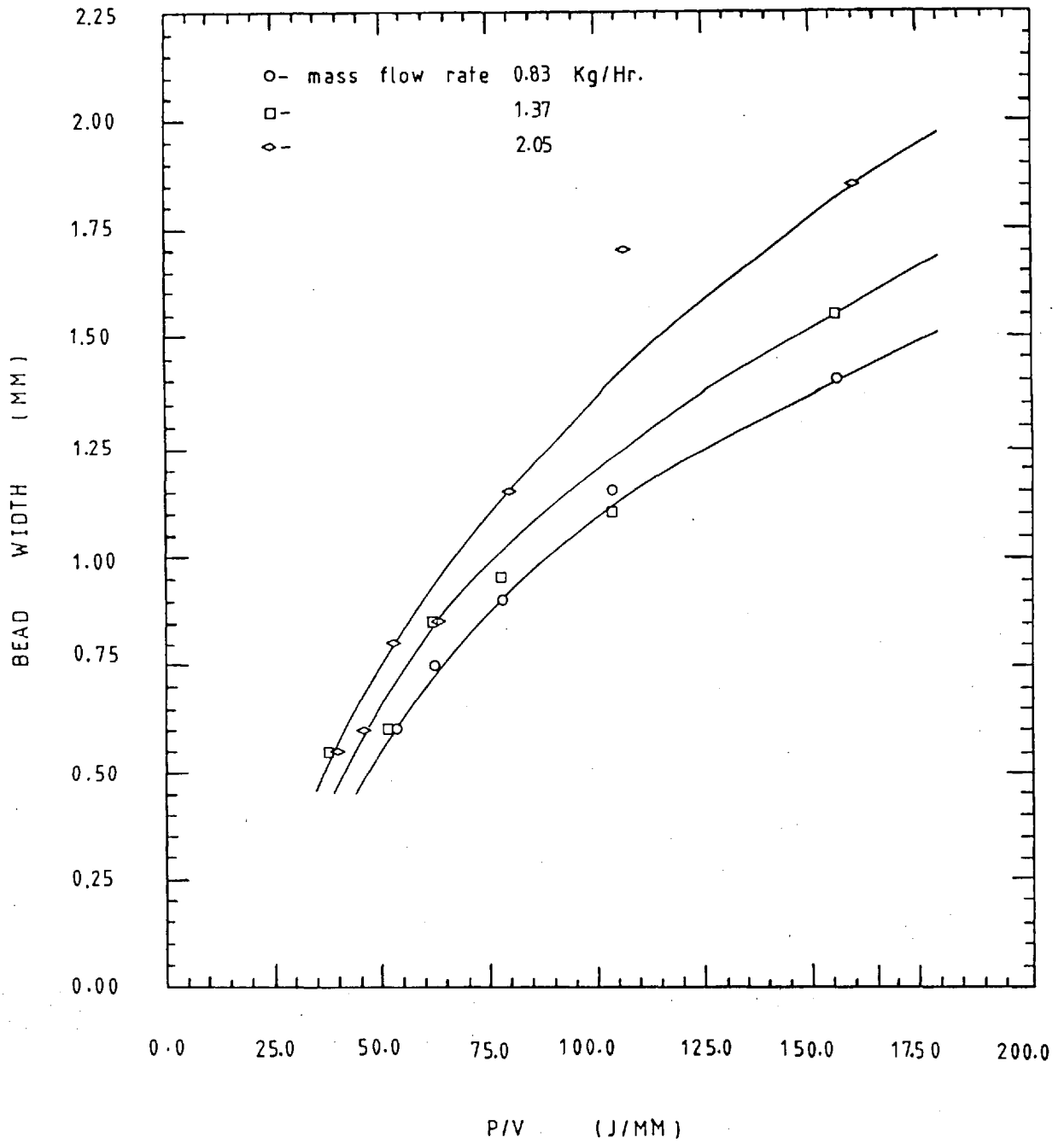


FIG 4.41 BEAD WIDTH (MM) vs ENERGY/UNIT LENGTH, P/V (J/MM) FOR A 2.00 MM BEAM DIAMETER.

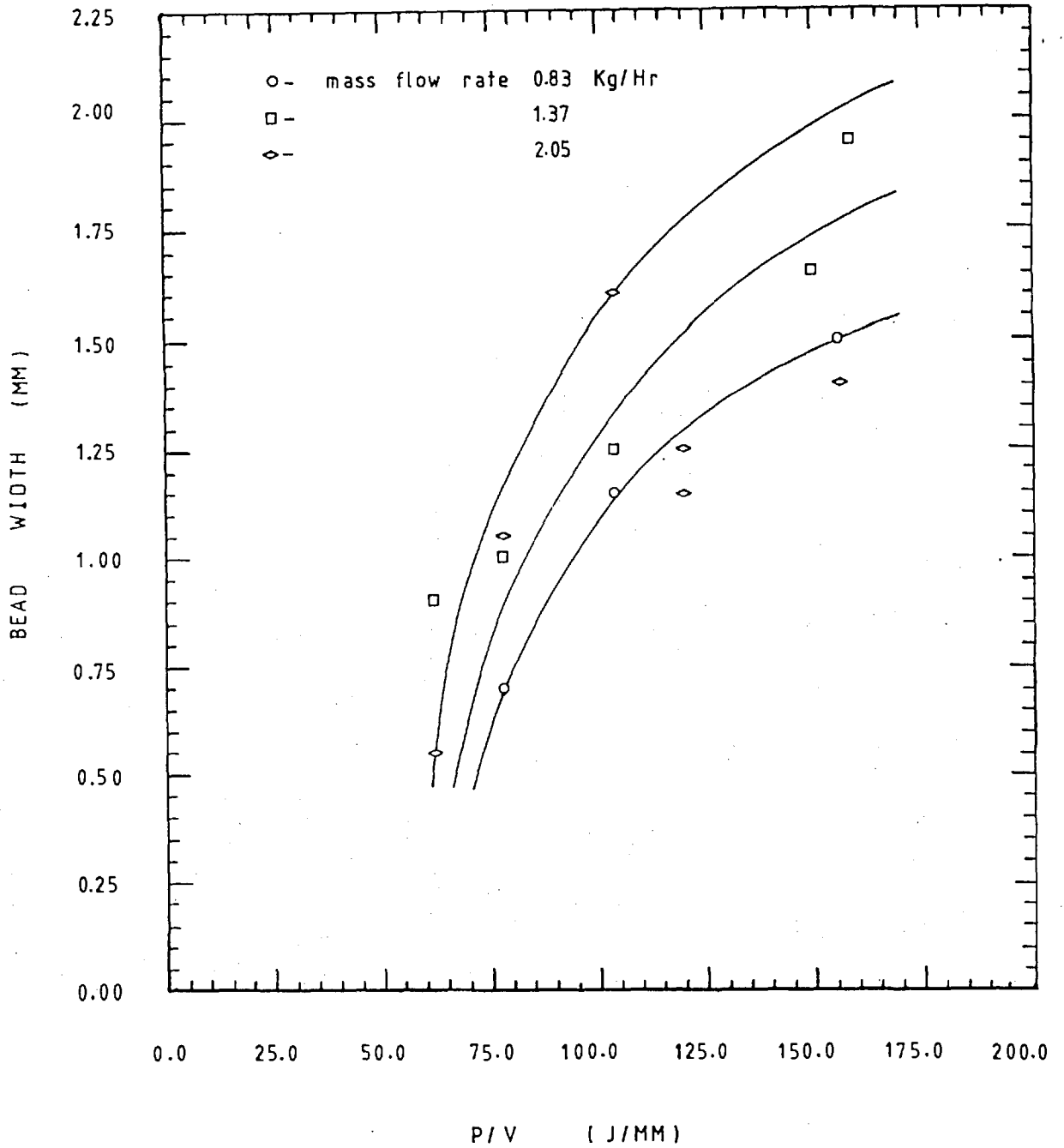


FIG 4.42 BEAD WIDTH (MM) vs ENERGY/UNIT LENGTH, P/V (J/MM) FOR A 3.00 MM BEAM DIAMETER.

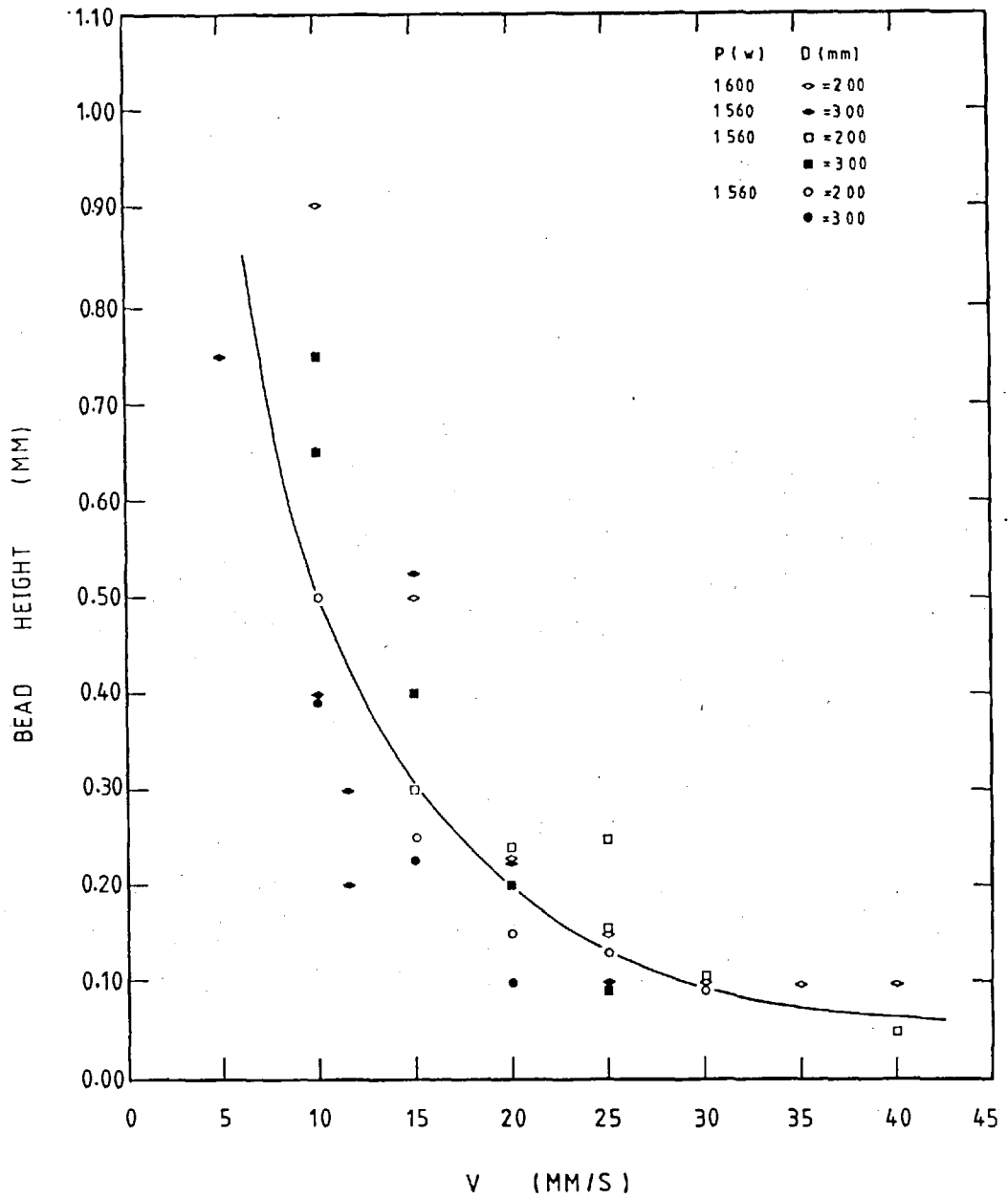


FIG 4.43 BEAD HEIGHT (MM) vs TRAVERSE SPEED (MM/S) FOR A MASS FLOW RATE OF $\diamond = 2.05$, $\square = 1.37$ AND $\circ = 0.87$ Kg/Hr.

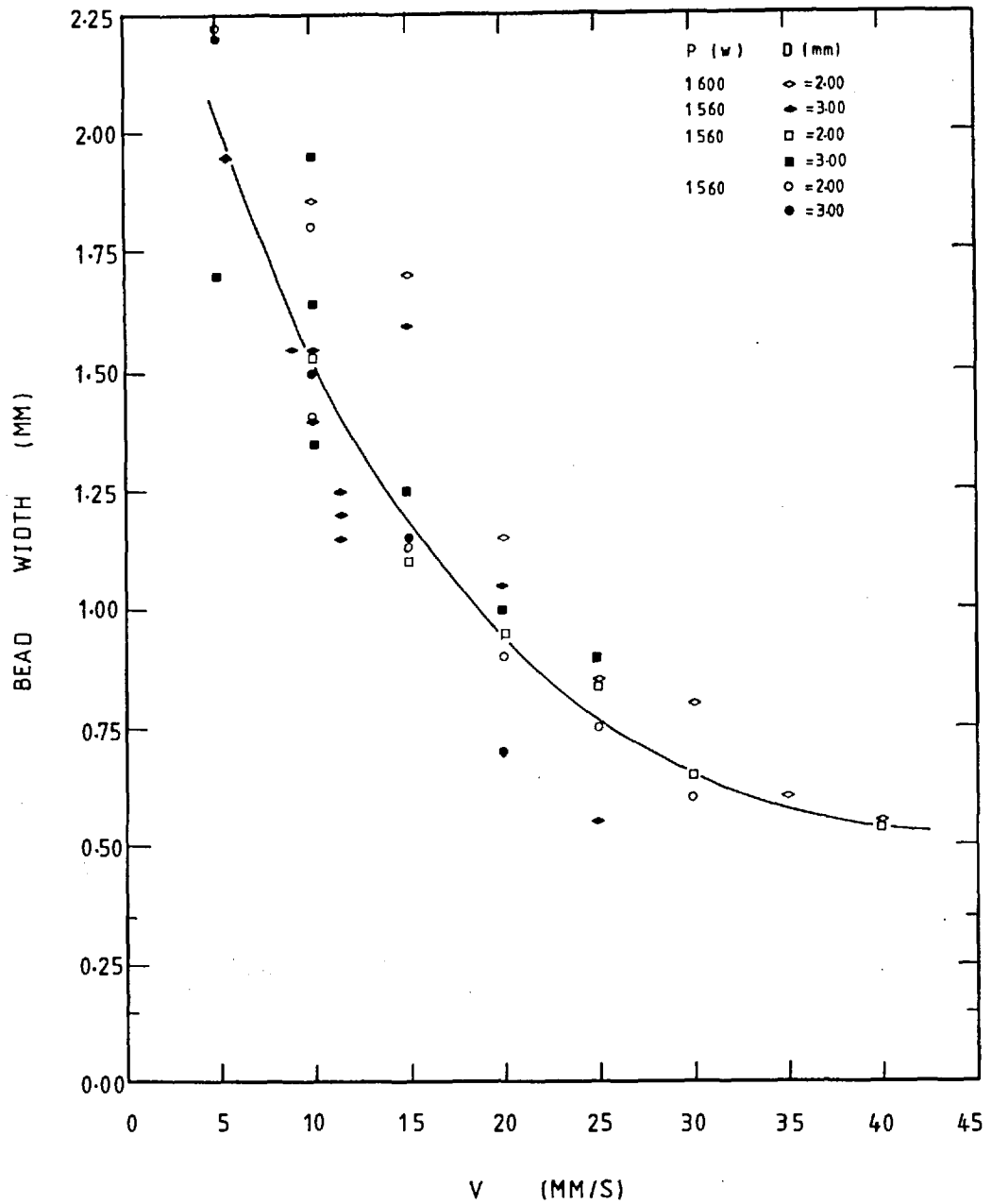


FIG 4.44 BEAD WIDTH (MM) vs TRAVERSE SPEED (MM/S) FOR A MASS FLOW RATE OF ◇ = 2.05, □ = 1.37 AND ○ = 0.87 Kg/Hr.

4.4 Developing Section Surface Cladding

All single-run specimens were cut, mounted, polished and etched in a 2% and 4% nital solution, proceeding to a microscopic analysis of each one, making use of a light microscope to observe the morphology at the interface between surface cladding alloy and base metal. Another object of the analysis was to check for possible underbead cracking as well as cracking in the bead .

All specimens were photographed at low magnification. These are shown in Appendix 1.1 in which the different areas of deposition can be observed.

The resultant sectional area was found to depend on the traverse speed as shown in graphs 4.45 - 4.47 for stainless steel and in graph 4.48 for tin-bronze. This implies more melting sideways in the fixed powder bed at slow speeds.

Another manifestation of this greater neat preparation is shown in graphs 4.49 and 4.51 for stainless steel and 4.52 for tin-bronze.

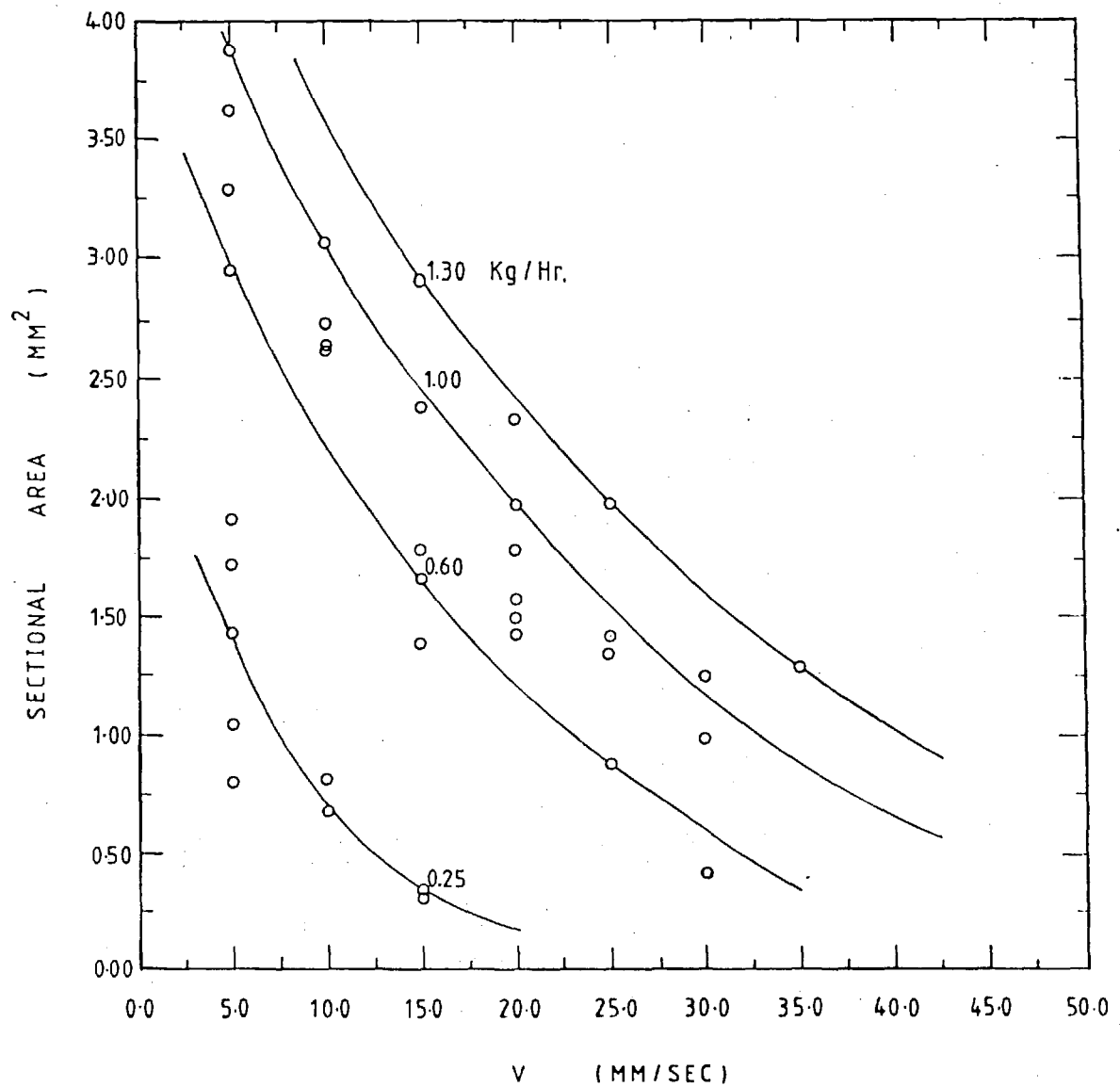


FIG 4.45 SECTIONAL AREA (MM²) vs TRAVERSE SPEED (MM/SEC) FOR A 1.00MM POWDER THICKNESS.

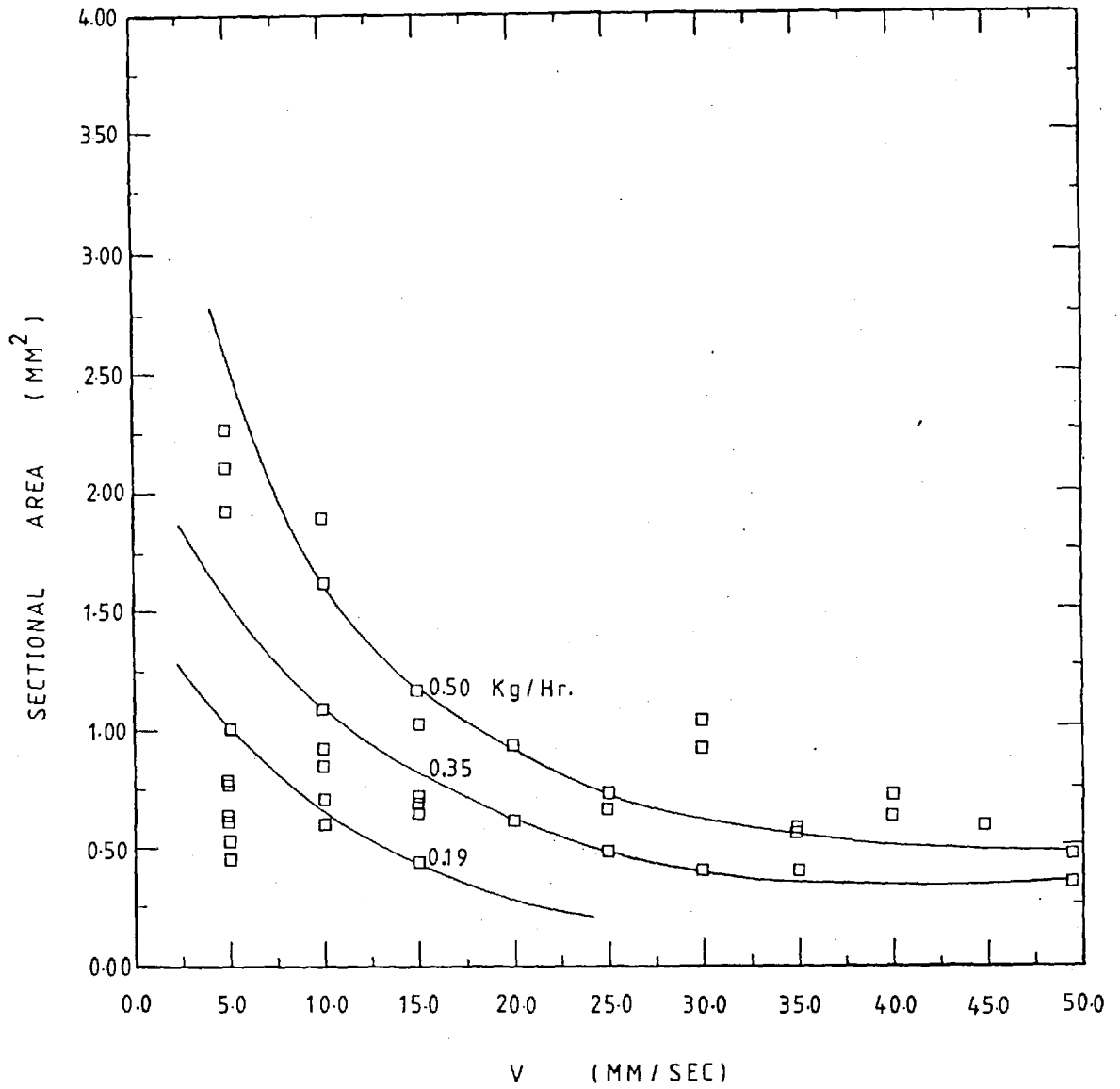


FIG 4.46 SECTIONAL AREA (MM²) vs TRAVERSE SPEED (MM/SEC) FOR A 0.50MM POWDER THICKNESS.

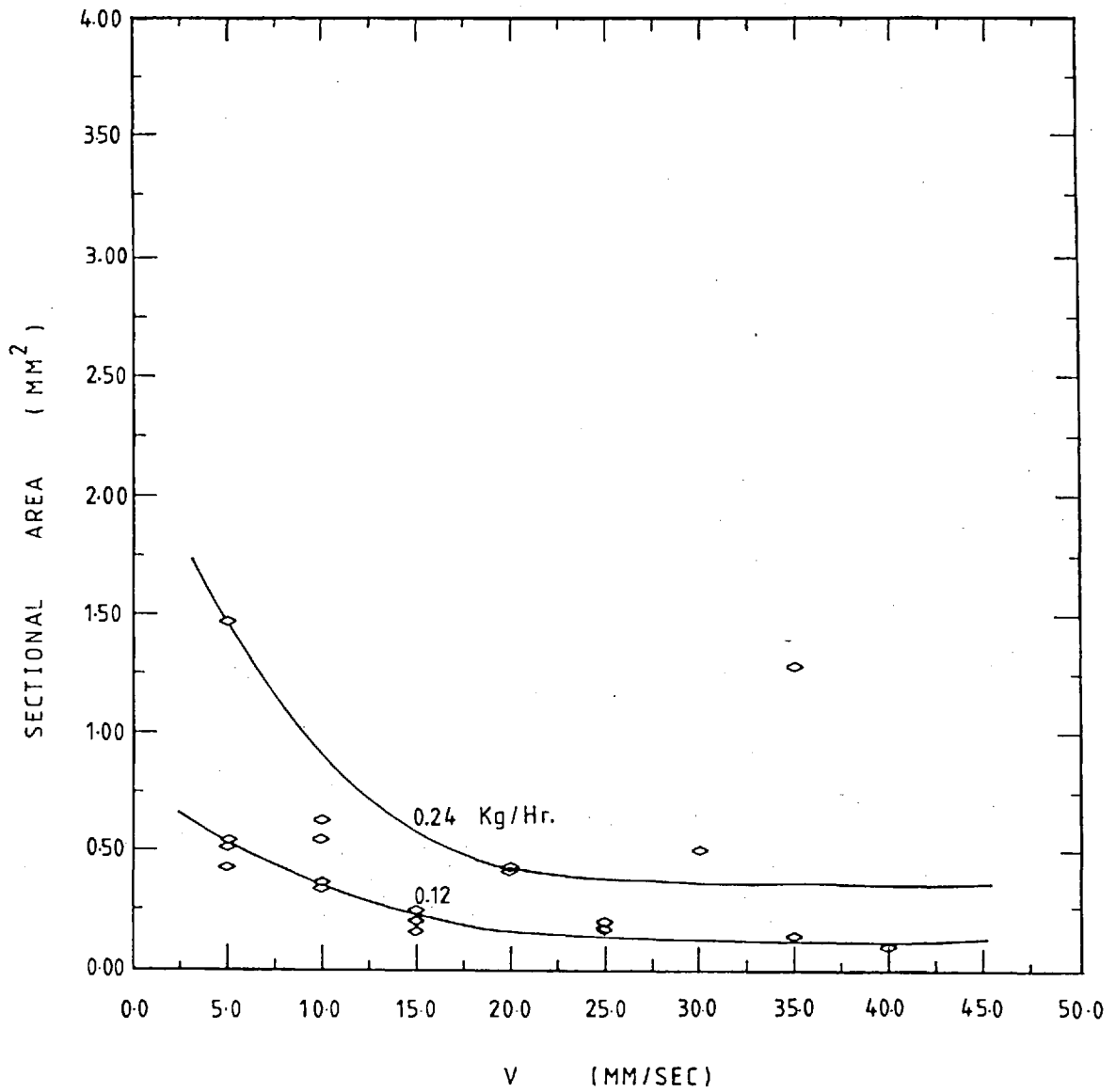


FIG 4.47 SECTIONAL AREA (MM²) vs TRAVERSE SPEED (MM/SEC) FOR A 0.25 MM POWDER THICKNESS.

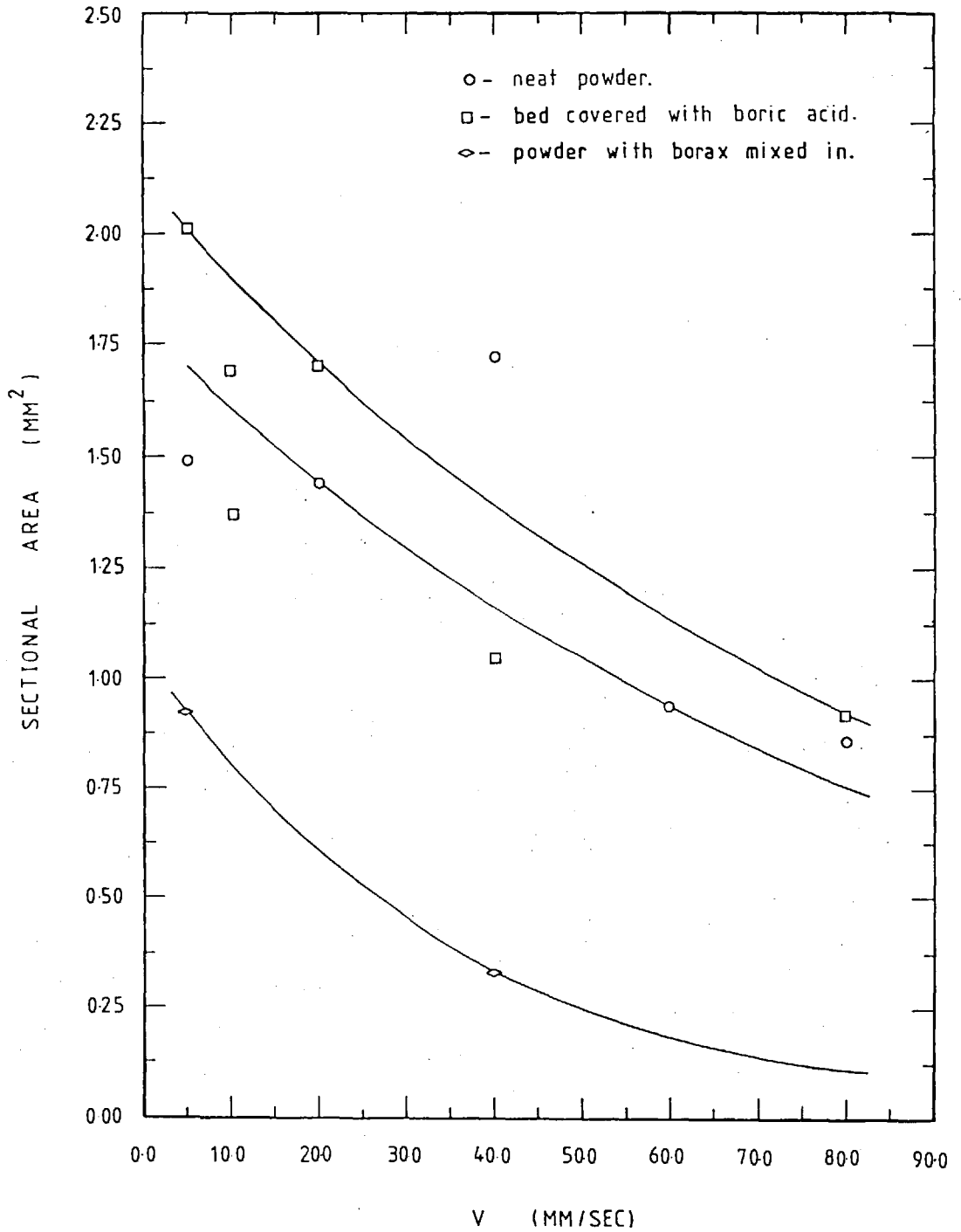


FIG 4.48 SECTIONAL AREA (MM²) vs TRAVERSE SPEED, V (MM/SEC) — FOR A 1.00 MM POWDER THICKNESS AND 2.00 MM BEAM — DIAMETER.

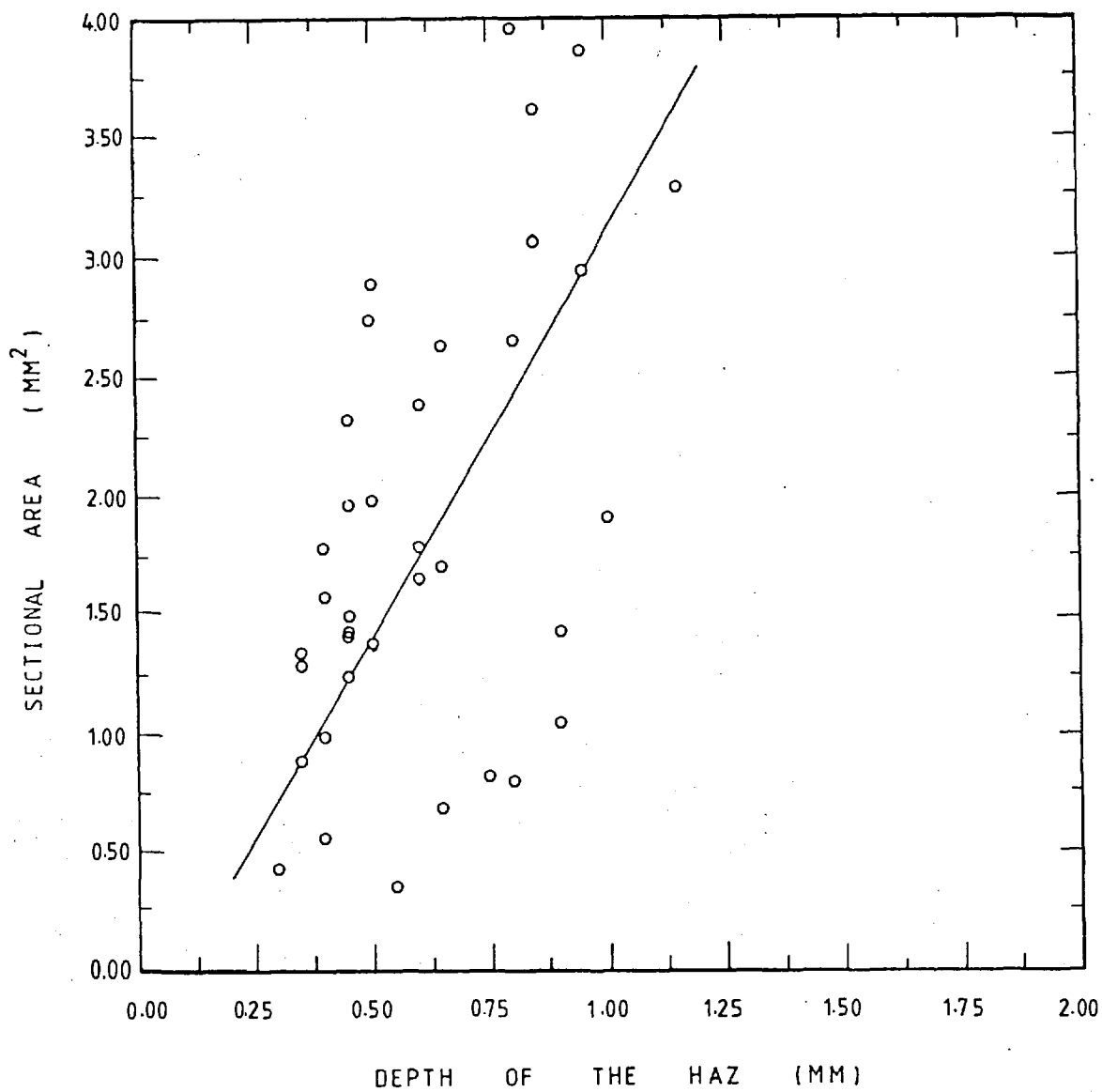
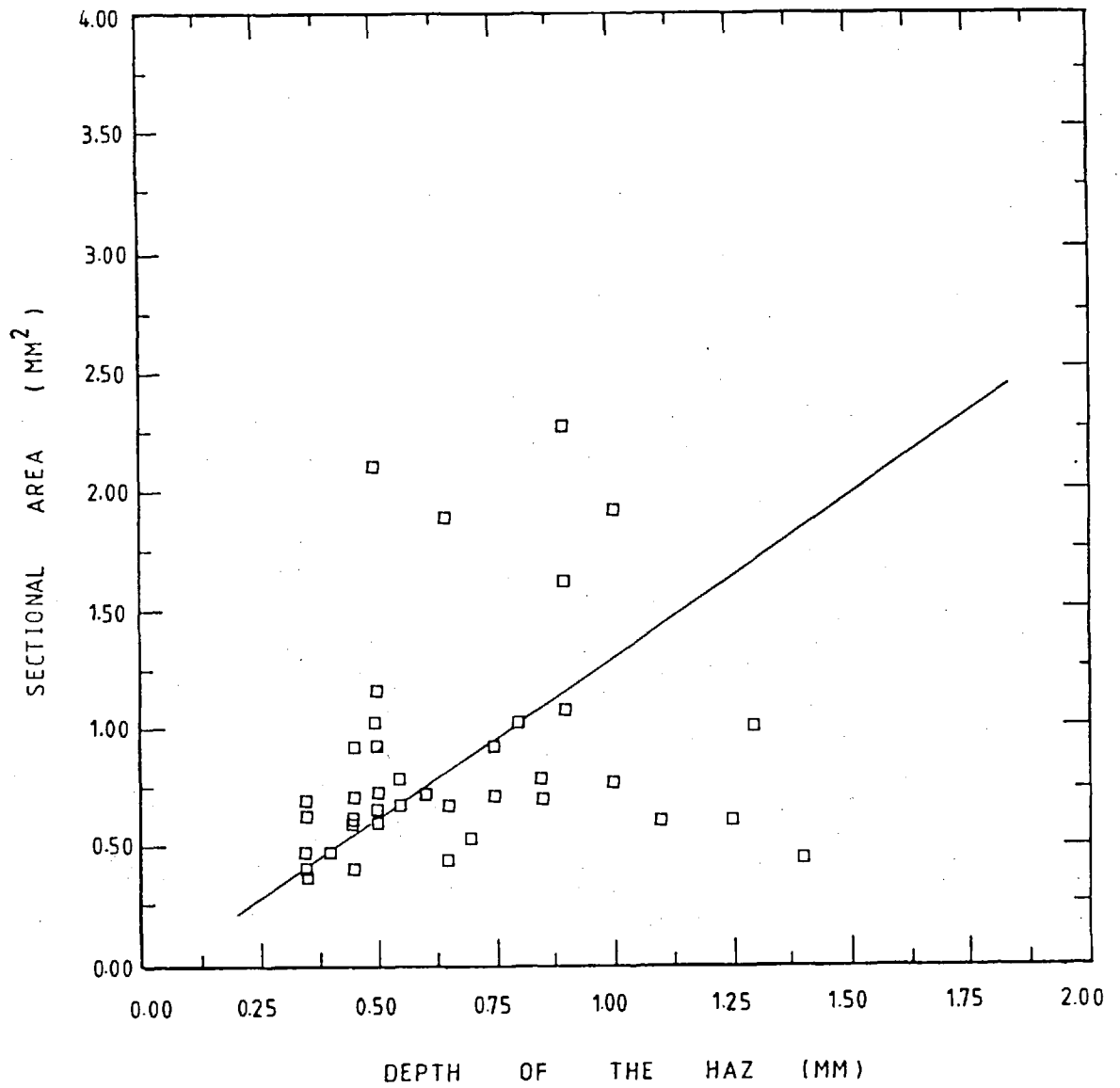


FIG 4.49 SECTIONAL AREA (MM²) vs DEPTH OF THE HAZ (MM) FOR A 1.00 MM POWDER THICKNESS.



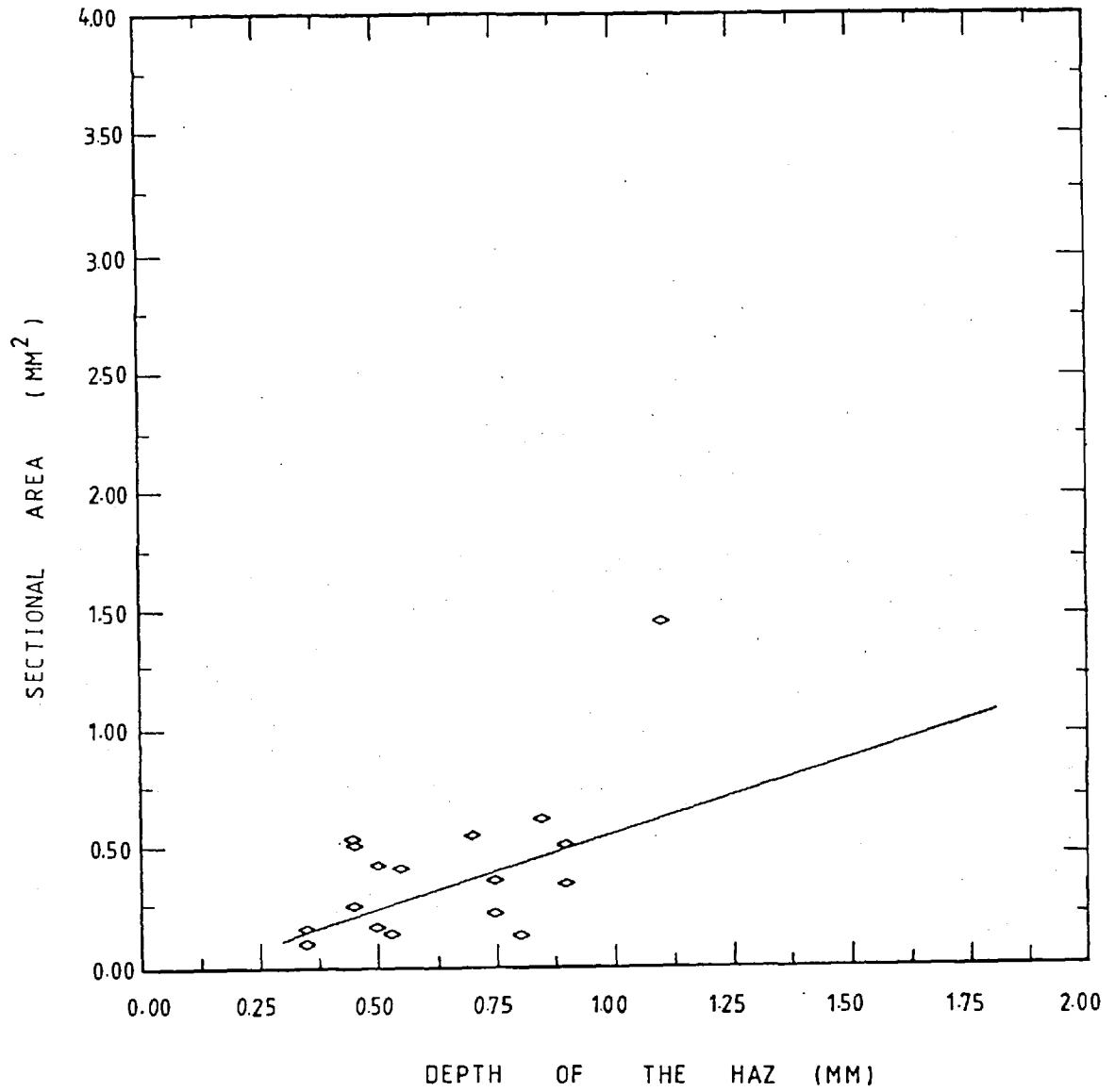


FIG 4.51 SECTIONAL AREA (MM²) vs DEPTH OF THE HAZ (MM) FOR A 0.25 MM POWDER THICKNESS.

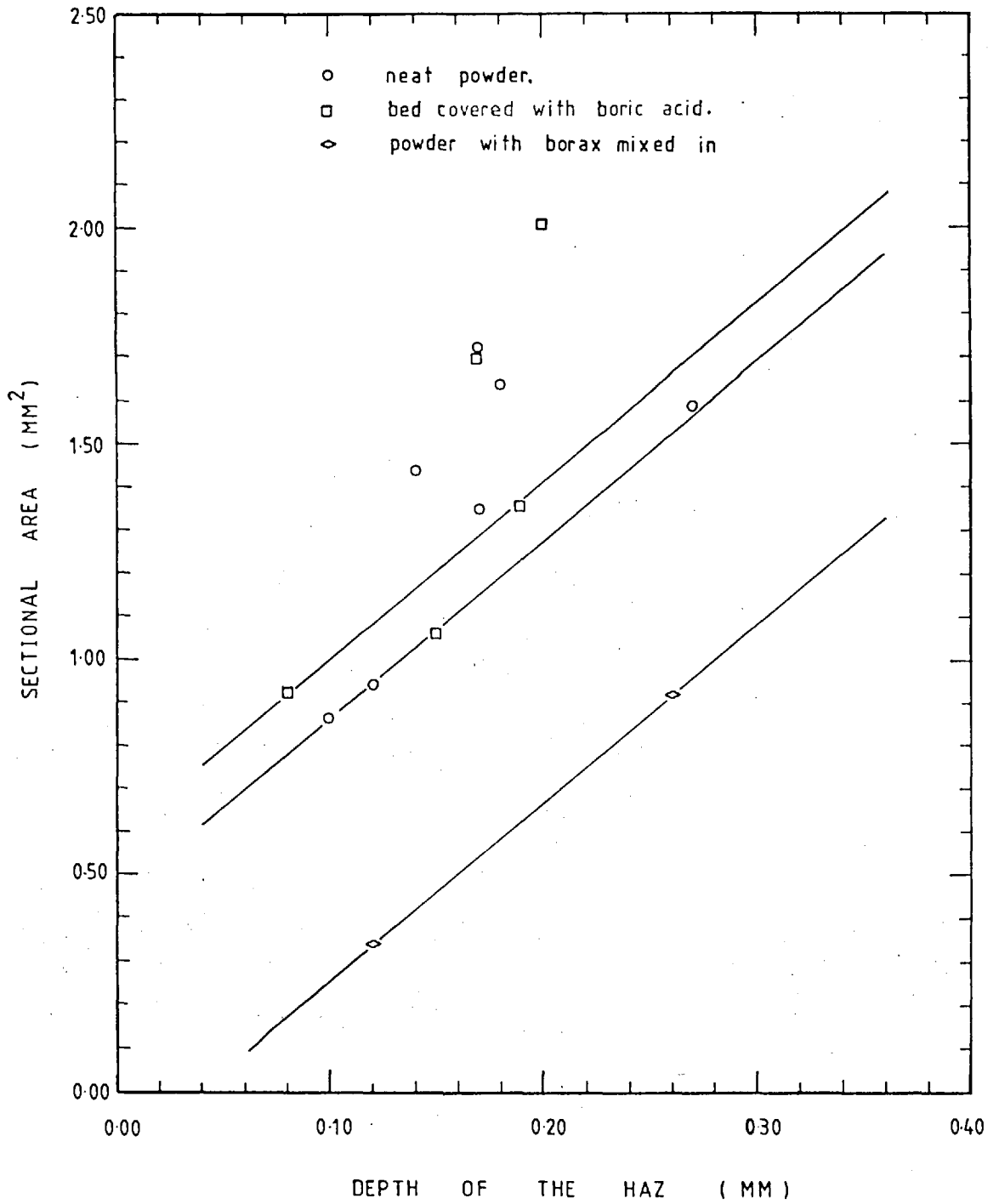


FIG 4.52 SECTIONAL AREA (MM²) vs DEPTH OF THE HAZ (MM) FOR A 1.00 MM POWDER THICKNESS AND 2.00 MM BEAM DIAMETER.

4.5 Quantitative Dilution

The resultant dilution measured on the basis described in section 2.2 for each run was found to vary, with the working conditions, as was expected and could be correlated with the specific energy, and powder bed thickness. From this it can be deduced that there exists an optimum specific energy for a given bed depth, which will produce a continuous adherent track with low dilution. Calculated dilution values are shown in Appendix II.

4.5.1 316 Stainless Steel - Dilution in Surface Cladding

The percentage dilution, calculated as described in section 2.2 and illustrated here by fig 4.53a and 4.53b, was found to be a function of the applied specific energy, as shown in figs 4.54, 4.55 and 4.56 in which it is seen that a decrease of specific energy causes less melting of the substrate and hence a decrease in dilution.

The dilution figures recorded here are artificial since they

assume that there is uniform mixing through the clad trace.

This is rarely found to be the case (ref 8). Even so in the region previously identified as "good" the dilution % is always below 12%.

Variation of dilution with traverse speed can be observed for selected samples having the same incident power and beam diameter.

(e.g. S4 - S7, S8 - S13 etc)

These values are plotted in fig 4.57 - 4.59.

No obvious correlation is noted. The considerable experimental scatter may be due to the intermittent flow of the weld bead causing rippling of the upper surface and interface which would cause a variation in dilution as measured in the manner described here.

For a given specific energy and traverse speed the % dilution increases with decreasing bed depth as shown in 4.54 - 4.56 and 4.57 - 4.59.

4.5.2 Tin-Bronze Dilution in Surface Cladding

No dilution was observed in any example of tin-bronze surface cladding. Probably due to the disparity in melting points between bronze and steel.

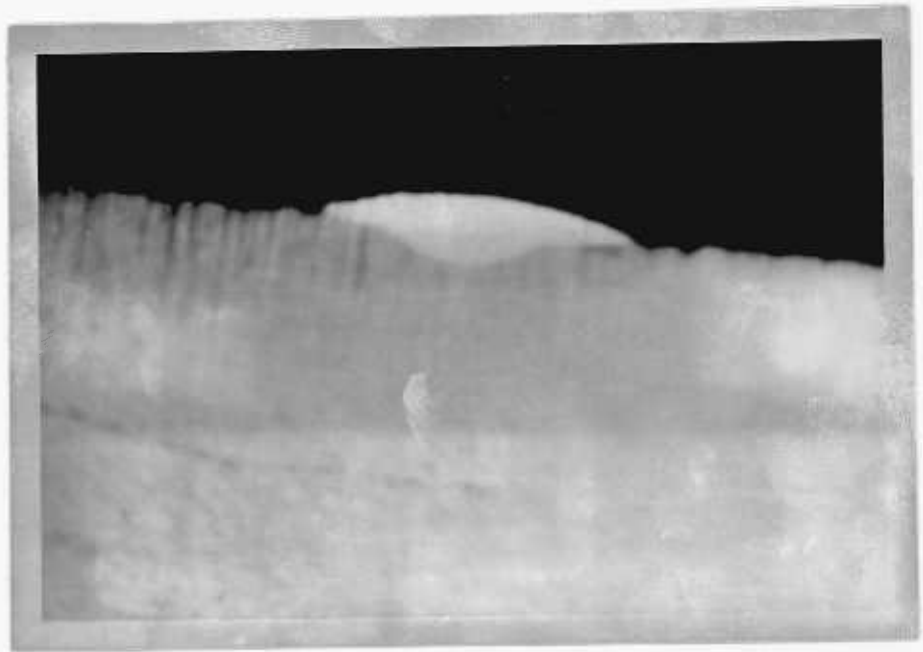


FIG 4.53 a NUGGET CHARACTERISTICS: SPECIMEN NUMBER S74,
 POWER=1 400 W; BEAM DIAMETER=3.2 MM; SPEED=5
 MM/S; POWDER THICKNESS =0.50 MM.
 TOTAL AREA=0.53 MM²; DEPOSITION RATE=0.08 Kg/Hr;
 DILUTION=57.5% .

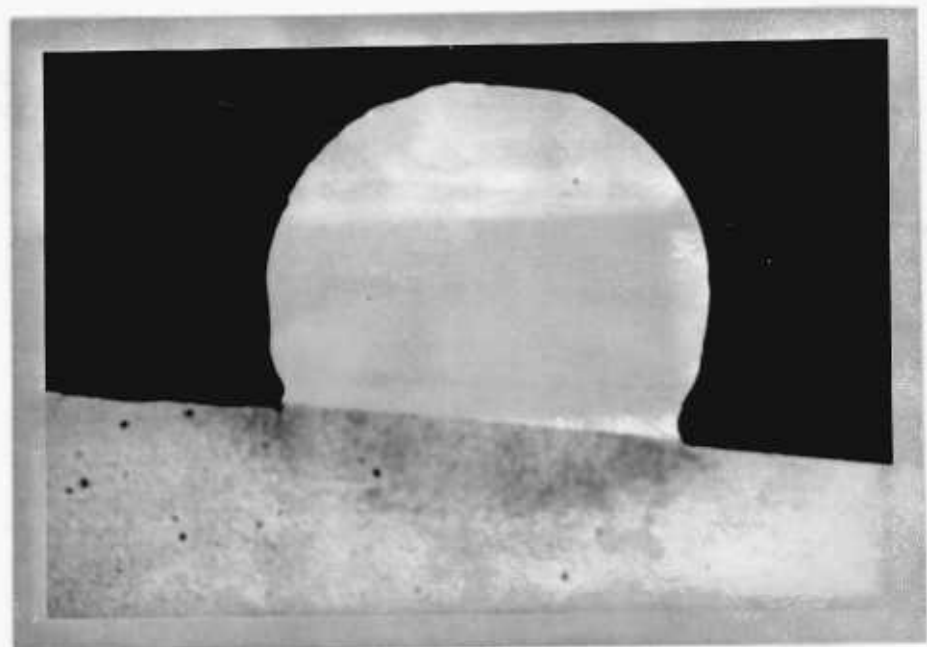


FIG 4.53 b NUGGET CHARACTERISTICS: SPECIMEN NUMBER S123,
 POWER=1800 W, BEAM DIAMETER=5.8 MM; SPEED=10
 MM/S; POWDER THICKNESS=1.00 MM.
 TOTAL AREA=4.19 MM²; DEPOSITION RATE=1.21 Kg/Hr,
 DILUTION=0.13% (0)

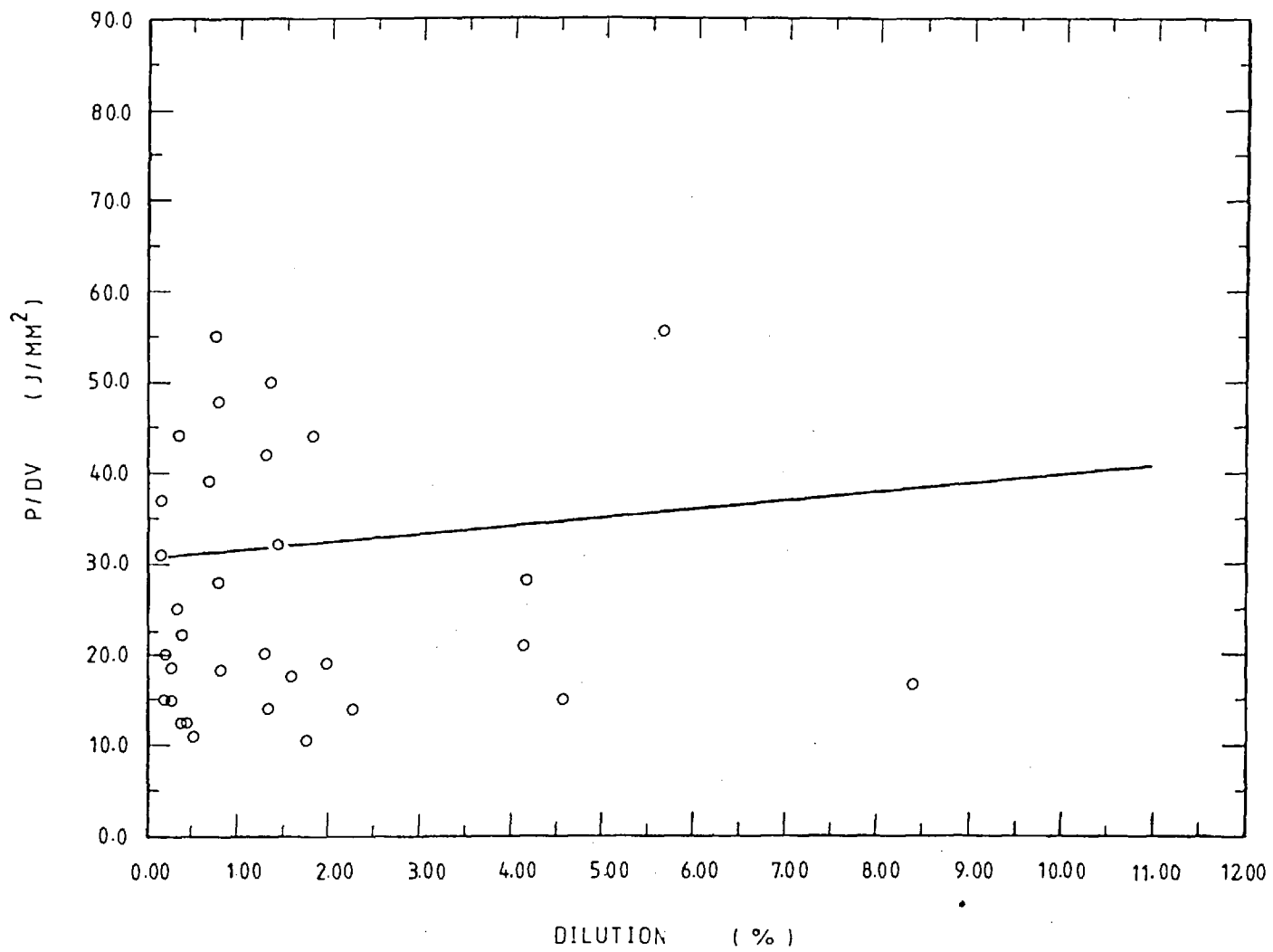


FIG 4.54 ENERGY/UNIT AREA, P/DV (J/MM²) vs DILUTION (%) FOR A 1.00 MM POWDER THICKNESS.

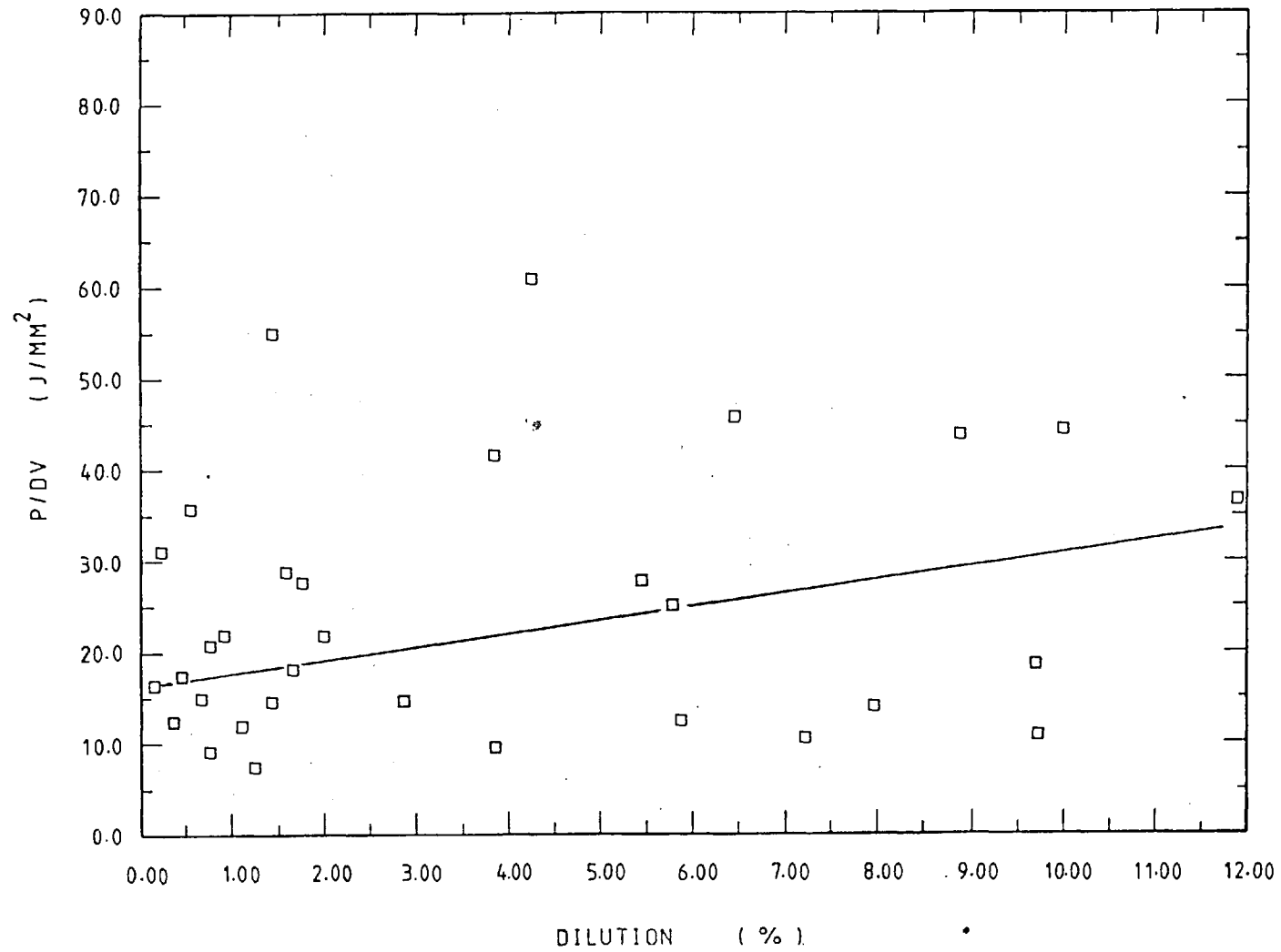


FIG 4.55 ENERGY/UNIT AREA, P/DV (J/MM²) vs DILUTION (%) FOR A 0.50 MM POWDER THICKNESS.

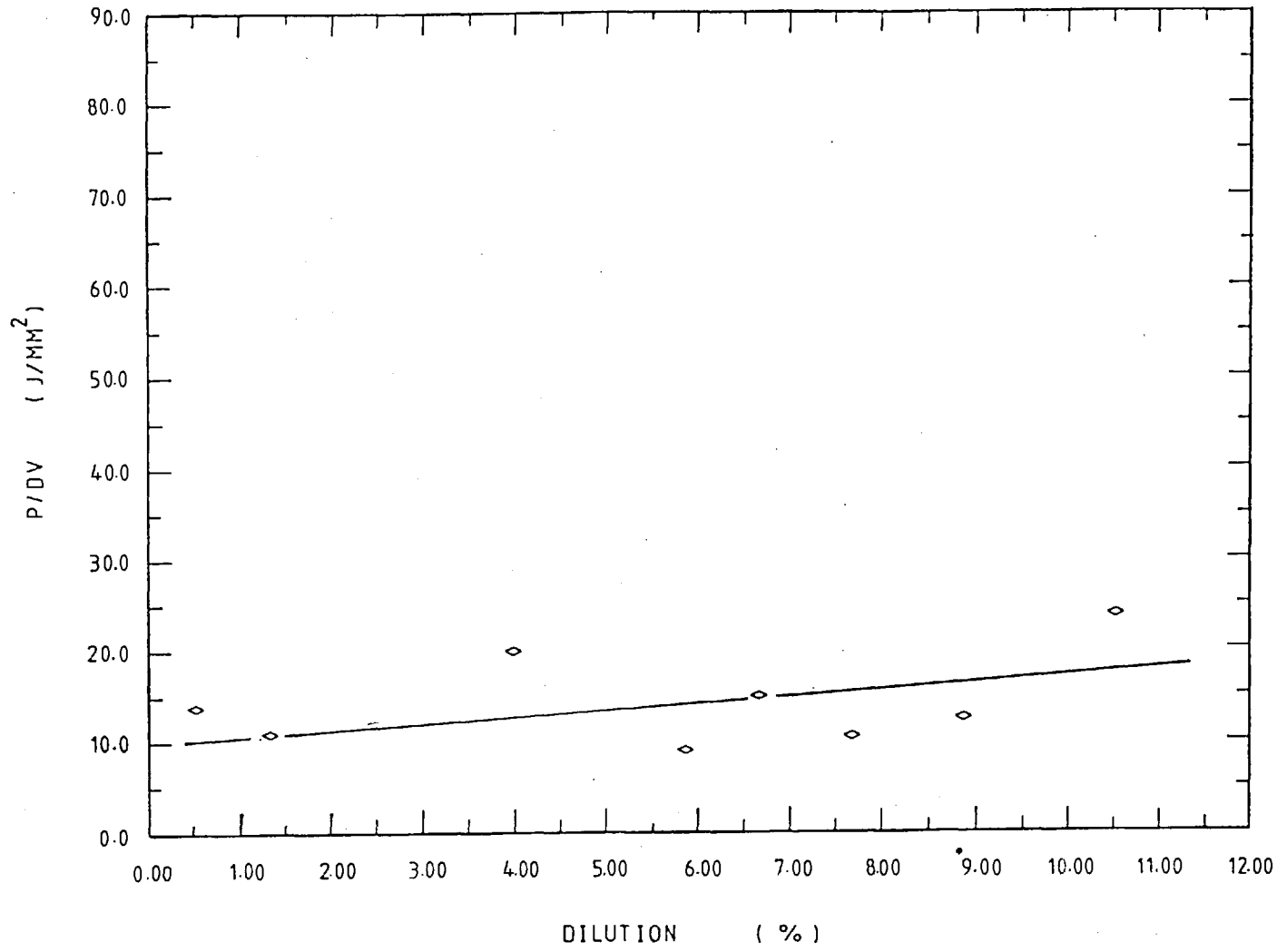


FIG 4.56 ENERGY/UNIT AREA, P/DV (J/MM²) vs DILUTION (%) FOR A 0.25 MM POWDER THICKNESS.

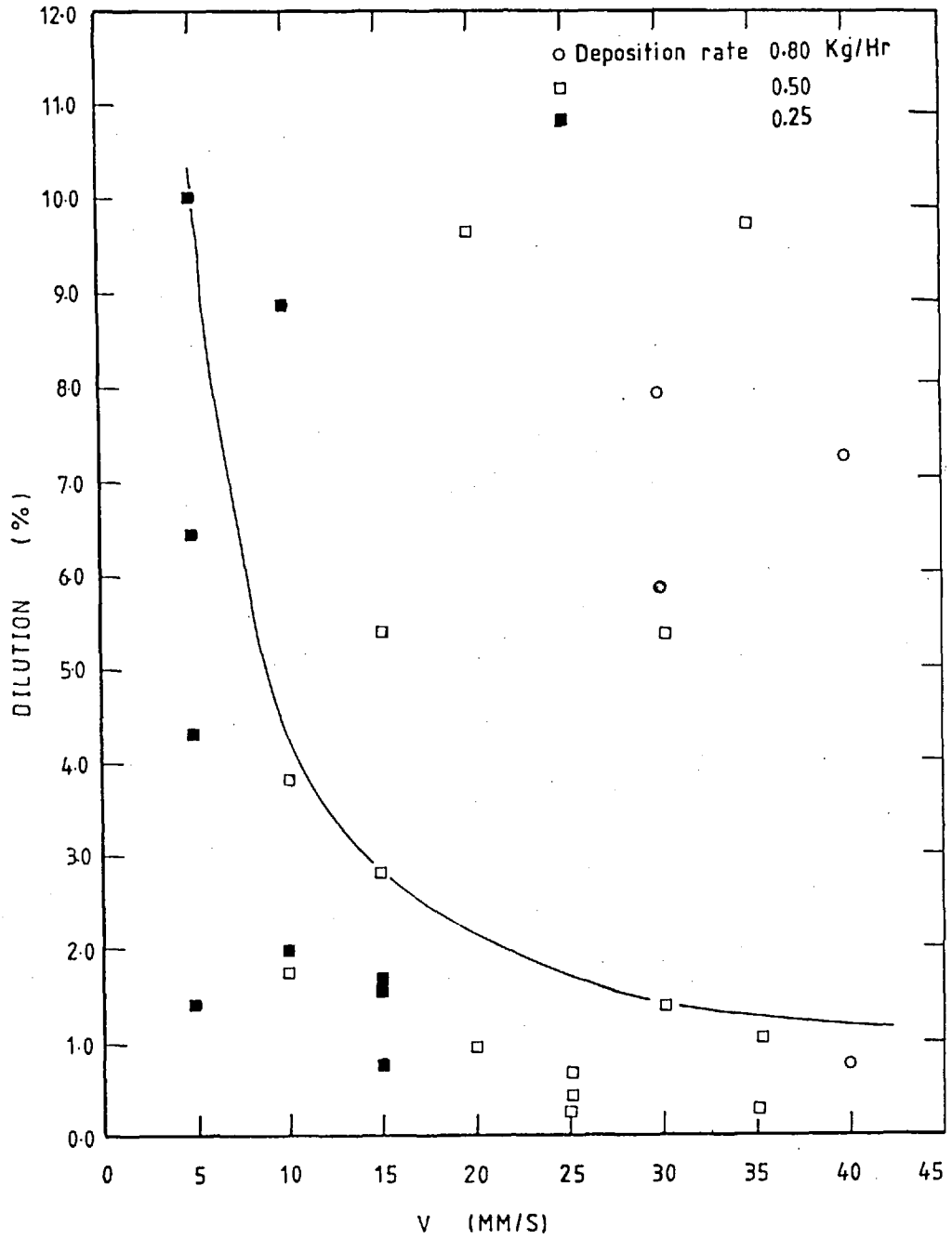


FIG 4.58 DILUTION (%) vs TRAVERSE SPEED (MM/S) FOR A 0.50 MM POWDER THICKNESS.

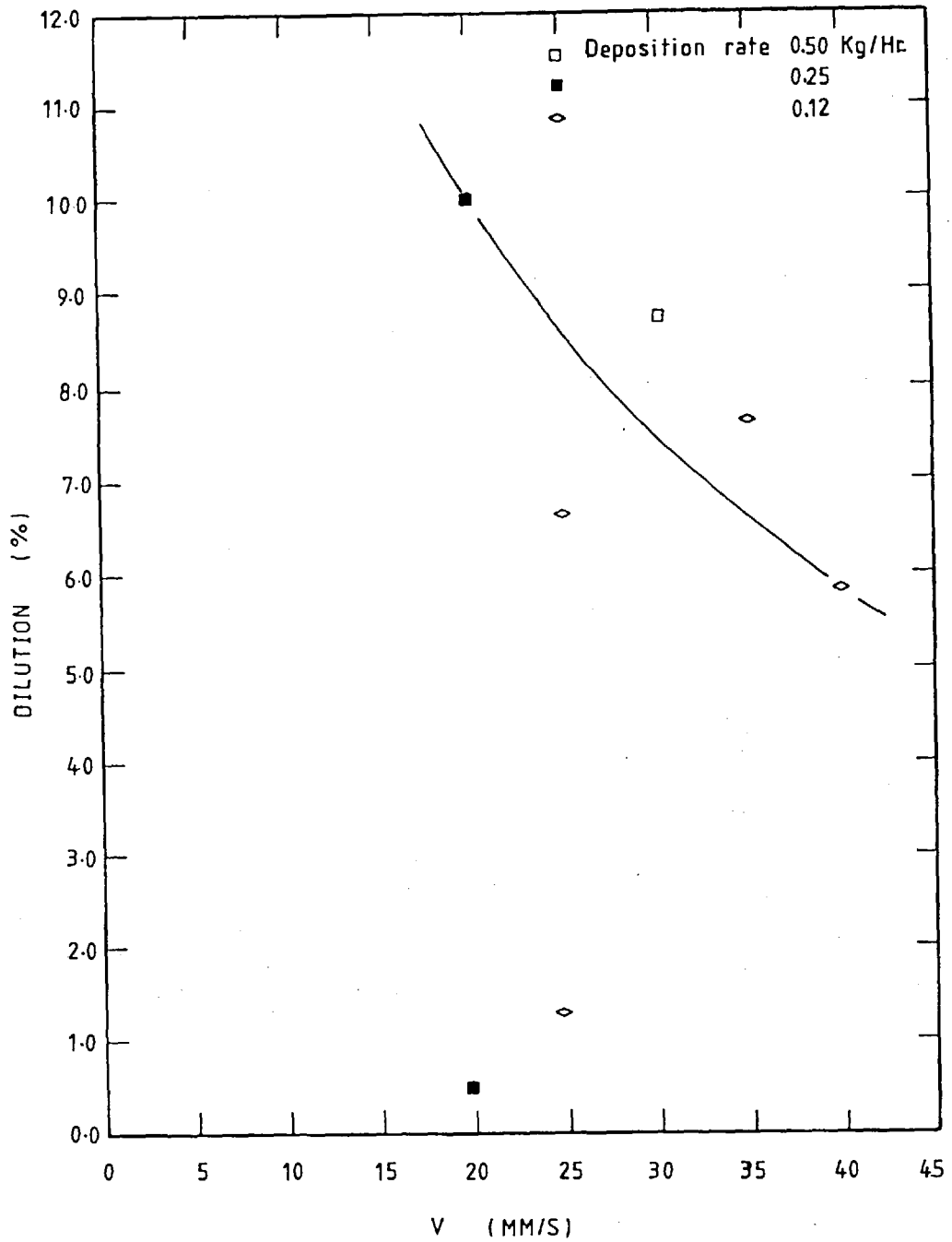


FIG 4.59 DILUTION (%) vs TRAVERSE SPEED (MM/S) FOR A 0.25 MM POWDER THICKNESS.

4.6 Deposition Rate in Surface Cladding

Deposition rate, in the surface cladding process can be measured as the weight of material deposited per unit of time.

The deposition rate using powdered stainless steel 316 and tin-bronze after melting with a laser beam was found to be dependent on powder bed thickness, type of powder alloy, beam power, beam diameter and traverse speed.

4.6.1 Deposition Rates for 316 Stainless Steel

The variation of deposition rate with traverse speed is shown in fig 4.60, 4.61 and 4.62 for various bed depths. The values of deposition rate observed are also given in Appendix II. The deposition rate increased with traverse speed as expected for fixed bed deposition as practical here, but a maximum deposition rate was observed at that speed corresponding to a specific energy near the onset of discontinuous traces. The observed rate of deposition rates are shown in Table 4.4.

TABLE 4.4 RANGE OF DEPOSITION RATE OBSERVED WITH DIFFERENT BED DEPTHS OF 316 STAINLESS STEEL

BED DEPTH mm	MINIMUM Kg/Hr	MAXIMUM Kg/Hr
1.00	0.12	1.43
0.50	0.06	0.89
0.25	0.03	0.44

The variation of deposition rate with traverse speed for constant beam power and beam diameter for three different bed depths is shown in fig 4.63.

To understand the relation between deposition rate, deposit thickness and dilution see fig 4.64 where the curves indicate the following:

- (a) for a given deposition rate, dilution decreases as the deposit thickness is increased.
- (b) for a given deposit thickness, dilution increases as the deposition rate is increased, which implies an increase in power density and this in turn increases dilution.

It can also be seen that the deposition rate is limited by the required deposit thickness and acceptable percentage dilution.

For example, if the proposed bead height of surface cladding is 1.00 mm, then, at the dilution of 2%, the maximum deposition rate is fixed at about 0.50 Kg/Hr. However, if the percentage dilution of 6% still acceptable, then a deposition rate of 0.80 Kg/Hr can be used for the purpose.

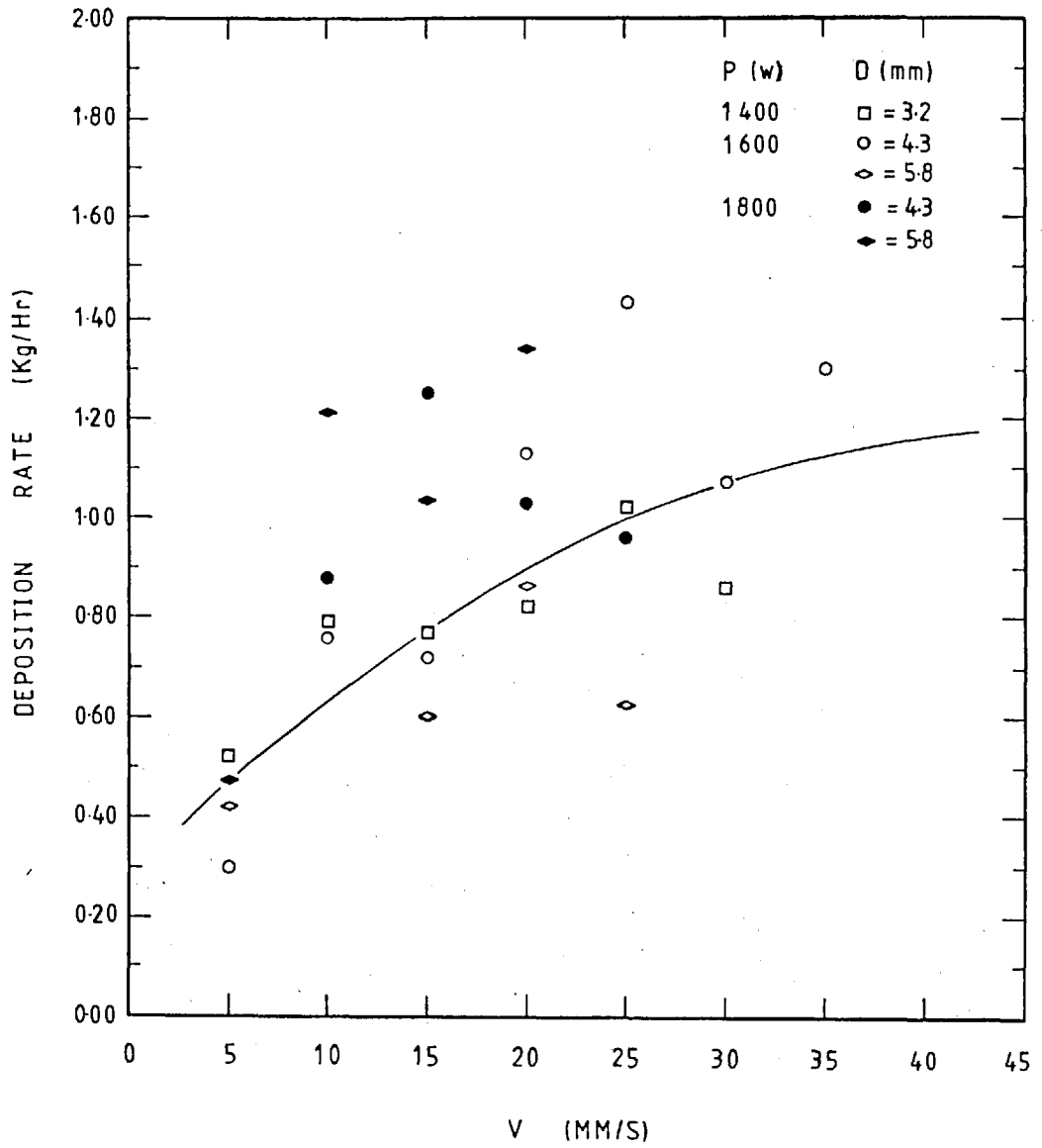


FIG 4.60 DEPOSITION RATE (Kg/Hr) vs TRAVERSE SPEED (MM/S) FOR A 1.00 MM POWDER THICKNESS.

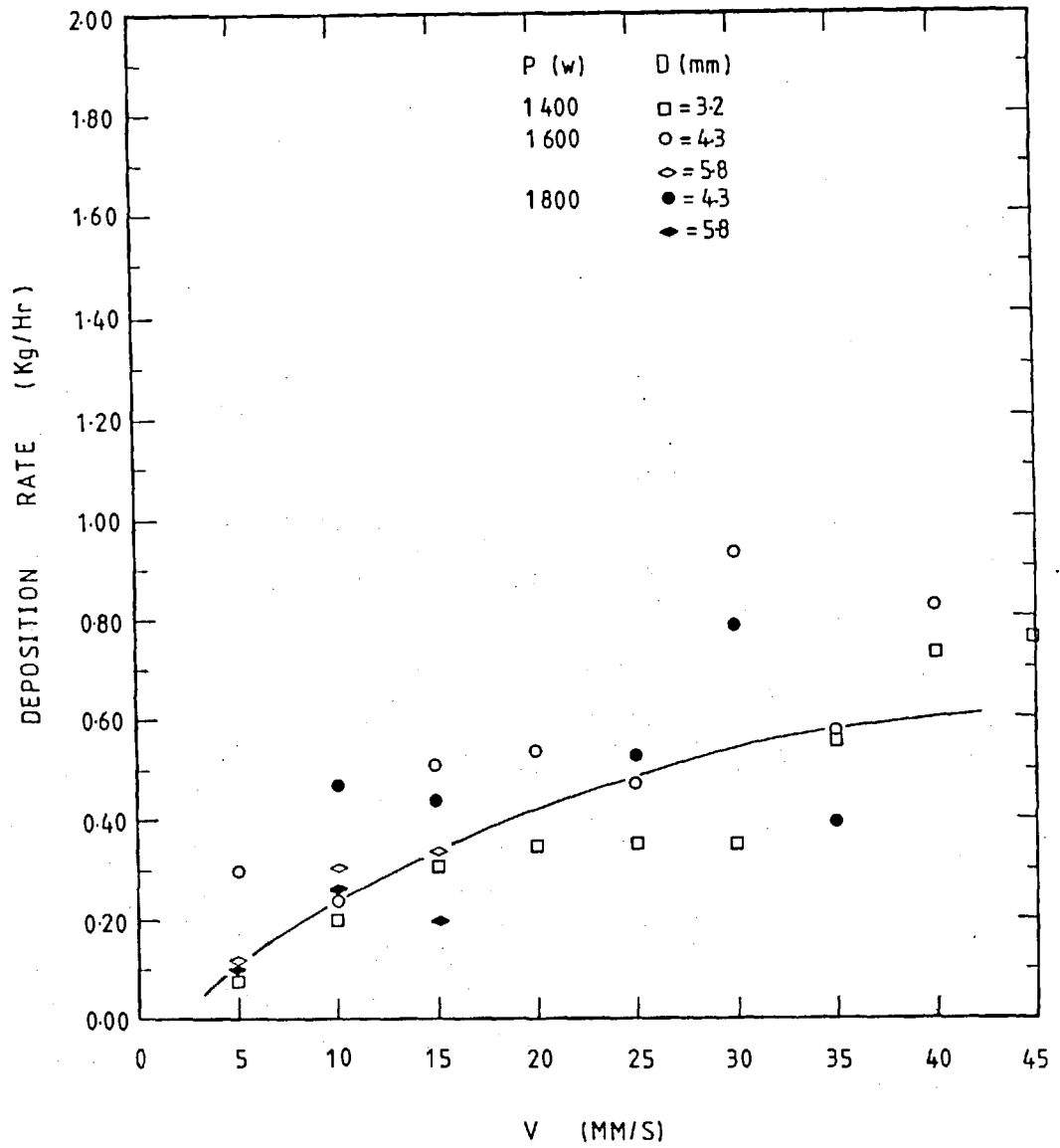


FIG 4.61 DEPOSITION RATE (Kg/Hr) vs TRAVERSE SPEED (MM/S) FOR A 0.50 MM POWDER THICKNESS.

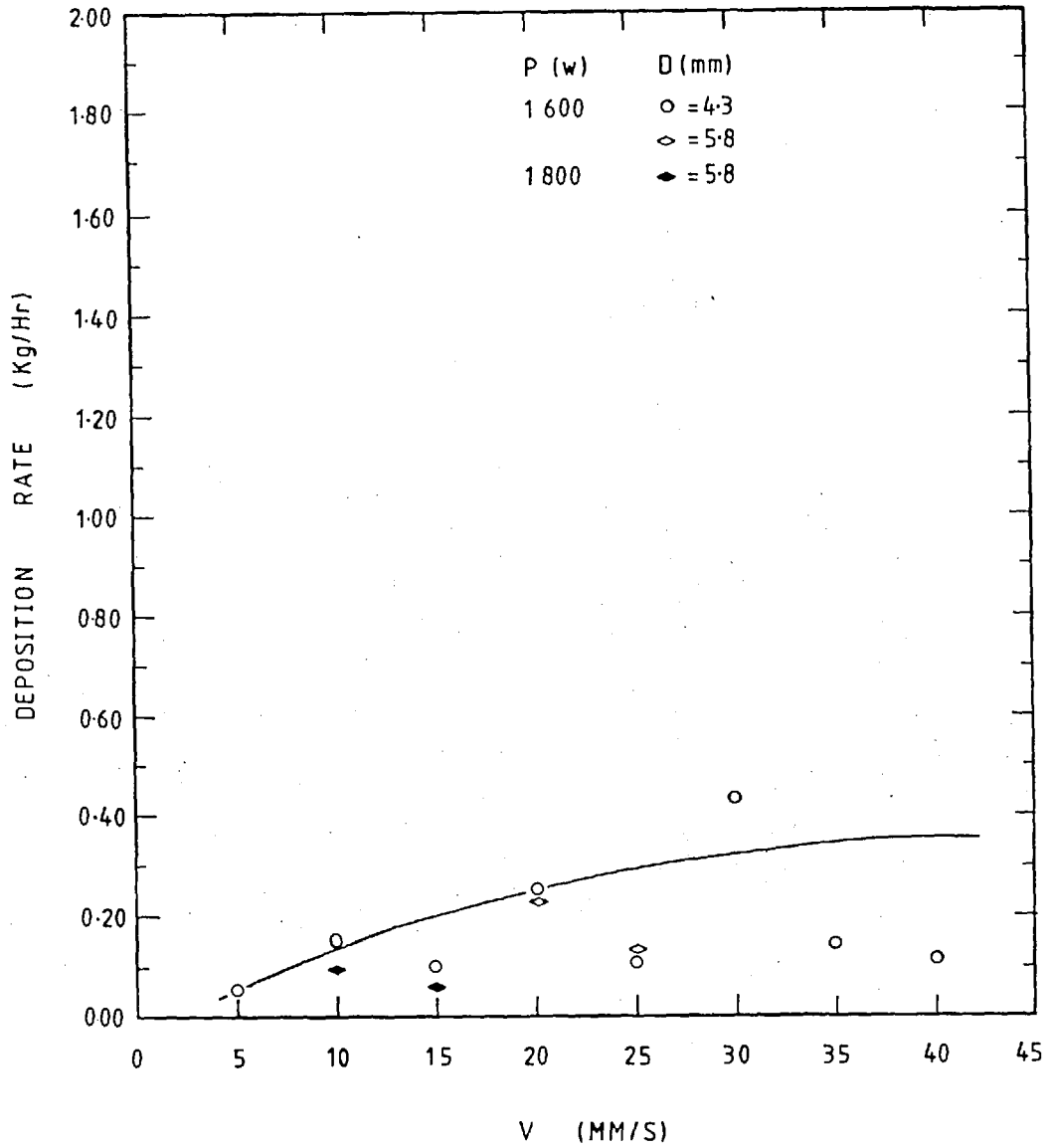


FIG 4.62 DEPOSITION RATE (Kg/Hr) vs TRAVERSE SPEED (MM/S) FOR A 0.25 MM POWDER THICKNESS.

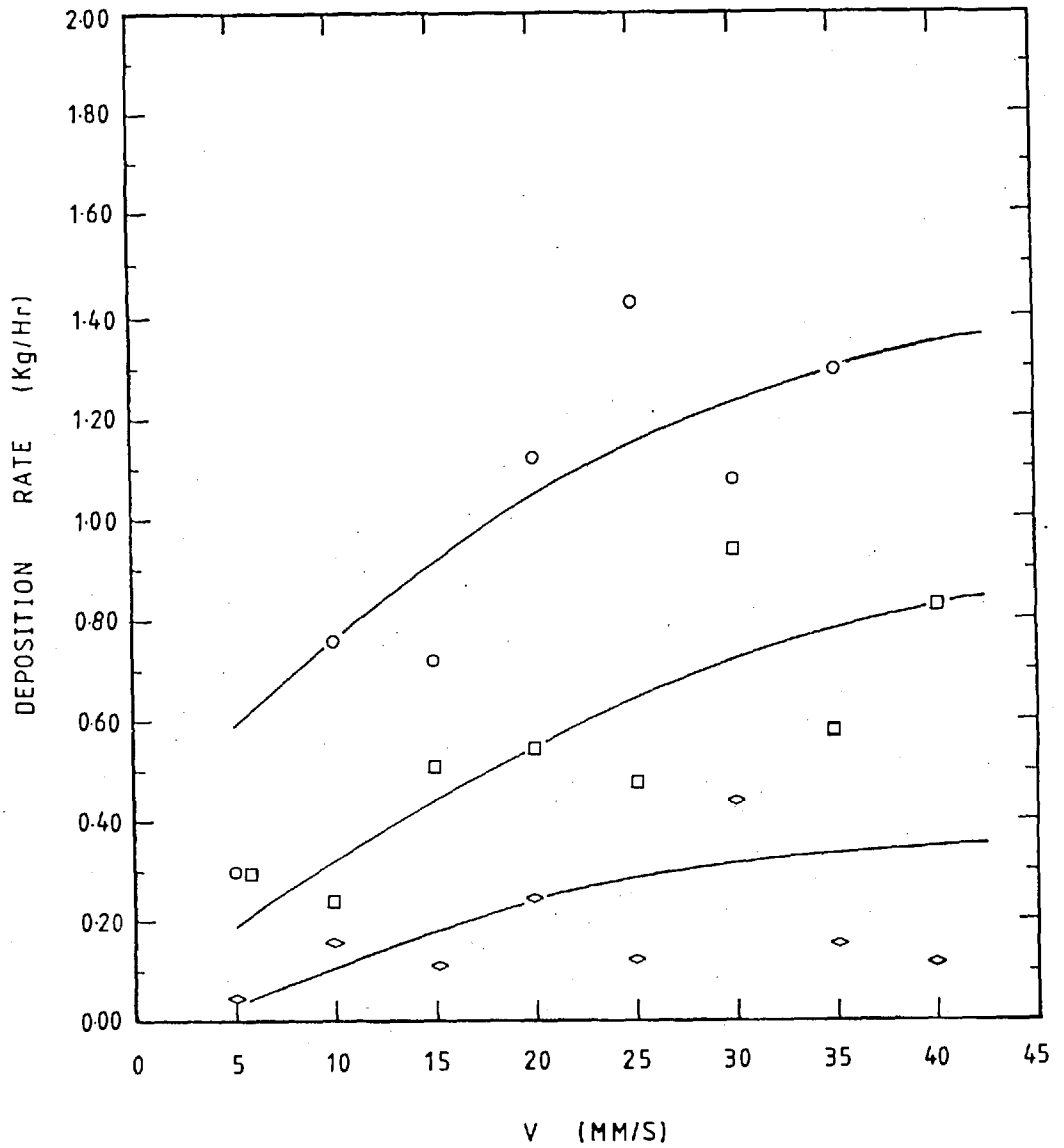


FIG 4.63 DEPOSITION RATE (Kg/Hr) vs TRAVERSE SPEED (MM/S) FOR A BEAM POWER=1600 W, BEAM DIAMETER=4.3 MM AND \circ = 1.00, \square = 0.50, \diamond = 0.25 MM POWDER THICKNESS.

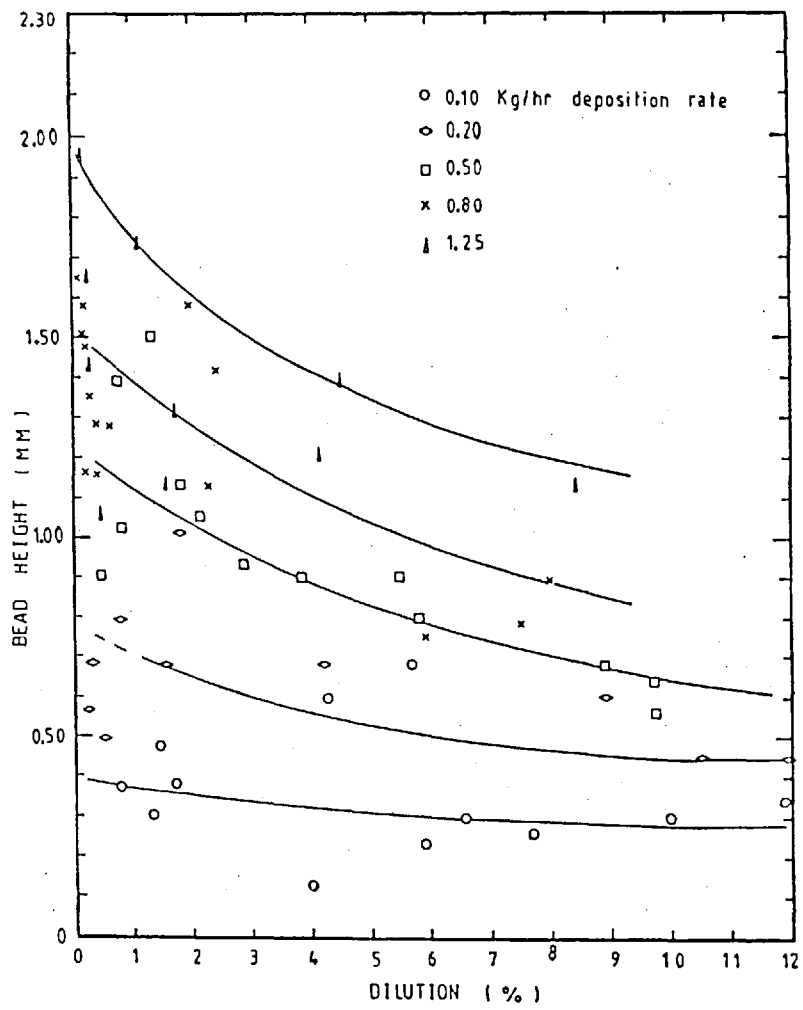


FIG 4.64 BEAD HEIGHT (MM) vs DILUTION (%), FOR 316 STAINLESS STEEL.

4.6.2 Deposition rate for tin-bronze, for a 1.00mm powder bed thickness of neat powder it is observed that for a constant beam power and beam diameter the deposition rate increases when traverse speed is increased, as can be seen in appendix 1.2 or in fig 4.65. The effect of boric acid, as an active surface agent was, that when the bed was covered with borax the deposition rate increased for a given traverse speed. However, the deposition rate decreased when the powder and borax were mixed for a constant traverse as can be seen in fig 4.65.

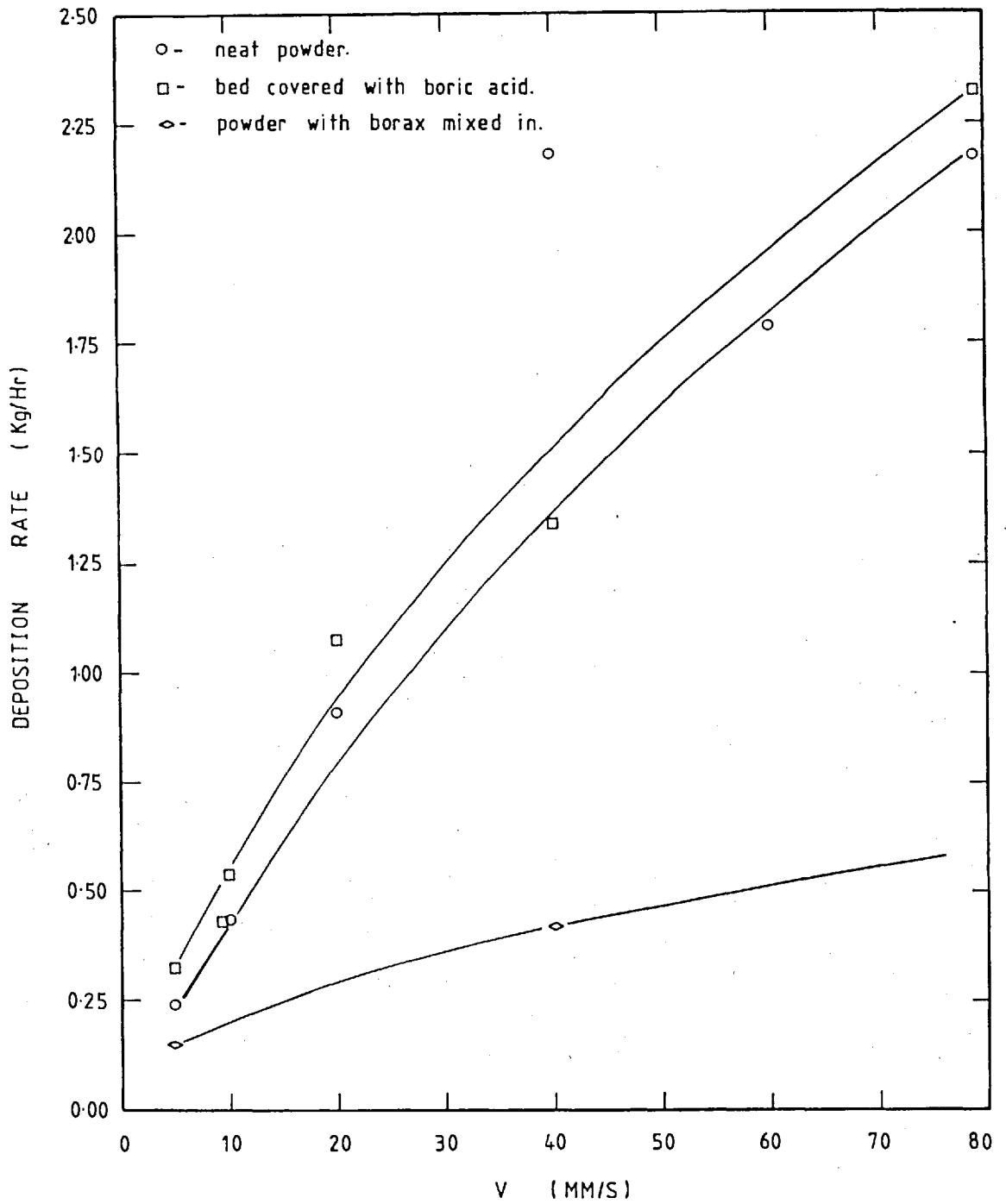


FIG 4.65 DEPOSITION RATE (Kg/Hr) vs TRAVERSE SPEED (MM/S) FOR A 1.00 MM POWDER THICKNESS AND 200 MM BEAM DIAMETER.

4.7 Solidification Structures in Type 316 Stainless Steel Surface Cladding

The solidification mechanism of austenitic stainless steel weldments are not fully understood and thus has prevented investigators from gaining a full understanding of the role of delta ferrite in reducing the hot cracking susceptibility of these alloys. The ratio of ferrite-stabilizing elements (Cr, Mo, Si) to austenite-stabilizing elements (Ni, Mn, C) has been adjusted to prevent the formation of cracks during solidification in austenitic stainless steel, the solidified structure should have a certain percentage of delta ferrite. All fusion welding processing involve microsegregation of the component alloying elements (19). In stainless steel weldments, chromium is rejected to the liquid during primary austenite solidification and nickel is rejected to the liquid during primary delta ferrite solidification. Elements such as silicon, molybdenum, sulphur and phosphorus which are more soluble in delta ferrite are rejected to the liquid during primary austenite solidification. Elements such as carbon and manganese are more soluble in austenite and are thus rejected to the liquid during primary delta ferrite solidification. Sulphur and phosphorus form low melting eutectics between sulphides

and phosphides, and silicon tends to form glassy silicate films. In alloys solidifying as primary austenite, sulphur phosphorus, and silicon are rejected to the liquid, form low melting constituents in the interdendritic regions and thus cause hot cracking. Alloys solidifying as primary delta ferrite reject less of these elements to the liquid and consequently are more resistant to hot cracking.

The content of delta ferrite in 316 stainless steel should be at least 1% to avoid cracking when this steel is welded.

According to the Schaeffler diagram fig 4.66 (Ref 16), if the chemical composition does not change during the deposition the percentage of delta ferrite should be in the range of 2% to 5% with a $C_{req}/N_{req} \simeq 1.45$ relation, where C_{req} is the chromium equivalent and N_{req} is the nickel equivalent.

Considering equilibrium solidification, fig 4.67 is a schematic pseudo-binary slice of the iron-chromium-nickel ternary system taken at 70% Fe. The approximate location of type 316 stainless steel (considering only the iron chromium and nickel contents) is shown by the vertical line. According to this diagram, the initial stage would begin at T_1 . The diagram also predicts that the end of solidification would be when the temperature reaches T_2 . As the alloy cools below

the solidus it must pass through the two phase $\gamma + \delta$ region, and then enter the single phase austenitic region as indicated in fig 4.67. However, the rate of cooling through the two phase $\gamma + \delta$ region is believed to be so fast that the diffusion-controlled transformation predicted by equilibrium cannot occur. Instead, the delta ferrite, is believed to transform to austenite by a diffusionless massive transformation. This is made possible by the fact that for the alloy in question, at temperatures below T_3 austenite is the stable phase. Therefore, it is merely necessary to convert the body-centered cubic ferritic crystal structure to the face-centered cubic crystal structure of austenite during rapid cooling.

Concerning the mode of solidification, and in accordance to the theory of metal solidification (20), the character of the substructure is determined by the degree of constitutional supercooling, by the temperature gradient (G) and the square root of solidification rate ($R^{1/2}$). The ratio $G/R^{1/2}$ influences in the mechanism of solidification. High $G/R^{1/2}$ ratios are associated with planar front cellular; low levels with equiaxed-dendritic; between these extreme possibilities there are transient types: cellular-dendritic, columnar-dendritic. Whereas the product $G.R$

gives the cooling rate (\dot{T}) which controls the scale of the structure forming.

It is known that the instantaneous solidification rate (R) in a given point of a solidification isotherm depends upon traverse speed (V) according to figs 4.68 (19).

$$R = V \cos \theta \quad (1)$$

where

θ = Angle between traverse vector and the normal to the isotherm in a given point

Thus the growth velocity would vary from $R=0$ at the sides of the pool (points A and C) where $\theta = 90^\circ$, to a maximum of $R = V$ at the centerline of the clad (point E) where $\theta=0$.

The cooling rate (\dot{T}) can be expressed as a time dependence of a temperature change,

$$\dot{T} = \frac{\partial T}{\partial t} \quad (2)$$

and the temperature gradient (G) as change of temperature with the distance in the direction of the normal

$$G = \frac{\partial T}{\partial x} \quad (3)$$

$$\text{then, } \dot{T} = \frac{\partial T}{\partial x} \cdot \frac{\partial x}{\partial t} = G \cdot R \quad (4)$$

from equations (1) and (4) it follows that

$$T = G \cdot V \cdot \cos \theta$$

in other words, the cooling rate at a given transverse speed varies with position in the molten pool area, for example at

at point A where θ approaches 90° the cooling rate approaches zero, at the same traverse speed but with different factors influencing the cooling rate in the clad axis, various types of structure and thus also various clad metal properties can be obtained.

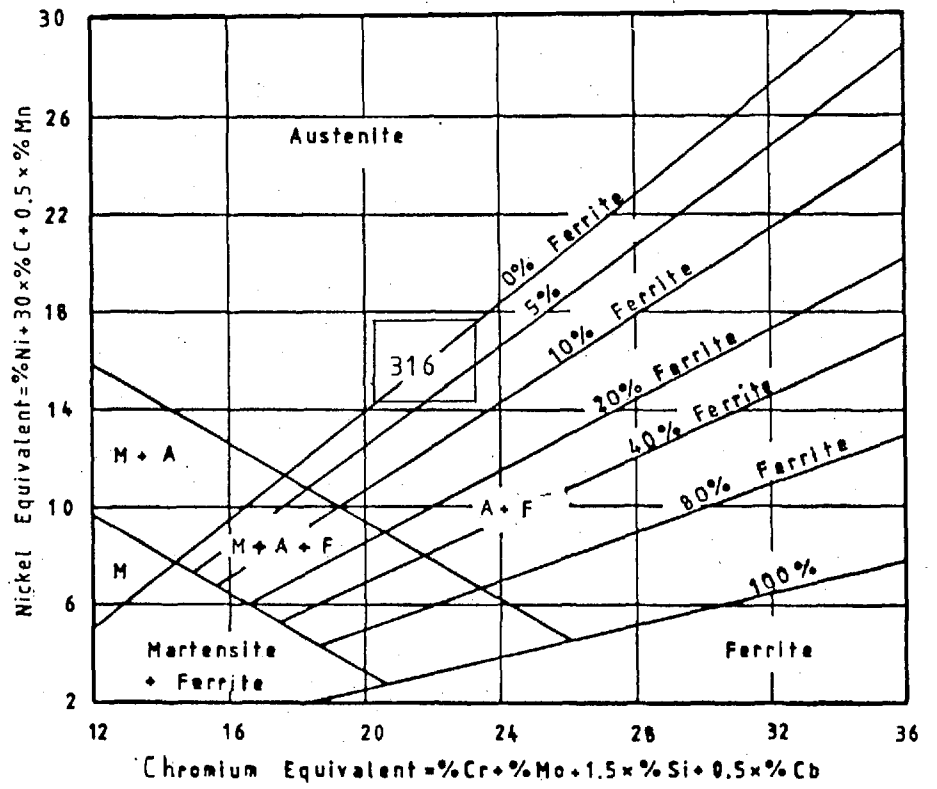


FIG 4.66 CONSTITUTION DIAGRAM FOR STAINLESS STEEL AS A WELD DEPOSIT (REF. 15).

4.8 Metallographic Observations

Observations on the cross section of a clad trace by optical microscopy show distinct variations in microstructure from the top of the trace down to the interface and into the heat-affected zone (HAZ) of the substrate.

4.8.1 316 Stainless Steel Surface Cladding

The structures resulting from solidification in austenitic 316 stainless steel cladding were found to be predominantly cellular-dendritic. In fig 4.69 there can be seen different forms of structures that could be dependent on the redistribution of the elements i.e. microsegregation, as well as on the different gradients and cooling rate during the solidification.

At the top of fig 4.69 cellular grain formation produced by solidification in the cellular mode is observed, a similar structure can be observed in fig 4.71, where the grain was, perhaps, quite well developed by etching. In the centre of fig 4.69 cellular-dendritic grains can be seen with different growth directions and grain sizes similar shapes of grain are observed in figs 4.71, 4.72 and 4.73.

At the bottom of fig 4.69, where the interface is located, the resultant grain is different from the others described; planar grains are observed which was produced by the planar growth mode of solidification.



FIG 4.69 MICROSTRUCTURE 316 STAINLESS STEEL CLADDING, SPECIMEN NUMBER S62; POWER=1400 W; BEAM DIAMETER=5.8 MM; SPEED=5 MM/S; POWDER THICKNESS=1.00 MM; ETCHED IN HCl + HNO₃ AND H₂O SOLUTION, X110.

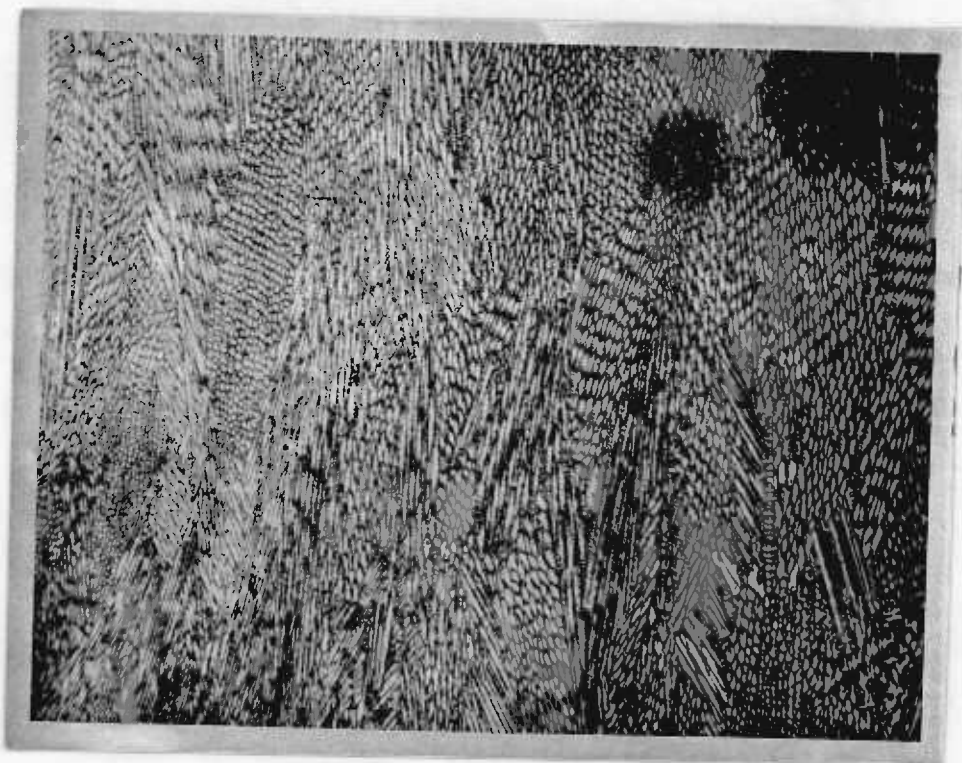


FIG 4.70 MICROSTRUCTURE 316 STAINLESS STEEL CLADDING, SPECIMEN NUMBER S68; POWER=1400 W; BEAM DIAMETER=3.2 MM; SPEED=10 MM/S; POWDER THICKNESS=1.00 MM; ETCHED IN HCl + HNO₃ AND H₂O SOLUTION, X110.

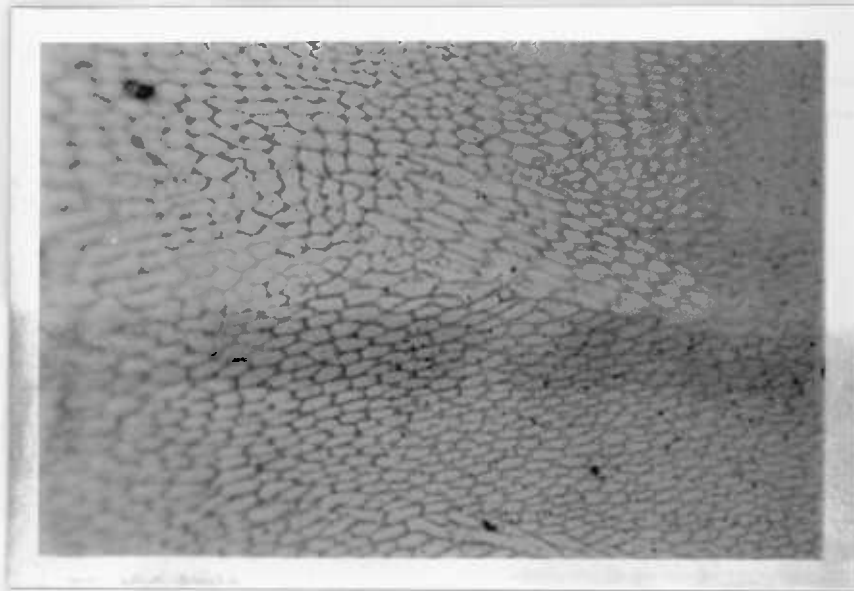


FIG 4.71 MICROSTRUCTURE 316 STAINLESS STEEL CLADDING, ———
SPECIMEN NUMBER M8 ; POWER = 1300 W; BEAM DIAMETER =
= 2.29 MM; SPEED = 25 MM/S; POWDER THICKNESS = 2.00 MM;
ETCHED IN KALLING'S REAGENT; X ———

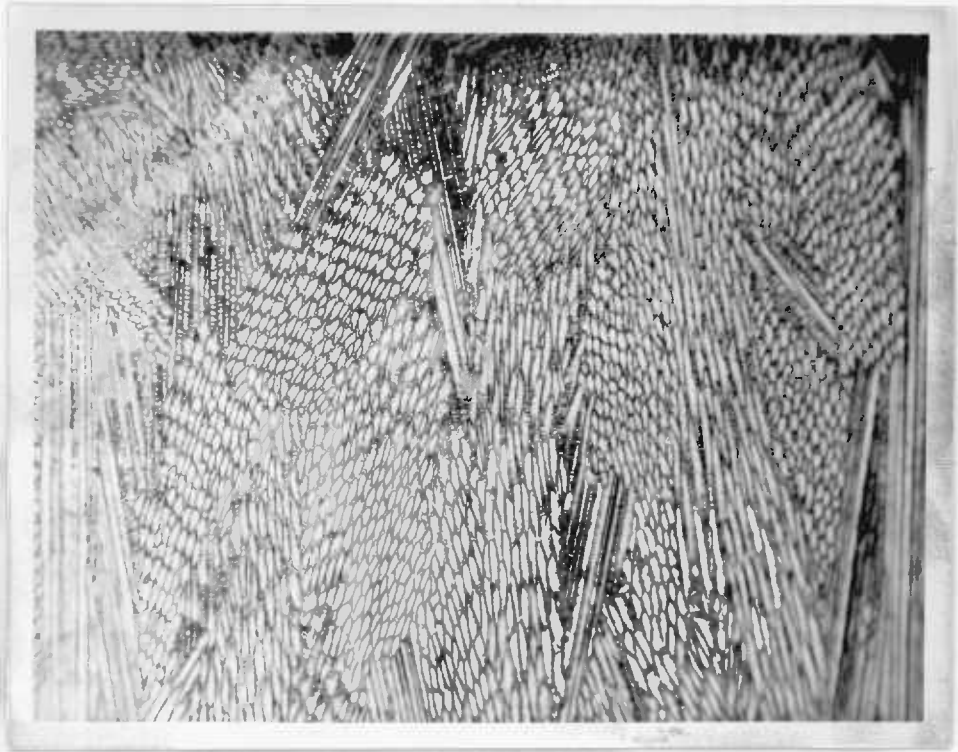


FIG 4.72 MICROSTRUCTURE 316 STAINLESS STEEL CLADDING, ——— SPECIMEN NUMBER M9; POWER=1 460 W; BEAM DIAMETER= 2.29 MM; SPEED=15 MM/S; POWDER THICKNEES=2.00 MM; GRADE OF PREHEATING =300 °C; OVERLAP=1.5 MM; ——— FORWARDS AND BACKWARDS, ETCHED IN A SOLUTION OF HCl + HNO₃ AND H₂O; X182.

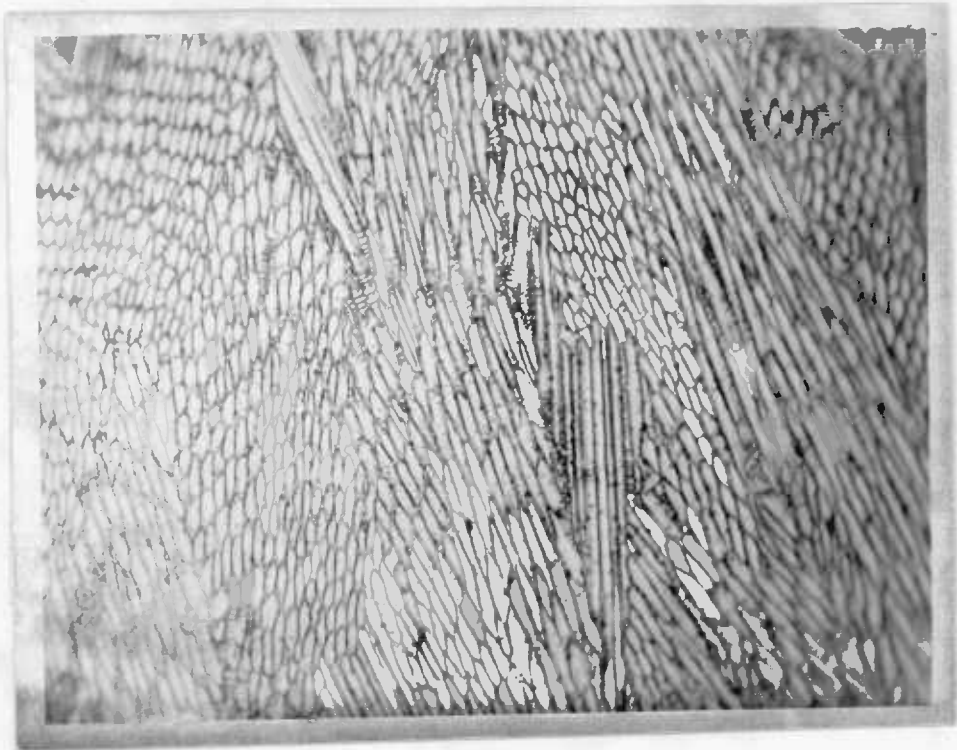


FIG 4.73 THE SAME AS ABOVE, BUT AT X442.

4.8.2 Microstructure in the Heat-affected Zone Structure

The microstructures in the heat-affected zone produced in the mild steel base plate after cladding with 316 stainless steel, consist of a number of different areas within its narrow thickness. This variation is due to the range of heating and cooling rates, as well as maximum temperatures possible with this process. The resultant dimensions of the heat-affected zone are shown in appendix 1.1, and the resultant structures are shown in figs 4.74 to 4.78. The different structures in the base metal are very fine and not quite clearly resolved by light microscopy. Those structures in regions which have been heated above A_3 , e.g. points "C" and "D" on fig 4.79, reached the single phase austenite which has been transformed into martensite on cooling and this is in agreement with the hardness value measured and with previous work (3). There was a decrease in microhardness value further into the base metal that perhaps corresponds to martensitic-bainitic structures, a bainitic structure has a tendency to form in this kind of steel, according to the isothermal transformation diagram in fig 4.80 (A+F+C).

On the other hand, regions heated to between A_1 and A_3 (fig 4.79, eg point B) reached a two phase condition proeutectoid ferrite and austenite, after cooling the structure consisted of proeutectoid ferrite and martensite which had formed from austenite.

The structures between A_1 and A_3 had not transformed completely to austenite, and the austenite may be inhomogeneous because areas that were ferrite formerly may be somewhat low in carbon, and those formerly carbides may be high in carbon concentration. The above mentioned conditions still persist when the steel reaches the austenitizing temperature; in an ordinary heat treatment these concentration gradients associated with these inhomogeneous can be eliminated by diffusion, so if homogeneous austenite is desired sufficient time must be allowed.

The last observed structure in the heat-affected zone had the appearance of a completely ferritic structure at low magnification, implying that the pearlite colonies had disappeared. However, these colonies are the starting point of the austenite formation by a nucleation and growth process. The carbon contained in the austenite must be always higher than in the ferrite with which it is in equilibrium, so the formation of austenite in the ferrite always needs the diffusion of carbon.



FIG 4.74 HEAT-AFFECTED ZONE IN En 3 STEEL AFTER LASER —
CLADDING 316 STAINLESS STEEL; SPECIMEN NUMBER S63; —
POWER=1 400 W, BEAM DIAMETER=4.6 MM, SPEED=10 MM/S;
POWDER THICKNESS=1.00 MM; ETCHED IN 2% NITAL, X110.

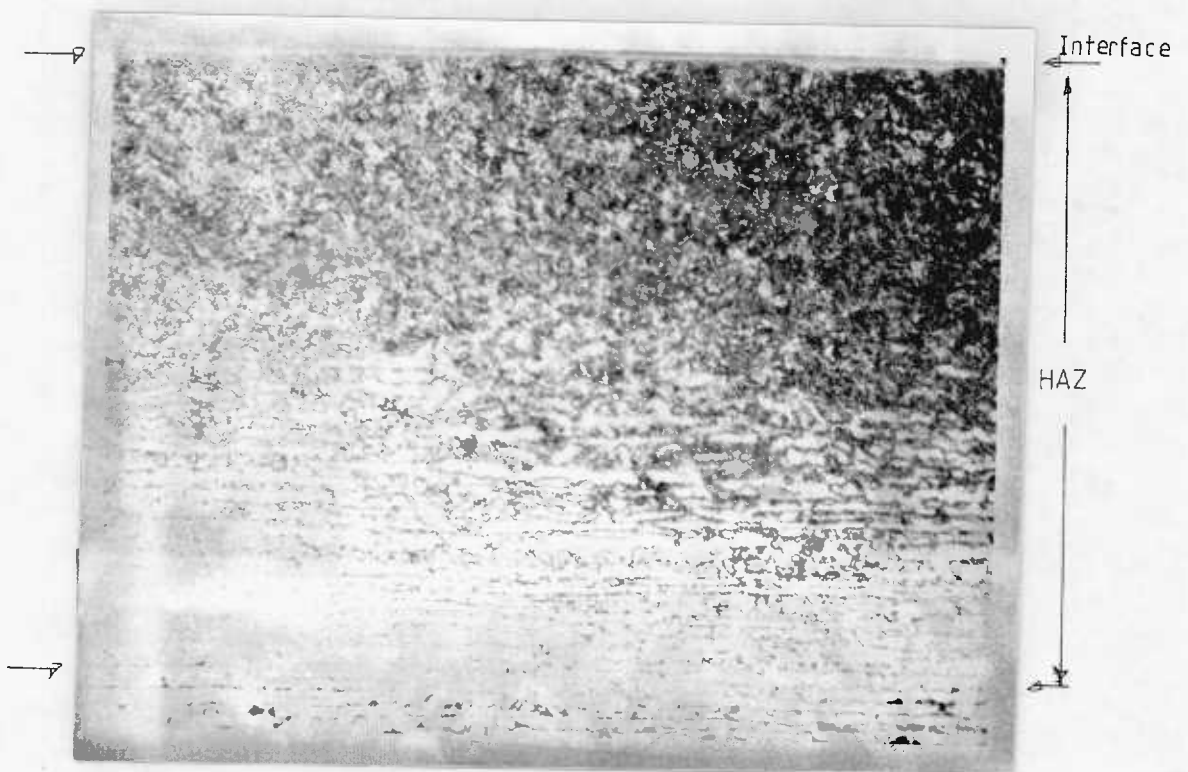


FIG 4.75 HEAT-AFFECTED ZONE IN En 3 STEEL AFTER LASER —
CLADDING 316 STAINLESS STEEL, SPECIMEN NUMBER S123;
POWER=1 800 W; BEAM DIAMETER=5.8 MM, SPEED=10 MM/S;
POWDER THICKNESS=1.00 MM, ETCHED IN 2% NITAL, X110.

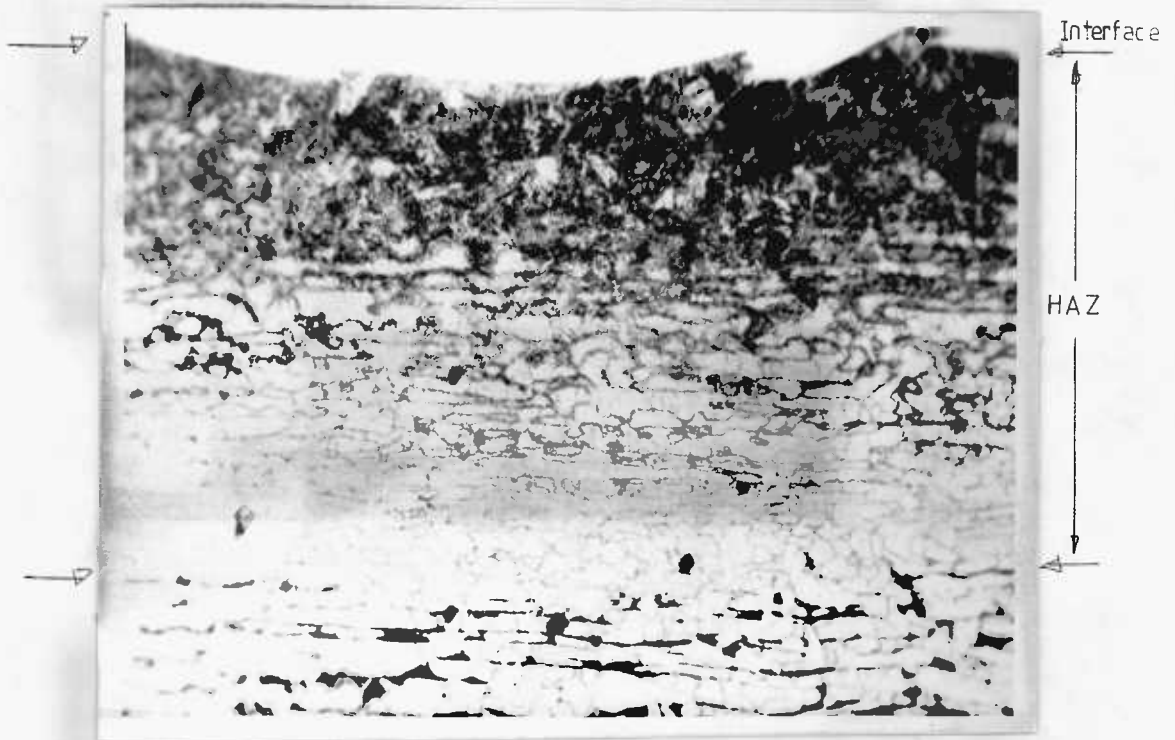


FIG 4.76 HEAT AFFECTED-ZONE IN EN 3 STEEL AFTER LASER CLADDING 316 STAINLESS STEEL, SPECIMEN NUMBER S 20, POWER = 1 600 W, BEAM DIAMETER = 4.3 MM, — SPEED = 35 MM/S, POWDER THICKNESS = 1.00 MM, — ETCHED IN A 2% NITAL SOLUTION, X182 . —



FIG 4.77 HEAT AFFECTED-ZONE IN En 3 STEEL AFTER LASER CLADDING - 316 STAINLESS STEEL, SPECIMEN NUMBER M4; POWER=1 300 W; BEAM DIAMETER=2.29 MM; SPEED=15 MM/S; POWDER THICKNESS=2.00 MM; NO PREHEAT; OVERLAP=1.88 MM; ETCHED IN 2% NITAL; X 110.



FIG 4.78 HEAT AFFECTED-ZONE IN En 3 STEEL AFTER LASER CLADDING - 316 STAINLESS STEEL, SPECIMEN NUMBER M16; POWER=1 400 W; BEAM DIAMETER=2.29 MM; SPEED=20 MM/S; POWDER THICKNESS=2.00 MM; DEGREE OF PREHEATING=150 °C; OVERLAP=1.5 MM; ETCHED IN 2% NITAL; X 110.

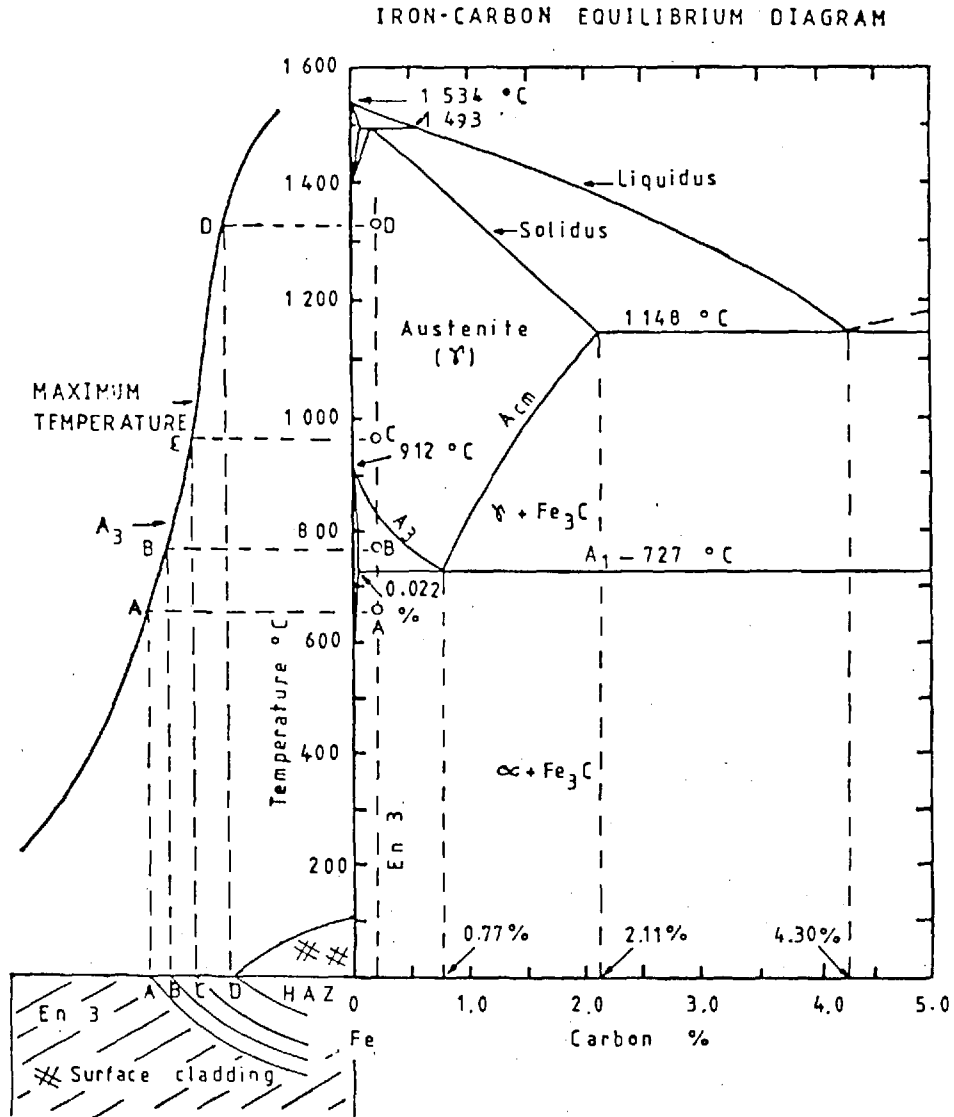


FIG 4.79 RELATION BETWEEN THE PEAK TEMPERATURES BY VARIOUS REGIONS IN HEAT AFFECT ZONE, AND HOW THESE CORRELATE WITH IRON-CARBON PHASE DIAGRAM

Austenitizing Temperature 913°C

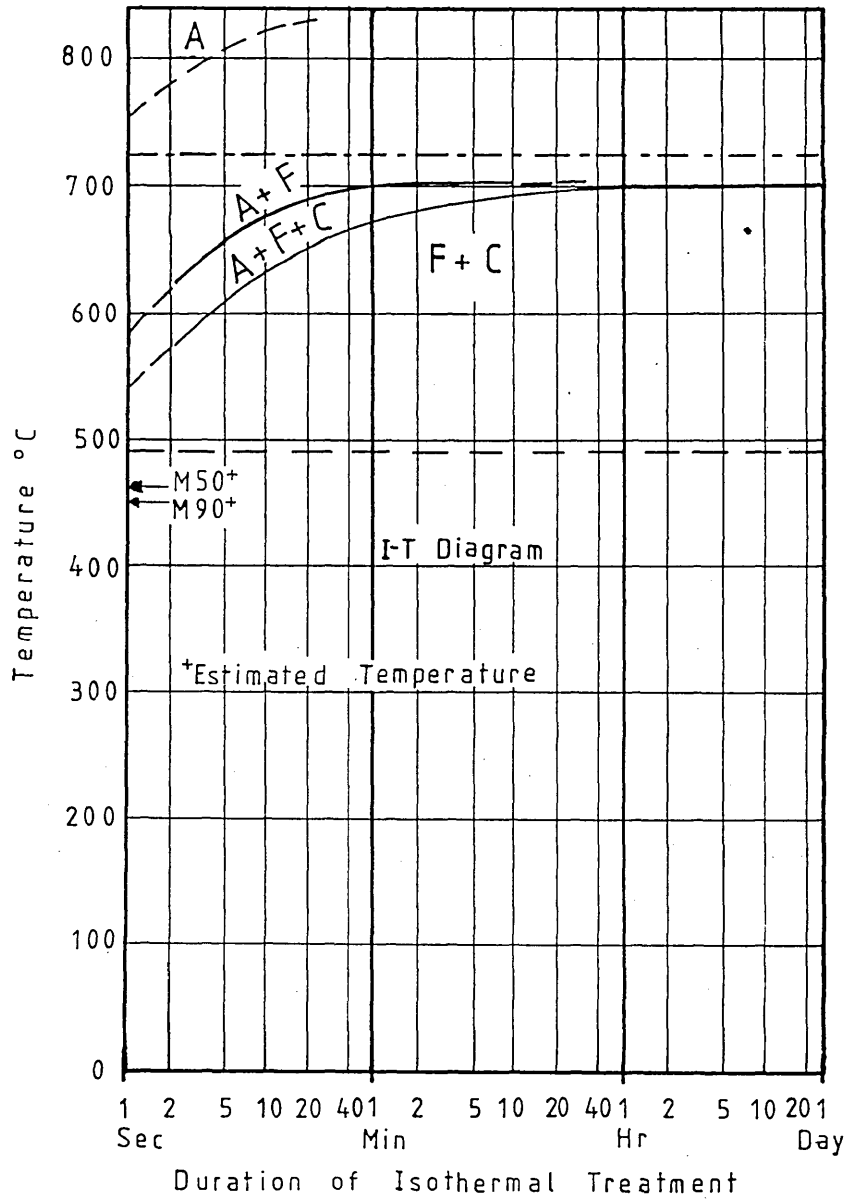


FIG 4.80 ISOTHERMAL TRANSFORMATION DIAGRAM FOR En 3 STEEL (REF. 16).

4.9 Surface Cladding Composition

The distribution of alloying elements in the surface cladding has been studied using a microprobe analyzer.

The aim of the analysis was to check the composition of the surface cladding, and it was found that nickel, chromium and molybdenum were suitable for tracing, but manganese and silicon too low to give reliable results. Iron was present strongly throughout, and so was not used. All specimens were therefore traced across the junction from about 200 μm into the surface cladding for chromium/nickel and nickel/molybdenum as can be seen in Figs 4.81 to 4.86.

All results show that the composition is constant, except that S26 showed a lower nickel and chromium content, and that S137 showed a short step just before the interface. Traces for nickel and chromium dropped off over the last 50, or so μm . Approximate calibrations were made by signal comparison with the pure metals, but because of the low nickel values obtained, these were checked by rough measurement on S118 and S137, and found to agree with the calibrations for both nickel and chromium. It seems that the nickel content of all of these surface cladding is about $\frac{1}{3}$ of that specified for 316 stainless steel. The small variations that have been registered with the

microprobe analyzer from nickel, chromium and molybdenum are due to the microsegregated caused by carbides and by the ferrite phase. The measured segregation ratios (C_{\max}/C_{\min}) of nickel, chromium and molybdenum are 1.13, 1.15 and 1.55 for S1, 1.15, 1.13 and 1.75 for S26; 1.13, 1.06 and 1.50 for S63; 1.12, 1.06 and 1.75 for S116; 1.05, 1.10 and 1.65 for S118; 1.10, 1.05 and 1.60 for S137 respectively.

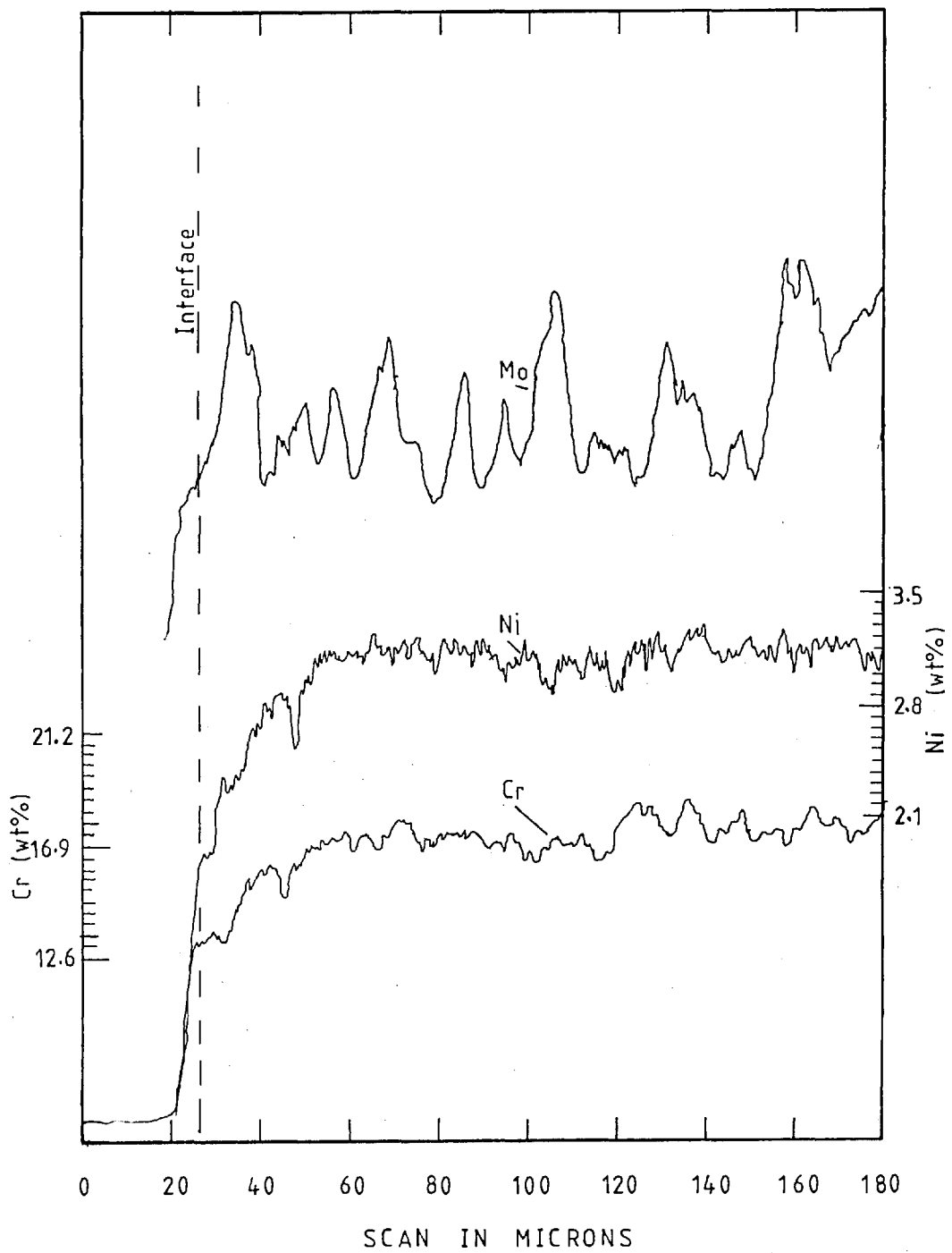


FIG 4.81 EPMA CONCENTRATION PROFILES FOR Cr, Ni, AND Mo IN 316 STAINLESS STEEL SURFACE CLADDING, SPECIMEN S1.

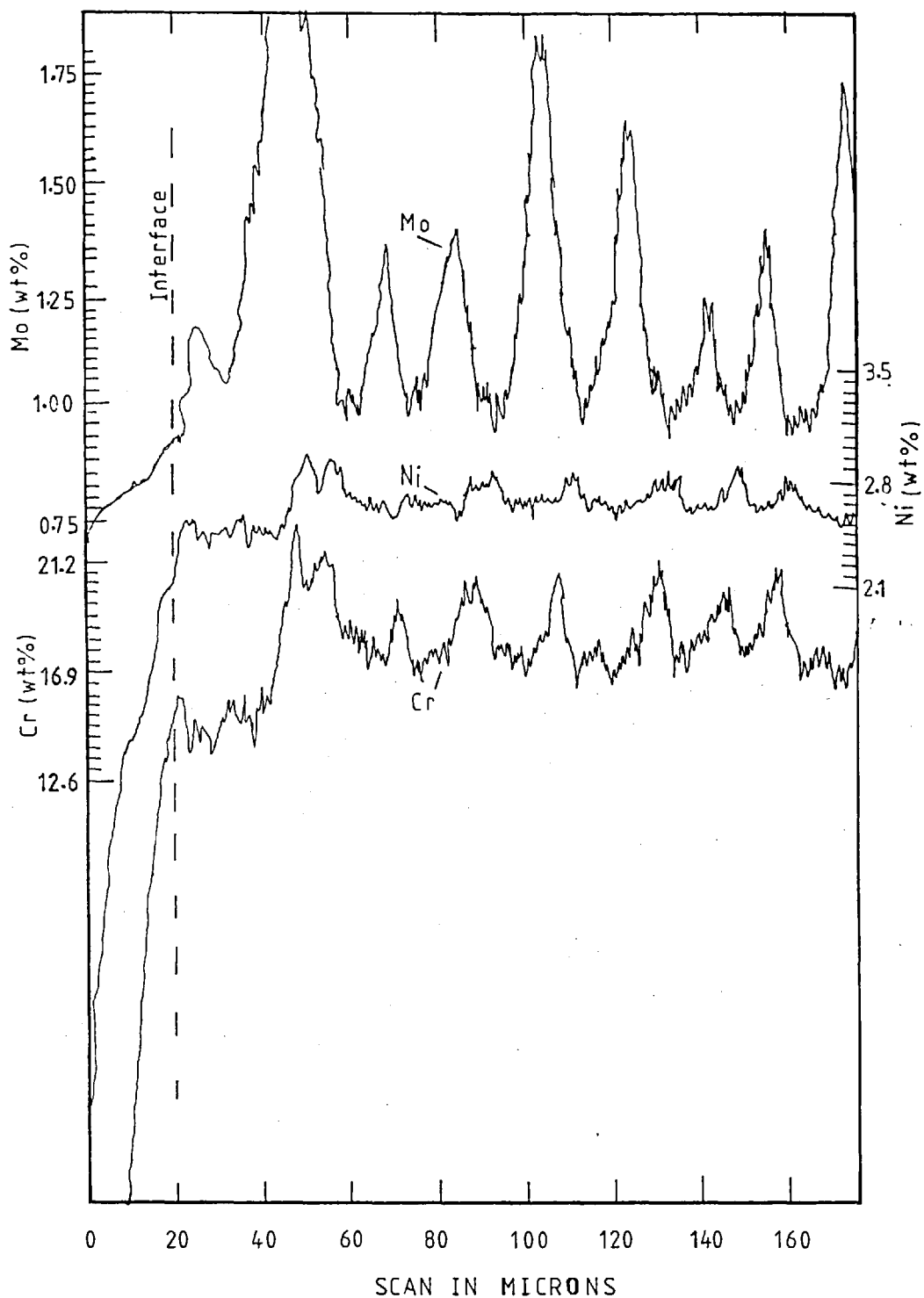


FIG 4.82 EPMA CONCENTRATION PROFILES FOR Cr, Ni, AND Mo IN 316 STAINLESS STEEL SURFACE CLADDING, SPECIMEN S26.

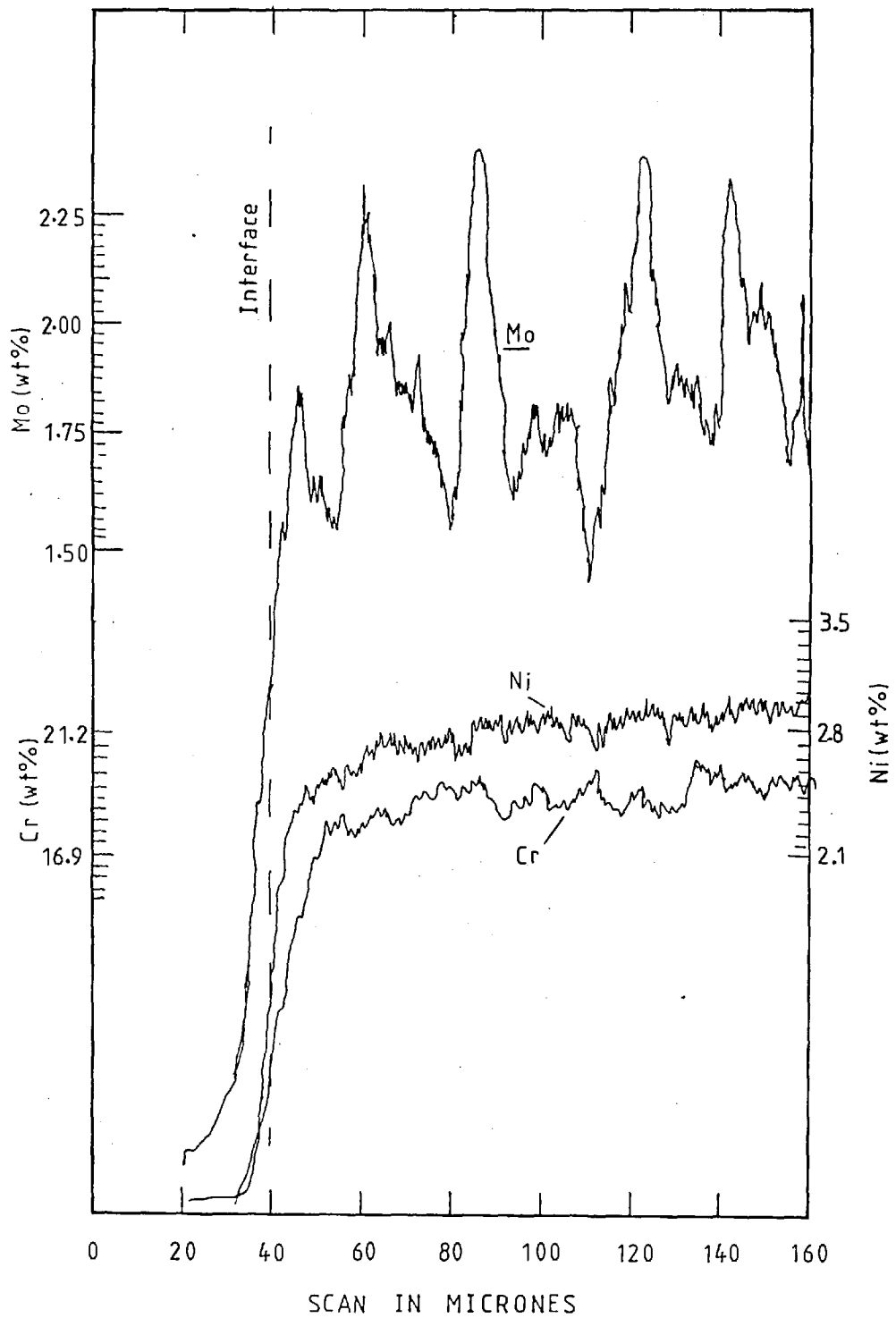


FIG 4.83 EPMA CONCENTRATION PROFILES FOR Cr, Ni, AND Mo IN 316 STAINLESS STEEL SURFACE CLADDING, SPECIMEN S63.

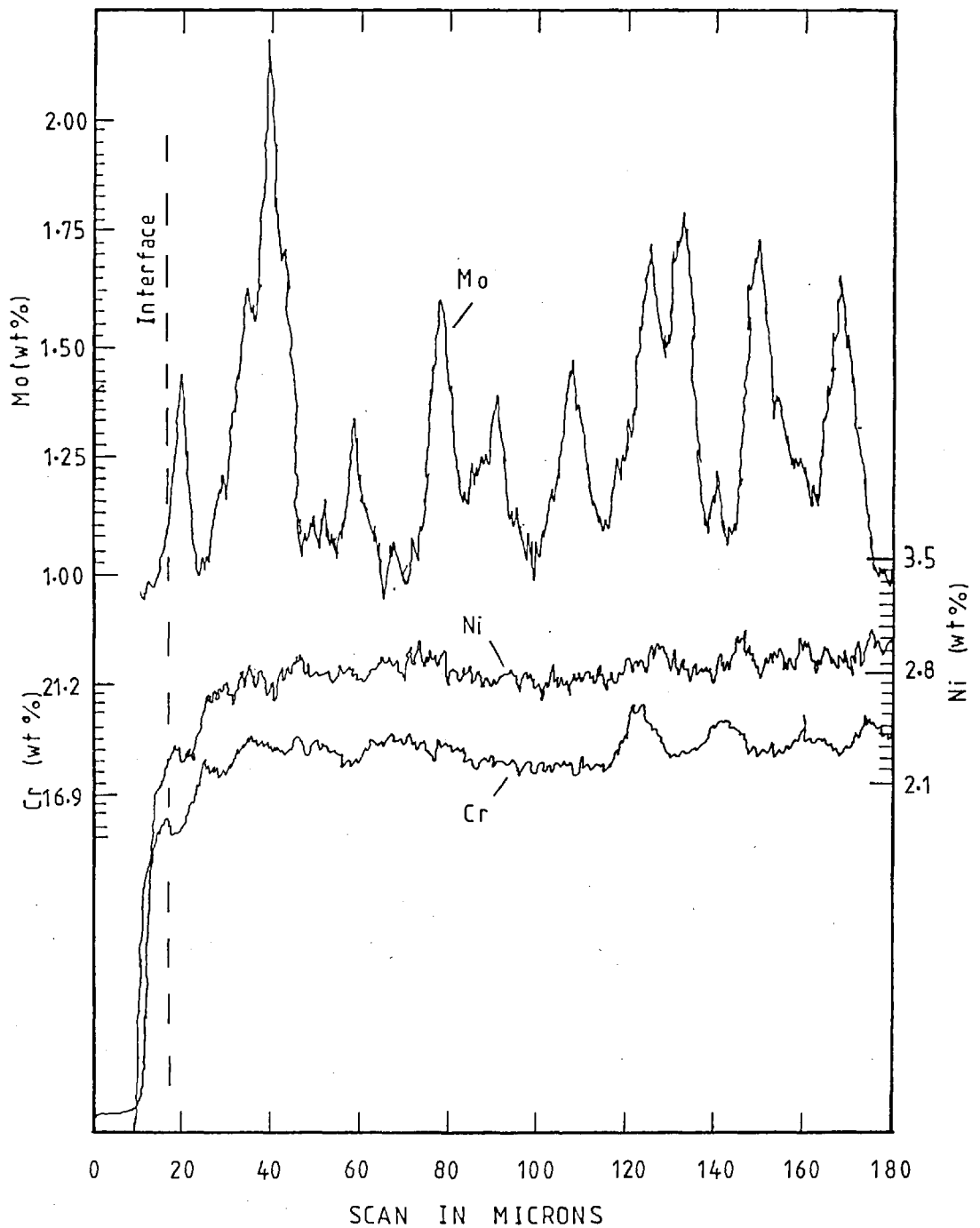


FIG 4.84 EPMA CONCENTRATION PROFILES FOR Cr, Ni, AND Mo IN 316 STAINLESS STEEL SURFACE CLADDING, SPECIMEN S116.

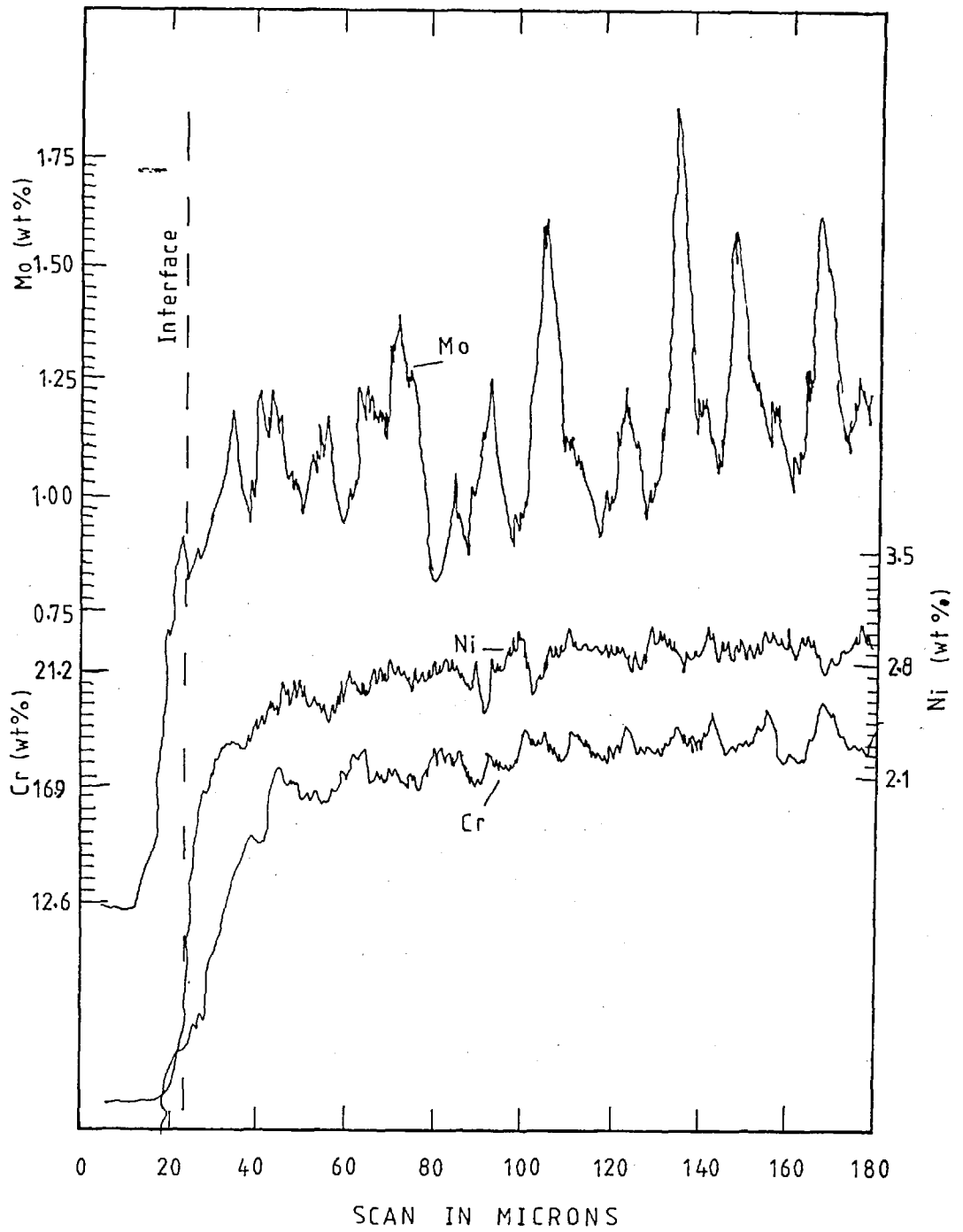


FIG 4.85 EPMA CONCENTRATION PROFILES FOR Cr, Ni, AND Mo IN 316 STAINLESS STEEL SURFACE CLADDING SPECIMEN S118.

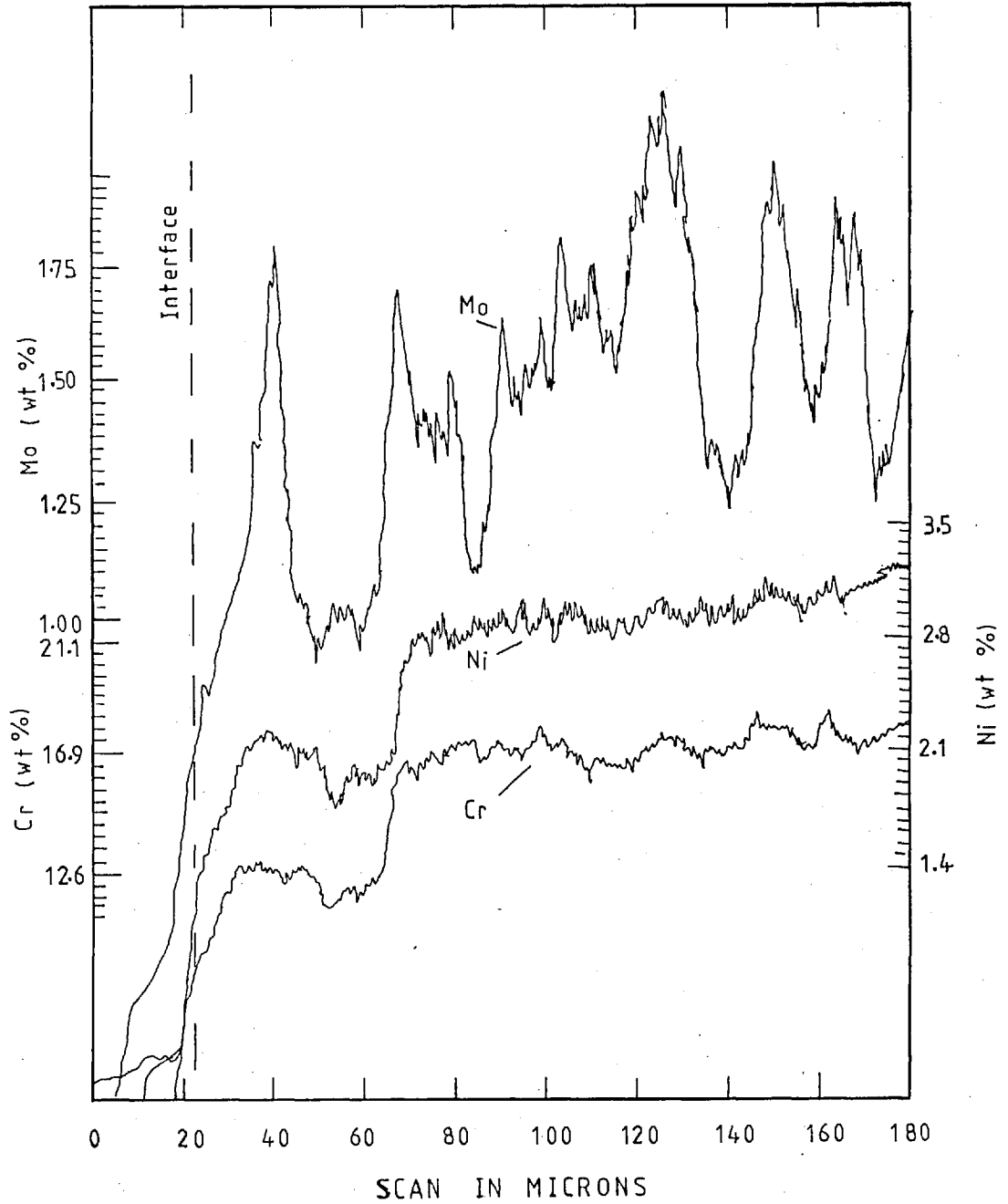


FIG 4.86 EPMA CONCENTRATION PROFILES FOR Cr, Ni, AND Mo IN 316 STAINLESS STEEL SURFACE CLADDING, SPECIMEN S137.

4.10 Resultant Hardness in the Clad Layer

The resultant microhardness measured across the specimens from the top surface of the cladding towards the base metal, and into the HAZ, was determined and its behaviour is shown in Figs 4.87 to 4.98.

4.10.1 Resultant Hardness in 316 Stainless Steel Cladding

The hardness measured across the 316 stainless steel surface cladding, from the top surface to the interface with the base metal is approximately constant in each case examined having a value of 239 ± 31 VPN; with the exception of specimen numbers S8 and S26, where the hardness was variable from 250 to 500 VPN.

This uniformity of hardness value implies a uniformity of structure with only slight variations in orientation and refinement within the predominantly columnar morphology of the homogeneous austenite.

4.10.2 Resultant Hardness in the Heat-Affected Substrate

The heat-affected zone of the base metal had its highest degree of hardness at a point adjacent to the clad alloy-base metal interface being 550 ± 62 VPN. This high level of hardness was expected, since this value corresponds to a martensitic structure prediction in Fig 4.99; due to the high cooling rates created in the bulk of the substrate. With small increases in the short distance from the interface, the resultant degree of hardness was decreased by the presence of other constituents whose values corresponded to the martensitic-bainitic structure. Where the hardness was found to be less than in the homogeneous transformation, the values correspond to mixture martensite-bainite and perhaps retained austenite. In the last affected area in the substrate, it corresponds to the thermally affected pearlite the degree of hardness was found to be higher than in the unaffected base metal.

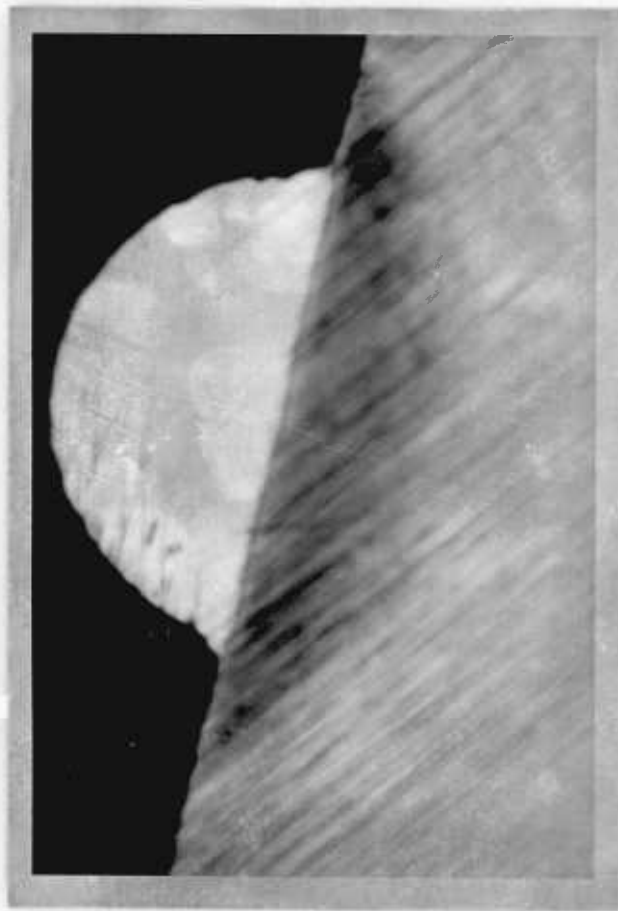
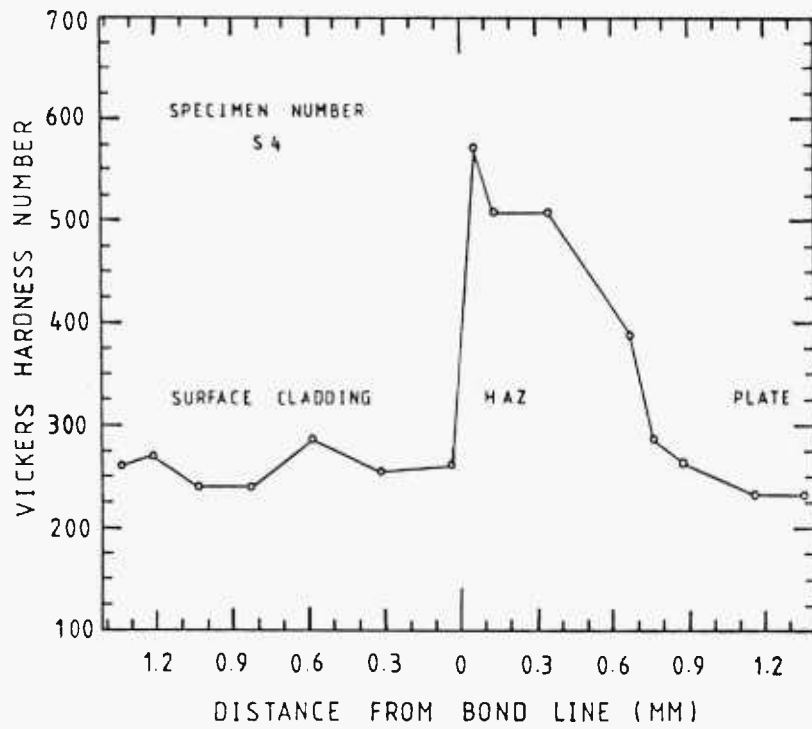


FIG 4.87 MICROHARDNESS AND MACROGRAPH SECTION VIEW THROUGH SURFACE CLADDING ETCHED 2% NITAL, X21. POWER=1 600 W BEAM DIAMETER=5.8 MM, SPEED=5 MM/S, POWDER THICKNESS=1.00 MM.

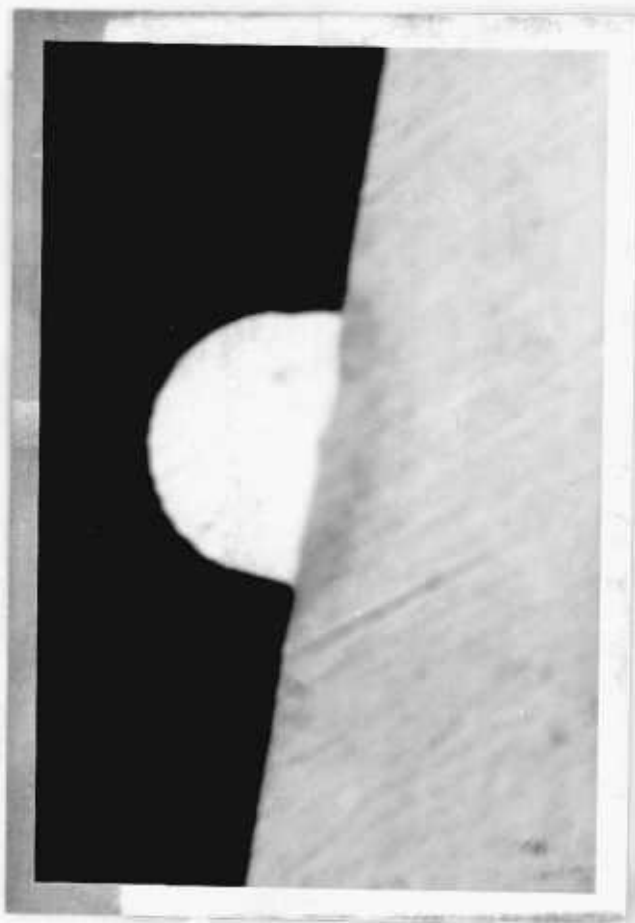
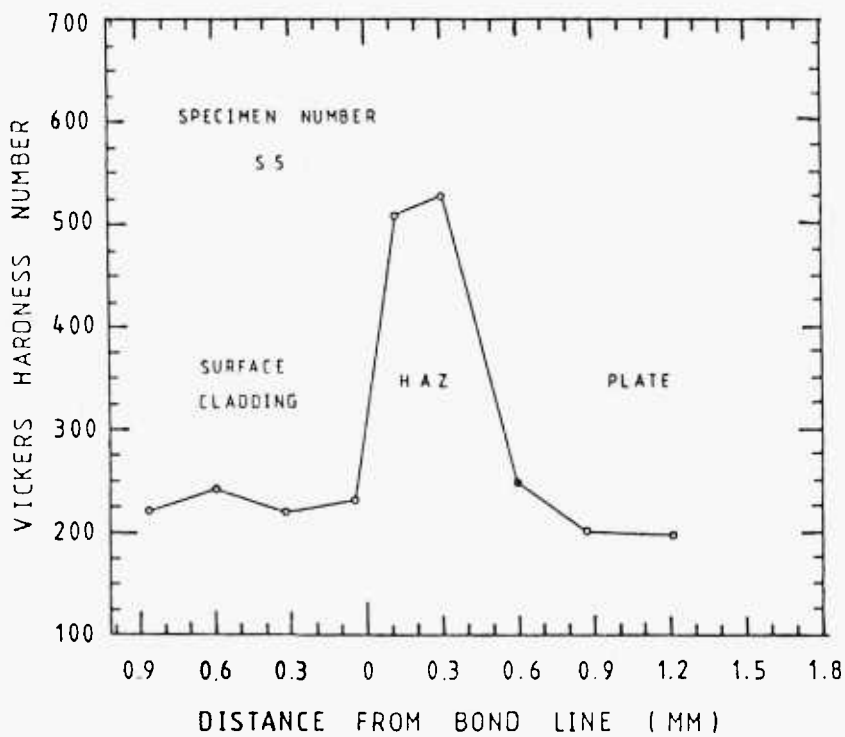


FIG4.88 MICROHARDNESS AND MACROGRAPH SECTION VIEW THROUGH SURFACE CLADDING FICED 2% NITAL, X21. POWER=1 600 W, BEAM DIAMETER = 5.8 MM, SPEED = 15 MM/S, POWDER THICKNESS = 1.00 MM.

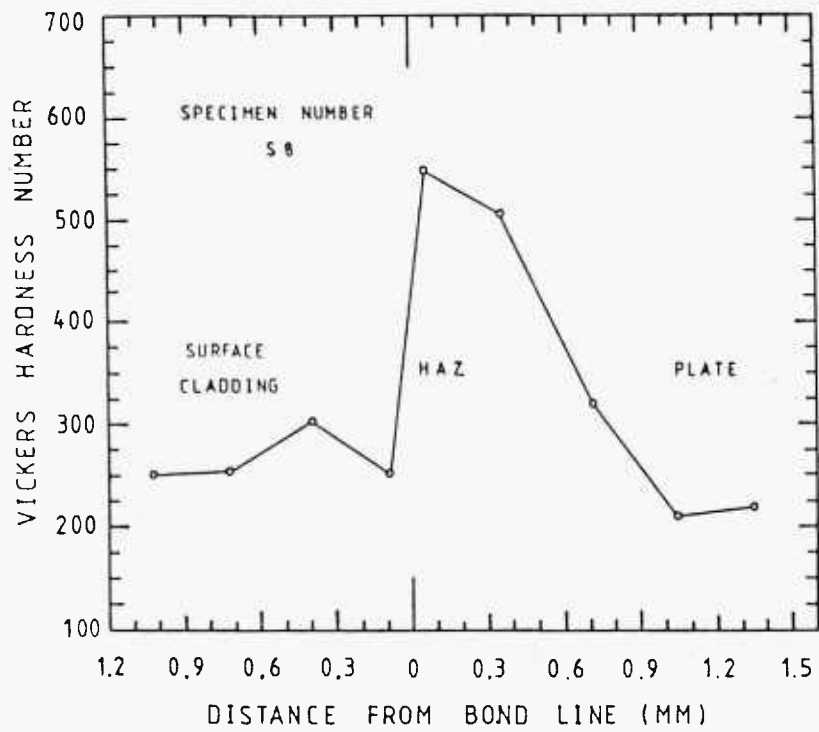


FIG 489 MICROHARDNESS AND MACROGRAPH SECTION VIEW THROUGH SURFACE CLADDING ETCHED 2% NITAL, X21, POWER=1 600 W BEAM DIAMETER = 4.3 MM, SPEED=5 MM/S, POWDER THICKNESS = 1.00 MM.

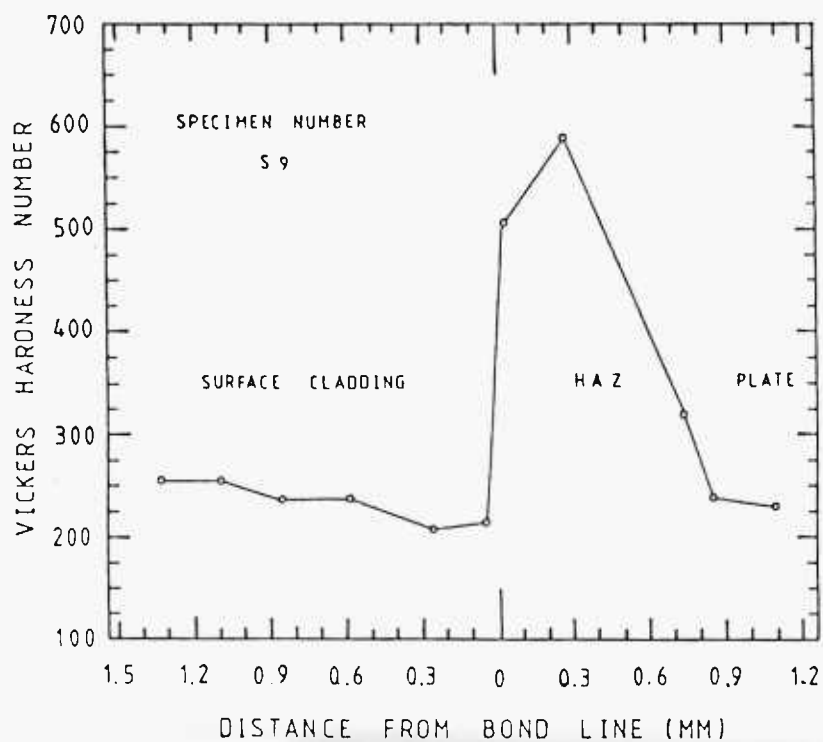


FIG 4.90 MICROHARDNESS AND MACROGRAPH SECTION VIEW THROUGH SURFACE CLADDING ETCHED 2% NITAL, X21. POWER=1600 W BEAM DIAMETER=4.3 MM, SPEED=15 MM/S, POWDER THICKNESS=1.00 MM.

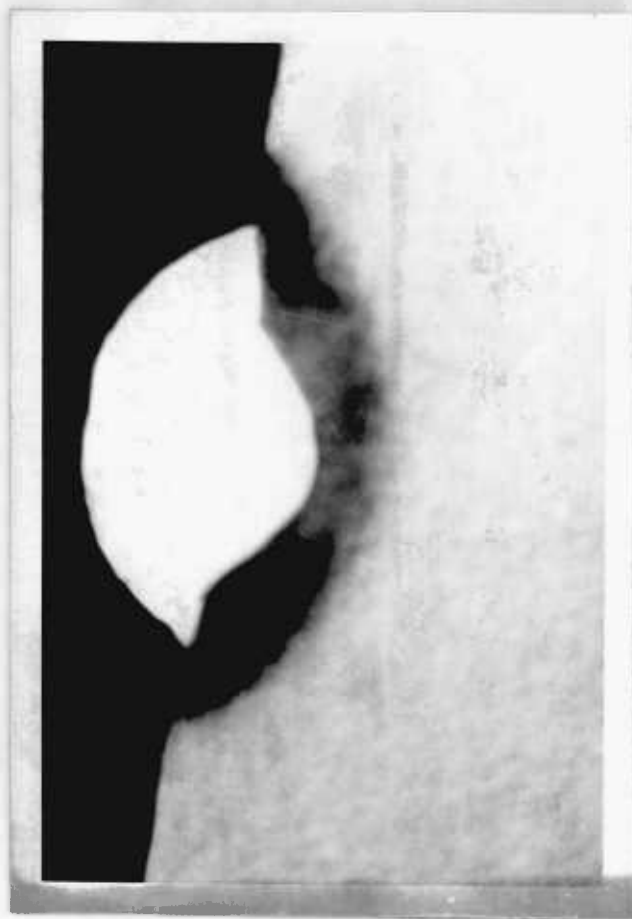
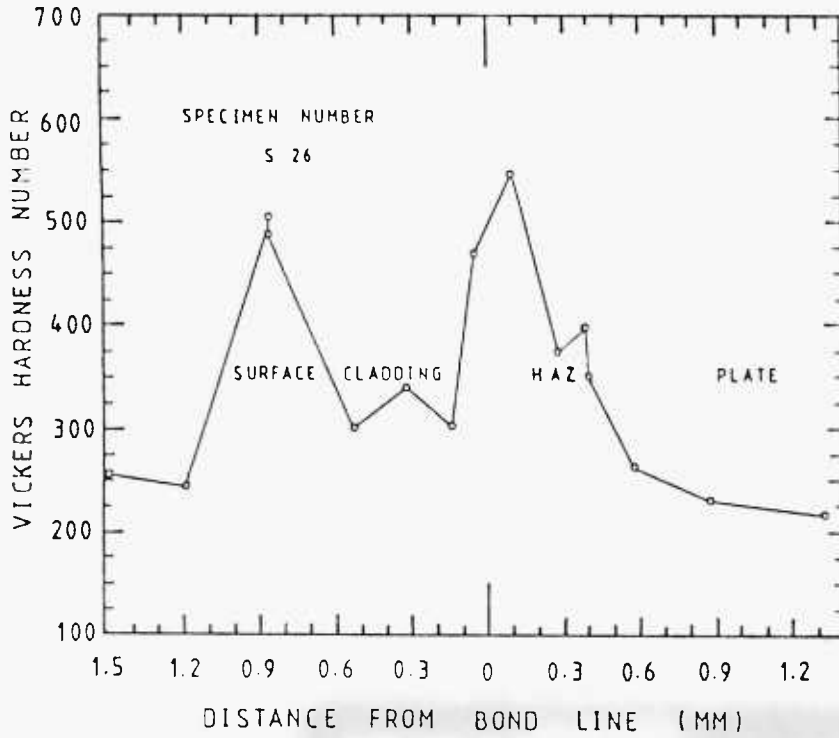


FIG 4.91 MICROHARDNESS AND MICROGRAPH SECTION VIEW THROUGH SURFACE CLADDING ETCHED 2% NITAL, X21. POWER=1 600 W BEAM DIAMETER=4.3 MM, SPEED 5 MM/S, POWDER THICKNESS = 0.50 MM.

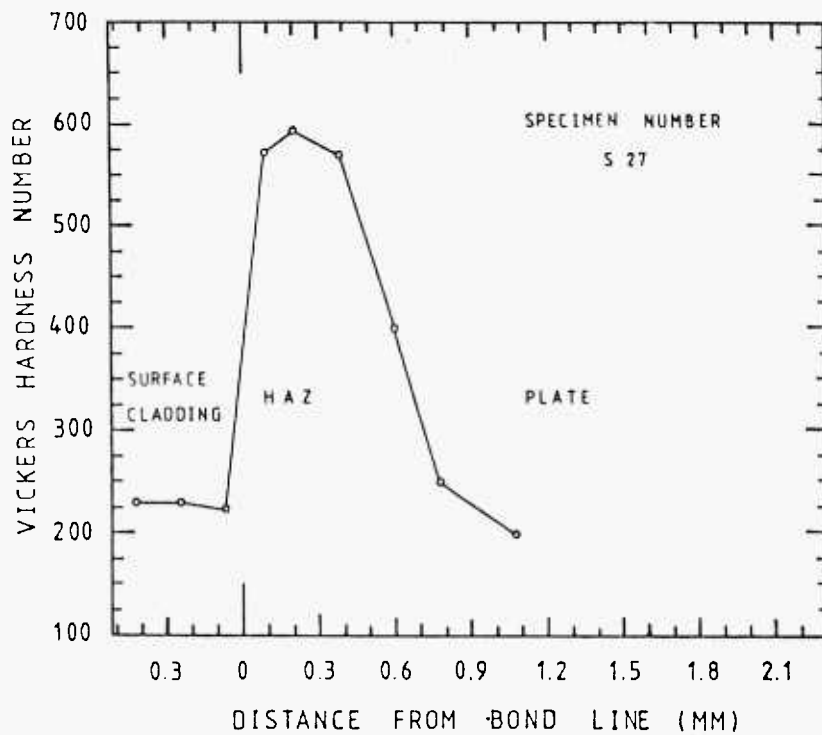


FIG 4.92 MICROHARDNESS AND MACROGRAPH SECTION VIEW THROUGH SURFACE CLADDING ETCHED 2% NITAL, X21, POWER=1 600 W BEAM DIAMETER=43 MM, SPEED=10 MM/S, POWDER THICKNESS = 0.50 MM.

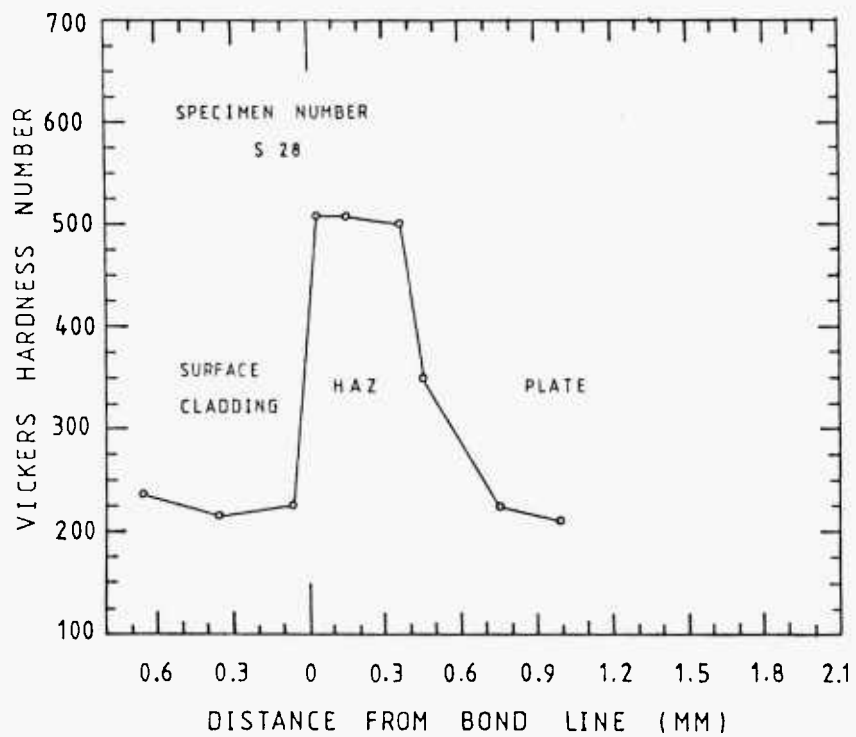


FIG 4.93 MICROHARDNESS AND MACROGRAPH SECTION VIEW THROUGH SURFACE CLADDING ETCHED 2% NITAL, X21. POWER=1 600 W BEAM DIAMETER=4.3 MM, SPEED=15 MM/S, POWDER THICKNESS=0.50 MM

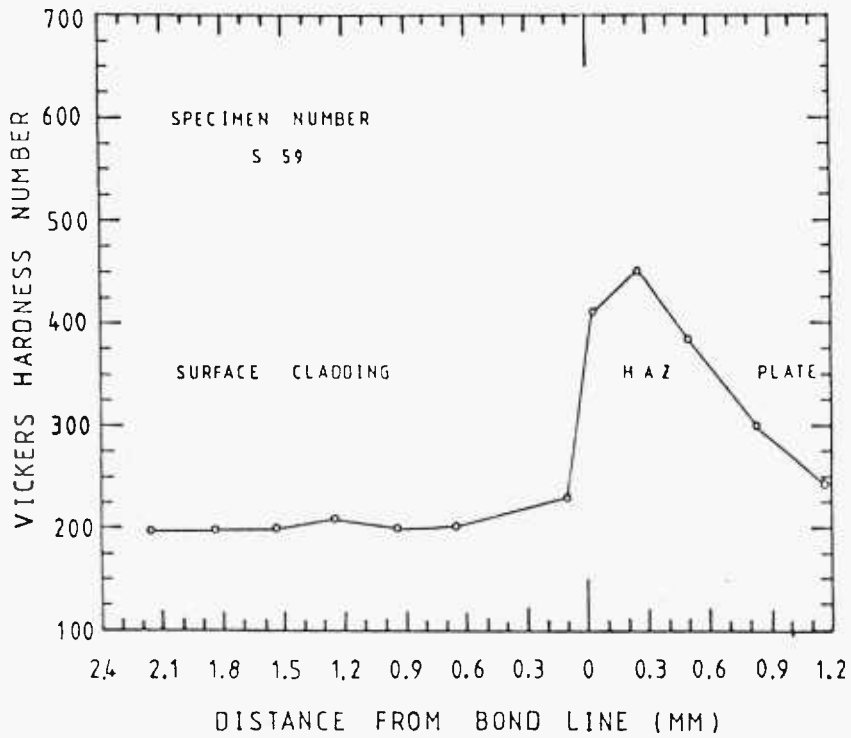


FIG. 4.94 MICROHARDNESS AND MACROGRAPH SECTION VIEW THROUGH SURFACE CLADDING ETCHED 2% NITAL, X21. POWER = 1 400 W BEAM DIAMETER = 0.7 MM, SPEED = 5 MM/S, POWDER THICKNESS = 1.00 MM.

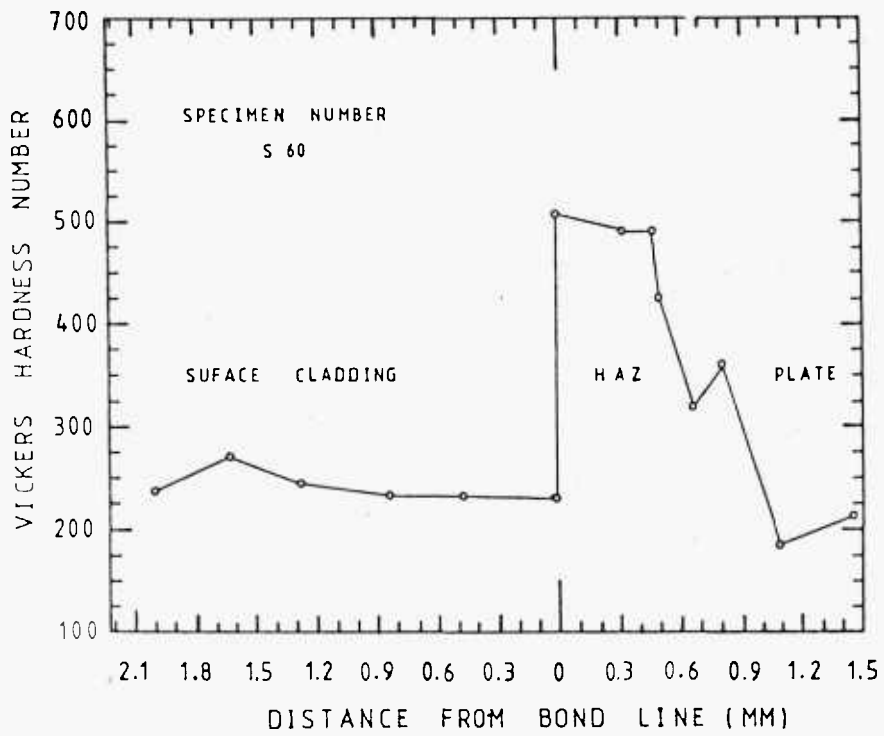


FIG495 MICROHARDNESS AND MACROGRAPH SECTION VIEW THROUGH SURFACE CLADDING ETCHED 2% NITAL, X21, POWER=1 400 W BEAM DIAMETER=7.2 MM, SPEED=5 MM/S, POWDER THICKNESS =1.00 MM.

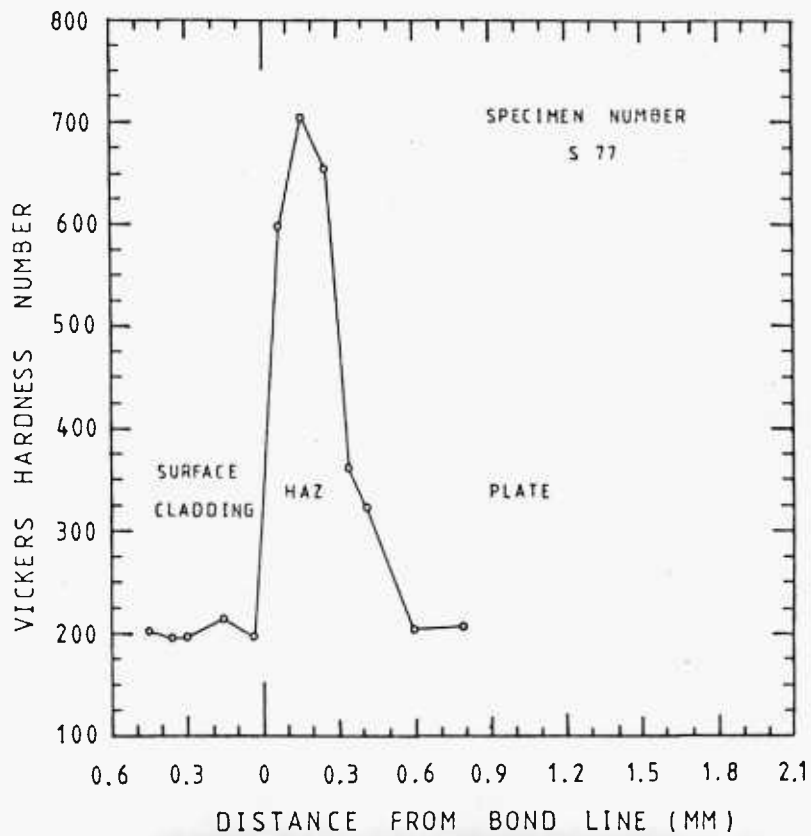


FIG 496 MICROHARDNESS AND MACROGRAPH SECTION VIEW THROUGH SURFACE CLADDING ETCHED 2% NITAL, X21, POWER=1400 W BEAM DIAMETER=3.2 MM, SPEED=20 MM/S, POWDER — THICKNESS=0.50 MM.

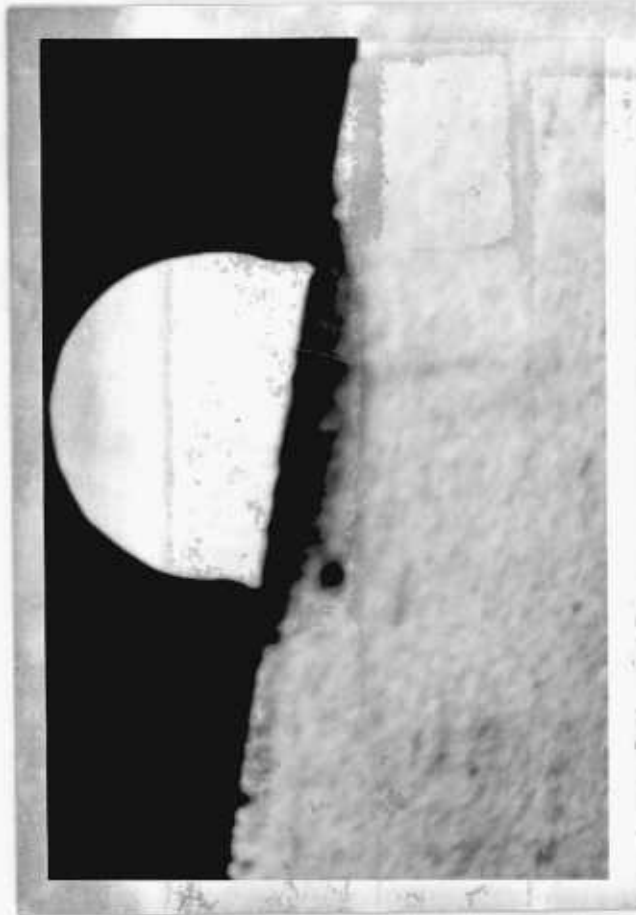
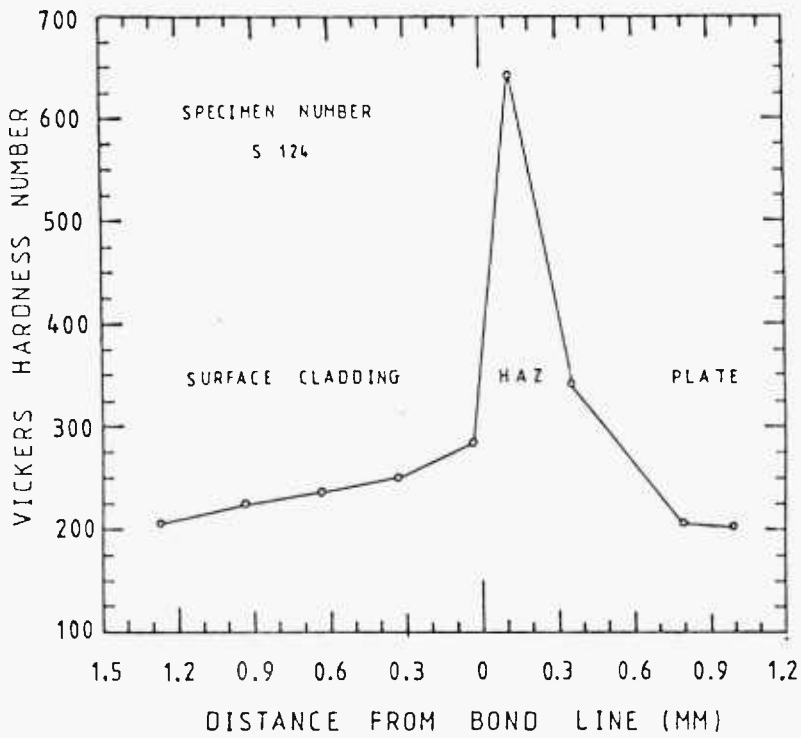


FIG 4.97 MICROHARDNESS AND MACROGRAPH SECTION VIEW THROUGH SURFACE CLADDING ETCHED 2% NITAL, X21. POWER=1800 W, BEAM DIAMETER=5.8 MM, SPEED = 15 MM/S, POWDER THICKNESS=1.00 MM.

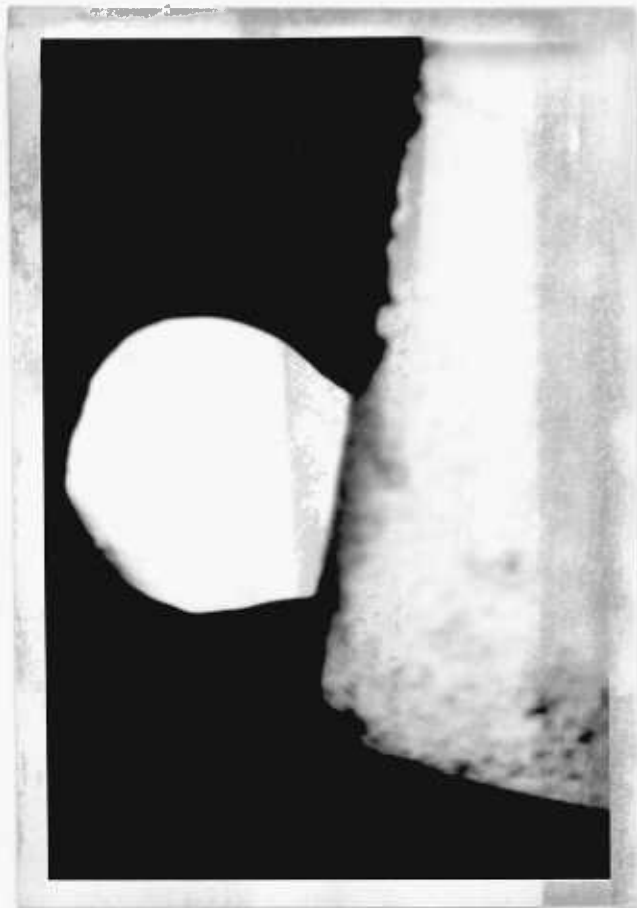
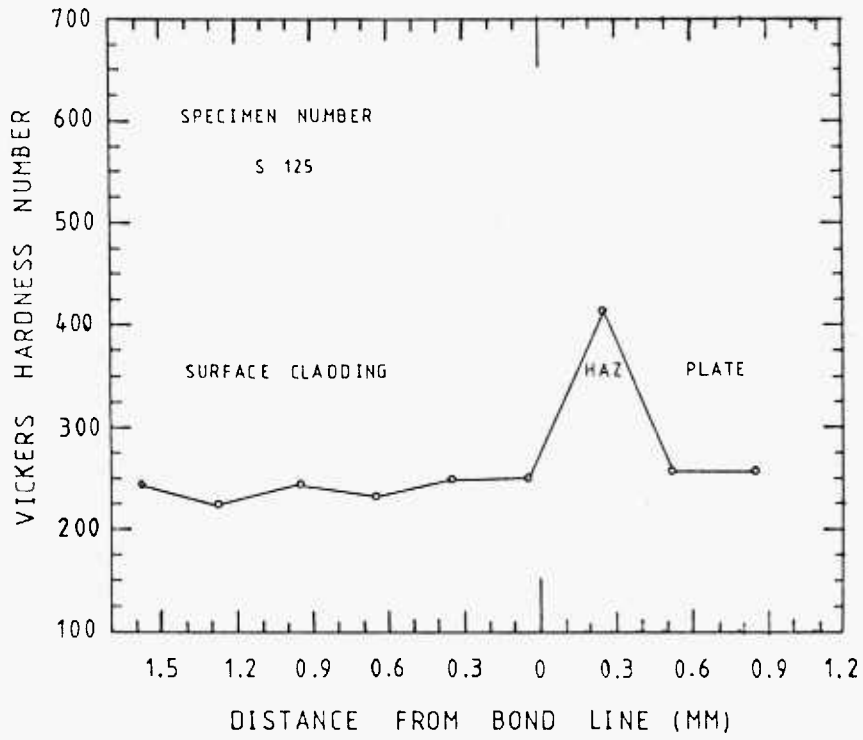


FIG498 MICROHARDNESS AND MACROGRAPH SECTION VIEW THROUGH SURFACE CLADDING ETCHED 2% NITAL, X21, POWER=1800 W BEAM DIAMETER=5.8 MM. SPEED=20 MM/S, POWDER THICKNESS=1.00 MM.

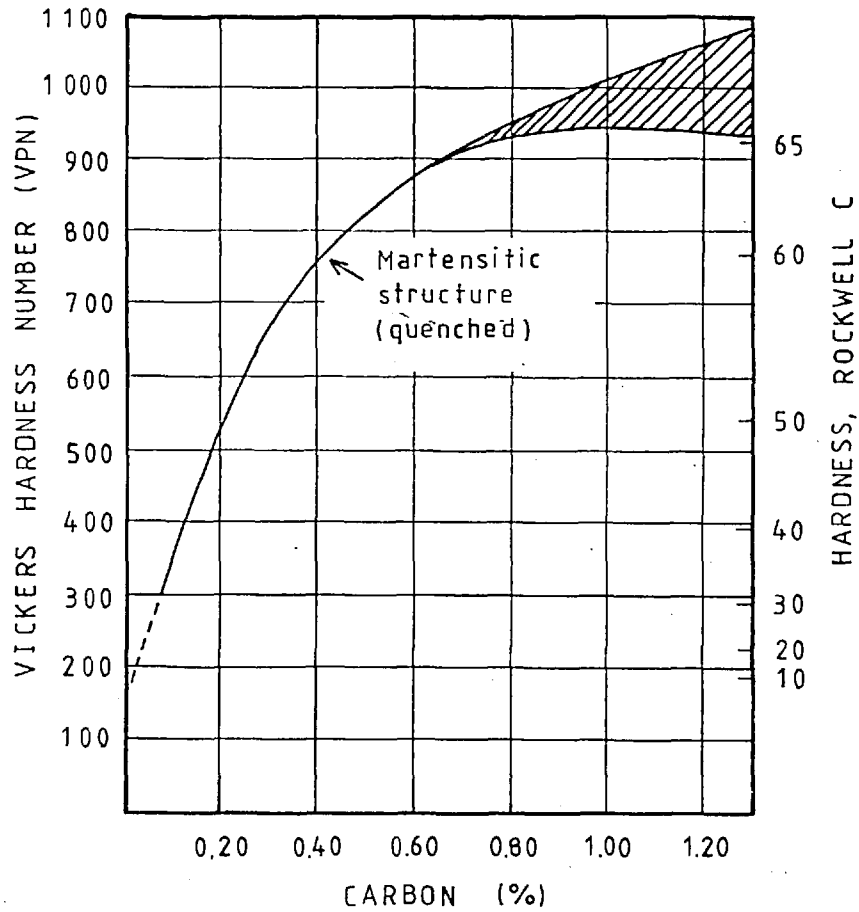


FIG 4.99 APPROXIMATE HARDNESS OF CARBON STEELS AS A FUNTION OF CARBON CONTENT. FULLY HARDENED MARTENSITE. (REF. 17)

4.10.3 Resultant Hardness on Selected Specimens 316 Stainless Steel

Surface Cladding

The heat input was applied by the laser beam under different operating conditions for each run, so it is to be expected that the microhardness of the surface cladding as well as within the heat-affected zone will vary between runs.

In each case the same or similar trend is seen.

- a) A reasonable constant value of hardness across the bead of between 220-280 VPN. The effect of dilution is seen in Fig 4.91.
- b) A fairly abrupt increase at the interface due to martensitic formation in the base metal.
- c) The hardness value falling in the HAZ away from the interface down to the constant value of the En 3 base metal of 220-280 VPN.

4.11 Results of Surface Cladding with Multiple Run Deposits

Multiple run deposits were made as described in section 3.5.1.

The principle variables studied were:-

- a) the overlap of consequential runs.
- b) degree of preheat of base metal

The operating conditions are shown in appendix 1.4 and the overall structural features are collated in table 4.5. In which it is seen that interrune inclusions are less frequent with increasing preheat temperature while surface smoothness improves with increasing overlap, though some improvement was noticed in traversing the laser back and forth across the powder bed instead of traversing in one direction alone (sample M3 for example).

TABLE 4.5 PHYSICAL CHARACTERISTICS OF MULTIPLE RUNS IN 316 STAINLESS STEEL, POWDER BED 2.0 mm DEEP

RUN NUMBER	PD/V (J/mm ²)	PREHEAT TEMPERATURE (°C)	PERCENTAGE OVERLAP (%)	PRESENCE SURFACE OF OXIDE RANKING	INTER-RUN INCLUSIONS RANKING	SURFACE SMOOTHNESS RANKING	METHOD OF TRAVERSE	COMMENTS
M1	33.96	500	21.0 [±] 1.56	20	1	10	B	Small ripples appeared
M2	33.96	300	38.0 [±] 0.68	19	2	6	B	See Fig 4.100 top view surface
M3	40.76	20	36.0 [±] 6.01	7	16	16	B	Smoother in fourth direction than back
M4	37.85	20	23.5 [±] 2.12	4	17	4	B	Disuniform overlap
M5	37.85	20	44.0 [±] 4.24	5	14	7	B	Shear test was made
M6	28.38	20	35.0 [±] 1.73	3	18	17	B	See Fig 4.102 with interrun inclusion
M7	28.38	20	27.5 [±] 0.71	2	19	18	A	See Fig 4.104 with big interrun inclusion
M8	22.71	20		1		20	A	Discontinuous track
M9	42.50	300	29.0 [±] 1.73	15	4	13	B	See Fig 4.103 with slight interrun inclusion
M10	31.88	300	33.0 [±] 4.0	8	8	3	B	See Fig 4.101 top view surface
M11	25.50	300	35.0 [±] 7.21	6	10	1	B	Shear test was made
M12	40.76	200	34.0 [±] 2.65	11	9	12	B	
M13	30.57	200	30.6 [±] 4.90	10	12	2	B	
M14	24.45	200	29.0 [±] 5.0	9	11	15	B	
M15	40.76	150	17.0 [±] 5.66	17	7	19	B	The backwards affected the for
M16	30.57	150	19.67 [±] 4.73	16	3	9	B	See Fig 4.105 without interrun inclusion
M17	24.45	150	29.0 [±] 2.89	14	6	8	B	Shear test was made
M18	37.85	400	31.0 [±] 6.24	18	13	11	B	
M19	28.38	400	22.0 [±] 4.24	13	15	5	B	
M20	22.71	400	20.0 [±] 4.36	12	5	14	B	Shear test was made

SCORED RANKING: 1 IS THE BEST, 20 IS THE WORST

A. SINGLE DIRECTION TRAVERSE

B. TRAVERSE IN BOTH DIRECTIONS

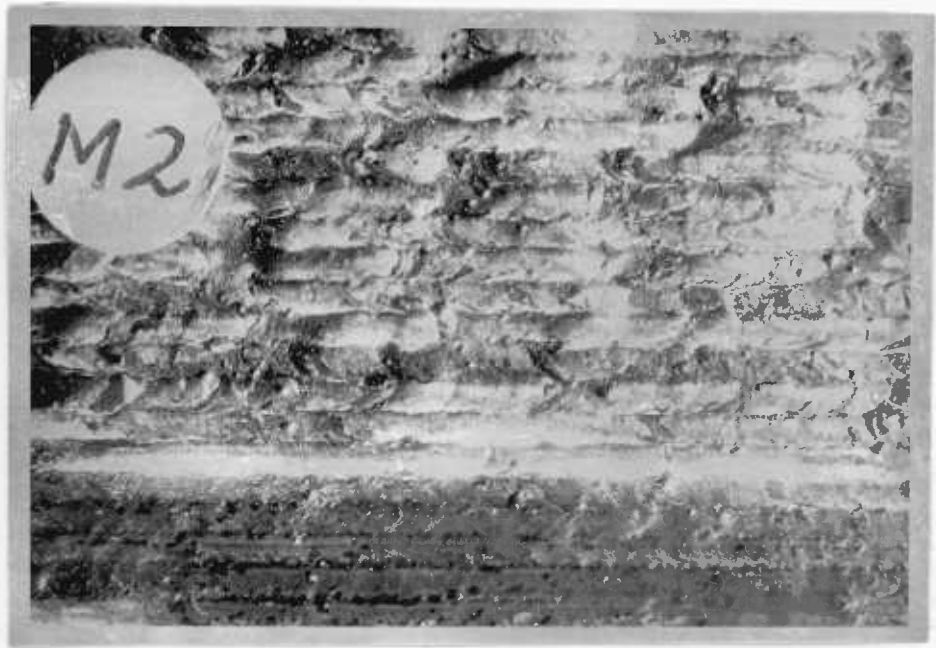


FIG 4.100 SURFACE CLADDING: POWER = 1 400 W; BEAM DIAMETER = 2.29 MM; SPEED = 18 MM/S; POWDER THICKNESS = 2.00 MM; GRADE OF PREHEATING = 300 °C; OVERLAP = 1.25 MM; — TOWARDS AND BACKWARDS, X3.

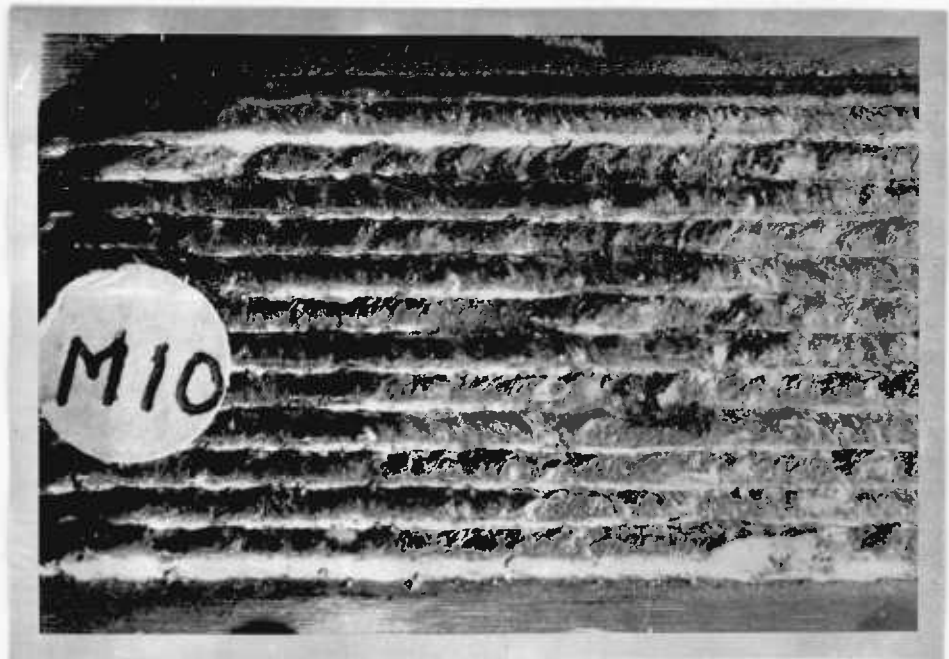


FIG 4.101 SURFACE CLADDING: POWER = 1 460 W, BEAM DIAMETER = 2.29 MM; SPEED = 20 MM/S; POWDER THICKNESS = 2.00 MM; GRADE OF PREHEATING = 300 °C; OVERLAP = 1.50 MM; — TOWARDS AND BACKWARDS, X3.

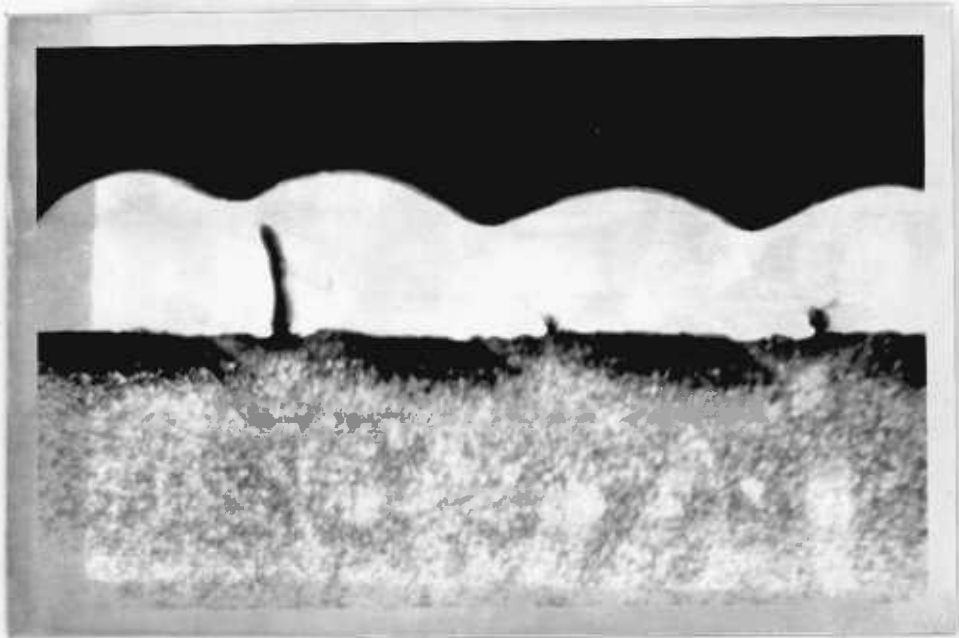


FIG 4.102 SECTION VIEW 316 STAINLESS STEEL CLADDING; SPECIMEN NUMBER M6; POWER=1300 W; BEAM DIAMETER=2.29 MM; — SPEED=20 MM/S; POWDER THICKNESS=2.00 MM; NO PREHEAT; OVERLAP=1.5 MM; FORWARDS AND BACKWARDS; ETCHED IN — 4% NITAL; X18.

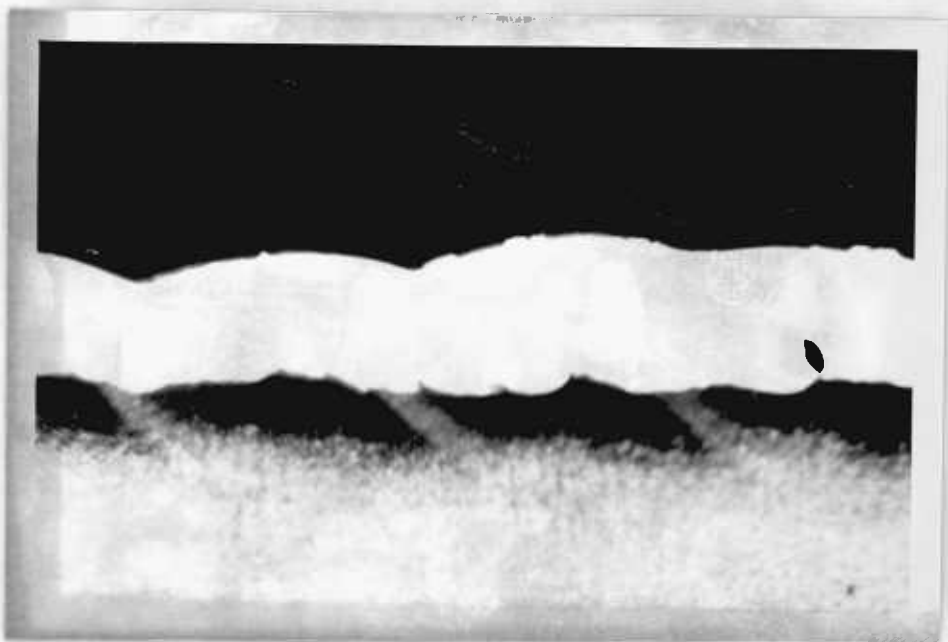


FIG 4.103 SECTION VIEW 316 STAINLESS STEEL CLADDING; SPECIMEN NUMBER M9; POWER=1450 W; BEAM DIAMETER=2.29 MM; — SPEED=15 MM/S; POWDER THICKNESS=2.00 MM; DEGREE OF — PREHEATING=300 °C; OVERLAP=1.50 MM; FORWARDS AND — BACKWARDS; ETCHED IN 4% NITAL; X18.

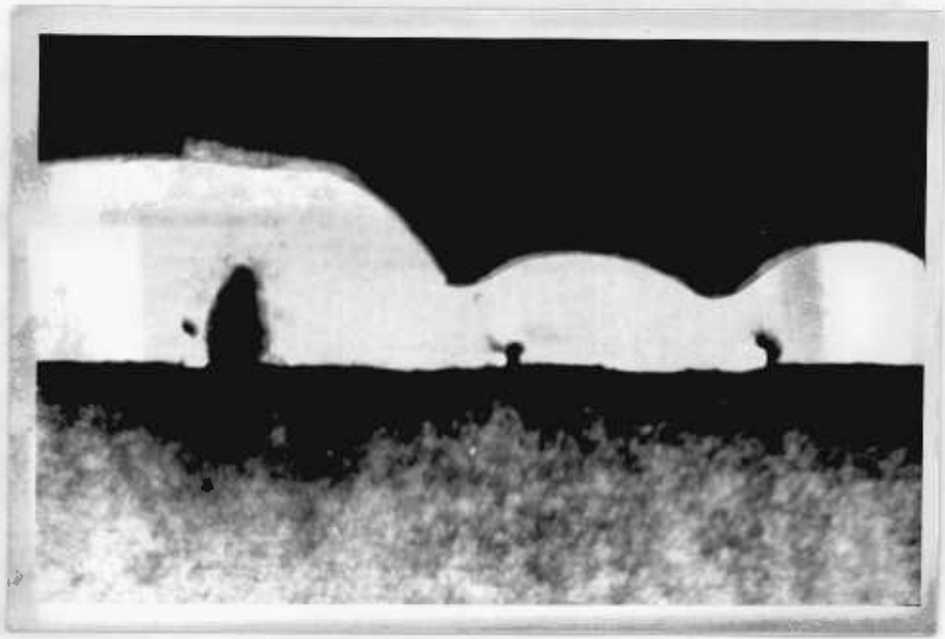


FIG 4.104 SECTION VIEW 316 STAINLESS STEEL CLADDING; SPECIMEN NUMBER M7; POWER=1300 W; BEAM DIAMETER=2.29 MM; — SPEED=20 MM/S; POWDER THICKNESS=2.00 MM; NO PREHEAT; OVERLAP=1.5 MM; FORWARDS; ETCHED IN 4% NITAL; X18.

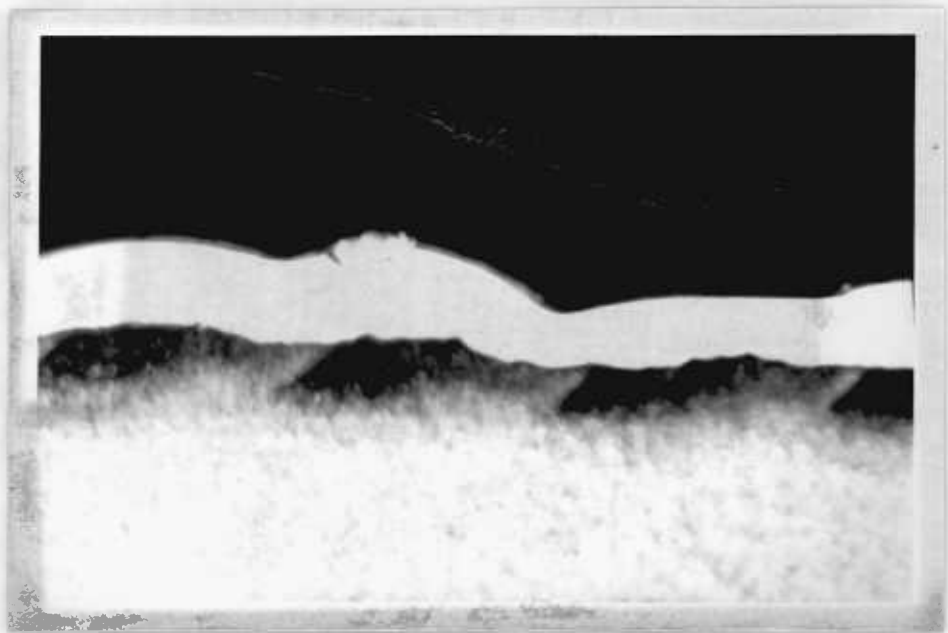


FIG 4.105 SECTION VIEW 316 STAINLESS STEEL CLADDING; SPECIMEN NUMBER M16; POWER=1400 W; BEAM DIAMETER=2.29 MM; — SPEED=20 MM/S; POWDER THICKNESS=2.00 MM; DEGREE OF — PREHEATING=150 °C; OVERLAP=1.5 MM; FORWARDS AND — BACKWARDS; ETCHED IN 4% NITAL; X18.

4.12 Metallographic Observation on Multiple Runs

4.12.1 316 Stainless Steel Surface Cladding

All specimens were cut, mounted, polished and etched in either Kalling's Reagent, or in a solution of 10 ml of HNO_3 , 20 ml of HCl , and 30 ml of H_2O also, to develop surface cladding structure, the acid etchant showed the stainless steel structure best.

On the transverse section view from the top surface cladding towards the HAZ, columnar-grained dendritic structure is observed, similar to single track runs with slight variations in grain size as well as in growth orientation, as can be seen in Figs 4.71 - 4.73.

4.12.2 Heat-Affected Zone Substrate

All specimens were polished and etched in a 2% nital solution to develop the HAZ structures.

Similar structures are observed in multiple runs to those found in single pass runs. That is a martensitic structure is present adjacent to surface cladding with martensitic - bainitic or non homogeneous martensite further removed from the cladding. However there are also zones of tempered martensitic in regions where the depth of the HAZ is overlapped.

4.13 Wetting & Spreading of Molten Cladding Alloy on a Base Metal

A basic factor which is involved in any cladding operation, is the wettability of the base metal by cladding alloy and it can be defined as the ability of the liquid cladding alloy to flow over the base metal surface which might be either liquid or solid.

The ability of spreading of the cladding alloy is dependent upon surface tension forces and the interaction between elements of the base metal and the cladding alloy.

A diagram of the forces acting on a liquid droplet of cladding alloy in two dimensions is shown in Fig 4.106. The vector system for this diagram can be derived from the Dupré' equation (18), to yield:

$$\gamma_{s/g} = \gamma_{l/s} + \gamma_{l/g} \cos \theta$$

by considering a force balance in the horizontal direction.

This expression means that spreading will occur at melt down when the base metal surface tension or the spreading tension $\gamma_{s/g}$ is of greater magnitude than the sum of the interfacial tension, $\gamma_{l/s}$ and the cosine component of the cladding alloy surface tension, $\gamma_{l/g}$ in some circumstances of penetrating $\gamma_{l/s}$ may no longer act horizontally but may be deflected downwards at some angle,

Φ so, the expression for spreading is now

$$\gamma_{s/g} > \gamma_{l/s} \cos \Phi + \gamma_{l/g} \cos \theta$$

thus the sessile drop will tend to spread outward under the influence of $\gamma_{s/g}$ until a new equilibrium of the above equation is established.

Spreading by the liquid cladding alloy could result from a high or low base metal surface energy as long as the condition of the above equation would prevail, low surface tension in the liquid cladding alloy $\gamma_{l/g}$ and the tendency towards superficial alloying between the liquid cladding alloy and the base metal (large $\gamma_{s/g}$) would favour the predominance of $\gamma_{s/g}$ and thus improve wettability.

Poor spreading would prevail when the magnitude of the spreading component is less than the sum of the interfacial tension and the cosine component of the cladding alloy surface tension, it can be represented symbolically, as:

$$\gamma_{s/g} < \gamma_{l/s} + \gamma_{l/g} \cos \theta$$

A high $\gamma_{l/g}$ or $\gamma_{l/s}$ would be expected when the liquid cladding alloy becomes contaminated as would be the case with oxide contamination.

In some cases this effect could be great enough to cause no-wetting or contraction to the cladding alloy upon melting, after it has initially spread over and reacted with some of the base metal surface film, in this instance, $\gamma_{l/g}$ and $\gamma_{l/s}$ try to contract the droplet into a spherical shape while attempting to obtain a minimum equilibrium surface energy level in the liquid.

Micrographs of all specimens were projected onto a screen and the solidified contact angles were measured between the cladding alloy and the base metal.

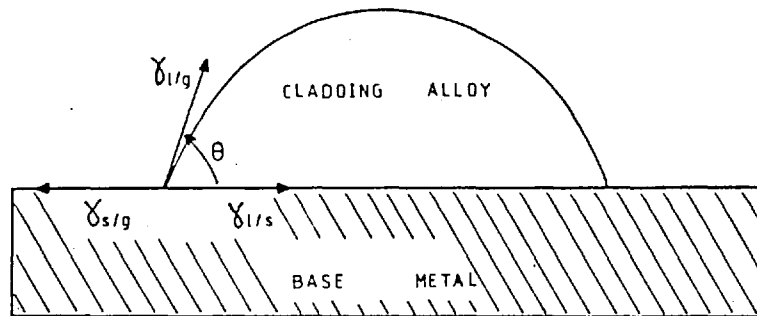
It is noticed that the resultant areas and solidified contact angles were quite different, as expected, for the different working conditions. For instance, with a 1.00 millimeter powder thickness on specimen number S65, the biggest contact angle was 127 degrees indicating that it did not exhibit good spreading. While another runs S128 had a small solidified contact angle of 23 degrees which did show good spreading.

Given a clean metal surface (true for all but preheat specimens)

$\gamma_{s/g} \approx \text{constant}$. The angle ϕ is a function of dilution while $\gamma_{l/g}$ and $\gamma_{l/s}$ would be expected to decrease with increased temperatures which is a function of (P/DV) the applied specific energy.

Fig 4. 107, 4.109 shows how the contact angle θ varies with dilution while Fig 4.110-4.112 shows the variation with (P/DV) . These two graphs are not unrelated since it has already been seen that dilution is a function of P/DV .

Likewise in Fig 4.113 shows the variation of the contact angle θ with (P/DV) , for tin-bronze surface cladding.



$\gamma_{s/g}$ - SURFACE TENSION OF SOLID SURFACE AND GAS.

$\gamma_{l/s}$ - INTERFACIAL TENSION OF LIQUID CLADDING ALLOY AND SOLID BASE METAL.

$\gamma_{l/g}$ - SURFACE TENSION OF THE LIQUID CLADDING ALLOY AND GAS.

θ - CONTACT ANGLE.

IN THE EQUILIBRIUM (DUPRÉ EQUATION)

$$\gamma_{s/g} = \gamma_{l/s} + \gamma_{l/g} \cos \theta$$

FIG 4.106 FORCE SYSTEM AFFECTING WETTABILITY IN TWO DIMENSIONS.

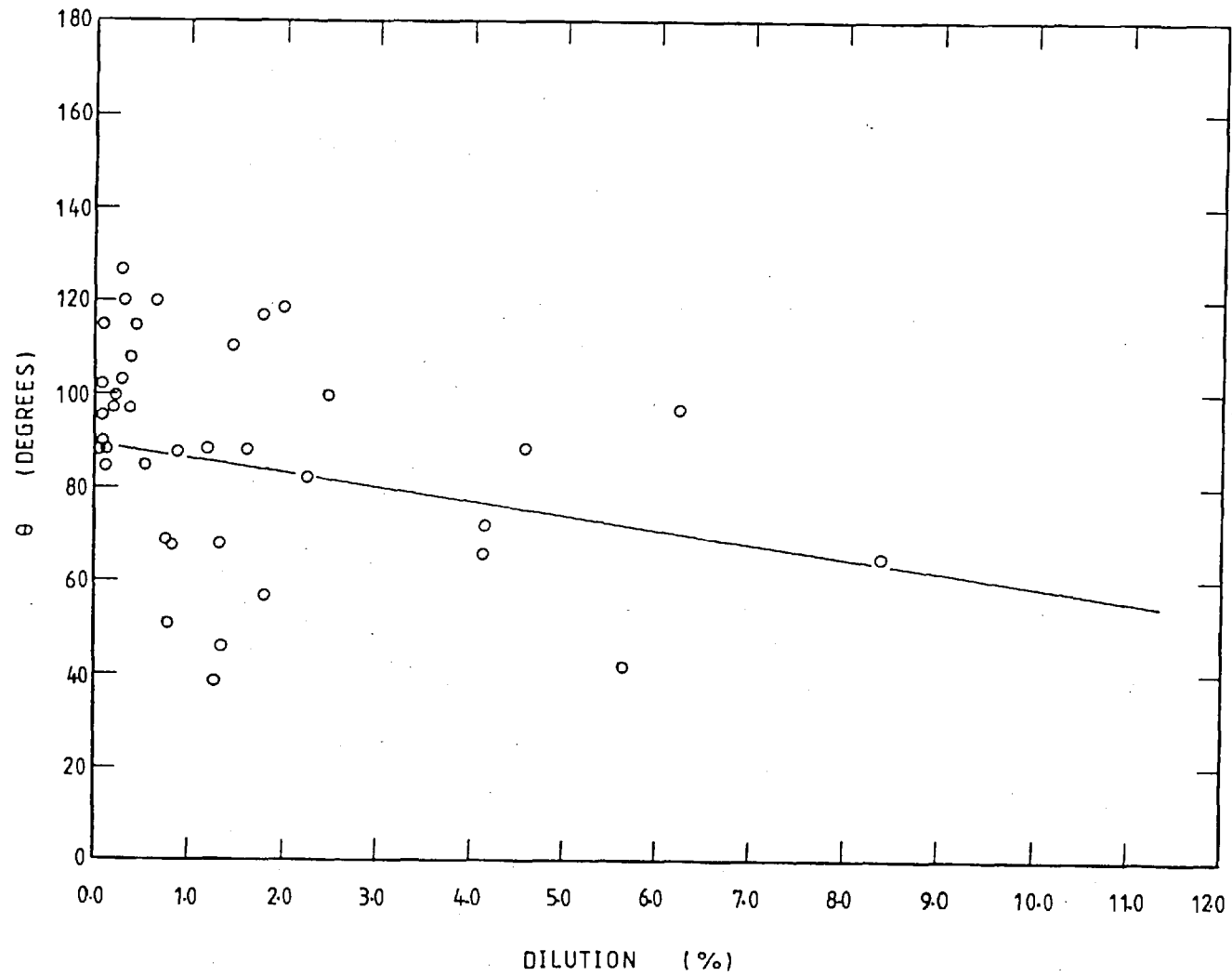


FIG 4.107 SOLIDIFIED CONTACT ANGLE, θ (DEGREES) vs DILUTION (%) FOR A 100 MM POWDER THICKNESS.

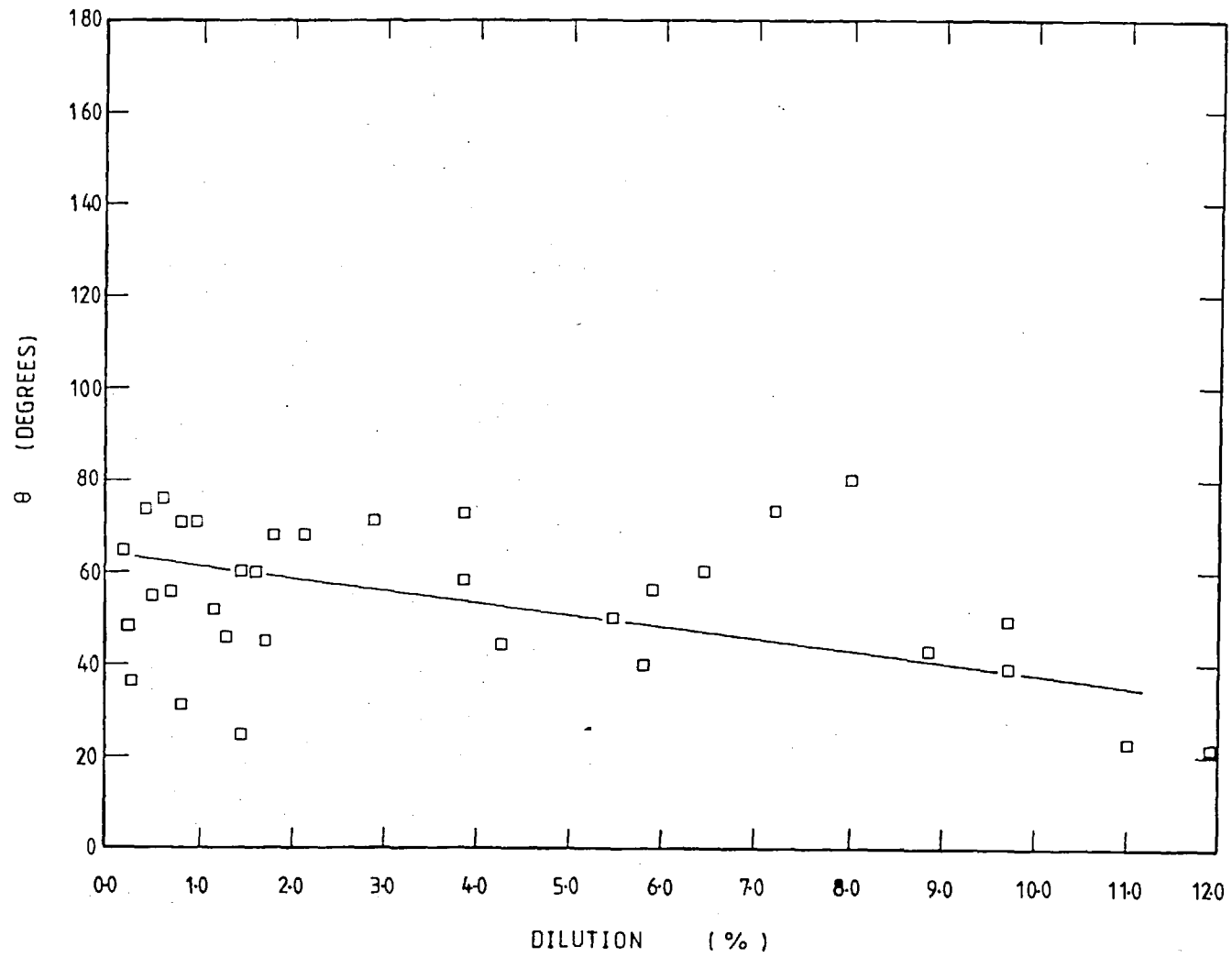


FIG 4.108 SOLIDIFIED CONTACT ANGLE, θ (DEGREES) vs DILUTION (%) FOR A 0.50 MM POWDER THICKNESS.

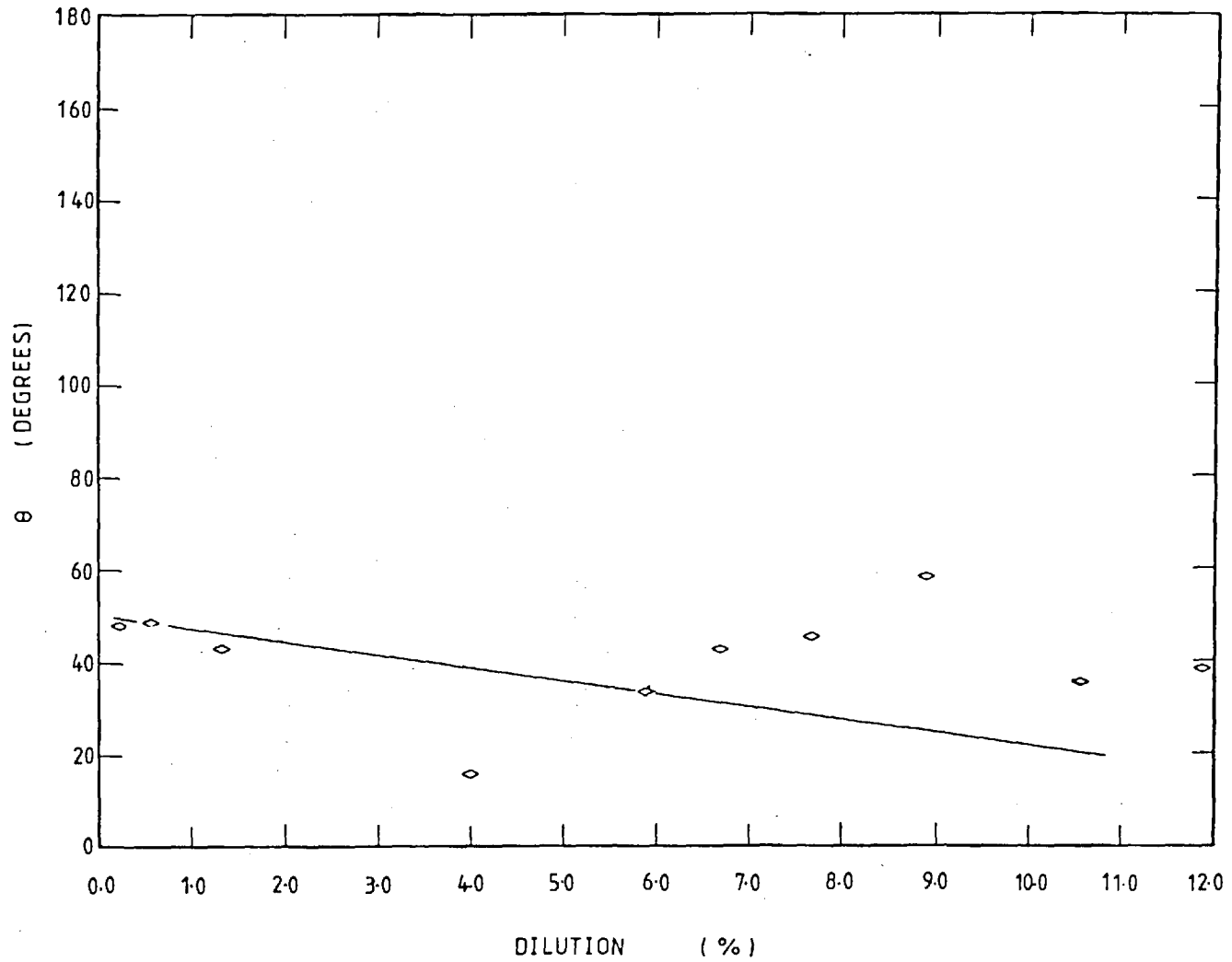


FIG 4.109 SOLIDIFIED CONTACT ANGLE, θ (DEGREES) vs DILUTION (%) FOR A 0.25 MM POWDER THICKNESS.

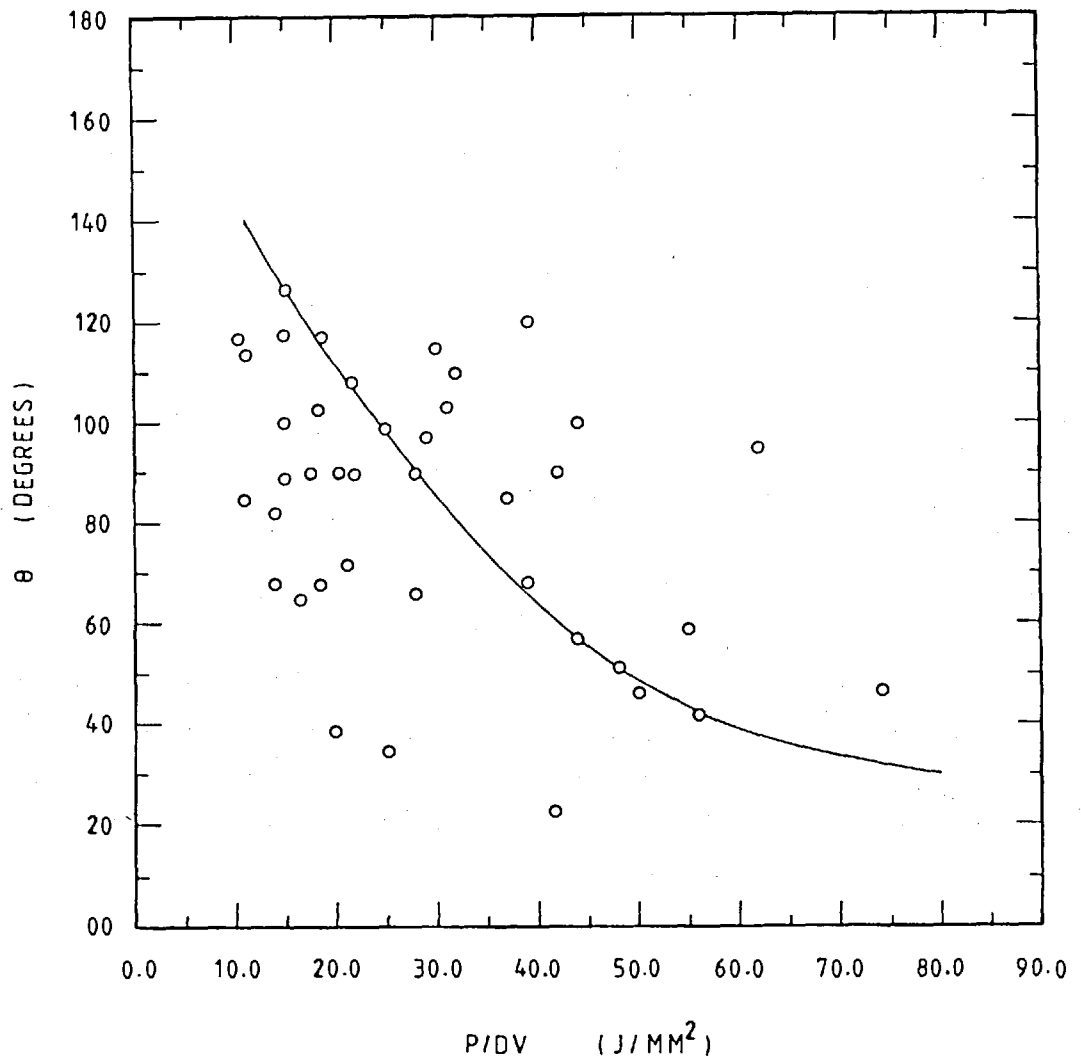


FIG 4.110 θ (DEGREES) vs ENERGY/UNIT AREA, P/DV (J/mm^2) FOR A 1.00 MM POWDER THICKNESS.

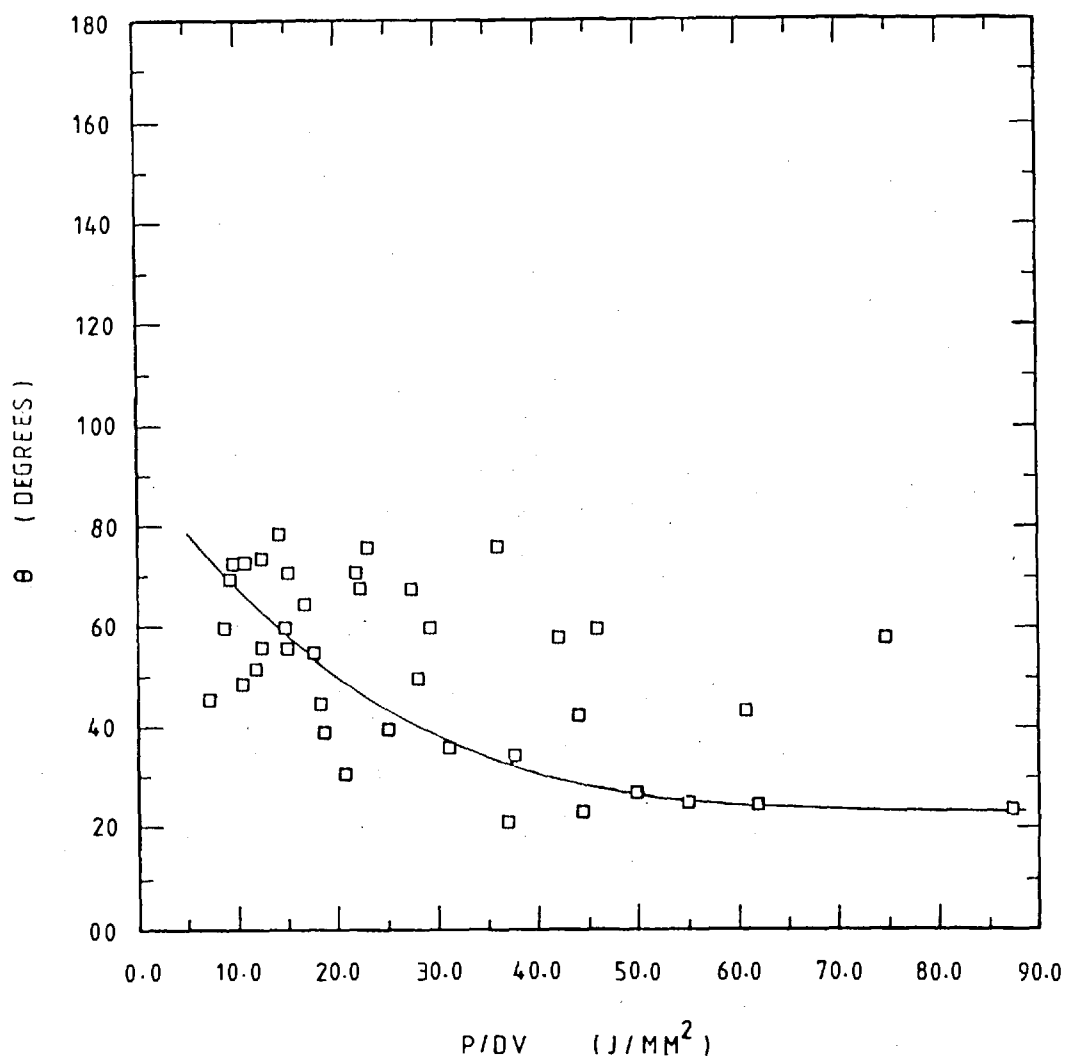


FIG 4.111 θ (DEGREES) vs ENERGY/UNIT AREA, P/DV (J/mm^2) FOR A 0.50 MM POWDER THICKNESS.

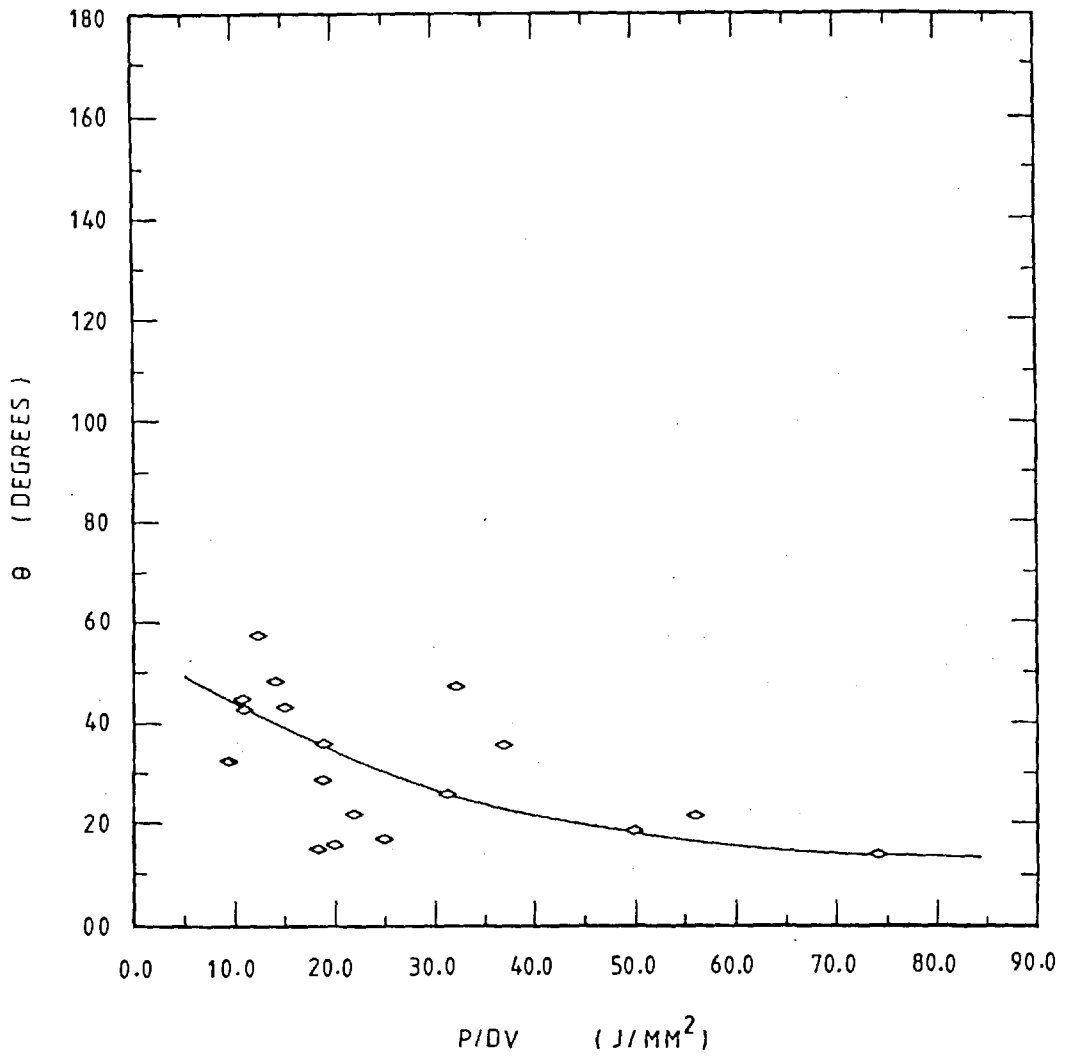


FIG 4.112 θ (DEGREES) vs ENERGY/UNIT AREA, P/DV (J/MM^2) FOR A 0.25 MM POWDER THICKNESS.

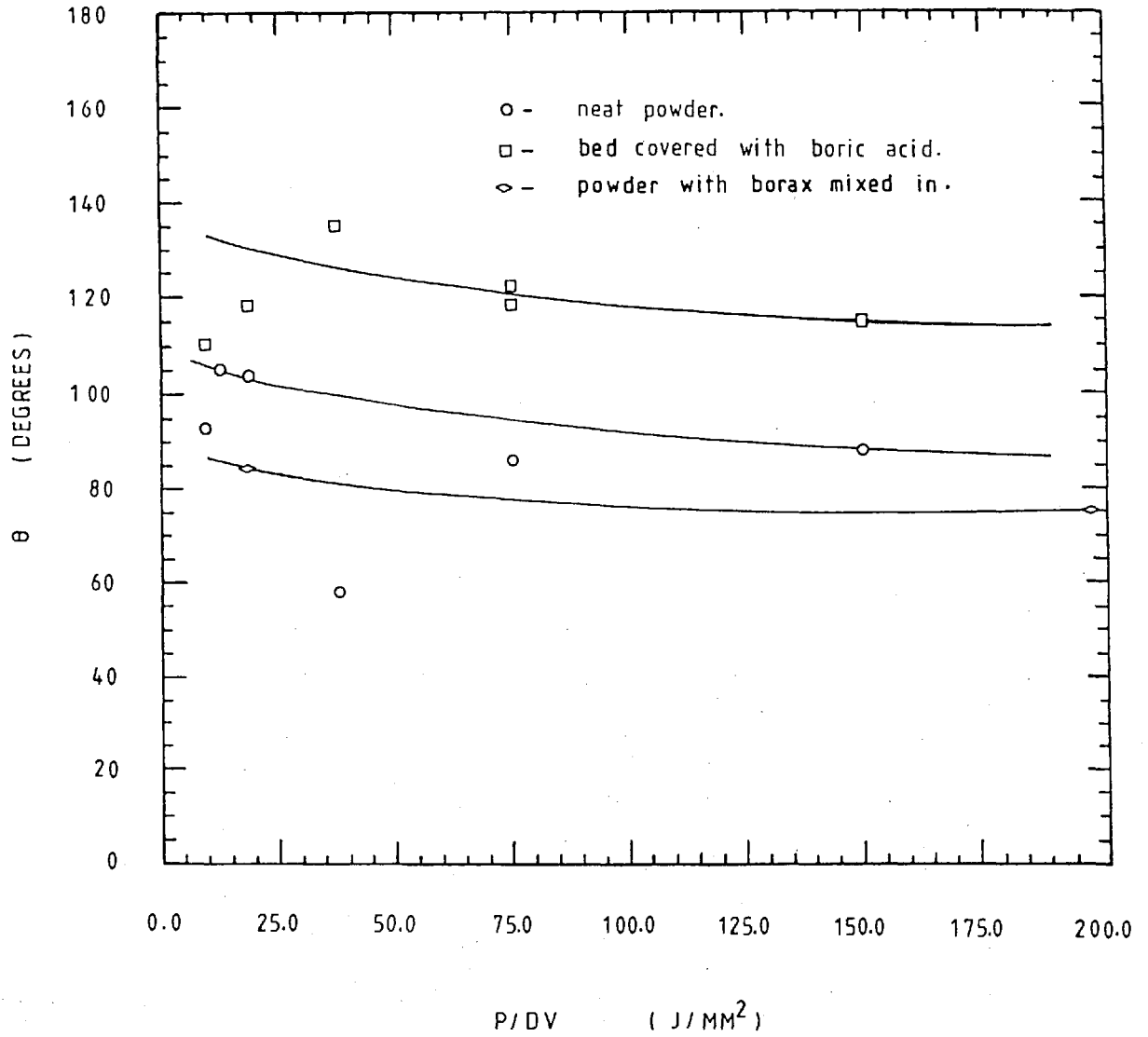


FIG 4.113 θ (DEGREES) vs ENERGY/UNIT AREA, P/DV (J/mm^2) FOR A 1.00 MM POWDER THICKNEES AND 2.00 MM BEAM DIAMETER.

4.14 Viscosity in Surface Cladding

Along the length of the clad trace there is a thermal gradient, which could be quite steep for the higher speed runs. This thermal gradient means there is a variation in surface tension, since surface tension is a function of temperature. The imbalance of surface tension forces causes surface movement the extent of which is governed by the molten pool viscosity and depth of the molten pool. The viscosity is also temperature dependent.

An oscillating backward flows from the molten pool is thus set up which results in the surface ripple structure.

4.15 Mechanical Properties in Surface Cladding

The determination of the bend and shear tests were made by B.S.C (S.L) according to A.S.T.M 264-74. The specimens were prepared according to the standard specification. The aim of the tests is to evaluate the ductility and adherence of the surface cladding.

4.15.1 Bend Test

The ASTM E290-77 describes a semi-guided bend test for ductility of metallic materials by bending through a specified angle and to a specified inside radius of curvature. The specimen shall be of the full section of the material and of

sufficient length to permit bending and the ratio of width to thickness shall be 2:1.

The results are recorded in table A.3 Appendix II.

From these results it is apparent that to avoid cracking preheat of around 350°C is necessary. The results are a little scattered probably due to lack of shielding gas.

4.15.2 Shear Test

The specimen is prepared according to standard specification and the aim of the test is to evaluate the adherence of the surface cladding onto the base metal.

The method consists in applying a force tangentially to the specimen in the top section until the surface cladding starts cracking from the base metal. The arrangement is illustrated in Fig 4.114. The results are reported in table A3, Appendix II, from which is concluded that there is adequate adherence of the surface cladding.

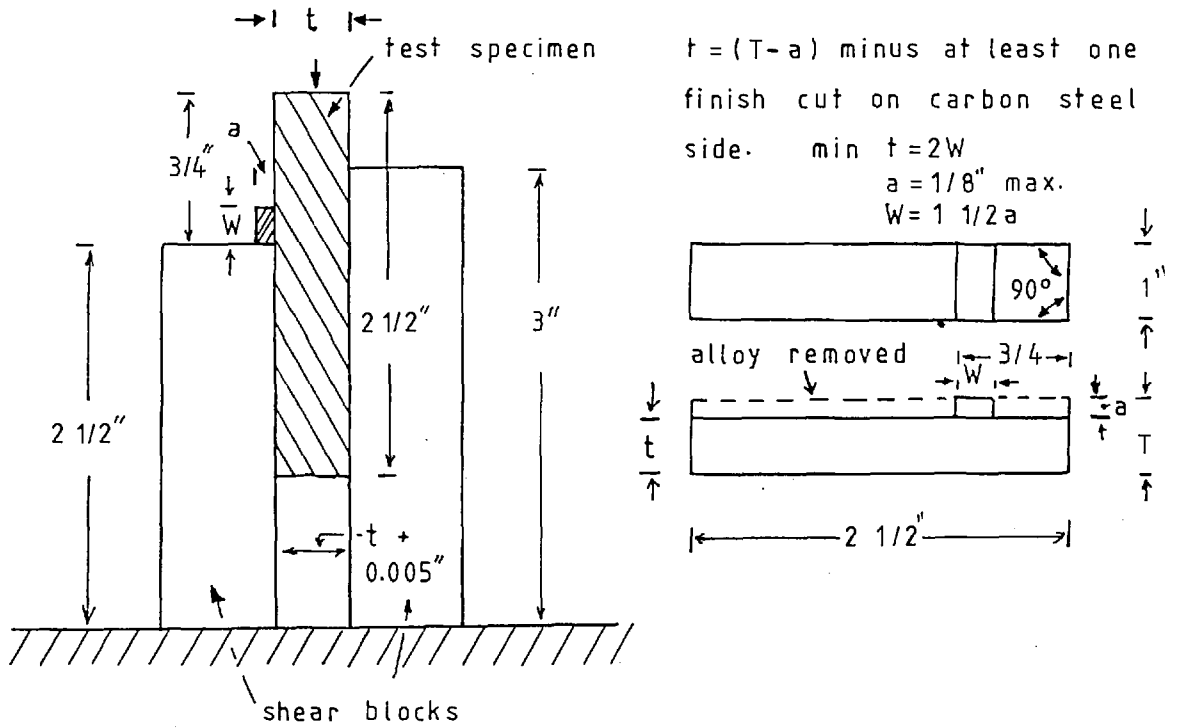


FIG 4.114 TEST SPECIMEN AND METHOD OF MAKING SHEAR TEST OF CLAD PLATE (FROM ASTM A 264-74 a).

Conclusion

The previously noted advantages of using a laser for cladding

have been justified in this work. Those advantages were

- precise control of energy input
- localisation of heat
- minimal heat affected zone and therefore thermal distortion and interface embrittlement
- a relatively tranquil process suffering from low dilution compared to other surfacing processes.
- a rapid process, resulting in high quench rates and therefore homogeneous deposits

The quality of the deposits made here has shown that smooth

surfaced deposits of controlled depth are possible, this could

be useful in reducing finishing costs in an industrial process.

The optimum operating conditions are described by the value of the applied specific energy (P/DV) J/mm^2 . Which for stainless steel, tin-bronze and monel is:

(a) Stainless Steel

1.00 mm	$44.0 \pm 8.0 J/mm^2$	$> P/DV > 14.0 \pm 5.0 J/mm^2$
0.50 mm	$35.0 \pm 8.0 J/mm^2$	$> P/DV > 11.0 \pm 5.0 J/mm^2$
0.25 mm	$22.0 \pm 8.0 J/mm^2$	$> P/DV > 10.0 \pm 5.0 J/mm^2$

(b) Tin-bronze

1.0 mm	$150 \pm 25.0 J/mm^2$	$> P/DV > 10.0 \pm 5.0 J/mm^2$.
1.0 mm	$150 \pm 25.0 J/mm^2$	$> P/DV > 10.0 \pm 5.0 J/mm^2$..
1.0 mm	$196 \pm 18.25 J/mm^2$	$> P/DV > 18.25 \pm 5.0 J/mm^2$...

(c) Monel

2.05 Kg/Hr	$80.0 \pm 20.0 J/mm^2$	$> P/DV > 30.0 \pm 12.0 J/mm^2$
1.27 Kg/Hr	$80.0 \pm 20.0 J/mm^2$	$> P/DV > 25.0 \pm 10.0 J/mm^2$
0.83 Kg/Hr	$80.0 \pm 20.0 J/mm^2$	$> P/DV > 25.0 \pm 10.0 J/mm^2$

- . Neat powder
- .. Bed covered with boric acid
- ... Powder and borax mixed in

These values were found to give continuous tracks with less than 12% dilution.

The microhardness of 316 Stainless Steel surface cladding from the apex to the interface is approximately constant with values of 239 ± 31 VPN, this implies that the resultant microstructure is homogeneous with only small variation in grain size and orientation.

The hardened martensitic zone is not homogeneous in structure through the HAZ perhaps because the short time at elevated temperature is insufficient to remove the effects of the prior ferrite-pearlite structure, so the resultant structure (deformed ferrite and bainite) contains alternating hard and soft regions. The maximum values of microhardness were found at the adjacent region to the interface. Typical values for the En3 steel were 550 ± 62 VPN.

The solidification structures formed during laser cladding are extremely fine cellular dendrites formed due to the rapid solidification rate characteristic of the process.

The microstructure in surface cladding is on a very fine scale and morphologically resembles that of the chilled zone of a solidifying bead, after the wide chilled zone has formed.

Relatively long columnar dendrites grow into the melt with differently grown direction and size, and finally a planar dendritic structure is developed in the bottom melt region adjacent to the interface.

In the multiple runs of 316 stainless steel surface cladding with preheating of the base metal of mild steel it is found that the interrun inclusions is less marked than without preheating where the oxide is present quite clearly in some runs. Good multiple-runs can be made with the correct or adequate preheat, though an improvement would be expected if a shielding gas were used.

In order to achieve a nearly smooth surface or overlap of 40-60% at least is required. There appears to be no harmful effect on the interface structure due to overlapping traces.

Adequate preheat, postheat and slow cooling after cladding could be useful to prevent possible cracks; and reduce residual thermal stress - as indicated by the bend test, while large differences in thermal and expansion coefficients between the clad alloy and the base metal should be avoided.

Low solidified contact angles may be dependent upon a low cladding-alloy surface tension combined in some cases with considerable dilution, diffusion and alloying with the base metal. High contact angles must be associated with high cladding-alloy surface tension, high interfacial tensions, and contaminated base-metal surface.

Substantial spreading of cladding alloy cannot occur unless the contact angle between alloy and solid substrate is low.

As equation ($\gamma_{l/g} \cos \theta = \gamma_{s/g} - \gamma_{s/l}$) shows factors which increase the difference between $\gamma_{s/g}$ and $\gamma_{s/l}$, or decrease the values of $\gamma_{l/g}$ favour low contact angles.

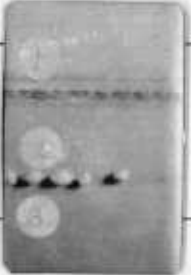

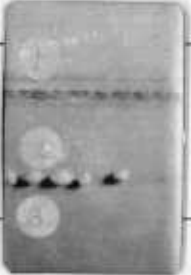

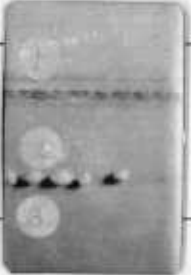

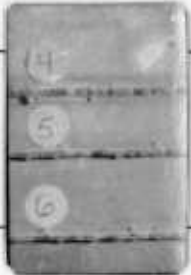
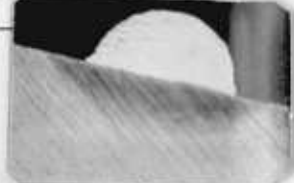
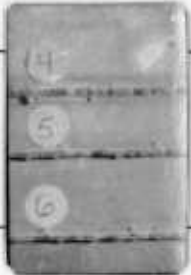

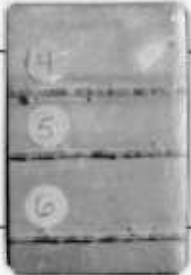

For data resulting from shear test which was made on some specimens indicates good adherence. The results are acceptable according to ASTM A264-74, consequently, successful multiple runs can be made.

It is thus concluded that laser cladding is a viable process having a promising industrial future.



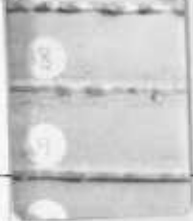









APPENDICES

- 1.1 OPERATING CONDITIONS AND RESULTS SINGLE TRACK
DEPOSITS, 316 STAINLESS STEEL SURFACE CLADDING
- 1.2 OPERATING CONDITIONS AND RESULTS SINGLE TRACK
DEPOSITS, TIN-BRONZE SURFACE CLADDING
- 1.3 OPERATING CONDITIONS AND RESULTS SINGLE TRACK
DEPOSITS, MONEL SURFACE CLADDING
- 1.4 OPERATING CONDITIONS AND RESULTS MULTIPLE TRACK
DEPOSITS, 316 STAINLESS STEEL SURFACE CLADDING
- 11.1 SECTIONAL AREA, PERCENTAGE DILUTION, DEPOSITION
RATE AND SOLIDIFIED CONTACT ANGLE AS A FUNCTION
OF THE APPLIED SPECIFIC ENERGY AND POWDER THICKNESS
- 11.2 SECTIONAL AREAS, PERCENTAGE DILUTION, DEPOSITION
RATE AND SOLIDIFIED CONTACT ANGLE AS A FUNCTION OF
THE APPLIED SPECIFIC ENERGY FOR A 1.00mm POWDER
THICKNESS OF TIN-BRONZE
- 11.3 DEPOSIT TOUGHNESS AND ADHERENCE AS MEASURED BY
BEND AND SHEAR TESTS













APPENDIX I-1 OPERATING CONDITIONS AND RESULTS SINGLE TRACK DEPOSITS, 316 STAINLESS STEEL SURFACE CLADDING.

Specimen Number	Laser Power (W)	Beam Diameter (mm)	Traverse Speed (mm/s)	Powder Thickness (mm)	Bead Width (mm)	Bead Height (mm)	HAZ Depth (mm)	Top View	Section View
S 1	1600	7.2	5	1.00	2.58 + - 0.18	1.20 + - 0.84	1.00		
S 2	1600	7.2	15	1.00	1.62 + - 2.70	1.39 + - 2.30	-		
S 3	1600	7.2	25	1.00	- -	- -	-		
S 4	1600	5.8	5	1.00	2.69 + - 0.18	1.18 + - 0.38	0.95		
S 5	1600	5.8	15	1.00	1.72 + - 0.08	1.37 + - 0.36	0.50		
S 6	1600	5.8	20	1.00	1.43 + - 1.20	1.36 + - 1.14	0.45		

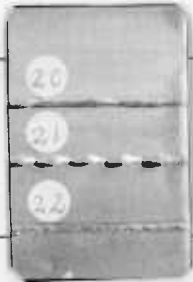
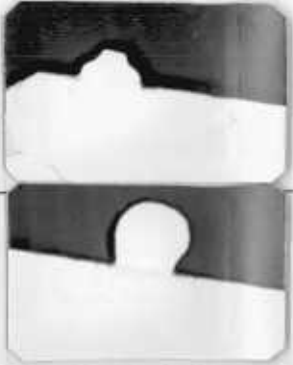
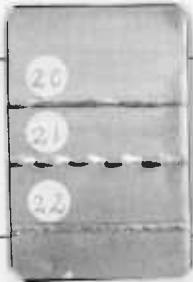
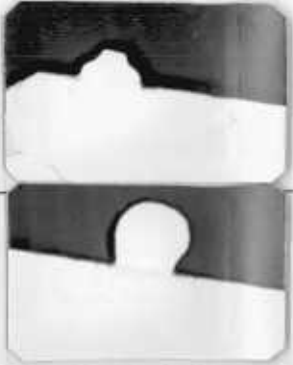
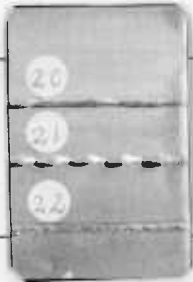
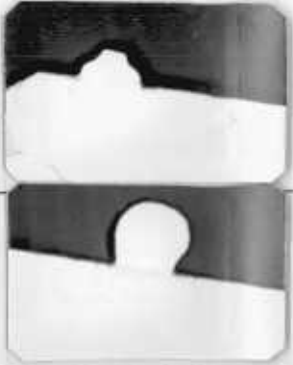
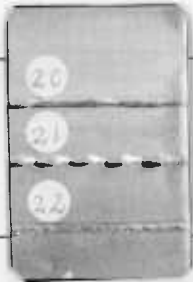
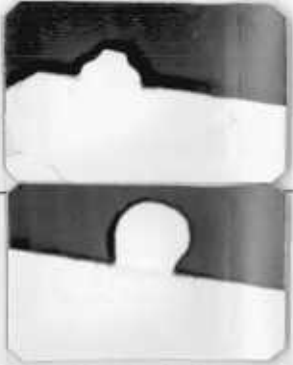
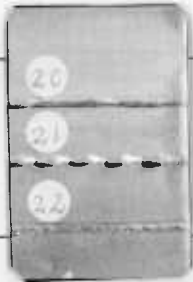
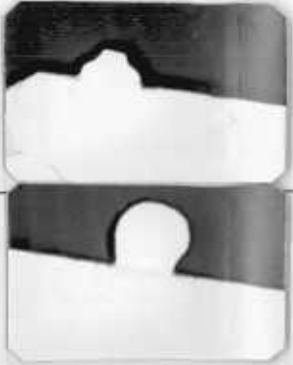
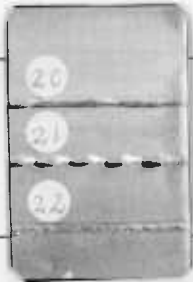
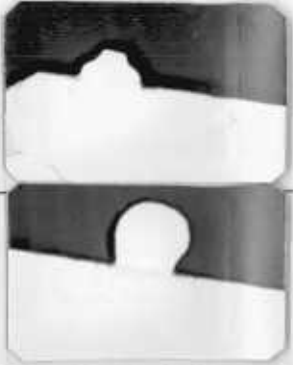
POWDER: STAINLESS STEEL 316, 300 MESH.

Specimen Number	Laser Power (W)	Beam Diameter (mm)	Traverse Speed (mm/s)	Powder Thickness (mm)	Bead		HAZ Depth (mm)	Top View	Section View
					Width (mm)	Height (mm)			
S 7	1600	5.8	25	1.00	1.50 + - 1.34	1.47 + - 1.26	0.35		
S 8	1600	4.3	5	1.00	2.39 + - 0.48	0.89 + - 0.42	0.65		
S 9	1600	4.3	10	1.00	2.14 + - 0.16	1.56 + - 0.76	0.80		
S 10	1600	4.3	15	1.00	1.84 + - 0.22	1.33 + - 0.32	0.60		
S 11	1600	4.3	20	1.00	1.70 + - 0.14	1.57 + - 0.34	0.45		
S 12	1600	4.3	25	1.00	1.52 + - 0.24	1.38 + - 0.28	0.50		


POWDER: STAINLESS STEEL 316, 300 MESH.

Specimen Number	Laser Power (W)	Beam Diameter (mm)	Traverse Speed (mm/s)	Powder Thickness (mm)	Bead Width (mm)	Bead Height (mm)	HAZ Depth (mm)	Top View	Section View
S 13	1600	4.3	30	1.00	1.34 + - 0.62	1.23 + - 0.16	0.45		
S 14	1600	4.3	5	0.25	- - -	0.25 + - 0.14	0.75		
S 15	1600	4.3	10	0.25	1.94 + - 0.20	0.44 + - 0.06	0.70		
S 16	1600	4.3	15	0.25	1.75 + - 0.34	0.36 + - 0.20	0.45		
S 17	1600	4.3	20	0.25	1.19 + - 0.98	0.27 + - 0.22	0.50		
S 18	1600	4.3	25	0.25	1.41 + - 0.16	0.47 + - 0.40	0.50		

POWDER: STAINLESS STEEL 316, 300 MESH.

Specimen Number	Laser Power (W)	Beam Diameter (mm)	Traverse Speed (mm/s)	Powder Thickness (mm)	Bead		HAZ Depth (mm)	Top View	Section View
					Width (mm)	Height (mm)			
S 19	1600	4.3	30	0.25	1.45 + - 0.22	0.63 + - 0.44	0.45		
S 20	1600	4.3	35	1.00	1.17 + - 1.00	1.22 + - 1.02	0.35		
S 21	1600	4.3	40	1.00	1.12 + - 1.42	1.11 + - 1.38	0.30		
S 22	1600	4.3	35	0.25	1.03 + - 0.28	0.29 + - 0.26	0.35		
S 23	1600	4.3	40	0.25	0.74 + - 0.96	0.21 + - 0.30	0.35		
S 24	1600	4.3	50	0.25	0.51 + - 1.14	0.18 + - 0.38	0.35		

POWDER: STAINLESS STEEL 316, 300 MESH.

Specimen Number	Laser Power (W)	Beam Diameter (mm)	Traverse Speed (mm/s)	Powder Thickness (mm)	Bead Width (mm)	Bead Height (mm)	HAZ Depth (mm)	Top View	Section View
S 25	1600	4.3	75	0.25	-	-	-		
S 26	1600	4.3	5	0.50	2.33 + - 0.26	0.76 + - 0.18	0.50		
S 27	1600	4.3	10	0.50	2.03 + - 0.20	0.51 + - 0.18	0.70		
S 28	1600	4.3	15	0.50	1.88 + - 0.18	0.77 + - 0.10	0.50		
S 29	1600	4.3	20	0.50	1.62 + - 0.12	0.77 + - 0.14	0.50		
S 30	1600	4.3	25	0.50	1.50 + - 0.20	0.80 + - 0.10	0.50		








POWDER: STAINLESS STEEL 316, 300 MESH.

Specimen Number	Laser Power (W)	Beam Diameter (mm)	Traverse Speed (mm/s)	Powder Thickness (mm)	Bead Width (mm)	Bead Height (mm)	HAZ Depth (mm)	Top View	Section View
S 31	1600	4.3	30	0.50	1.50 + - 0.18	0.78 + - 0.34	0.50		
S 32	1600	4.3	35	0.50	1.43 + - 0.12	0.78 + - 0.32	0.45		
S 33	1600	4.3	40	0.50	1.44 + - 0.16	0.77 + - 0.14	0.60		
S 34	1600	4.3	50	0.50	0.85 + - 0.70	0.54 + - 0.46	0.35		
S 35	1600	4.3	75	0.50	0.76 + - 1.30	0.76 + - 1.26	0.25		
S 36	1600	5.8	5	0.50	2.81 + - 0.36	0.69 + - 0.20	1.00		





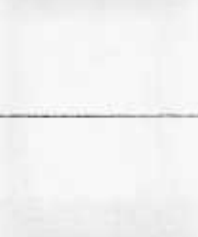







POWDER: STAINLESS STEEL 316, 300 MESH.

Specimen Number	Laser Power (W)	Beam Diameter (mm)	Traverse Speed (mm/s)	Powder Thickness (mm)	Bead Width (mm)	Bead Height (mm)	HAZ Depth (mm)	Top View	Section View
S 37	1600	5.8	10	0.50	2.05 + -	1.13 + -	0.65		
S 38	1600	5.8	15	0.50	1.68 + -	0.76 + -	0.65		
S 39	1600	5.8	20	0.50	1.04 + -	0.53 + -	0.50		
S 40	1600	5.8	25	0.50	0.73 + -	0.34 + -	0.20		
S 41	1600	7.2	5	0.50	3.18 + -	0.43 + -	1.40		
S 42	1600	7.2	10	0.50	1.89 + -	0.98 + -	0.80		













POWDER: STAINLESS STEEL 316, 300 MESH.

Specimen Number	Laser Power (W)	Beam Diameter (mm)	Traverse Speed (mm/s)	Powder Thickness (mm)	Bead Width (mm)	Bead Height (mm)	HAZ Depth (mm)	Top View	Section View
S 43	1600	7.2	15	0.50	-	-	0.55		
S 44	1600	7.2	20	0.50	-	-	-		
S 45	1600	8.7	5	0.50	2.16 + - 2.66	0.34 + - 0.44	1.25		
S 46	1600	8.7	10	0.50	-	-	-		
S 47	1600	8.7	15	0.50	-	-	-		
S 48	1600	5.8	5	0.25	2.70 + - 0.34	0.22 + - 0.08	1.20		













POWDER: STAINLESS STEEL 316, 300 MESH.

Specimen Number	Laser Power (W)	Beam Diameter (mm)	Traverse Speed (mm/s)	Powder Thickness (mm)	Bead		HAZ Depth (mm)	Top View	Section View
					Width (mm)	Height (mm)			
S 49	1600	5.8	10	0.25	2.33	0.16	0.80		
					+ -	+ -			
S 50	1600	5.8	15	0.25	1.75	0.16	0.50		
					+ -	+ -			
S 51	1600	5.8	20	0.25	0.97	0.53	0.55		
					+ -	+ -			
S 52	1600	5.8	25	0.25	0.48	0.39	0.50		
					+ -	+ -			
S 53	1600	7.2	5	0.25	2.75	0.27	1.50		
					+ -	+ -			
S 54	1600	7.2	10	0.25	1.26	0.15	0.85		
					+ -	+ -			
					1.58	0.22			


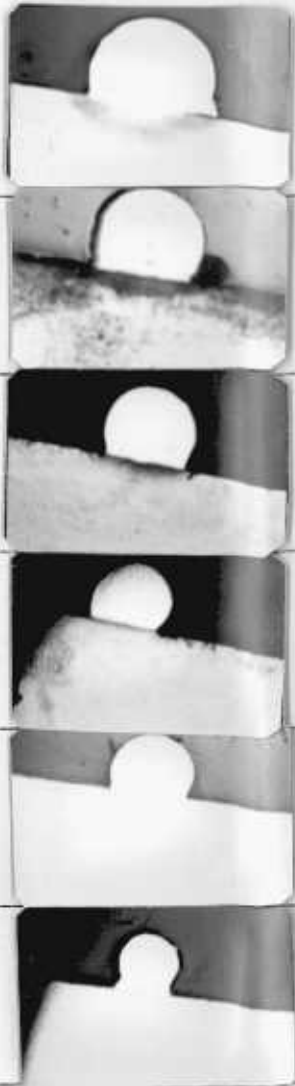
POWDER: STAINLESS STEEL 316, 300 MESH.

Specimen Number	Laser Power (W)	Beam Diameter (mm)	Traverse Speed (mm/s)	Powder Thickness (mm)	Bead		HAZ Depth (mm)	Top View	Section View
					Width (mm)	Height (mm)			
S 55	1600	7.2	15	0.25	0.70 + - 1.50	0.13 + - 0.28	0.40		
S 56	1600	7.2	20	0.25	- - -	- - -	-		
S 57	1600	8.7	5	0.25	2.31 + - 1.94	0.21 + - 0.18	0.60		
S 58	1600	8.7	10	0.25	- - -	- - -	0.75		
S 59	1400	8.7	5	1.00	2.00 + - 1.70	1.97 + - 1.68	1.00		
S 60	1400	7.2	5	1.00	2.65 + - 0.30	2.25 + - 0.58	0.95		













POWDER: STAINLESS STEEL 316, 300 MESH.

Specimen Number	Laser Power (W)	Beam Diameter (mm)	Traverse Speed (mm/s)	Powder Thickness (mm)	Bead		HAZ Depth (mm)	Top View	Section View
					Width (mm)	Height (mm)			
S 61	1400	7.2	10	1.00	0.86	0.51	0.60		
					+	+			
					-	-			
S 62	1400	5.8	5	1.00	2.56	1.25	0.80		
					+	+			
					-	-			
S 63	1400	4.6	10	1.00	2.05	1.63	0.65		
					+	+			
					-	-			
S 64	1400	4.6	15	1.00	1.31	0.55	0.55		
					+	+			
					-	-			
S 65	1400	4.6	20	1.00	1.64	1.42	0.40		
					+	+			
					-	-			
S 66	1400	4.6	25	1.00	1.26	1.13	-		
					+	+			
					-	-			
					2.10	1.88			

POWDER: STAINLESS STEEL 316, 300 MESH.







Specimen Number	Laser Power (W)	Beam Diameter (mm)	Traverse Speed (mm/s)	Powder Thickness (mm)	Bead		HAZ Depth (mm)	Top View	Section View
					Width (mm)	Height (mm)			
S 67	1400	3.2	5	1.00	2.27 + - 0.34	1.91 + - 0.60	0.85		
S 68	1400	3.2	10	1.00	2.02 + - 0.06	1.48 + - 0.40	0.50		
S 69	1400	3.2	15	1.00	1.82 + - 0.16	1.40 + - 0.12	0.60		
S 70	1400	3.2	20	1.00	1.62 + - 0.04	1.24 + - 0.06	0.45		
S 71	1400	3.2	25	1.00	1.53 + - 0.16	1.24 + - 0.14	0.45		
S 72	1400	3.2	30	1.00	1.44 + - 0.10	1.35 + - 0.18	0.40		

POWDER: STAINLESS STEEL 316, 300 MESH












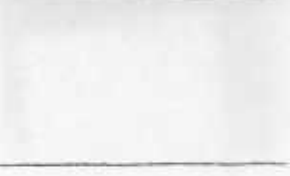
Specimen Number	Laser Power (W)	Beam Diameter (mm)	Traverse Speed (mm/s)	Powder Thickness (mm)	Bead		HAZ Depth (mm)	Top View	Section View
					Width (mm)	Height (mm)			
S 73	1400	3.2	35	1.00	0.92	1.23	0.25		
					+ -	+ -			
S 74	1400	3.2	5	0.50	2.06	0.50	0.70		
					+ -	+ -			
S 75	1400	3.2	10	0.50	1.86	0.64	0.75		
					+ -	+ -			
S 76	1400	3.2	15	0.50	1.57	0.69	0.45		
					+ -	+ -			
S 77	1400	3.2	20	0.50	1.43	0.57	0.45		
					+ -	+ -			
S 78	1400	3.2	25	0.50	1.35	0.62	0.40		
					+ -	+ -			
					0.06	0.12			

215







POWDER: STAINLESS STEEL 316, 300 MESH.

Specimen Number	Laser Power (W)	Beam Diameter (mm)	Traverse Speed (mm/s)	Powder Thickness (mm)	Bead Width (mm)	Bead Height (mm)	HAZ Depth (mm)	Top View	Section View
S 79	1400	3.2	30	0.50	1.35 + - 0.08	0.70 + - 0.12	0.35		
S 80	1400	3.2	35	0.50	1.11 + - 0.90	0.57 + - 0.48	0.50		
S 81	1400	3.2	40	0.50	1.17 + - 0.06	0.69 + - 0.12	0.35		
S 82	1400	3.2	45	0.50	1.08 + - 0.06	0.64 + - 0.06	0.35		
S 83	1400	3.2	50	0.50	0.99 + - 0.12	0.72 + - 0.22	0.35		
S 84	1400	3.2	75	0.50	- -	- -	-		

POWDER: STAINLESS STEEL 316, 300 MESH.




Specimen Number	Laser Power (W)	Beam Diameter (mm)	Traverse Speed (mm/s)	Powder Thickness (mm)	Bead		HAZ Depth (mm)	Top View	Section View
					Width (mm)	Height (mm)			
S 85	1400	4.6	5	0.50	2.32 + - 0.14	0.36 + - 0.10	0.85		
S 86	1400	4.6	20	0.50	0.67 + - 1.12	0.26 + - 0.44	0.45		
S 87	1400	4.6	35	0.50	- -	- -	-		
S 88	1400	6.1	5	0.50	2.29 + - 0.36	0.63 + - 0.82	0.80		
S 89	1400	6.1	10	0.50	- -	- -	0.50		
S 90	1400	6.7	20	0.50	- -	- -	-		

POWDER: STAINLESS STEEL 316, 300 MESH








Specimen Number	Laser Power (W)	Beam Diameter (mm)	Traverse Speed (mm/s)	Powder Thickness (mm)	Bead Width (mm)	Bead Height (mm)	HAZ Depth (mm)	Top View	Section View
S 91	1400	6.7	25	0.50	-	-	-		
S 92	1400	8.4	5	0.50	-	-	-		
S 93	1400	9.0	20	0.50	-	-	-		
S 94	1400	5.5	20	0.50	-	-	-		
S 95	1400	4.9	20	0.50	1.17 + - 2.04	0.75 + - 1.34	0.40		
S 96	1400	6.4	20	0.50	-	-	0.25		

218


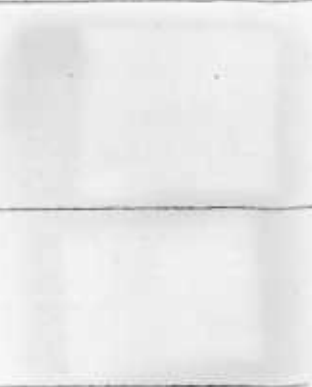
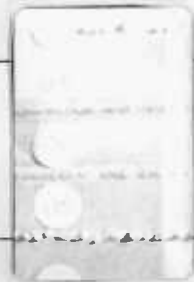

POWDER: STAINLESS STEEL 316, 300 MESH.

Specimen Number	Laser Power (W)	Beam Diameter (mm)	Traverse Speed (mm/s)	Powder Thickness (mm)	Bead Width (mm)	Bead Height (mm)	HAZ Depth (mm)	Top View	Section View
S 97	1400	7.8	5	0.50	1.09 + - 2.34	0.73 + - 1.56	1.00		
S 98	1400	8.7	5	0.25	- - -	- - -	1.10		
S 99	1400	8.7	15	0.25	- - -	- - -	-		
S 100	1400	8.7	25	0.25	- - -	- - -	-		
S 101	1400	7.2	15	0.25	- - -	- - -	-		
S 102	1400	7.2	40	0.25	- - -	- - -	-		



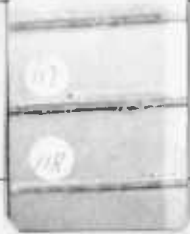









POWDER: STAINLESS STEEL 316, 300 MESH

Specimen Number	Laser Power (W)	Beam Diameter (mm)	Traverse Speed (mm/s)	Powder Thickness (mm)	Bead Width (mm)	Bead Height (mm)	HAZ Depth (mm)	Top View	Section View
S 103	1200	4.3	5	0.25	2.14 + -	0.25 + -	0.95		
S 104	1200	4.3	15	0.25	- -	- -	-		
S 105	1200	4.3	25	0.25	- -	- -	-		
S 106	1200	5.8	10	0.25	1.43 + -	0.13 + -	-		
S 107	1200	5.8	30	0.25	- -	- -	-		
S 108	1200	5.8	10	0.50	- -	- -	-		









POWDER: STAINLESS STEEL 316, 300 MESH

Specimen Number	Laser Power (W)	Beam Diameter (mm)	Traverse Speed (mm/s)	Powder Thickness (mm)	Bead Width (mm)	Bead Height (mm)	HAZ Depth (mm)	Top View	Section View
S 109	1200	5.8	25	0.50	-	-	-		
S 110	1200	8.7	10	0.50	-	-			
S 111	1200	8.7	15	1.00	-	-			
S 112	1200	4.3	25	1.00	-	-	-		
S 113	1200	4.3	10	1.00	1.69 + -	0.84 + -	0.75		
S 114	1200	4.3	5	1.00	2.21 + -	0.50 + -	0.80		
					0.16	0.10			
					0.06	0.20			

POWDER: STAINLESS STEEL 316, 300 MESH

Specimen Number	Laser Power (W)	Beam Diameter (mm)	Traverse Speed (mm/s)	Powder Thickness (mm)	Bead		HAZ Depth (mm)	Top View	Section View
					Width (mm)	Height (mm)			
S 115	1200	4.3	15	1.00	0.47	0.36	0.40		
					+	+			
S 116	1800	4.3	10	1.00	1.30	1.06	0.85		
					+	+			
S 117	1800	4.3	15	1.00	2.29	1.57	0.50		
					+	+			
S 118	1800	4.3	20	1.00	0.12	0.20	0.40		
					+	+			
S 119	1800	4.3	25	1.00	2.23	1.71	0.35		
					+	+			
S 120	1800	4.3	30	1.00	0.06	0.26	0.30		
					+	+			
					0.10	0.32			
					1.79	1.11			
					0.08	0.16			
					1.62	1.26			
					+	+			
					-	-			
					0.54	0.38			

POWDER: STAINLESS STEEL 316, 300 MESH.

Specimen Number	Laser Power (W)	Beam Diameter (mm)	Traverse Speed (mm/s)	Powder Thickness (mm)	Bead		HAZ Depth (mm)	Top View	Section View
					Width (mm)	Height (mm)			
S 121	1800	4.3	35	1.00	0.89	0.74	0.20		
					+ -	+ -			
S 122	1800	5.8	5	1.00	1.94	1.60	1.15		
					+ -	+ -			
S 123	1800	5.8	10	1.00	2.45	1.73	0.80		
					+ -	+ -			
S 124	1800	5.8	15	1.00	2.01	1.44	0.60		
					+ -	+ -			
S 125	1800	5.8	20	1.00	2.09	1.78	0.45		
					+ -	+ -			
S 126	1800	7.2	5	1.00	3.02	1.28	0.95		
					+ -	+ -			
					0.12	0.38			

POWDER: STAINLESS STEEL 316, 300 MESH.


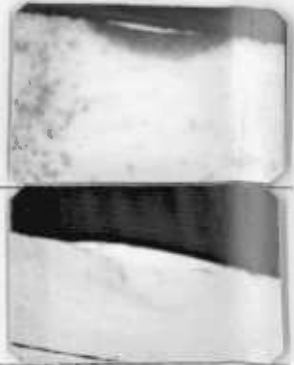



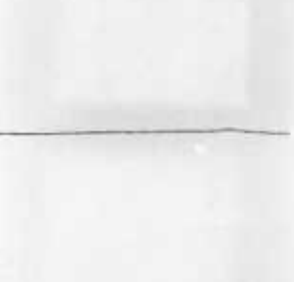

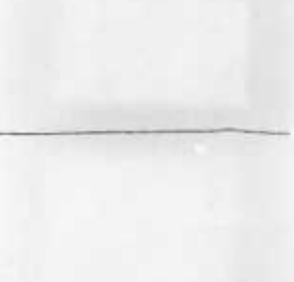
Specimen Number	Laser Power (W)	Beam Diameter (mm)	Traverse Speed (mm/s)	Powder Thickness (mm)	Bead		HAZ Depth (mm)	Top View	Section View
					Width (mm)	Height (mm)			
S 127	1800	7.2	10	1.00	2.14	0.53	0.65		
					+ -	+ -			
S 128	1800	8.7	5	1.00	0.34	0.38	0.90		
					2.75 -	0.93 -			
S 129	1800	8.7	15	1.00	2.26	1.64	-		
					- -	- -			
S 130	1800	8.7	5	0.50	2.47	0.44	0.95		
					+ -	+ -			
S 131	1800	7.2	5	0.50	3.12	0.68	1.30		
					2.80 +	0.66 +			
S 132	1800	7.2	15	0.50	1.22	0.54	-		
					- -	- -			

Specimen Number	Laser Power (W)	Beam Diameter (mm)	Traverse Speed (mm/s)	Powder Thickness (mm)	Bead Width (mm)	Bead Height (mm)	HAZ Depth (mm)	Top View	Section View
S 133	1800	5.8	5	0.50	2.87 + -	0.70 + -	1.10		
S 134	1800	5.8	10	0.50	2.30 + -	0.71 + -	0.75		
S 135	1800	5.8	15	0.50	1.80 + -	0.64 + -	0.65		
S 136	1800	4.3	10	0.50	2.27 + -	0.97 + -	0.90		
S 137	1800	4.3	15	0.50	2.05 + -	0.99 + -	0.75		
S 138	1800	4.3	20	0.50	1.77 + -	0.61 + -	0.80		

POWDER: STAINLESS STEEL 316, 300 MESH

Specimen Number	Laser Power (W)	Beam Diameter (mm)	Traverse Speed (mm/s)	Powder Thickness (mm)	Bead Width (mm)	Bead Height (mm)	HAZ Depth (mm)	Top View	Section View
S 139	1800	4.3	25	0.50	1.73 + -	1.15 + -	0.50		
					0.22	0.50			
S 140	1800	4.3	30	0.50	1.63 + -	1.33 + -	0.45		
					0.36	0.76			
S 141	1800	4.3	35	0.50	1.24 + -	0.94 + -	0.45		
					0.20	0.12			
S 142	1800	4.3	10	0.25	2.24 + -	0.17 + -	1.00		
					0.08	0.08			
S 143	1800	4.3	30	0.25	-	-	0.45		
					-	-			
S 144	1800	5.8	10	0.25	1.89 + -	0.30 + -	0.90		
					1.58	0.44			

POWDER: STAINLESS STEEL 316, 300 MESH


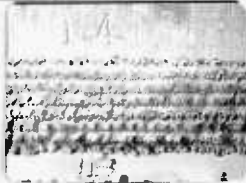












Specimen Number	Laser Power (W)	Beam Diameter (mm)	Traverse Speed (mm/s)	Powder Thickness (mm)	Bead Width (mm)	Bead Height (mm)	HAZ Depth (mm)	Top View	Section View
S 145	1800	5.8	15	0.25	1.37	0.13	0.80		
					+	+			
S 146	1800	7.2	5	0.25	1.70	0.24	0.90		
					+	+			
S 147	1800	7.2	25	0.25	2.96	0.21	-		
					-	-			
S 148	1800	8.7	10	0.25	0.14	0.16	-		
					-	-			

POWDER: STAINLESS STEEL 316, 300 MESH.

APPENDIX I-2 OPERATING CONDITIONS AND RESULTS SINGLE TRACK DEPOSITS, TIN-BRONZE SURFACE CLADDING

Specimen Number	Laser Power (w)	Beam Diameter (mm)	Traverse Speed (mm/s)	Powder Thickness (mm)	Bead Width (mm)	Bead Height (mm)	H.A.Z. Depth (mm)	Top View	Section View
B1	1500	2.0	5	1.0	2.80	0.67	0.27		
B2	1500	2.0	10	1.0	2.44	0.80	0.17		
B3	1500	2.0	20	1.0	2.50	0.74	0.14		
B4	1500	2.0	40	1.0	2.80	0.95	0.17		
B5	1500	2.0	60	1.0	1.80	0.77	0.12		
B6	1480	2.0	80	1.0	1.55	0.84	0.10		
B07	1500	2.0	5	1.0	2.74	0.90	0.20		
B08	1500	2.0	10	1.0	2.36	0.72	0.19		
B09	1500	2.0	20	1.0	2.60	0.58	0.17		
B010	1500	2.0	40	1.0	2.30	0.60	0.15		
B011	1490	2.0	80	1.0	1.51	0.94	0.08		
BI12	1460	2.0	5	1.0	2.51	0.58	0.26		

POWDER: 90% Cu, 9.5% Sn, 0.2% P, 0.3% OTHERS

Specimen Number	Laser Power (w)	Beam Diameter (mm)	Traverse Speed (mm/s)	Powder Thickness (mm)	Bead Width (mm)	Bead Height (mm)	H.A.Z. Depth (mm)	Top View	Section View
BI 13	1460	2.0	40	1.0	1.66	0.29	0.12		
BM 14	1490	2.0	10	1.0					
BO 15	1500	2.0	10	1.0	2.40	0.88	0.18		
BMOS 16	1500	2.0	10	1.0					
BMS 17	1500	2.0	10	1.0					
BMS 19	1560	2.0	10	1.0					
BMS 19	1560	2.0	20	1.0					

O - BED WAS LIGHT COVERED OF BORIC ACID
 I - POWDER WITH BORAX MIXED IN
 S - LENS GAS SHIELDING
 M - OVERLAP 1.25 mm

POWDER: 90% Cu, 9.5% Sn, 0.2% P, 0.3% OTHERS

APPENDIX I-3 OPERATING CONDITIONS AND RESULTS SINGLE TRACK DEPOSITS, MONEL SURFACE CLADDING.


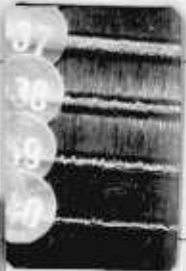
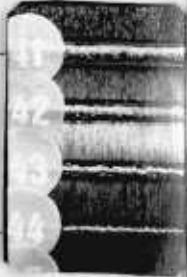

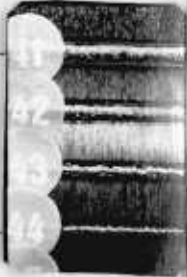

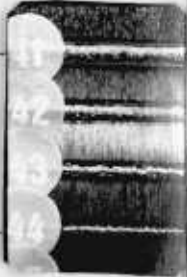

Specimen Number	Laser Power (W)	Beam Diameter (mm)	Traverse Speed (mm/s)	Mass Flow Rate (Kg/Hr)	Bead Width (mm)	Bead Height (mm)	HAZ Depth (mm)	Top View	Section View
M 1	1560	2.0	5	0.83					
M 2	1560	2.0	5	0.83					
M 3	1560	2.0	3	0.83					
M 4	1560	2.0	3	1.37					
M 5	1560	2.0	3	2.05					
M 6	1560	2.0	5	2.05					
M 7	1560	2.0	18	2.05					
M 8	1600	2.0	10	2.05	1.85	0.90			
M 9	1600	2.0	15	2.05	1.70	0.55			
M 10	1600	2.0	20	2.05	1.15	0.23			
M 11	1600	2.0	25	2.05	0.85	0.15			
M 12	1600	2.0	30	2.05	0.80	0.10			
M 13	1600	2.0	35	2.05	0.60	0.10			
M 14	1600	2.0	40	2.05	0.55	0.10			
M 15	1560	2.0	45	2.05					
M 16	1560	2.0	50	2.05					

230

POWDER MONEL : PRE-ALLOYED APB2/TVKO619 (150 μm)

Specimen Number	Laser Power (W)	Beam Diameter (mm)	Traverse Speed (mm/s)	Mass Flow Rate (Kg/Hr)	Bead Width (mm)	Bead Height (mm)	HAZ Depth (mm)	Top View	Section View
M 17	1560	2.0	10	1.37	1.55	1.30			
M 18	1560	2.0	15	1.37	1.10	0.30			
M 19	1560	2.0	20	1.37	0.95	0.23			
M 20	1560	2.0	25	1.37	0.85	0.15			
M 21	1560	2.0	30	1.37	0.60	0.10			
M 22	1560	2.0	40	1.37	0.55	0.05			
M 23	1560	2.0	10	0.83	1.40	0.50			
M 24	1560	2.0	15	0.83	1.15	0.25			
M 25	1560	2.0	20	0.83	0.90	0.15			
M 26	1560	2.0	25	0.83	0.75	0.13			
M 27	1560	2.0	30	0.83	0.60	0.10			
M 28	1560	2.0	40	0.83					
M 29	1560	3.0	10	1.37					
M 30	1500	3.0	10	1.37	1.65	0.65			
M 31	1590	3.0	10	1.37	1.95	0.75			
M 32	1560	3.0	15	1.37	1.25	0.40			

POWDER MONEL : PRE-ALLOYED APB2/TVK0619 (150 μm)

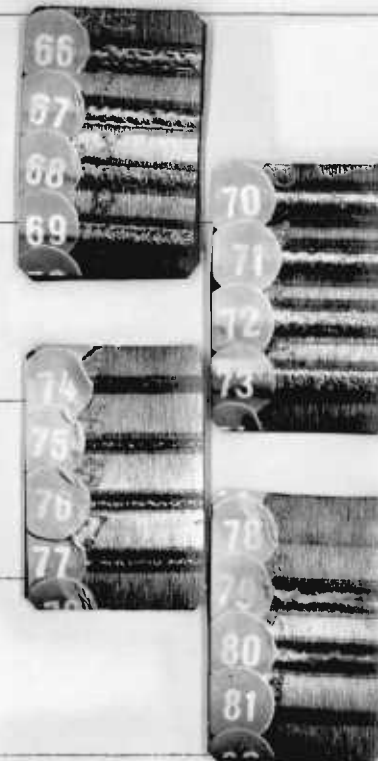
Specimen Number	Laser Power (W)	Beam Diameter (mm)	Traverse Speed (mm/s)	Mass Flow Rate (Kg/Hr)	Bead Width (mm)	Bead Height (mm)	HAZ Depth (mm)	Top View	Section View
M 33	1560	3.0	20	1.37	1.00	0.20			
M 34	1560	3.0	25	1.37	0.90	0.10			
M 35	1560	3.0	30	1.37					
M 36	1560	3.0	10	2.05	1.40	1.40			
M 37	1560	3.0	15	2.05	1.60	0.55			
M 38	1560	3.0	20	2.05	1.05	0.25			
M 39	1560	3.0	25	2.05	0.55	0.10			
M 40	1560	3.0	30	2.05					
M 41	1560	3.0	10	0.83	1.50	0.40			
M 42	1560	3.0	15	0.83	1.15	0.23			
M 43	1560	3.0	20	0.83	0.70	0.10			
M 44	1560	3.0	25	0.83					
M 45	1560	3.0	30	0.83					
M 46	1560	3.0	13	2.05	1.25	0.30			
M 47	1560	3.0	13	2.05	1.15	0.20			
M 48	1560	3.0	13	2.05	1.25	0.30			

POWDER MONEL : PRE-ALLOYED APB2/TVKO619 (150 μm)

Specimen Number	Laser Power (W)	Beam Diameter (mm)	Traverse Speed (mm/s)	Mass Flow Rate (Kg/Hr)	Bead Width (mm)	Bead Height (mm)	HAZ Depth (mm)	Top View	Section View
MM 49	1560	3.0	13	2.05					
MM 50	1530	3.0	10	1.37					
MM 51	1460	3.0	10	2.05					
MM 52	1560	3.0	10	2.05					
MM 53	1500	3.0	6	1.37					
MM 54	1500	3.0	6	1.37					
MM 55	1500	3.0	8	1.37					
M 56	1560	3.0	10	0.83	1.70	0.15			
M 57	1560	3.0	10	1.37	1.50	0.13			
M 58	1560	3.0	10	2.05	1.55	0.25			
M 59	1560	3.0	6.6	0.83	1.40	0.08			
M 60	1560	3.0	6.6	1.37	1.70	0.18			
M 61	1560	3.0	6.6	2.05	1.95	0.25			
M 62	1560	3.0	20	0.83					
M 63	1560	3.0	20	1.37					
M 64	1560	3.0	20	2.05					

POWDER MONEL : PRE-ALLOYED APB2/TVKO619 (150 μm)

Specimen Number	Laser Power (W)	Beam Diameter (mm)	Traverse Speed (mm/s)	Mass Flow Rate (Kg/Hr)	Bead Width (mm)	Bead Height (mm)	HAZ Depth (mm)	Top View	Section View
M 65	1560	3.0	20	2.74					
M 66	1560	4.0	10	0.83	1.5	0.20			
M 67	1560	4.0	10	1.37	1.3	0.15			
M 68	1560	4.0	10	2.05	1.8	0.30			
M 69	1560	4.0	10	2.74	1.9	0.35			
M 70	1560	4.0	5	0.83	2.35	0.35			
M 71	1560	4.0	5	1.37	2.30	0.37			
M 72	1560	4.0	5	2.05	2.25	0.75			
M 73	1560	4.0	5	2.74	2.15	1.45			
M 74	1560	4.0	15	0.83					
M 75	1560	4.0	15	1.37					
M 76	1560	4.0	15	2.05					
M 77	1560	4.0	15	2.74					
M 78	1560	4.0	8	0.83					
M 79	1560	4.0	8	1.37					
M 80	1560	4.0	8	2.05					



234

POWDER MONEL : PRE-ALLOYED APB2/TVKO619 (150 μm)


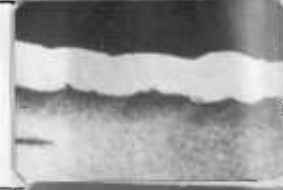



Specimen Number	Laser Power (W)	Beam Diameter (mm)	Traverse Speed (mm/s)	Mass Flow Rate (Kg/Hr)	Bead Width (mm)	Bead Height (mm)	HAZ Depth (mm)	Top View	Section View
M 81	1560	4.0	8	2.74					
M 82	1560	2.0	8	0.83	1.50	0.05			
M 83	1560	2.0	8	1.37	1.20	0.15			
M 84	1560	2.0	8	2.05	1.60	0.18			
M 85	1560	2.0	8	2.74					
M 86	1560	2.0	13	0.83					
M 87	1560	2.0	13	1.37					
M 88	1560	2.0	13	2.05					
M 89	1560	2.0	13	2.74					
M 90	1560	2.0	13	0.83	1.35				
M 91	1560	2.0	13	1.37	1.20				
M 92	1560	2.0	13	2.05	1.20				
M 93	1560	2.0	13	2.74	1.25				
M 94	1560	2.0	20	0.83	0.90				
M 95	1560	2.0	20	1.37	1.25				
M 96	1560	2.0	20	2.05	1.10				

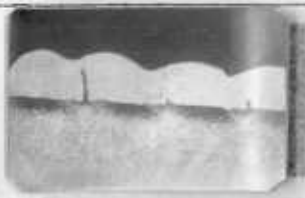


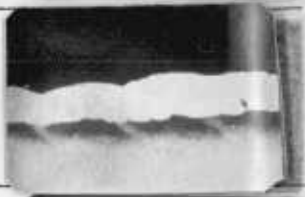

POWDER MONEL : PRE-ALLOYED APB2/TVKO619 (150 μm)

Specimen Number	Laser Power (W)	Beam Diameter (mm)	Traverse Speed (mm/s)	Mass Flow Rate (Kg/Hr)	Bead Width (mm)	Bead Height (mm)	HAZ Depth (mm)	Top View	Section View
M 97	1560	2.0	20	2.74	1.15				
MM 98	1560	2.0	15	2.05					
MM 99	1560	2.0	15	2.05					
M 100	1520	2.0	25	0.83	0.90				
M 101	1520	2.0	25	0.83	0.65				
M 102	1520	2.0	25	2.05	0.75				
M 103	1520	2.0	25	2.74	1.5				
M 104	1520	2.0	10	2.05					
M 28A	1500	2.0	13	1.37					
MM 110	1400	3.0	13	2.05					
MM 111	1400	3.0	13	2.05					
MM 112	1400	3.0	13	2.05					

POWDER MONEL : PRE-ALLOYED APB2/TVKO619 (150 μm)



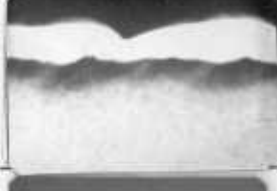

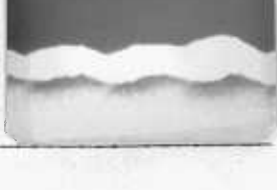
APPENDIX I-4 OPERATING CONDITIONS AND RESULTS MULTIPLE TRACK DEPOSITS, 316 STAINLESS STEEL SURFACE CLADDING

Specimen number	Laser power (W)	Beam diameter (mm)	Traverse speed (mm/s)	Powder thickness (mm)	AISI powder	Preheat (°C)	Overlap (mm)	Bead height (mm)	HAZ depth (mm)	Section View
M 1	1400	2.29	18	2.0	316 300	500	1.25	0.70 ± 0.34	0.12 ± 0.06	
M 2	1400	2.29	18	2.0	316 300	300	1.25	0.68 ± 0.22	0.28 ± 0.08	
M 3	1400	2.29	15	2.0	316 -300	20	1.25	0.88 ± 0.80	0.32 ± 0.32	
M 4	1300	2.29	15	2.0	316 -300	20	1.88	0.78 ± 0.26	0.26 ± 0.12	
M 5	1300	2.29	15	2.0	316 -300	20	1.50	0.82 ± 0.41	0.33 ± 0.30	

Specimen number	Laser power (W)	Beam diameter (mm)	Traverse speed (mm/s)	Powder thickness (mm)	AISI powder	Preheat (°C)	Overlap (mm)	Bead height (mm)	HAZ depth (mm)	
M 6	1300	2.29	20	2.0	316 -300	20	1.50	0.79 ± 0.12	0.21 ± 0.06	
M 7	1300	2.29	20	2.0	316 -300	20	1.50	0.81 ± 0.26	0.35 ± 0.16	
M 8	1300	2.29	25	2.0	316 -300	20	single run	width 1.9 height 1.8	0.2	
M 9	1460	2.29	15	2.0	316 -300	300	1.50	0.84 ± 0.54	0.26 ± 0.06	
M10	1460	2.29	20	2.0	316 -300	300	1.50	0.74 ± 0.20	0.26 ± 0.06	

Specimen number	Laser power (W)	Beam diameter (mm)	Traverse speed (mm/s)	Powder thickness (mm)	AISI powder	Preheat (°C)	Overlap (mm)	Bead height (mm)	HAZ depth (mm)
M 11	1460	2.29	25	2.0	316 -300	300	1.50	0.73 ± 0.26	0.28 ± 0.08
M 12	1400	2.29	15	2.0	316 -300	200	1.50	0.86 ± 0.88	0.30 ± 0.20
M 13	1400	2.29	20	2.0	316 -300	200	1.50	0.71 ± 0.22	0.24 ± 0.08
M 14	1400	2.29	25	2.0	316 -300	200	1.50	0.63 ± 0.44	0.26 ± 0.08
M 15	1400	2.29	15	2.0	316 -300	150	1.50	0.68 ± 0.50	0.27 ± 0.16



Specimen number	Laser power (W)	Beam diameter (mm)	Traverse speed (mm/s)	Powder thickness (mm)	AISI powder	Preheat (°C)	Overlap (mm)	Bead height (mm)	HAZ depth (mm)	
M16	1400	2.29	20	2.0	3.16 -300	150	1.50	0.56 ± 0.12	0.28 ± 0.06	
M17	1400	2.29	25	2.0	3.16 -300	150	1.50	0.73 ± 0.20	0.28 ± 0.06	
M18	1300	2.29	15	2.0	316 300	400	1.50	0.77 ± 0.38	0.32 ± 0.06	
M19	1300	2.29	20	2.0	316 300	400	1.50	0.72 ± 0.46	0.29 ± 0.08	
M20	1300	2.29	25	2.0	316 300	400	1.50	0.56 ± 0.26	0.26 ± 0.04	

APPENDIX 11.1

TABLE A1 SECTIONAL AREA PERCENTAGE DILUTION DEPOSITION RATE AND SOLIDIFIED CONTACT ANGLE AS A FUNCTION OF THE APPLIED SPECIFIC ENERGY AND BED POWDER THICKNESS.

SPECIMEN NUMBER	APPLIED SPECIFIC ENERGY (J/mm ²)	POWDER THICKNESS (mm)	SECTIONAL AREA (mm ²)	DILUTION (%)	RATE OF DEPOSITION (Kg/Hr)	SOLIDIFIED CONTACT ANGLE (DEGREES)
S 1	44.0	1.00	1.91	1.78	0.28	57
S 2	14.8	1.00	-	-	-	-
S 3	8.9	1.00	-	-	-	-
S 4	55.2	1.00	2.95	0.76	0.42	69
S 5	18.4	1.00	1.39	0.81	0.60	68
S 6	13.8	1.00	1.50	2.26	0.85	82
S 7	11.0	1.00	0.88	0.51	0.63	85
S 8	74.4	1.00	1.72	22.88	0.25	47
S 9	37.2	1.00	2.65	0.71	0.76	85
S10	24.8	1.00	1.66	0.34	0.72	99
S11	18.6	1.00	1.97	0.29	1.13	103
S12	14.9	1.00	1.98	4.55	1.43	89
S13	12.4	1.00	1.25	0.45	1.08	114
S14	74.4	0.25	0.23	50.00	0.03	14
S15	37.2	0.25	0.55	12.24	0.16	36
S16	24.8	0.25	0.25	36.36	0.11	17
S17	18.6	0.25	0.43	10.53	0.25	36
S18	14.9	0.25	0.17	6.67	0.12	43
S19	12.4	0.25	0.51	8.89	0.44	58
S20	10.6	1.00	1.29	1.73	1.30	117
S21	9.3	1.00	-	-	-	-
S22	10.6	0.25	0.15	7.69	0.15	45
S23	9.3	0.25	0.10	5.88	0.12	33
S24	7.4	0.25	-	-	-	-
S25	5.0	0.25	-	-	-	-
S26	74.4	0.50	2.11	30.40	0.30	58
S27	37.2	0.50	0.85	20.00	0.24	34
S28	24.8	0.50	1.17	5.80	0.51	40
S29	18.6	0.50	0.93	9.70	0.54	39
S30	14.9	0.50	0.66	0.68	0.48	56
S31	12.4	0.50	1.03	5.88	0.89	56
S32	10.6	0.50	0.58	9.71	0.58	49
S33	9.3	0.50	0.72	0.79	0.83	70
S34	7.4	0.50	0.36	1.27	0.52	46
S35	5.0	0.50	-	-	-	-
S36	55.2	0.50	0.78	1.44	0.11	25
S37	27.6	0.50	1.89	1.79	0.54	68
S38	18.4	0.50	0.68	1.67	0.29	45
S39	13.8	0.50	-	-	-	-
S40	11.0	0.50	-	-	-	-
S41	44.4	0.50	0.45	10.00	0.06	23
S42	22.2	0.50	1.08	2.08	0.31	68
S43	14.8	0.50	0.79	2.85	0.34	71
S44	11.1	0.50	-	-	-	-
S45	36.8	0.50	0.61	11.93	0.09	21
S46	18.4	0.50	-	-	-	-
S47	12.3	0.50	-	-	-	-
S48	55.2	0.25	-	-	-	-
S49	27.6	0.25	-	-	-	-
S50	18.4	0.25	-	-	-	-

SPECIMEN NUMBER	APPLIED SPECIFIC ENERGY (J/mm ²)	POWDER THICKNESS (mm)	SECTIONAL AREA (mm ²)	DILUTION (%)	RATE OF DEPOSITION (Kg/Hr)	SOLIDIFIED CONTACT ANGLE (DEGREES)
S51	13.8	0.25	0.42	0.54	0.24	49
S52	11.0	0.25	0.17	1.32	0.12	43
S53	44.4	0.25	-	-	-	-
S54	22.2	0.25	0.63	42.86	0.18	22
S55	14.8	0.25	-	-	-	-
S56	11.1	0.25	-	-	-	-
S57	36.8	0.25	-	-	-	-
S58	18.4	0.25	0.37	51.52	0.11	15
S59	32.2	1.00	5.15	1.42	0.74	110
S60	39.0	1.00	5.07	0.67	0.73	120
S61	19.4	1.00	-	-	-	-
S62	48.3	1.00	1.43	0.79	0.21	51
S63	30.4	1.00	2.64	0.09	0.76	115
S64	20.3	1.00	0.35	1.27	0.15	39
S65	15.2	1.00	1.58	0.28	0.91	127
S66	12.2	1.00	-	-	-	-
S67	87.5	1.00	3.62	6.23	0.52	97
S68	43.8	1.00	2.74	2.47	0.79	100
S69	29.2	1.00	1.79	0.31	0.77	97
S70	21.9	1.00	1.43	0.40	0.82	109
S71	17.5	1.00	1.42	1.58	1.02	88
S72	14.6	1.00	0.99	0.23	0.86	100
S73	12.5	1.00	-	-	-	-
S74	87.5	0.50	0.53	57.45	0.08	24
S75	43.8	0.50	0.71	8.87	0.20	43
S76	29.2	0.50	0.71	1.59	0.31	60
S77	21.9	0.50	0.61	0.93	0.35	71
S78	17.5	0.50	0.48	0.47	0.35	55
S79	14.6	0.50	0.40	1.41	0.35	60
S80	12.15	0.50	0.57	0.39	0.57	74
S81	10.9	0.50	0.63	7.21	0.73	73
S82	9.7	0.50	0.59	3.85	0.76	73
S83	8.8	0.50	0.46	19.51	0.66	59
S84	5.8	0.50	-	-	-	-
S85	60.8	0.50	0.79	4.26	0.11	44
S86	15.2	0.50	-	-	-	-
S87	8.7	0.50	-	-	-	-
S88	45.9	0.50	2.27	6.47	0.33	60
S89	23.0	0.50	0.60	15.89	0.17	76
S90	10.5	0.50	-	-	-	-
S91	8.4	0.50	-	-	-	-
S92	33.3	0.50	-	-	-	-
S93	7.8	0.50	-	-	-	-
S94	12.7	0.50	-	-	-	-
S95	14.3	0.50	-	-	-	-
S96	10.9	0.50	-	-	-	-
S97	35.9	0.50	1.92	0.59	0.28	76
S98	32.2	0.25	1.47	0.23	0.21	48
S99	10.7	0.25	-	-	-	-
S100	6.4	0.25	-	-	-	-

SPECIMEN NUMBER	APPLIED SPECIFIC ENERGY (J/mm ²)	POWDER THICKNESS (mm)	SECTIONAL AREA (mm ²)	DILUTION (%)	RATE OF DEPOSITION (Kg/Hr)	SOLIDIFIED CONTACT ANGLE (DEGREES)
S101	13.0	0.25	-	-	-	-
S102	4.9	0.25	-	-	-	-
S103	55.8	0.25	0.52	34.41	0.07	22
S104	18.6	0.25	0.14	48.00	0.06	29
S105	11.2	0.25	-	-	-	-
S106	20.7	0.25	-	-	-	-
S107	6.9	0.25	-	-	-	-
S108	20.7	0.50	-	-	-	-
S109	8.3	0.50	-	-	-	-
S110	13.8	0.50	-	-	-	-
S111	9.2	1.00	-	-	-	-
S112	11.2	1.00	-	-	-	-
S113	27.9	1.00	0.82	4.14	0.24	66
S114	55.8	1.00	0.80	5.64	0.12	42
S115	18.6	1.00	0.57	1.98	0.25	118
S116	41.9	1.00	3.06	1.29	0.88	88
S117	27.9	1.00	2.89	0.78	1.25	88
S118	20.9	1.00	1.78	4.13	1.03	72
S119	16.7	1.00	1.34	8.40	0.96	65
S120	14.0	1.00	0.42	1.33	0.36	68
S121	12.0	1.00	-	-	-	-
S122	62.1	1.00	3.29	3.29	0.47	80
S123	31.0	1.00	4.14	4.19	1.21	103
S124	20.7	1.00	2.38	2.38	1.03	88
S125	15.5	1.00	2.33	2.33	1.34	118
S126	50.0	1.00	3.87	1.31	0.56	70
S127	25.0	1.00	0.68	33.33	0.20	35
S128	41.4	1.00	1.05	41.18	0.15	23
S129	13.8	1.00	-	-	-	-
S130	41.4	0.50	-	-	-	-
S131	50.0	0.50	1.01	34.00	0.15	27
S132	16.7	0.50	-	-	-	-
S133	62.1	0.50	0.61	14.81	0.09	25
S134	31.0	0.50	0.92	0.25	0.26	36
S135	20.7	0.50	0.44	0.76	0.19	31
S136	41.9	0.50	1.62	3.82	0.47	58
S137	27.9	0.50	1.03	5.46	0.44	50
S138	20.9	0.50	-	-	-	-
S139	16.7	0.50	0.73	0.15	0.53	65
S140	14.0	0.50	0.92	7.98	0.79	79
S141	12.0	0.50	0.40	1.11	0.40	52
S142	41.9	0.25	-	-	-	-
S143	13.0	0.25	-	-	-	-
S144	31.0	0.25	0.35	21.67	0.10	26
S145	20.7	0.25	0.14	4.00	0.06	16
S146	50.0	0.25	0.52	39.13	0.07	19
S147	10.0	0.25	-	-	-	-
S148	20.7	0.25	-	-	-	-

APPENDIX 11.2

TABLE A.2 SECTIONAL AREAS, PERCENTAGE DILUTION, DEPOSITION RATE AND SOLIDIFIED CONTACT ANGLE AS A FUNCTION OF THE APPLIED SPECIFIC ENERGY FOR A 1.00mm POWDER THICKNESS OF TIN-BRONZE.

SPECIMEN NUMBER	APPLIED SPECIFIC ENERGY (J/mm ²)	SECTIONAL AREA (mm ²)	DILUTION (%)	DEPOSITION RATE (Kg/Hr)	SOLIDIFIED CONTACT ANGLE (Degrees)
B1	150.00	1.49	-*	0.24	88
B2	75.00	1.35	-	0.43	86
B3	37.50	1.44	-	0.91	58
B4	18.75	1.72	-	2.18	104
B5	12.50	0.94	-	1.79	105
B6	9.25	0.86	-	2.18	93
B07	150.00	2.74	-	0.32	115
B08	75.00	1.36	-	0.43	122
B09	37.50	1.70	-	1.08	135
B010	18.75	1.06	-	1.34	118
B011	9.32	0.92	-	2.33	110
BI12	196.00	0.92	-	0.15	55
BI13	18.25	0.33	-	0.42	84
B015	75.00	1.69	-	0.54	118

* No dilution was found.

APPENDIX 11.3

TABLE A.3 DEPOSIT TOUGHNESS AND ADHERENCE AS MEASURED BY BEND AND SHEAR TESTS

SPECIMEN NUMBER	DEGREE OF PREHEATING (°C)	OVERLAP (mm)	TRAVERSE SPEED (mm/s)	ANGLE OF BEND TEST BEFORE CRACKING (DEGREES) *	PEAK LOAD (TONF OR T.S.I.) *
M 1	500	1.25	18	90-100	
M 2	300	1.25	18	80	
M 3	20	1.25	15	90	
M 4	20	1.88	15	DITTO HA2	
M 5	20	1.50	15	120	2.99/15.95
M 6	20	1.50	20	120	
M 7	20	1.50	20	90	
M 8	20	SINGLE RUN	25	120	
M 9	300	1.50	15	140	
M10	300	1.50	20	120	
M11	300	1.50	25	OK 180	3.653/19.48
M12	200	1.50	15	160+180	
M13	200	1.50	20	90	
M14	200	1.50	25	160+180	
M15	150	1.50	15	120	
M16	150	1.50	20	120	
M17	150	1.50	25	OK 180	1.605/8.56**
M18	400	1.50	15	OK 180	
M19	400	1.50	20	160+180	
M20	400	1.50	25	OK 180	2.91/15.52

* TESTS DONE BY B.S.C. (S.L.)

** RUN No. 17 FAILED TO MEET THE MINIMUM SPECIFIED OF 20 000 P.S.I.

NOMENCLATURE

SYMBOL	MEANING	UNITS
A	AUSTENITE	
A	PARTIAL AREA OF DEPOSITION ON THE BASE METAL	mm ²
A	SINGLE DIRECTION TRAVERSE	
A+B	TOTAL AREA OF DEPOSIT ON THE BASE METAL	mm ²
B	PARTIAL AREA OF DEPOSIT PENETRATED ON THE BASE METAL	mm ²
B	TRAVERSE IN BOTH DIRECTIONS	
C	CARBIDES	
C _{req}	CHROMIUM EQUIVALENT = %Cr + Mo + 1.5 X % Si + 0.5 X % N ₆	
C _{Max}	MAXIMUM SEGREGATION MEASURED	
C _{Min}	MAXIMUM SEGREGATION MEASURED	
D	INCIDENT BEAM DIAMETER	mm
d	POWDER BED THICKNESS	mm
F	FERRITE	
H _v	VICKERS HARDNESS NUMBER	
h	HEIGHT OF THE BEAD	mm
L	LIQUID PHASE	

M	MARTENSITE	
Nieq	NICKEL EQUIVALENT = %Ni + 30 x %C + 0.05 x % Mn	
P	TOTAL INCIDENT BEAM POWER	W
(P/DV)	APPLIED SPECIFIC ENERGY	J/mm ²
T	TEMPERATURE	°C
V	TRAVERSE SPEED OF INCIDENT BEAM	MM/S
W	WIDTH OF THE BEAD	mm
X-Y	DIRECTIONS OF MOVEABLE TABLE	
Z	DEPTH OF THE HEAT-AFFECTED ZONE	mm
α (alpha)	^X FERRITE	
γ (gamma)	AUSTENITE	
$\gamma_{s/g}$	SURFACE TENSION OF SOLID SURFACE AND GAS	
$\gamma_{l/s}$	INTERFACIAL TENSION OF LIQUID CLADDING ALLOY AND SOLID BASE METAL	
$\gamma_{l/g}$	SURFACE TENSION OF THE LIQUID CLADDING ALLOY AND GAS	
δ (delta)	DELTA FERRITE	
η (eta)	LAVES PHASE	
θ (theta)	SOLIDIFIED CONTACT ANGLE, DEGREES	
λ	WAVELENGTH (m μ)	

- μ_1 (Nu) SYMMETRIC STRETCH MODE OF CO₂ VIBRATION
- μ_2 BENDING MODE OF CO₂ VIBRATION
- μ_3 ASSYMETRIC STRETCH MODE OF CO₂ VIBRATION
- σ (Sigma) SIGMA PHASE
- ϕ (Phi) DEFLECTED DOWNWARDS ANGLE IN DILUTION SURFACE CLADDING,
DEGREES
- χ (Chi) CHI PHASE

TABLES

- 1.1 Commercial laser used in material processing
- 4.1 Quality of tracks form 316 stainless steel
- 4.2 Quality of tracks made with tin-bronze
- 4.3 Quality of tracks made with monel
- 4.4 Range of deposition rate observed with different bed depths of 316 stainless steel
- 4.5 Physical characteristics of multiple runs in 316 stainless steel
- A.1 Sectional area, percentage dilution, deposition rate and solidified contact angle as a function of the applied specific energy and powder bed thickness
- A.2 Sectional area, percentage dilution deposition rate and solidified contact angle as a function of the applied specific energy for a 1.00 mm powder thickness of tin-bronze
- A.3 Deposit toughness and adherence as measured by bend and shear tests.

REFERENCES

1. Desforges C.D.
Technical File No 46
Engineering, October 1977
2. Megaw J.H and I.J Spalding
Physics in Technology, 186-194, September 1976
3. Steen W.M and C. Courtney
Surfaces Heat Treatment of En 8 Steel
using a 2 kw continuous-wave CO₂ Laser
Metals Technology, 456-462 December 1979
4. Eduard U. Locke and Richard A. Hella
Metal Processing with High Power CO₂ Laser
ICE Journal of Quantum Electronics, Vol QE-10 No 2, 179-
185, February 1974.
5. Peter Bletzinger and others.
IEEE Journal of Quantum Electronics Vol QE-11 No 7, 317-
322, July 1975.
6. Seaman F.D and D.S Gnanamuthu using the Industrial Laser
to surface Harden and Alloy.
Metal progress, 67-74 August 1975,
7. Breinan E.M, B.H. Kear and C.M. Banas
Processing Materials with Lasers
Physics Today, 44-50 November 1976.
8. Steen W.M and C.G.H Courtney
Hardfacing Ninonic 75
Metals Technology, 232-237 June 1980
9. Suchowsky R.S and E Garrabrant
Welding Journal, 43 (1), 13-20 1964

10. Gabrabrant E.C and R.S. Suchowsky
Welding Journal, 48 (5) 385-395 1969
11. Raynolds G.H and E.J. Kachelmeier
Metal Construction, 429-430 1978
12. Courtney C. and W.M. Steen
Measurement of the Diameter of a Laser Beam
Applied Physics 17, 303-307, 1978
13. Ream S.L.
Laser Focus, 68-71 November 1979
14. Making Light Work
Metalworking Production, 75 August 1979.
15. Shaeffler, A
Metal Progress 56, 680-680B, 1949
16. Physical and Mechanical Properties of
British Steels
17. Bain E.C and A.W. Paxton
Alloy Elements in Steel
23rd Ed. American Society for Metals, Metal
Park, Ohio. 1961
18. Adams A.W.
Physical Chemistry of Surfaces
Ad. John Wiley & Sons
Third Edition 1976.

19. G J Davies and J G Garland
Solidification Structures and Properties
of Fusion Welds
International Metallurgical Reviews
March 1975, Vol 20, P 83

20. M C Flemings
Solidification Processing
McGraw-Hill 1974

21. J. E. READY
Industrial Applications of Lasers
Academic Press 1978

22. D. Peckner & I. M. Bernstein
Handbook of Stainless Steel
McGraw Hill Book Co 1977

List of Figures

FIGURE	TITLE
1.1	Oscillation modes and vibrating energy levels of carbon and nitrogen molecules.
1.2	Chemical reactions in gas laser.
2.1	Dilution of surface cladding, the bead, A, and penetration B, both areas A and B are the same cladding alloy, but are shaded different to illustrate the calculation of dilution.
3.1	Arrangement of the apparatus for making a single bead surface cladding.
3.2	Arrangement of the apparatus.
3.3	Photograph of the arrangement of apparatus for monel surface cladding.
3.4	BCO 2kw CO ₂ laser-gas and discharge path (ref 14).
3.5	Photograph of the equipment.
4.1	High penetration and dishomogeneous deposits, power = 1800 w; beam diameter = 7.2, 7.2 and 5,8mm; speed = 5, 15, 5 mm/S; powder thickness = 0.50mm.
4.2	Homogeneous deposits; power = 1600 w; beam diameter = 4.3 mm; speed = 15, 20 and 25 mm/s; powder thickness = 1.00mm.
4.3	Bead height vs energy/unit area p/dv (J/mm ²) for a 1.00mm powder thickness.
4.4	Bead height vs energy/unit area p/dv (j/mm ²) for a 0.50mm powder thickness.
4.5	Bead height vs energy/unit area p/dv (J/mm ²) for a 0.25 mm powder thickness.
4.6	Bead width vs energy/unit area p/dv (J/mm ²) for a 1.00mm powder thickness.
4.7	Bead width vs energy/unit area p/dv (J/mm ²) for a 0.50 mm powder thickness.

- 4.8 Bead width vs energy/unit area p/dv (J/mm^2) for a 0.25 mm powder thickness.
- 4.9 Ratio (W/H) vs energy/unit area, p/dv (J/mm^2) for a 1.00mm powder thickness.
- 4.10 Ratio (W/H) vs energy/unit area, p/dv (J/mm^2) for a 0.50mm powder thickness.
- 4.11 Ratio (W/H) vs energy/unit area, p/dv (J/mm^2) for a 0.25mm powder thickness.
- 4.12 Depth of the HAZ (heat-affected zone) vs energy/unit area, p/dv (J/mm^2) for a 1.00mm powder thickness.
- 4.13 Depth of the HAZ (heat-affected zone) vs energy/unit area, p/dv (J/mm^2) for a 0.50mm powder thickness.
- 4.14 Depth of the HAZ (heat-affected zone) vs energy/unit area, p/dv (J/mm^2) for a 0.25 powder thickness.
- 4.15 Bead height (mm) vs traverse speed (mm/s) for a 1.00mm powder thickness.
- 4.16 Bead height (mm) vs traverse speed (mm/s) for a 0.50mm powder thickness.
- 4.17 Bead height (mm) vs traverse speed (mm/s) for a 0.25mm powder thickness.
- 4.18 Bead width (mm) vs traverse speed for a 1.00mm powder thickness.
- 4.19 Bead width (mm) vs traverse speed for a 0.50mm powder thickness.
- 4.20 Bead width (mm) vs traverse speed for a 0.25mm powder thickness.
- 4.21 Powder thickness (mm) vs energy/unit area, p/dv (J/mm^2) for 316 stainless steel.
- 4.22 Good and discontinuous tracks, power = 1500 w; beam diameter = 2.00mm speed = 20, 40, and 80 mm/s; powder thickness = 1.00mm.
- 4.23 Different cross section produced between
- a) tin-bronze surface cladding
 - b) stainless steel surface cladding

- 4.24 Bead height (mm) vs energy/unit area, p/dv (J/mm^2) for a 1.00 mm powder thickness and 2.00mm beam diameter.
- 4.25 Bead width (mm) vs energy/unit area, p/dv , (J/mm^2) for a 1.00 mm powder thickness and 2.00mm beam diameter.
- 4.26 Ratio (W/H) (bead width/bead height) vs energy/unit area, p/dv for a 1.0mm powder thickness and 2.00mm beam diameter.
- 4.27 Depth of the HAZ (mm) vs energy/unit area p/dv (J/mm^2) for a 1.00mm powder thickness and 2.00mm beam diameter.
- 4.28 Bead height (mm) vs traverse speed (mm/s) for a 1.00mm powder thickness and 2.00mm beam diameter.
- 4.29 Bead width (mm) vs traverse speed (mm/s) for a 1.00mm powder thickness and 2.00mm beam diameter.
- 4.30 Discontinuous tracks = 1600 w; beam diameter = 2.00mm; speed = 35, 40, 45 and 50mm/s; mass flow rate = 2.05Kg/Hr.
- 4.31 Continuous tracks; power = 1560 w; beam diameter = 2.00mm; speed 10,15, 20 and 25mm/s; mass flow rate= 1.37 Kg/Hr.
- 4.32 Bead height (mm) vs energy/unit area, p/dv (J/mm^2) for a mass flow rate of 2.05 Kg/Hr, $\diamond = 2.00$ and $\blacklozenge = 3.00$ mm beam diameter.
- 4.33 Bead height (mm) vs energy/unit area, p/dv (J/mm^2) for a mass flow rate of 1.37 Kg/Kg, $\square = 2.00$ and $\blacksquare = 3.00$ mm beam diameter.
- 4.34 Bead height (mm) vs energy/unit area, p/dv (J/mm^2) for a mass flow rate of 0.83 Kg/Hr, $\circ = 2.00$ and $\bullet = 3.00$ mm beam diameter.
- 4.35 Bead width (mm) vs energy/unit area. p/dv (J/mm^2) for a mass flow rate of 2.05 Kg/Hr, $\diamond = 2.00$ and $\blacklozenge = 3.00$ mm beam diameter.
- 4.36 Bead width (mm) vs energy/unit area, p/dv (J/mm^2) for a mass flow rate of 1.37 Kg/Hr, $\square = 2.00$ and $\blacksquare = 3.00$ mm beam diameter.
- 4.37 Bead width (mm) vs energy/unit area, p/dv (J/mm^2) for a mass flow rate of 0.87 Kg/Hr, $\circ = 2.00$ and $\bullet = 3.00$ mm beam diameter.
- 4.38 Ratio (W/H) (bead width/bead height) vs energy/unit area, p/dv (J/mm^2) for a mass flow rate of 2,05 Kg/Hr, $\diamond = 2.00$ and $\blacklozenge = 3.00$ mm beam diameter.

- 4.39 Ratio (W/H) (bead width/bead height) vs energy unit area, p/dv (J/mm^2) for a mass flow rate of 1.37 Kg/Hr, $\square = 2.00$ and $\blacksquare = 3.00$ mm beam diameter.
- 4.40 Ratio (W/H) (bead width/bead height) vs energy/unit area, p/dv (J/mm^2) for a mass flow rate of 0.87 Kg/Hr, $\circ = 2.00$ and $\bullet = 3.00$ mm beam diameter.
- 4.41 Bead width (mm) vs energy/unit length, p/v (J/mm) for a 2.00mm beam diameter.
- 4.42 Bead width (mm) vs energy/unit length p/v (J/mm) for a 3.00mm beam diameter.
- 4.43 Bead height (mm) vs traverse speed (mm/s) for a mass flow rate of $\diamond = 2.05$, $\square = 1.37$ and $\circ = 0.87$ Kg/Hr.
- 4.44 Bead width (mm) vs traverse speed (mm/s) for a mass flow rate of $\diamond = 2.05$, $\square = 1.37$ and $\circ = 0.87$ Kg/Hr.
- 4.45 Sectional area (mm^2) vs traverse speed (mm/s) for a 1.00mm powder thickness.
- 4.46 Sectional area (mm^2) vs traverse speed (mm/s) for a 0.50mm powder thickness.
- 4.47 Sectional area (mm^2) vs traverse speed (mm/s) for a 0.25mm powder thickness.
- 4.48 Sectional area (mm^2) vs traverse speed v (mm/s) for a 1.00mm powder thickness and 2.00mm beam diameter.
- 4.49 Sectional area (mm^2) vs depth of the HAZ (mm) for a 1.00mm powder thickness.
- 4.50 Sectional area (mm^2) vs depth of the HAZ (mm) for a 0.50mm powder thickness.
- 4.51 Sectional area (mm^2) vs depth of the HAZ (mm) for a 0.25mm powder thickness.

- 4.52 Sectional area (mm^2) vs depth of the HAZ (mm) for a 1.00mm powder thickness and 2.00mm beam diameter.
- 4.53a Nugget characteristics: specimen number S74, power = 1400 W, beam diameter = 3.2mm; speed = 5mm/s, powder thickness = 0.50mm total area = 0.53mm^2 , deposition rate = 0.08 Kg/Hr, dilution = 57.5%.
- 4.53b Nugget characteristics: specimen number S123, power = 1800 W, beam diameter = 5.8mm; speed = 10mm/s, powder thickness = 1.00mm total area = 4.19mm^2 , deposition rate = 1.21 Kg/Hr, dilution = 0.13%. (0)
- 4.54 Energy/unit area, p/dv (J/mm^2) vs dilution (%) for a 1.00mm powder thickness.
- 4.55 Energy/unit area, p/dv (J/mm^2) vs dilution (%) for a 0.50mm powder thickness.
- 4.56 Energy/unit area, p/dv (J/mm^2) vs dilution (%) for a 0.25mm powder thickness.
- 4.57 Dilution (%) vs traverse speed (mm/s) for a 1.00mm powder thickness.
- 4.58 Dilution (%) vs traverse speed (mm/s) for a 0.50mm powder thickness.
- 4.59 Dilution (%) vs traverse speed (mm/s) for a 0.25mm powder thickness.
- 4.60 Deposition rate (Kg/Hr) vs traverse speed (mm/s) for a 1.00mm powder thickness.
- 4.61 Deposition rate (Kg/Hr) vs traverse speed (mm/s) for a 0.50mm powder thickness.
- 4.62 Deposition rate (Kg/Hr) vs traverse speed (mm/s) for a 0.25mm powder thickness.
- 4.63 Deposition rate (Kg/Hr) vs traverse speed (mm/s) for a beam power = 1600 W; beam diameter = 4.3mm and $\theta = 1.00$, $\alpha = 0.50$,

ϕ = 0.25mm powder thickness.

- 4.64 Bead height (mm) vs dilution (%), for 316 stainless steel.
- 4.65 Deposition rate (Kg/Hr) vs traverse speed (mm/s) for a 1.00mm powder thickness and 2.00mm beam diameter.
- 4.66 Constitution diagram for stainless steel as weld deposit (Ref 15).
- 4.67 Fe - Cr - Ni Pseudo-binary diagram taken at 70% Fe.
- 4.68 Schematic diagrams showing competitive growth for a moving pool with,
 a) An elliptical shaped puddle
 b) A teardrop shaped puddle
- 4.69 Microstructure 316 stainless steel cladding, specimen number S62, power = 1400 W; beam diameter = 5.8mm, speed = 5mm/s, powder thickness = 1.0mm, etched in HCl + HNO₃ and H₂O solution, X 110.
- 4.70 Microstructure 316 stainless steel cladding, specimen number S68; powder thickness = 1.00mm etched in HCl + HNO₃ and H₂O solution X110.
- 4.71 Microstructure 316 stainless steel cladding, specimen number M 8, power = 1300 W, beam diameter = 2.29mm, speed = 25mm/s, powder thickness = 2.00mm, etched in Kalling's Reagent, X.
- 4.72 Microstructure 316 stainless steel cladding, specimen number M 9, power = 1460 W, beam diameter = 2.29mm, speed 15mm/s, powder thickness = 2.0mm, grade of preheating = 300 °C overlap = 1.15mm, forwards and backwards, etched in a solution of HCl + HNO₃ and H₂O, X182.
- 4.73 The same as above, but at X 442.
- 4.74 Heat-affected zone in En 3 steel after laser cladding 316 stainless steel, specimen number S63, power = 1400 W; beam diameter = 4.6mm, speed = 10mm/s, powder thickness = 1.0mm etched in 2% nital X110.

- 4.75 Heat-affected zone in En 3 steel after laser cladding 316 stainless steel, specimen number S123, power = 1800 W; D = 5.8mm, V = 10mm/s, powder thickness = 1.00mm, etched in 2% nital X 110.
- 4.76 Heat-affected zone in En 3 stainless steel, specimen number S20, P = 1600 W; D = 4.3mm, V = 35mm/s, powder thickness 1.00mm, etched in nital, X182.
- 4.77 Heat-affected zone in En 3 steel after laser cladding 316 stainless steel, specimen number M4, P = 1300 W; D = 2.29mm, V = 15mm/s, powder thickness = 2.00mm, not preheat overlap, 1.88mm, etched in 2.00% nital X110.
- 4.78 Heat-affected zone in En 3 steel after laser cladding 316 stainless steel, specimen number M16, P = 1400 W; D = 2.29, V = 20mm/s, powder thickness = 2.0mm.
- 4.79 Relation between the peak temperatures by various regions in heat-affected zone, and how these correlate with iron-carbon phase diagram.
- 4.80 Isotherm transformation for En 3 steel (Ref 16).
- 4.81 EPMA concentration profiles for Cr, Ni and Mo in 316 stainless steel surface cladding, specimen S1.
- 4.82 EPMA concentration profiles for Cr, Ni and Mo in 316 stainless steel surface cladding, specimen S26.
- 4.83 EPMA concentration profiles for Cr, Ni and Mo in 316 stainless steel surface cladding, specimen S63.
- 4.84 EPMA concentration profiles for Cr, Ni and Mo in 316 stainless steel surface cladding, specimen S116.
- 4.85 EPMA concentration profiles for Cr, Ni and Mo in 316 stainless steel surface cladding, specimen number S118.
- 4.86 EPMA concentration profiles for Cr, Ni and Mo in 316 stainless steel surface cladding, specimen number S137.
- 4.87 Microhardness and macrograph section view through surface

- cladding of specimen number S4, etched 2% nital, X21 power 1600 W, beam diameter = 5.8mm, traverse speed = 5mm/s, powder thickness = 1.0mm.
- 4.88 Microhardness and macrograph specimen view through surface cladding of specimen number S5, etched 2% nital, X21, power = 1600 W, beam diameter = 5.8mm, traverse speed = 15mm/s, powder thickness = 1.0mm.
- 4.89 Microhardness and macrograph specimen view through surface cladding of specimen number S8, etched 2% nital, X21, power = 1600 W, beam diameter = 4.3mm, traverse speed = 5mm/s, powder thickness = 1.0mm.
- 4.90 Microhardness and macrograph section view through surface cladding of specimen number S9, power = 1600 W, beam diameter = 4.3mm, traverse speed = 15mm/s, powder thickness = 1.0 mm.
- 4.91 Microhardness and macrograph section view through surface cladding of specimen number S26, power = 1600 W, beam diameter = 4.3mm, traverse speed = 5mm/s, powder thickness = 0.50mm.
- 4.92 Microhardness and macrograph section view through surface cladding of specimen number S27, power = 1600 W, beam diameter = 4.3mm, traverse speed = 10mm/s, powder thickness = 0.50mm.
- 4.93 Microhardness and macrograph section view through surface cladding of specimen number S28, power = 1600 W, beam diameter = 4.3mm, traverse speed = 15mm/s, powder thickness = 0.50mm.
- 4.94 Microhardness and macrograph section view through surface cladding of specimen number S59, power = 1400 W, beam diameter = 8.7mm, traverse speed = 5mm/s, powder thickness = 1.0mm.
- 4.95 Microhardness and macrograph section view through surface cladding of specimen number S60, power = 1400 W, beam diameter = 7.2mm, traverse speed = 5mm/s, powder thickness = 1.00mm.

- 4.96 Microhardness and macrograph section view through surface cladding of specimen number S77, power = 1400 W, beam diameter = 3.2mm, traverse speed = 20mm/s, powder thickness = 0.50mm.
- 4.97 Microhardness and macrograph section view through surface cladding of specimen number S124, power = 1800 W, beam diameter = 5.8mm, traverse speed = 15mm/s, powder thickness = 1.00mm.
- 4.98 Microhardness and macrograph section view through surface cladding of specimen number S125, power = 1800 W, beam diameter = 5.8mm, traverse speed = 20mm, powder thickness = 1.0mm.
- 4.99 Approximation hardness of carbon steel as a function of carbon content, fully hardening martensite (Ref 17).
- 4.100 Surface cladding; power 1400 W, beam diameter = 2.29mm, speed = 18mm/s, powder thickness = 2.00mm, grade of preheating = 300°C, overlap = 1.25mm, towards and backwards, X3.
- 4.101 Surface cladding, power = 1460W, beam diameter = 2.29mm, speed = 20mm/s, powder thickness = 2.00mm, grade of preheating = 300°C, overlap = 1.50mm, towards and backwards, X3.
- 4.102 Section view 316 stainless steel cladding, specimen number M6, power = 1300 W, beam diameter = 2.29mm, speed = 20mm/s, powder thickness = 2.00mm, no preheat, overlap = 1.5mm forwards and backwards etched in 4% nital.
- 4.103 Section view 316 stainless steel cladding, specimen number M9, power = 1450 W, beam diameter = 2.29mm, speed 15mm/s, powder thickness = 2.00mm, degree of preheating = 300°C, overlap = 1.50mm, forwards and backwards, etched in 4% nital, X18.
- 4.104 Section view 316 stainless steel cladding, specimen number M7, power = 1300 W, beam diameter = 2.29mm, speed = 20mm/s, powder thickness = 2.0mm, no preheat, overlap = 1.5mm, forwards etched in 4% nital, X18.
- 4.105 Section view 316 stainless steel cladding, specimen number M16, power = 1400 W, beam diameter = 2.29mm, speed = 20mm/s, powder thickness = 2.00mm, degree of preheating = 150°C, overlap = 1.5mm, forwards and backwards, etched in 4% nital, X18.

- 4.106 Force system affecting wettability in two dimensions.
- 4.107 Solidified contact angle, θ (degrees) vs dilution (%) for a 1.00mm powder thickness.
- 4.108 Solidified contact angle, θ (degrees) vs dilution (%) for a 0.50mm powder thickness.
- 4.109 Solidified contact angle, θ (degrees) vs dilution (%) for a 0.25mm powder thickness.
- 4.110 θ (degrees) vs energy/unit area, P/DV (J/mm^2) for a 1.00mm powder thickness.
- 4.111 θ (degrees) vs energy/unit area, P/DV (J/mm^2) for a 0.50mm powder thickness.
- 4.112 θ (degrees) vs energy/unit area, P/DV (J/mm^2) for a 0.25mm powder thickness.
- 4.113 θ (degrees) vs energy/unit area, P/DV (J/mm^2) for a 1.00mm powder thickness and 2.00mm beam diameter.
- 4.114 Test specimen and method of making shear test of clad plate (from ASTM A264-74a).

ACKNOWLEDGEMENTS

Thanks are due to British Steel Corporation (S. L.) for providing the materials used in this project.

I am very grateful and I express my thanks to Dr W. M. Steen, not only for introducing me to the field of lasers, but also for his invaluable guidance and contribution to this thesis.

Thanks are also due to Dr D. R. F. West for many suggestions.

I would like to thank all members of John Percy Research Group for their help.

I am very grateful to all members of the Laser Group, and Mr and Mrs Courtney for their invaluable help.

Thanks to all Technicians of the Department of Metallurgy for their help.

I am very grateful to T. Clarke who patiently typed this work.

And last but not least my thanks to all persons who kept me happy during the elaboration of this thesis, and Mr M. Sandwith, chairman of the Society of Friendship for Oversea Students.